2002 NASA SATS DESIGN

IKELOS

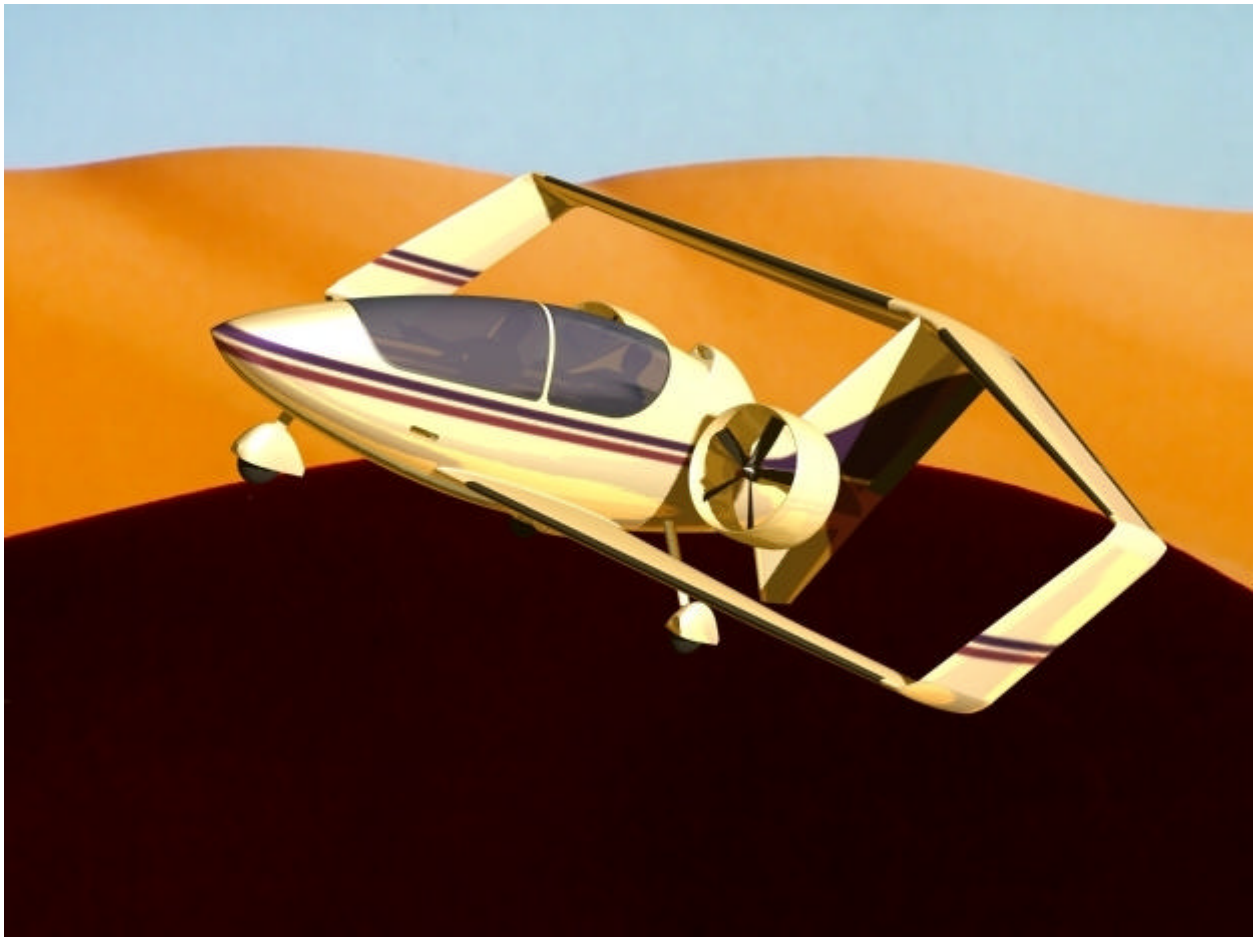

VirginiaTech

VIRGINIA POLYTECHNIC INSTITUTE AND STATE UNIVERSITY

Loughborough University

IKELOS

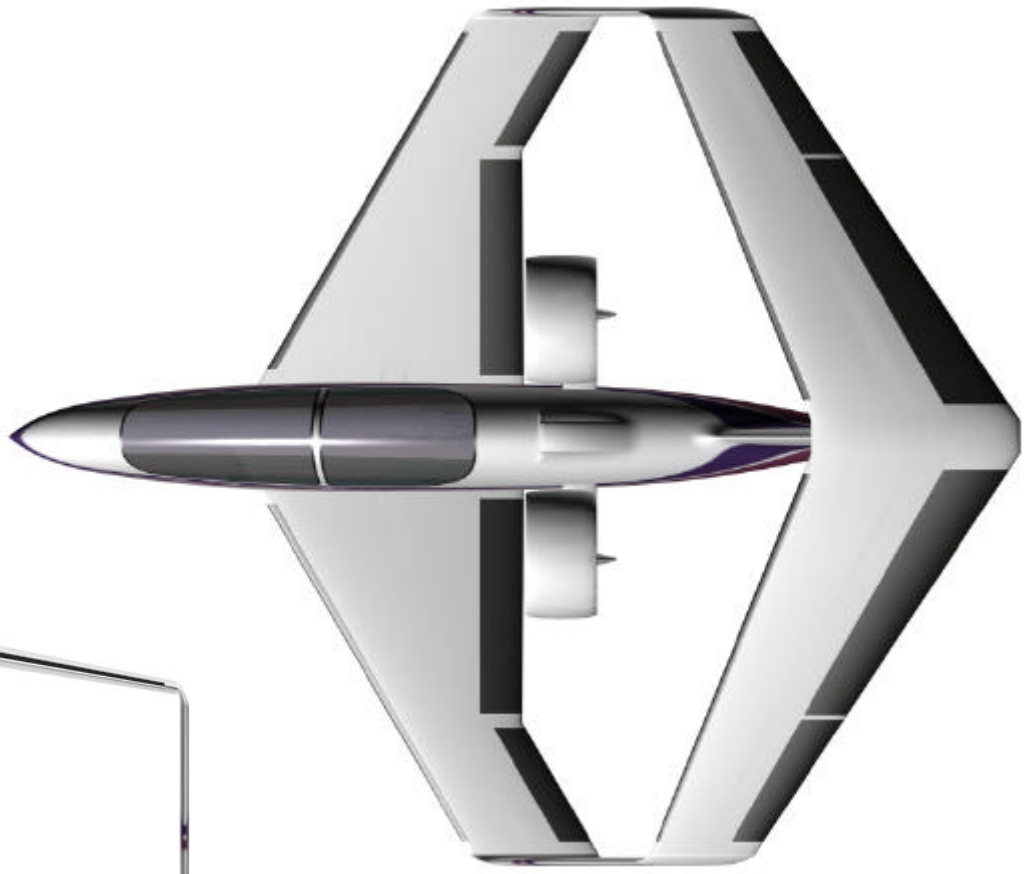

IKELOS

2002 NASA SATS Design Competition

Virginia Polytechnic Institute and State University
and
Loughborough University

Advisors:
James F. Marchman, III
Gary J. Page
Lloyd R. Jenkinson

May 1, 2002

TABLE OF CONTENTS

TEAM MEMBER INFORMATION…… ii
ABSTRACT……..iii
EXECUTIVE SUMMARY…….. 1
1. PROJECT DESCRIPTION……1
2. DESIGN SPECIFICATIONS…… 2
2.1 Introduction……2
2.2 Performance…… 5
2.2.1 Takeoff and Landing……..5
2.2.2 Cruise Performance……6
2.2.3 Climb and Turn Performance……6
2.2.4 Performance Comparison……...7
2.3 Propulsion……... 8
2.3.1 Rand Cam Engine…….. 8
2.3.2 Engine Installation…… 9
2.3.3 Ducted Fans……... 10
2.4 Aerodynamics…… 11
2.5 Stability and Control……... 13
2.6 Structures…… 15
2.6.1 Structural Design Aspects…….....15
2.6.2 Structural Overview……...15
2.6.3 Landing Gear…… 16
2.7 Avionics and Systems……17
2.7.1 Avionics……17
2.7.2 Systems…….. 19
2.8 Ergonomics/Human Factors……19
2.9 Manufacturing……20
2.10 Cost……... 20
2.11 Practical Applications……... 21
3. SATS ISSUES…… 21
4. DECRIPTION OF STUDENT WORK…….. 22
APPENDIX A: COMPETITION INFORMATION…… A-1
APPENDIX B: PERFORMANCE……... B-1
APPENDIX C: PROPULSION…… C-1
APPENDIX D: AERODYNAMICS…… D-1
APPENDIX E: STABILITY AND CONTROL……... E-1
APPENDIX F: WEIGHT AND BALANCE…… F-1
APPENDIX G: STRUCTURES……... G-1
APPENDIX H: AVIONICS AND SYSTEMS……H-1
APPENDIX I: COCKPIT…… I-1
APPENDIX J: MANUFACTURING……... J-1
APPENDIX K: COST…….. K-1
APPENDIX L: DESIGN SELECTION PROCESS..... L-1

Team Member Information

Virginia Tech

Name	Citizenship	Level of Study	Major	Career Aspirations	Project Task(s)
Trisha Basuray	US	Freshman	AE	Undecided	Stability & Control
Nicole Bratt	US	Senior	AE	Design & Development	Aerodynamics & Webpage
Jill Harper	US	Senior	ISE	NASA	Cockpit Design., Ergo., Manufact.
Andrew Kates	US	Senior	AE	Aerospace Industry	Performance
Ernest Keen	US	Senior	AE	R&D of new Aerospace Technology	Stability & Control
Joe Kehoe	US	Senior	AE	NLX Corporation	Stability & Control
John Leonard	US	Senior	AE	Advance Flight Control & Simulation	Stability & Control
Steve Penn	US	Senior	AE	Gas Turbine Engine Design	Team Leader, Propulsion
Carrie Phelps	US	Senior	AOE	Naval Architecture Field	Structures
Bryan Racine	US	Senior	AE	Flight Test Engineering, Test Pilot	Aerodynamics
Adam R. Shuty	US	Senior	ISE	Undecided	Manufacturing & Costs
Jessica Walker	US	Senior	AOE	Graduate School & Aircraft Design	Performance
Mike Willemann	US	Freshman	AE	Undecided	Aerodynamics
Lyndsey Wuethrich	US	Senior	ISE	Aviation Industry	Ergonomics & Cockpit Design

Loughborough University

Name	Citizenship	Level of Study	Major	Career Aspirations	Project Task(s)
Dave Etchells	British	Third Year, Undergrad.	AE	ATPL Qual. & Air Accident Investigation	Avionics
Matt Fletcher	British	Third Year, Undergrad.	AE	Aviation Industry	Mass Calculation, CG Location, Costs
Stuart Frizzel	British	Third Year, Undergrad.	AE	Work Abroad	Propulsion, Propeller & Duct Design
Michelle Hill	British	Third Year, Undergrad.	AE	Gas Turbine Engine Design & Testing	Structures
Will James	British	Third Year, Undergrad.	AE	Aviation Industry	Avionics & Systems
Graham Joyce	British	Third Year, Undergrad.	AE	Aircraft Design & Test Engineer, Astronautics	Configuration Manager, CAD
Jonathan Newton	British	Third Year, Undergrad.	AE	Pilot	Team Leader, Performance
Joshua Phelps	British	Third Year, Undergrad.	AE	Pilot	Structures
Melissa Puran	Singaporean	Third Year, Undergrad.	AE	Flight Test Engineer & Roller Coaster Design	Stability & Control
Greg Reid	British	Third Year, Undergrad.	AE	Alternate Transportation Development	Circulation Control, Mass Balance
Paul Whitehouse	British	Third Year, Undergrad.	AE	Royal Navy Pilot	Performance
Jamie Wright	British	Third Year, Undergrad.	AE	Flight Dynamics Div. of Marshall Aerospace	Aerodynamics

ABSTRACT

An international/multidisciplinary aircraft design team of 14 students from Virginia Tech (U.S.) and 12 from Loughborough University (England) was tasked with designing an innovative new general aviation aircraft. The original specifications called for the aircraft to be able to takeoff and land in 46 m (150 ft) including clearance of a 5 m (16 ft) obstacle, have a cruise speed greater than 90 kts, and a maximum range greater than 150 nm. These targets were modified as the project evolved.

Fourteen initial concepts were explored by members of the VT and LU teams. This field was then narrowed to six, which were examined in more detail. The entire team met in England in November 2001, and a final concept was selected through the use of a detailed rating process. The selected concept was chosen based on its performance, cost effectiveness, aesthetic appeal, marketability, and the degree to which SATS goals were satisfied. The evaluation process included comparative performance analysis between concepts, and open discussion on the pros and cons of each of the final six concepts.

The selected concept was a swept, box-wing design powered by dual ducted fans. Further detailed analysis of this concept was performed by specialized sub-groups within the design team. The aircraft was modified to be a 2-place design with the pilots seated in a tandem configuration. The original range and cruise speed specifications were increased to 500+ nautical miles and 140 kts, respectively. In addition, the landing specification was revised to require a 46 m (150 ft) ground roll and meet a 152 m (500 ft) Super-Short Takeoff and Landing requirement. These modifications allow the aircraft to be more competitive in the general aviation market while retaining its short field capabilities. The resulting design was named Ikelos after a Greek god of dreams.

The use of the unique box-wing for Ikelos required detailed analysis of the aircraft's aerodynamics, stability, and handling qualities to ensure safe and reliable SSTOL operation. The selection of an innovative rotary diesel engine design for Ikelos gave significant reductions in the weight, cost, and complexity of the propulsion system. Ikelos also features wings that are designed to be disassembled for trailer towing.

The goals of the Small Aircraft Transportation System were an important motivation in the design of Ikelos. Its short-field performance takes the SATS goal of making better use of small airports one step further to very short field use. The selection of modern avionics promises to make flying simpler and safer, another goal of SATS. The estimated aircraft cost of $156,000 lies within the current price range of general aviation aircraft, while offering new short field capabilities within the SATS operational framework.

1. PROJECT DESCRIPTION

The design problem was approached as an internationally collaborative project by students at Virginia Tech (VT) and Loughborough University (LU). At the start of the project, the team was given the following criteria for the design of the aircraft:

- Vertical or very short takeoff and landing in order to operate from confined areas
- Ability to fit on a small trailer for easy transportation
- Simple, lightweight, and easy-to-use design with a modern propulsion system
- Failsafe modes to ensure pilot safety – particularly during takeoff and landing
- Meet certification requirements where applicable
- Ability to takeoff and land over a 5 m (16.4 ft) obstacle in 46 m (150 ft)
- Stall speed not to exceed 37 kts in wingborne flight
- Maximum cruising speed at sea level in excess of 90 kts
- Range at typical cruising speed greater than 150 nm
- Endurance greater than two hours
- Sea level maximum rate of climb greater than 1000 feet per minute.

All of the design criteria were established in order to develop a light aircraft capable of expanding the utility of the SATS program with a vehicle that might meet new certification requirements for "Sport Aircraft." Initially, fourteen concept proposals were submitted by members of the design team. The team evaluated these proposals over the course of several months, and the selection of a final design concept was made in November, 2001. The final concept was chosen on the basis of performance, cost, compliance with SATS requirements, and the degree of innovation offered by the design.

The initially selected concept was capable of Vertical Takeoff and Landing (VTOL) if needed. Its box-wing design featured tilting, ducted propellers and was arranged to enhance VTOL operation. Due to the technical complexity, high cost, and high noise of VTOL design, this was modified for conventional takeoff and landing without vectored thrust. As more detailed analysis was performed, the original takeoff and landing specification of 46 m (150 ft) was reexamined and found too demanding for conventional operation. The operational goal was then changed to one meeting the NASA definition for Super Short Takeoff and Landing (SSTOL) flight of takeoff/landing within 152 m (500 ft) and clearance over a 15 m (50 ft) obstacle.[(1)] The design was also modified to be a two-person aircraft, allowing the design to retain its short field performance while dramatically improving the marketability and flexibility of the design. Note that the original box-wing and duct configuration was kept as the foundation of the design to allow future use of thrust vectoring and VTOL operation if desired.

2. DESIGN SPECIFICATIONS

2.1 Introduction

In recent years, flying has become a frustrating mode of transportation. Commercial airports have become huge waiting rooms filled with irritated passengers waiting for delayed flights and time-consuming security checks. Multiple connecting flights can make a simple trip much more complicated. Even if commercial airlines can be avoided by using smaller chartered or private aircraft, there is still the hassle of rush hour traffic and the long drive to the airport.

The new "Ikelos" aircraft, named after the Greek god of dreams, is designed to avoid all the hassles of airports and to make flying both fun and functional once again. This innovative aircraft allows the user to avoid both ground and air congestion with its ability to land and takeoff from 46 m (150 ft) strips. Ikelos can cut hours from the normal time needed for business or pleasure travel by using elements soon to be available within the SATS infrastructure.

Ikelos is designed to take full advantage of a combination of new technologies. These include its advanced swept box-wing, which is removable to allow Ikelos to be towed on a trailer. Its unique propulsion system consists of quiet dual ducted propellers driven by the lightweight Rand Cam rotary diesel engine. State of the art instrumentation combines with luxury seat design to make the cockpit a pilot's dream. Ikelos' ability to takeoff and land with a mere 46 m (150 ft) ground run gives the craft utility far beyond conventional aircraft while bringing excitement back into the world of general aviation flying.

Ikelos is an innovative two place SSTOL general aviation aircraft with a unique combination of features. A detailed drawing of the general arrangement appears in Figure 2.1-1. An overview of the specifications of Ikelos appears in Table 2.1-1.

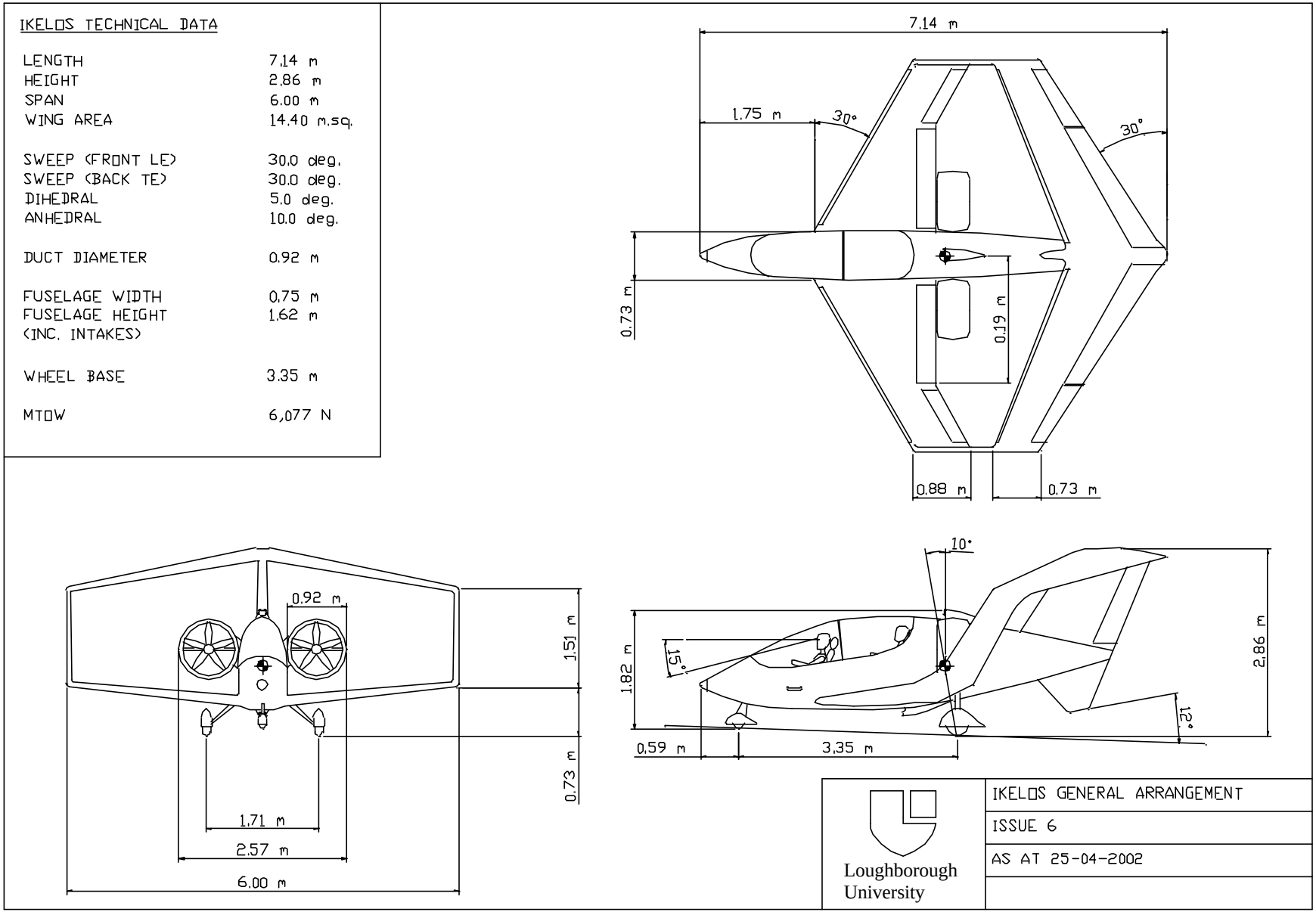

Figure 2.1-1: General arrangement of the Ikelos

Table 2.1-1: Aircraft specifications (sea level standard conditions)

Max Takeoff Weight	6095 N	1370 lbs
Takeoff Run (MTOW)	45 m	148 ft
Takeoff Field Length (MTOW including 50 ft obstacle)	150 m	492 ft
Landing Run (1 pilot only, full fuel)	46 m	150 ft
Landing Run (2 pilots, reserve fuel remaining)	49 m	160 ft
Landing Run (2 pilots, 20% fuel remaining)	50 m	163 ft
Landing Run (emergency at MTOW)	55 m	180 ft
Landing Field Length (MTOW, including 50 ft obstacle)	152 m	500 ft
Max Cruise Speed	140 kts	
Range @ 124 kts	500 nm	
Max Range @ 80 kts	650 nm	
Stall Speed	35 kts	
Max Rate of Climb @ 90 kts	1364 ft/min	
Engine Power	112 kW	150 hp
Fuel Capacity	84 L	22 gal
Empty Weight	3530 N	795 lbs
Payload Weight	1785 N	400 lbs

2.2 Performance

The unique design of Ikelos is complemented by its unprecedented performance. The key to the performance is the short field takeoff and landing capability complemented by a competitive cruise speed. Complete details of performance and all calculations are shown in Appendix B, a summary of the results is presented here.

2.2.1 Takeoff and Landing

Upon takeoff, Ikelos becomes airborne in only 46 m (150 ft) at Maximum Takeoff Weight (MTOW). In addition, with an 8 degree climb out, a 15m (50ft) obstacle can be cleared within the SSTOL requirement of 152 m (500 ft).

In terms of landing performance, Ikelos is equally capable of SSTOL performance. Approaching on a 9 degree glideslope with 3.1 m/s (10.2 ft/s) sink rate over a 15 m (50 ft) obstacle, Ikelos is capable of landing in 152m (500 ft) at all weights. The array of high lift devices on the front wing allows for a low stall speed and hence a relatively slow approach for landing. For added safety and reduced stopping distance, Ikelos is equipped with an automatic Anti-Lock Braking System (ABS). The system automatically engages approximately one second after touchdown to allow the aircraft to stabilize. The result of this is a total landing ground roll of 55 m (180 ft) at full load or 46 m (150 ft) if only one pilot is aboard. Figure 2.2-1 and Figure 2.2-2 show how takeoff and landing performances vary with weight.

With the inclusion of vectored thrust on future variants, the takeoff and landing performance will be further enhanced to enable Ikelos to operate from much smaller fields without significantly affecting the cruise performance.

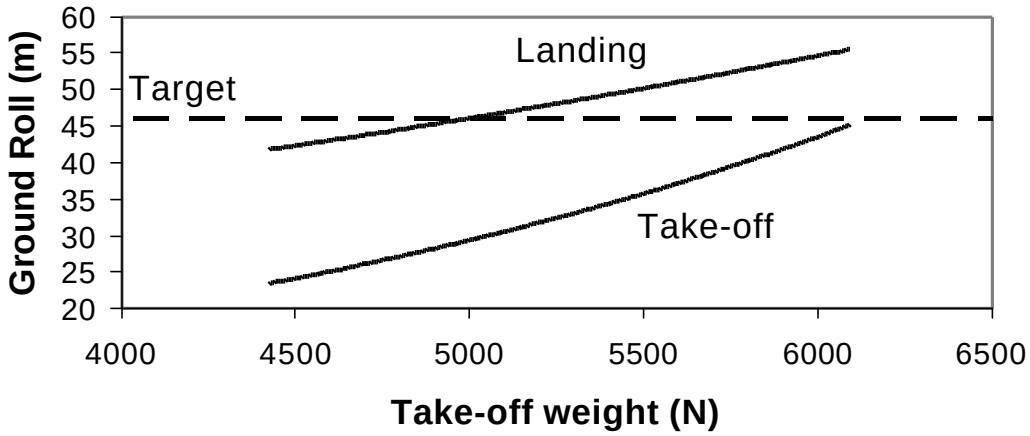

Figure 2.2-1: Takeoff and landing ground roll

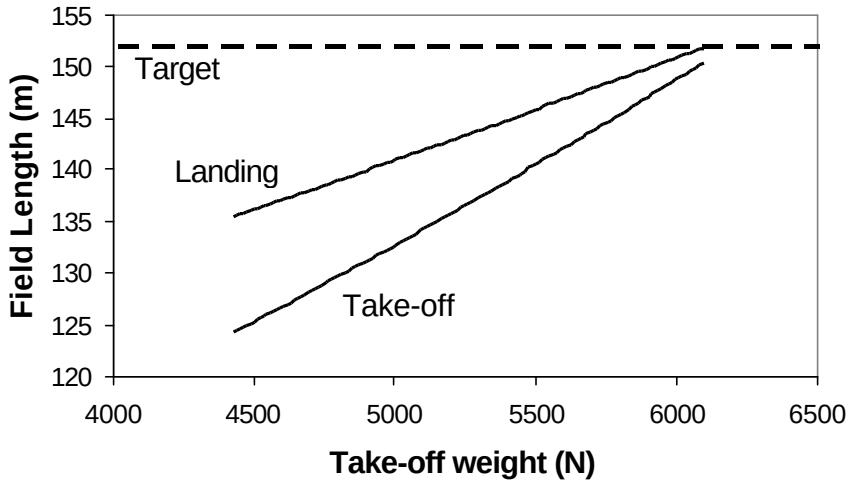

Figure 2.2-2: Takeoff and landing field length (including 15 m (50 ft) obstacle)

2.2.2 Cruise Performance

The cruise performance of Ikelos was intended to be competitive with other typical general aviation aircraft despite their inability to match the takeoff and landing performance of Ikelos. The powerful, lightweight engine provides excellent cruise performance despite the large wing that is so crucial for takeoff and landing. Ikelos features a maximum cruise speed of 140 kts. By cruising at 124 kts, Ikelos can fly 500 nm and at 80 kts, it can achieve its maximum range of 650 nm. Full details of the cruise performance of Ikelos appear in Figure 2.2-3.

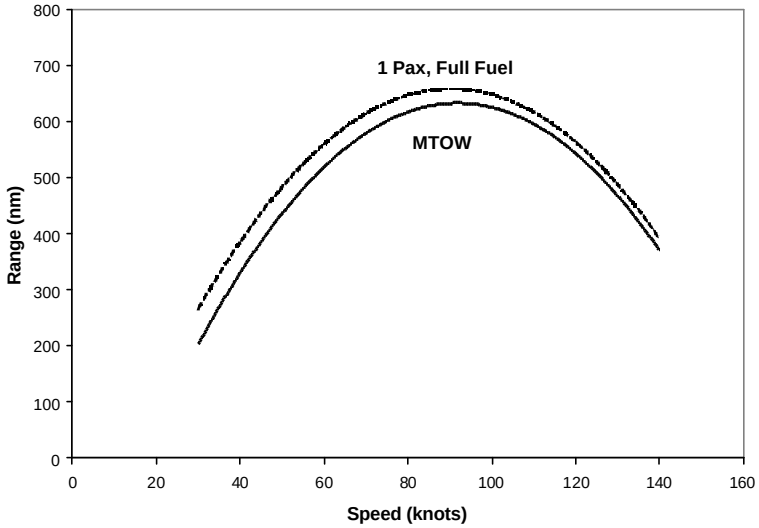

Figure 2.2-3: Range at different cruise speeds and weights

2.2.3 Climb and Turn Performance

In addition to superb takeoff and landing performance and impressive cruise performance, Ikelos is quite nimble. With a sea level max rate of climb of 1364 ft/min, it is capable of climbing to 3050 m (10000 ft) in just 10 minutes in a 90 kts climb at 85% power.

The recreational sport pilot might wish to push the envelope a little and Ikelos can deliver. Ikelos is as agile as it is powerful, with a maximum turn rate of 70 degrees per second at 305 m (1000 ft).

2.2.4 Performance Comparison

As shown in Figures 2.2-4 and 2.2-5, no other aircraft on the market can match both the landing distance and cruise speed that Ikelos offers.

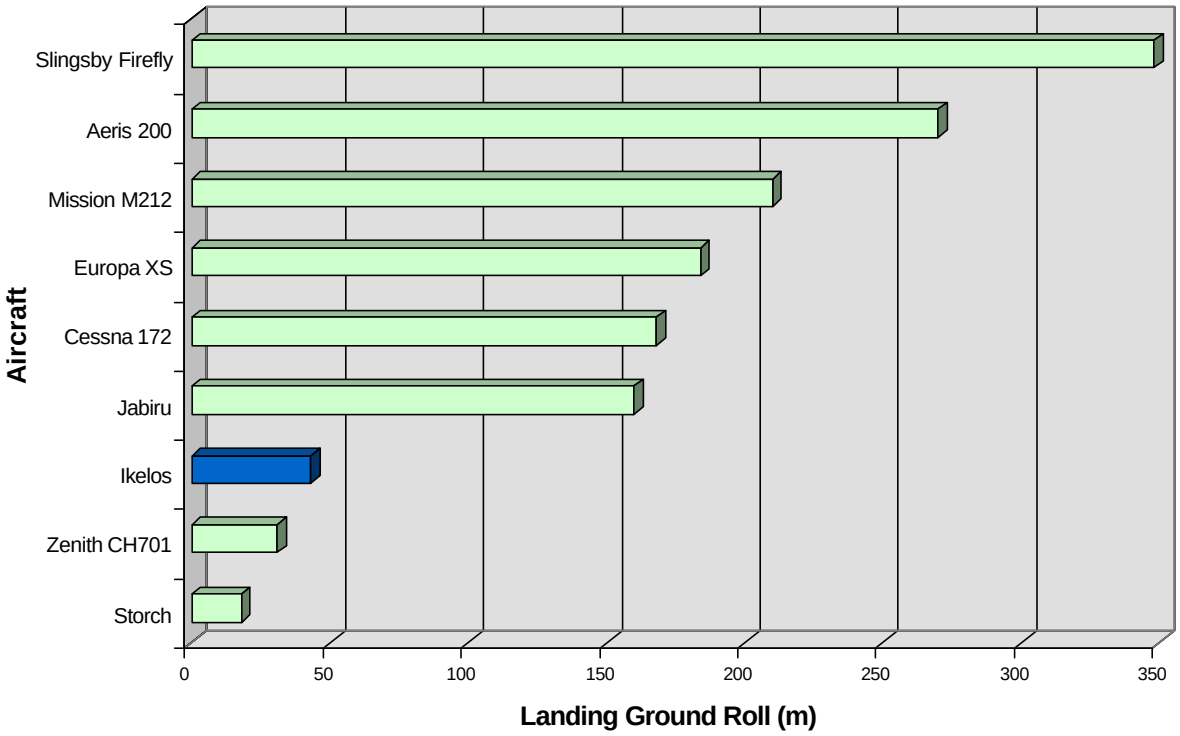

Figure 2.2-4: Landing ground roll comparison [2-9]

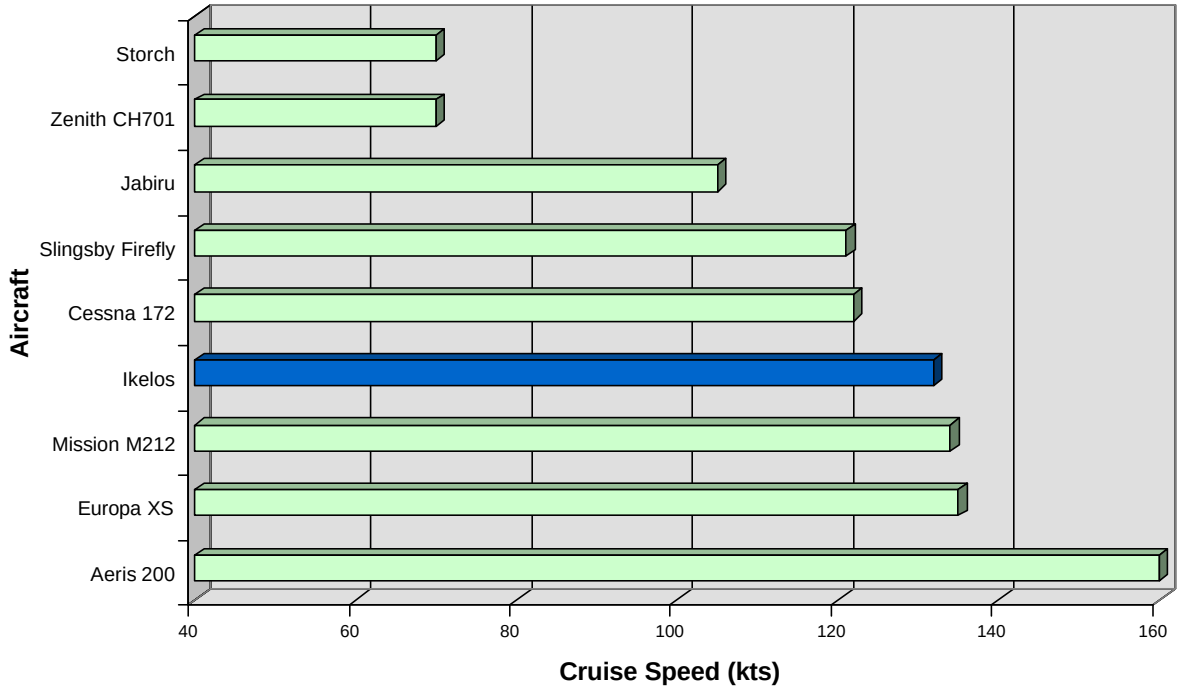

Figure 2.2-5: Cruise speed performance [2-9]

2.3 Propulsion

Complete details of all propulsion related calculations are in Appendix C with the highlights given in the following section.

2.3.1 Rand Cam Engine

Ikelos derives its superior performance from a revolutionary propulsion system, the Rand Cam engine. This innovative engine can produce 112 kW (150 hp) with a bare engine weight of only 245 N (55lbs). The engine is also very compact, with a diameter of 24.4 cm (9.6 in) and a length of 20.3 cm (8 in).[10] The Rand Cam (Figure 2.3-1) is a simple yet powerful rotary diesel engine that eliminates pistons, cylinders, crankshafts, spark plugs, and valve actuation camshafts. Instead, the Rand Cam consists of a rotor disk with 12 translating axial vanes. Cavities are formed between the vanes that trap the working fluid and serve as individual combustion chambers. The rotor is mounted in a cam-shaped housing, which causes the vanes to translate axially as the rotor spins. As a result, the size of the individual chambers change with circumferential location. This oscillation in chamber size forms the basis of a novel internal combustion engine.[11] The cycle of intake, compression, combustion, and expansion all takes place in each individual chamber for each revolution. Since there are 12 chambers on both the front and back faces of the rotor, the Rand Cam essentially has 24 power strokes per revolution.[12] A complete description of the engine's unique design and operation is given in Appendix C.

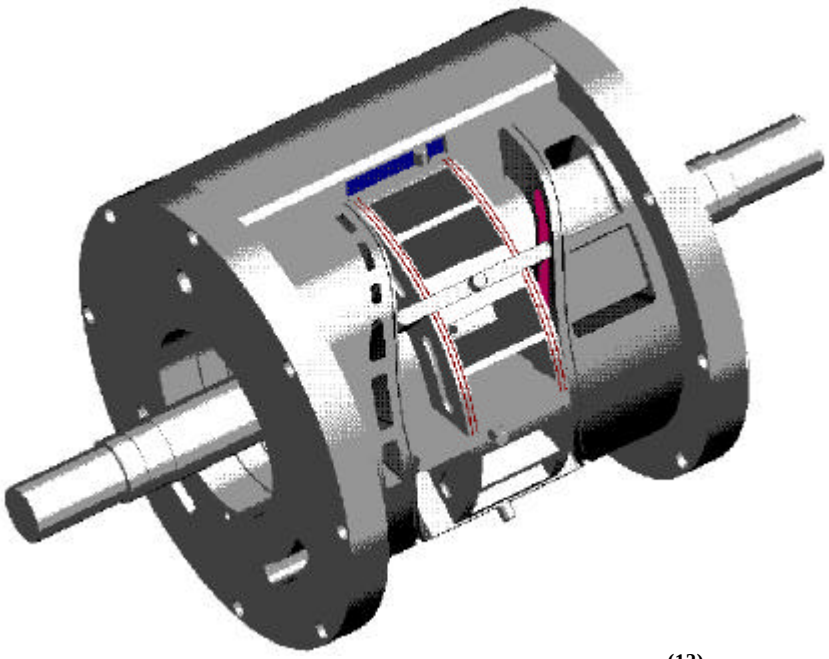

Figure 2.3-1: Rand Cam engine cutaway [12]

Not only does the Rand Cam offer a higher power to weight ratio than piston engines, but there are other advantages due to its inherently simple design. Since the engine is mechanically simple, it is anticipated that manufacturing cost will be cheap enough to allow the engine to be sold for $10000 if more than 2000 units are produced per year. [13] Also, the engine would require minimal maintenance making it very economical in operation.[12] The Rand Cam also features a Brake Specific Fuel Consumption (BSFC) that is lower than most engines of comparable power. At full throttle, the Rand Cam has a very impressive BSFC of 0.18 kg/kW-hr (0.3 lbs/hp-hr).[10]

The Rand Cam can run on either diesel or jet fuels, giving Ikelos added flexibility.[10] The aircraft will always be ready, whether operating from an airport where jet fuel is readily available or from private property where diesel fuel can be obtained from a nearby automobile service station. Of course, it is strongly advised that operators not mix the two fuel types.

2.3.2 Engine Installation

The Rand Cam is mounted inside the fuselage (Figure 2.3-2), bolted to the aft side of a slanted bulkhead that is located between the fans. The bulkhead is slanted in order to deflect the engine away from the cockpit in the event of a crash in which the engine breaks free of its mountings. Also located in the engine compartment are most of the necessary accessories such as the alternator, starter, oil tank, oil pump, oil cooler and cooling fan. Cooling air enters the engine compartment though a scoop inlet on the underside of the fuselage and engine intake air enters through an inlet on top of the fuselage.

The engine is mounted transversely, with the shaft parallel to the lateral axis of the aircraft and extending outward from each side. This allows the engine to drive both the fans directly with minimal gearing. The only gearing required is a set of spiral bevel gears for each fan which also features a gear reduction of 2:1 to drive the fans at 2700 RPM. The fans also rotate in opposite directions which negates any net torque they may produce.

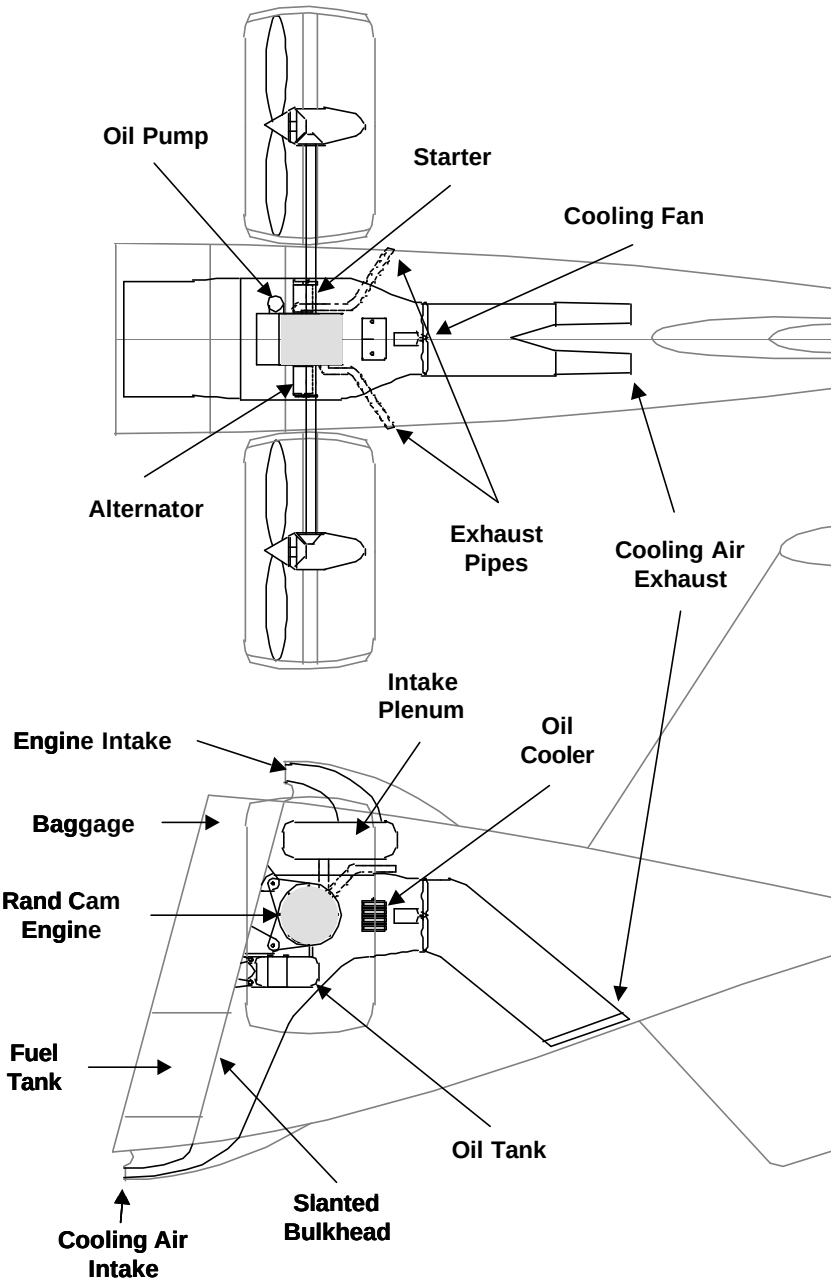

Figure 2.3-2: General layout of the propulsion system

2.3.3 Ducted Fans

The Rand Cam engine is used to drive two ducted fans mounted on the sides of the fuselage. Ducted fans, despite their comparably higher weight, were chosen because they offer several performance advantages over unducted propellers. Ducted fans require a smaller diameter for a given amount of thrust compared to a typical propeller. Also, ducted fans prove to be especially efficient at low speeds. Ducted fans are more attractive when noise is a major consideration because they are inherently quieter than standard propellers.[14]

Each 0.8 m (31.5 in) diameter fan has five blades made of light-weight Kevlar. The fan tip speed at full power is less than 152 m/s (500 ft/s), which generates less than 60 dBA of noise when flying overhead at 305 m (1000 ft).[15] Since this value represents the maximum noise produced by the aircraft, it makes for a very quiet aircraft.

2.4 Aerodynamics

Complete details of all aerodynamics related calculations are in Appendix D with the highlights given in the following section.

The box-wing design was chosen because of its capability for high lift for short-field capabilities, and due to its extremely low induced drag. The box-wing is an extension of the joined wing concept developed by Wolkovitch.[16] Studies by Kroo and McMasters[17] have shown the box-wing to be superior to the joined wing and conventional wings. The wingspan efficiency factor, which is less than the ideal value of unity for monoplane configurations, can be increased to a value of 1.46 for box-wing configurations.[17]

To analyze this complex, non-planar configuration, a *Matlab* code called *Tornado* was used. *Tornado* is a vortex lattice method written by Tomas Melin of the Royal Institute of Technology KTH, Sweden.[18] *Tornado* takes the input wing geometry and flight states and calculates the basic aerodynamic coefficients, stability derivatives, and other useful results for non-planar 3-D wing designs. Although *Tornado* is not used in industry, it provided a quick and powerful means of 3-D aerodynamic analysis.

To determine an optimum box-wing configuration, comparisons of lift coefficient curve slopes (C_{Lalpha}), induced drag, and wing loadings were examined for numerous wing geometries including variations in sweep, dihedral, and vertical and horizontal spacing of the wings. *Tornado* was used to define an optimum 3-D wing design in terms of planform, sweep, camber, etc.

The GAW-2 or NASA LS-1 airfoil was selected as the wing section for both wings because of its high C_{Lmax}.[19] Lift coefficient and moment coefficient predicted by *Tornado* are plotted versus angle of attack in Figure 2.4-1. Note that these coefficients may be higher than typical values since they were calculated using the front wing planform area, not the total wing planform area as the reference area. From a 2-D stall angle prediction for the chosen GAW-2 airfoil, Ikelos should have a flapped C_{Lmax} of 4.19. Both leading and trailing edge devices are employed to obtain superior short field landing performance. The trailing edge of the front (main) wing consists of two sets of double-slotted Fowler flaps (Fig 2.4-2), occupying the entire span. For mechanical simplicity, a system was used that is similar to that used on the T-45 Goshawk, in which the main element has a fixed slot. A spring-loaded leading edge slat, which automatically deploys at high angles of attack, increases the maximum lift angle of attack. The effect of these flaps can also be seen in Figure 2.4-1.

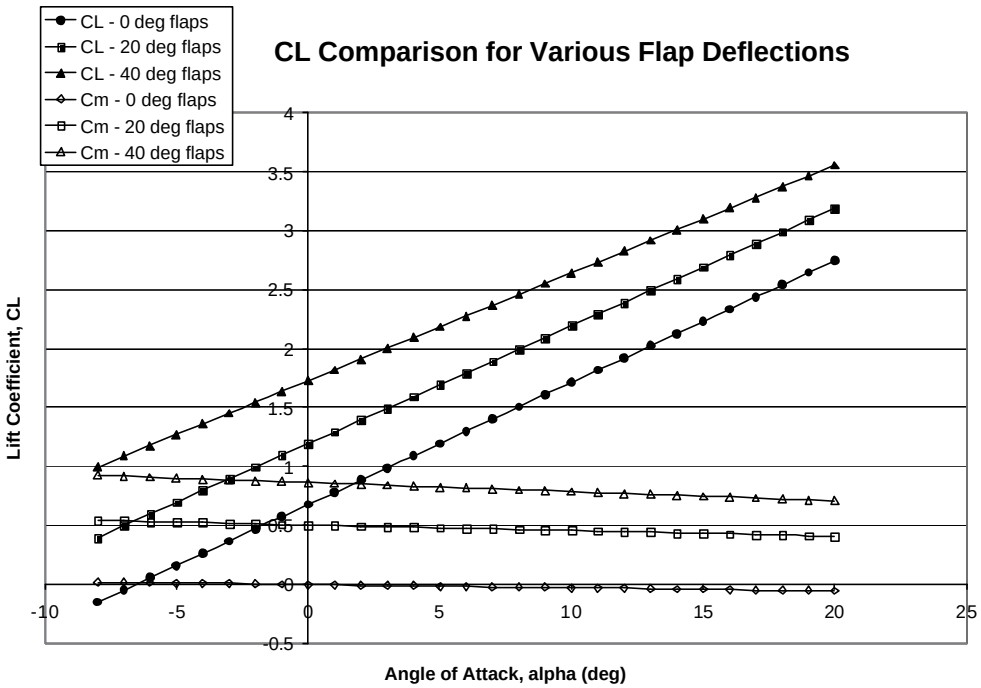

Figure 2.4-1: Plot of C_L versus angle of attack for various flap deflections

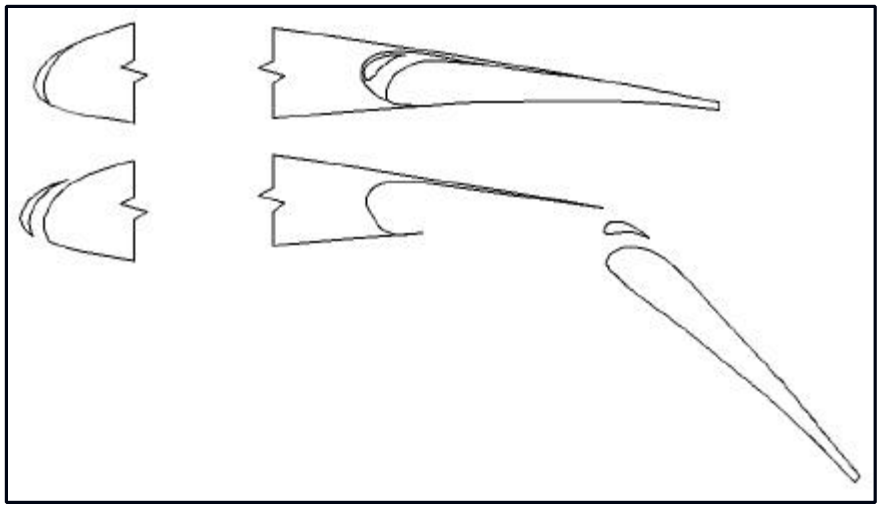

Figure 2.4-2: Front wing flap configuration

The concept of the Circulation Control Wing was studied in some detail as an alternative method of achieving high lift performance. More details of the work surrounding this concept are discussed in Appendix D. Much research has been done on circulation control by Robert Englar[20]. These systems have been shown to give significant increases in lift coefficient while eliminating the need for heavy mechanical flap systems. The possibility of incorporating such a system into Ikelos was examined and found to be unnecessary for this design. While an increase in high lift performance could have been achieved, this increase was not great enough to warrant the increase in aircraft noise and loss of engine performance when using circulation control.

Figure 2.4-3 shows an example of the pressure distribution across the wing geometry, as calculated using *Tornado*. This pictorial output proved useful in the setup and design of the wing configuration, as it allowed a visualization of how the lift was distributed between the two wings at a specified flight state. In the configuration shown in Figure 2.4-3, it can be seen that the front wing provides the primary source of lift, as indicated by the darker shading of the vortex panels.

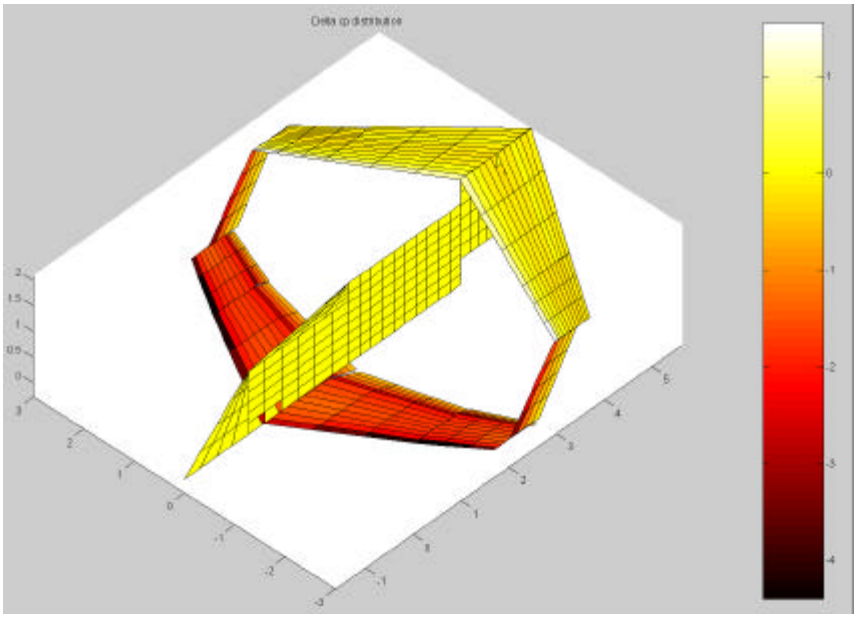

Figure 2.4-3: Pressure distribution as calculated by *Tornado*

Estimation of drag coefficients for the wing and fuselage were based on methods described by Hoerner.[21] This involved using the wetted area of individual components and empirical formulas to arrive at an estimation of drag coefficient for the whole aircraft. Using these methods along with the inviscid vortex lattice method results, C_{D0} was predicted to be 0.045 in a cruise condition.

2.5 Stability and Control

Complete details of all stability and control related calculations are in Appendix E with the highlights given in the following section.

For general aviation aircraft, having smooth, responsive handling qualities is a must. Ikelos meets these requirements even though its flight envelope includes very low speeds. The design has inherent longitudinal stability. This can be seen by the pitching moment curve in Fig. 2.4-1. Due to the significant amount of mass located high on the aircraft, care was taken to ensure that this design demonstrated lateral-directional stability, particularly in roll. Ikelos still retains maneuverability by preventing over-stability in cruise configurations.

Ikelos has a conventional vertical fin and plain flap rudder, along with powerful plain flap elevators and ailerons on the rear wing. Trim drag was minimized by designing for natural trim in cruise. Details on the analysis and sizing of these devices can be found in Appendix E. The control surface sizes are shown in Table 2.5-1.

Table 2.5-1: Control surfaces

Control Surfaces				
	Area (m^2)	% Chord	Span (m)	Sizing Condition
Ailerons	0.586	30	0.9	Comparable Aircraft
Elevators	1.496	30	1.9	Takeoff Rotation
Rudder	0.41	24	1.29	Maximum Crosswind Landing

Dynamic stability was also investigated to ensure that Ikelos exhibits acceptable flight qualities. Specifications from MIL-F-SPEC 8785C were used to gauge dynamic stability. Analysis was performed for a variety of control surface deflections in cruise and landing configurations.

A standard cable system provides actuation of the control surfaces. This method is both simple and cost-effective and gives the pilot the appropriate control "feel" that fly-by-wire systems can only mimic. The result is a well-mannered aircraft that provides a smooth, safe ride but is still agile enough to be exciting to fly. A complete analysis of pilot stick forces (Appendix E) showed that the aircraft can be easily flown at all attitudes.

Due to the structural benefits of box-wing designs, wing weight can be reduced for a given load bearing requirement. Coupled with a lightweight propulsion system, Ikelos has a maximum takeoff weight of 6095 N (1370 lbs). This is over 40% less than a Cessna 172.[6] A complete weight breakdown can be found in Appendix F.

Of major importance is the distribution of weight in the aircraft, which determines the center of gravity (CG) and the level of static stability. Expendable weight was placed as close as possible to the CG to prevent excessive changes in stability during flight. Ikelos, at maximum takeoff weight, has 5% static stability at takeoff and increases to 13% static stability at landing. A CG excursion plot for Ikelos is shown in Figure 2.5-1.

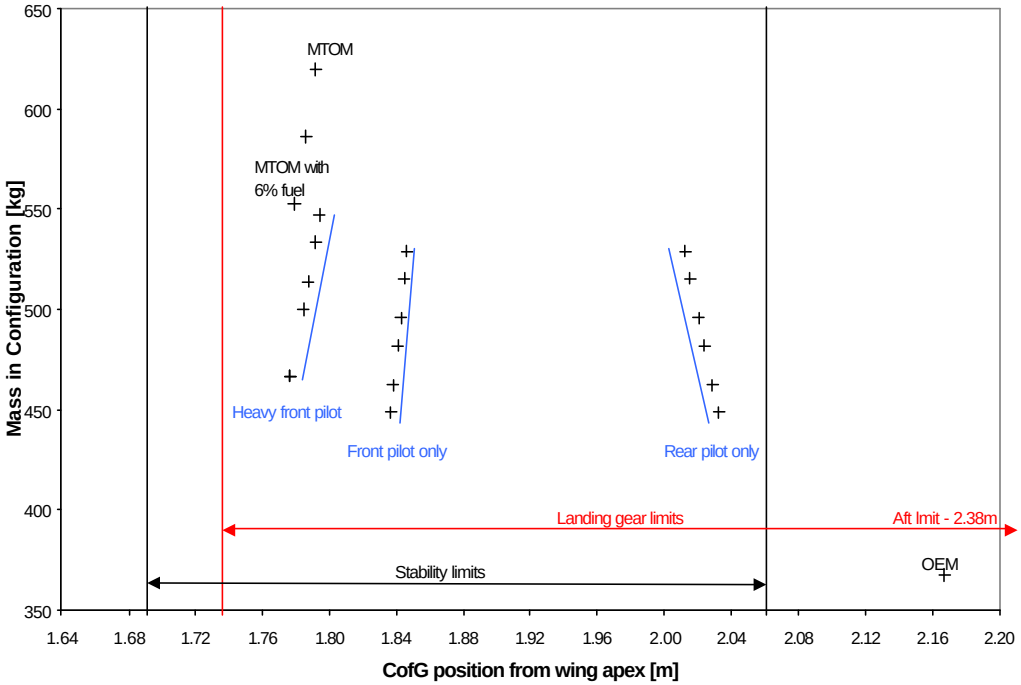

Figure 2.5-1: Ikelos CG Excursion plot

2.6 Structures

A detailed structural analysis is presented in Appendix G. Highlights and results of that work are given in the following sections.

2.6.1 Structural Design Aspects

The primary design driver from a structural viewpoint is the need to keep the aircraft as light and simple as possible. Because of the truss-like structure of the box-wing, many of the moments created during flight are transferred throughout the wing structure, which decreases the structural reinforcement needed.[16] Weight consideration is also the reason that the aircraft is constructed primarily from composites. The choice of which composites to use was also highly linked to material and manufacturing costs. In order to achieve both a lightweight and cost-effective structure, the fuselage and wing skins are made from Glass epoxy with a Nomex honeycomb core for added stiffness, while the spars, ribs and longerons are made from Carbon epoxy. For impact resistance, Kevlar reinforcements have been included on the inboard front wing skins to allow the crew to step onto the wing when entering Ikelos.

To meet the transportation requirements both the wings and one of the ducts needs to be removed. Therefore, a wing attachment method similar to that found on gliders has been used in the design.

2.6.2 Structural Overview

The main structural skeleton includes four longerons, positioned in a box shape, which run the entire length of the fuselage. Seven bulkheads connect the longerons together vertically and are positioned at high load areas along the fuselage. All critical components are connected to the bulkheads to allow the loads to be easily distributed though the fuselage. The main bulkhead, made from aluminum, is located behind the rear seat not only acts as a connection point for the engine and firewall but also is designed to deflect the engine downwards, away from the cockpit in the event of a crash. The fuselage structural layout is shown in Figure 2.6-1.

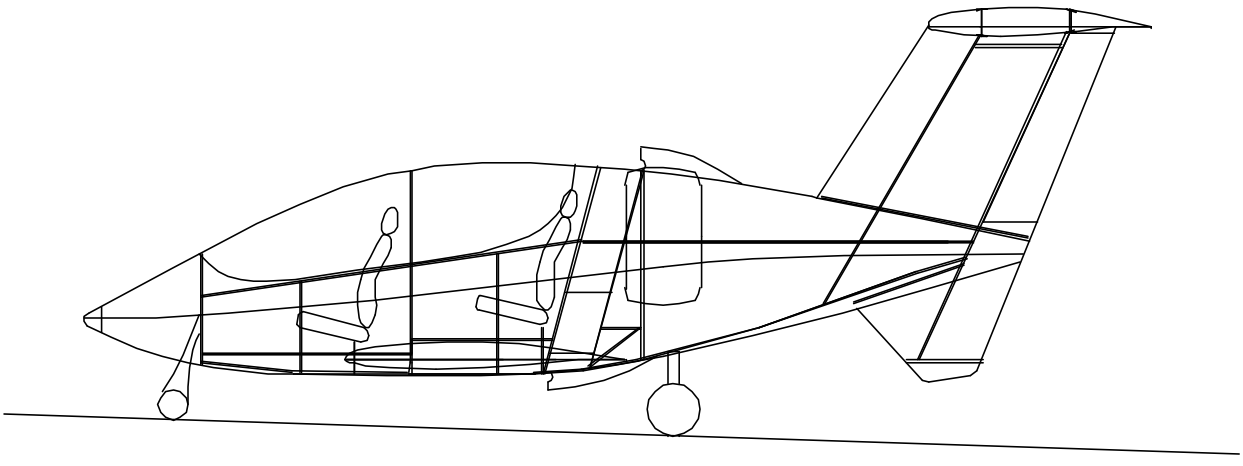

Figure 2.6-1: Fuselage Structural layout

Both front and rear wings contain two main I-section spars which run the entire length of the wing with one additional C-section spar running along the rear inboard section of the front wing mainly for the flap connections. Three C-section ribs are positioned at critical points along each wing - at the root, tip, and at mid span of the rear wings and at the bend in the front wings. The skin's honeycomb core will provide sufficient stiffness against buckling, eliminating the need for stringers. The vertical surfaces joining the wing tips together connect to the outer wing ribs and consist only of a hollow aluminum tube and two end ribs for shaping purposes. The wing layout is shown below in Figure 2.6-2.

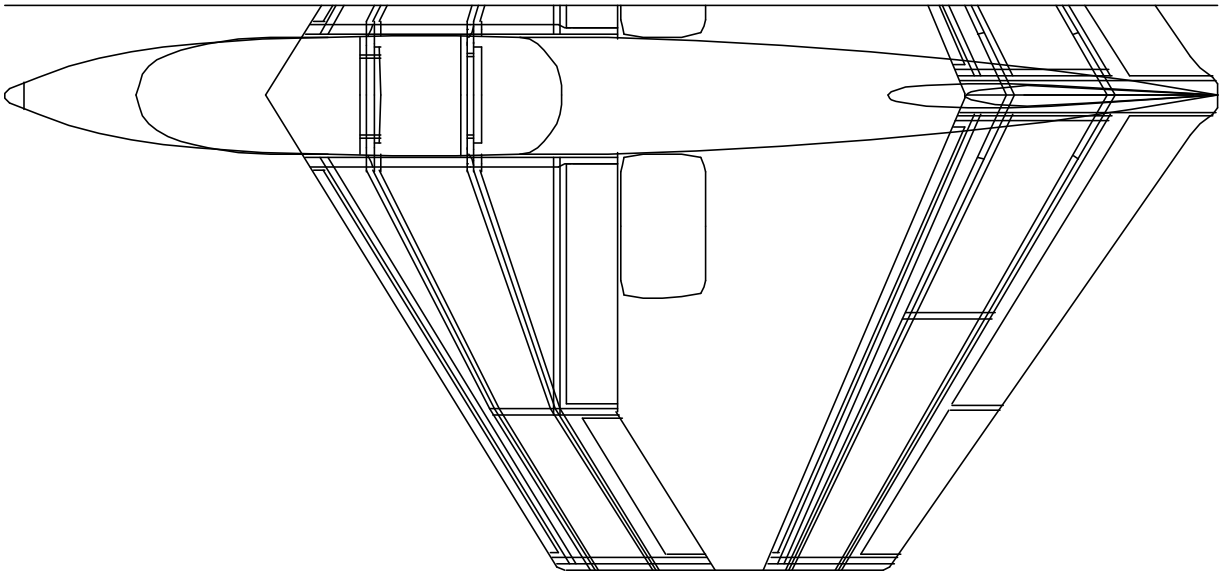

Figure 2.6-2: Wing structural layout

2.6.3 Landing Gear

The tricycle configuration landing gear, chosen for ease of landing and steering, has been designed not only for robustness, but also for low cost and simplicity. The main landing gear (Figure 2.6-3) is made from steel tubes that connect onto the fuselage with rubber dampers to help absorb the shock of landing. The nose gear is a hollow tube connected to a liquid spring shock absorber to absorb the shocks in takeoff and while taxiing on the ground.

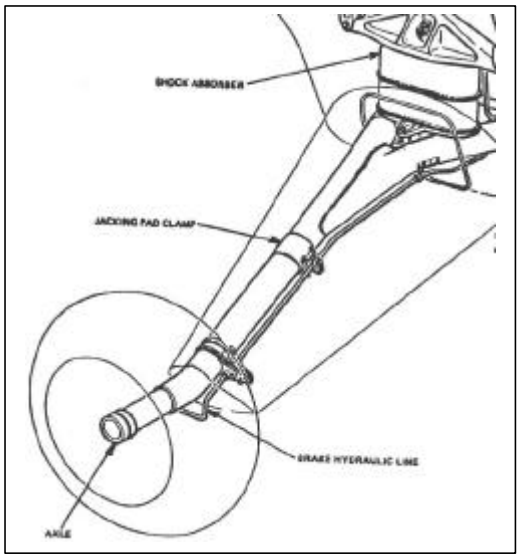

Figure 2.6-3: Main landing gear [22]

2.7 Avionics and Systems

2.7.1 Avionics

To be competitive in today's general aviation market, it is essential to minimize the physical and mental stress on the pilot during flight. Ikelos' combination of innovative technology and relative simplicity provide for the most enjoyable and relaxing flight experience possible, while taking advantage of all the information to be available in the SATS infrastructure.

The primary function of the avionics in any aircraft is to provide the pilot with the information necessary to fly the aircraft from one location to another in a safe and efficient manner. The baseline version of Ikelos includes all the avionics required by the FARs along with several additional instruments that allow for IFR (Instrument Flight Rules) flight. The basic instruments required by the FARs include an airspeed indicator, altimeter, magnetic compass, and necessary engine instruments. Also included in basic version of Ikelos would be a transponder, artificial horizon, VHF nav/com radio, and Electronic Flight Information System (EFIS).

While the standard instruments are included to meet the current FARs, the SATS environment calls for a much more integrated, digital avionics system in order to utilize the latest technology and to make as much real time information available to the pilot as possible. Ikelos' pilot receives most of his/her flight information through the fully integrated EFIS system. Current EFIS systems, such as the Op Technologies Flight Op 200,[23] feature a Liquid Crystal Display (LCD) screen with all the basic flight and engine instruments, while also acting as a single cue flight/navigation director. The Flight Op 200 is driven by a powerful computing unit which contains map/chart information and is integrated with an internal GPS receiver. This combination allows for a continuously moving map display with current position readout. The onboard database contains all public, military and private airfield information. This is perfect for the SATS program, in that it will present the pilot with the option of the currently underutilized, smaller, uncontrolled airports. What is even better is that the decision to land at a certain strip

can be made while in-flight. The destination is simply changed on the display, and the computer does the work for the pilot. The new navigation information is ready within seconds.

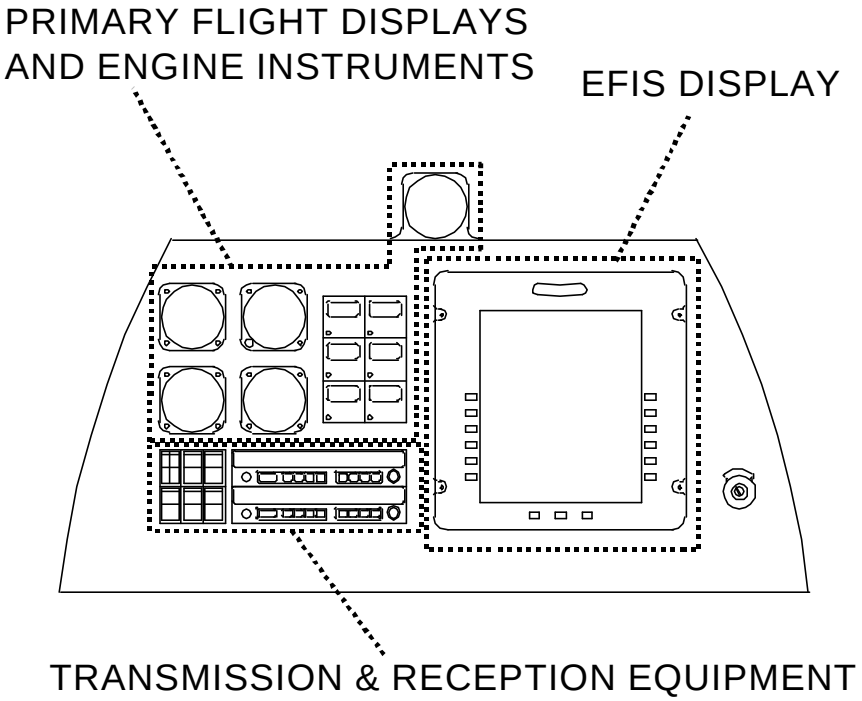

Figure 2.7-1: Cockpit instrument panel

The instruments are organized on the primary control panel in a standard arrangement (Figure 2.7-1). The standard flight and engine instruments, as well as the radios are located to the left, while a large LCD screen occupies the entire right half of the panel. The LCD screen displays information from the EFIS Computer, which effectively provides the pilot with easy to read, real-time flight information.

The passenger/co-pilot is also provided with a repeater EFIS display in the rear seat. This provides the same flight parameters as seen by the pilot without the need for a secondary EFIS unit. All the needed information is consolidated on a single display, and can be easily read with a quick glance to the EFIS screen.

In the future, it is anticipated that fully electronic avionics systems will not only be available, but will be the norm. In the future, regulation changes may allow the standard instruments to be replaced by a second LCD screen, displaying pertinent weather, engine, and flight path information, or to corroborate data shown on the right-hand screen. Future developments focusing on wireless networking technology could be incorporated into the Ikelos avionics system. The use of ground-based data streams to provide a steady pipeline of weather and air traffic information could give a dramatic reduction in radio communication required, thus freeing the pilot to enjoy flying the aircraft. This would allow full use of the SATS “Highway in the Sky” flight system in which the pilot would simply select the lane to occupy instead of tracking a heading. Touch screen technology and HUDs could all also be employed to improve the ergonomic environment for the pilots by removing the need for analog dials and buttons.

Ikelos is well adapted to conform to the future general aviation environment envisioned by the SATS program.

2.7.2 Systems

The aircraft has been equipped with a full authority anti-lock braking system (ABS). This has been done to improve performance and increase safety. Based on BMW motorbike brakes developed in conjunction with Brembo, world renowned brake specialists, these brakes produce maximum available braking force without the risk of skidding and loss of control.[24]

Another system available to increase safety is the optional ballistic parachute recovery system. Produced by Ballistic Recovery Systems Inc., the small size of the system allows it to be added to the upper section of the baggage compartment. The parachute canister weighs approximately 172 N (39 lbs) and is 53 cm (21 in) long with a diameter of 23 cm (9 in). When activated a small explosive charge propels the parachute out, immediately beginning to slow the aircraft and produce a survivable touchdown on the ground with reduced damage to the aircraft.[25]

Also included for safety are a five point seat harness, fire extinguisher and an axe. In the event of the aircraft ending up upside down on the ground the roll bar would provide the structural rigidity required but it would be very difficult to exit the aircraft without an axe.

A conventional mechanical control system of rods and pulleys has been adopted over a fly by wire (FBW) system because if a FBW system were used the redundancy required would be substantial, especially if a mechanical backup was not used. A mechanical system is easily maintainable, and offers vastly reduced costs.

The electrical system is of conventional layout, using a 24 Volt battery and a 28 Volt 120 Amp alternator. The large electrical power requirements are due to the engine accessories all being electrically driven.

Cabin conditioning is provided by the facility to control the mixture of external air and air taken from the oil cooler entering the cabin. Positional vents allow the air to be used for de-misting.

2.8 Ergonomics/Human Factors

Complete details of all ergonomics related calculations are in Appendix I with the highlights given in the following section.

The Ikelos two-person cockpit is ergonomically designed with main emphasis placed on pilot and passenger safety, comfort, and user-friendliness. The interior of the cockpit is sized to accommodate a wide range of people, from a 95^{th} percentile male to a 5^{th} percentile female.[26] Fully adjustable seats and rudder pedals are included for maximum flexibility. The tandem-style cockpit is approximately 2.35 m (7.7 ft) in length, 0.66 m (26 in) in width, and 1.18 m (3.87 ft) high. Located behind the cockpit is a 0.135 m^3 (4.75 ft^3) baggage compartment capable of accommodating 267 N (60 lbs) of baggage.

As far as primary controls, a center stick control was chosen for aileron and elevator control, while traditional pedals control the rudder and brakes. The pilot has maximum control because he has the option of single-hand control.

In order to protect the pilots from highly loaded landing conditions, ergonomically designed seats are made with Confor™ Foam, a high energy absorbing material used in military pilot ejection seats as well as in spacecraft. [27] A five-point harness style seatbelt was chosen for the restraint system, again to protect the occupants against any potential impact situations. The

entrance/exit to the cockpit is a right-side hinged canopy. The clear acrylic canopy is equipped with gas struts, and is split into two separate sections to allow for a roll bar to be placed between the two seats.

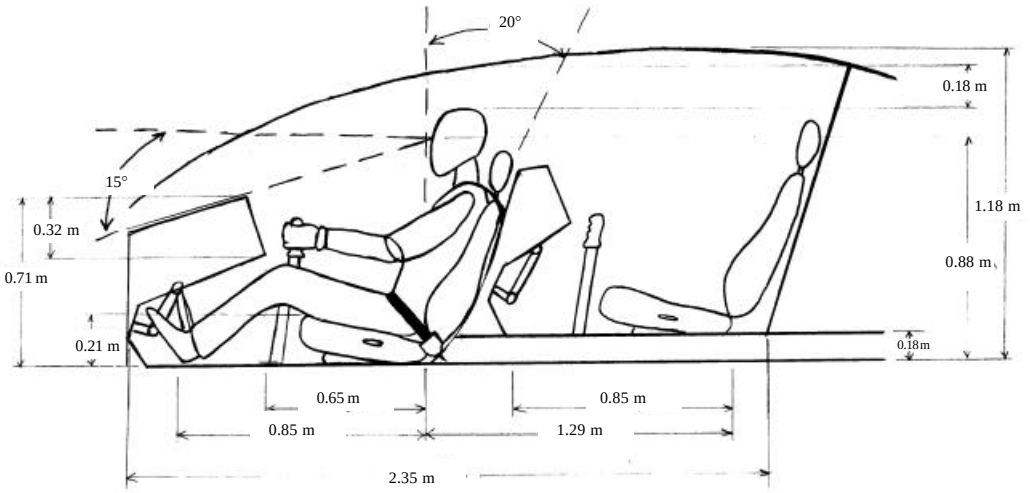

Figure 2.8-1: Cockpit layout and dimensions

2.9 Manufacturing

Detailed descriptions of the manufacturing estimates are shown in Appendix J. Manufacturing has been planned using the most contemporary methods available to create an environment where the highest quality product while giving the consumer highest priority. Ikelos will be manufactured using team-structured methods. The plane will remain stationary during assembly. Teams with individuals specializing in each aspect of the manufacturing process will start and finish each individual aircraft. The emphasis on teamwork produces a level of pride resulting in a higher quality product.[28]

2.10 Cost

Complete details of all cost related calculations are in Appendix K with the highlights given in the following section.

One of the goals of SATS is to make buying an aircraft more affordable. Ikelos has been designed to simplify manufacturing procedures and reduce production costs. However, the final price of an aircraft is still a strong function of classic laws of production that state for every 10 fold increase in production, the cost will be cut in half (Table 2.10-1).[29]

Table 2.10-1: Cost Analysis

Production Number	Cost Per Plane	Total Selling Cost
50,000	$68,000	$78,000
5,000	$136,000	$156,000
500	$272,000	$312,000

2.11 Practical Applications

Ikelos has been designed to fulfill many of the goals of the Small Aircraft Transportation System. However, the unique short-field and slow flight capabilities of Ikelos take the SATS vision one step further. With Ikelos, no airport is necessary, only a small field or parking lot. Thus it creates access to more communities in less time and expands the opportunities for people in those communities. As described by the SATS homepage, the Arlington, Charlottesville, Danville, Norfolk round trip would easily be completed in one day, as would any combination where a small airport or field is present.[30]

Such a convenience would be a great fit in transporting vital supplies between rural areas. Not only would a person in Farmville, VA have access to the Johns Hopkins Medical Center in Baltimore, MD, but also any person in a 300 nm radius from Baltimore would have access. Crucial business deliveries could be made in the same day without the cargo ever having to go an airport. Thus, Ikelos has potential to become an important business tool.[30]

The superior short field performance of Ikelos makes it a perfect match for many military applications. The SSTOL capabilities would certainly fit military search and rescue operations. This ability, coupled with Ikelos' slow flight capabilities could also be useful in military reconnaissance. In the reconnaissance role, the cockpit could be replaced with more extensive avionics to make Ikelos into an Unmanned Aerial Vehicle (UAV). Many applications where helicopters are currently used could also be potential markets. Such applications include weather/traffic reporting and rapid response law enforcement. In these cases, a nearby aircraft capable of getting airborne quickly is everything. Ikelos would offer dramatic reductions in maintenance and operations cost over helicopters or gyroplanes.

The area where Ikelos might be most appealing, however, is in sport aviation. Pilots who fly for fun or sightseeing typically do not need excessive range or payload capabilities, but value convenience, safety, and good flight qualities. Ikelos is an excellent fit for the sport pilot. It's an eye-catching aircraft that brings a new level of fun and convenience to the sport aviation enthusiast.

3. SATS ISSUES

The aviation industry is critical to economic health and welfare. However, increases in both passenger and freight travel, the aviation industry may soon face a serious problem! One recent report from the FAA projects a 63% increase in air passengers over the next 12 years, going from 733 million in 2000 to 1.2 billion in 2012.[31] SATS seeks to eliminate many of the problems with current air and land travel. The purpose of SATS is to use small aircraft to provide a safe and inexpensive alternative to highway travel and the "hub-and-spoke" air transportation system while increasing travel accessibility and decreasing time and cost. This goal seems quite feasible considering that the FAA estimates that 98% of the U.S. population lives within 20 miles of at least one public-use airport.[32]

Ikelos is designed to meet many of the SATS goals and to help eliminate some of the problems inherent in airline and highway travel. A strong point of Ikelos is its ability to achieve SSTOL as defined by NASA.[1] Ikelos meets these takeoff criteria with a 46 m (150 ft) ground run in all of its configurations, and in several configurations it can land with a 46m (150 ft)

ground-roll. This shows Ikelos can not only takeoff and land on almost all small airstrips, but can easily land in fields and even large backyards. With a range of about 500 nm at a cruise speed of about 124 kts, Ikelos can easily be used for the business or weekend traveler. Furthermore, Ikelos is easily transportable on a trailer, increasing storage options.

Safety issues were a major concern in the design of Ikelos. It is designed for the comfort of the pilot and passenger. The cockpit is sized for the majority of the adult population. The seats are built to be ergonomically correct, with extra cushioning to absorb the impact of a hard landing. Thus, the pilot and passenger should experience less spine and neck fatigue and fewer injuries. Both seats also are fitted with a 5-point harness to evenly distribute impact loads on the body.

Ikelos was designed for increased vertical loading in landing and for crash survivability. An extra flooring structure was added below the cockpit to attach the cockpit and absorb some of the energy of a crash landing. Also, the engine is exceptionally light, 245 N (55lbs), so that its placement behind the cockpit does not pose as much of a threat to the passengers in the event of a crash landing. Even so, the engine bulkhead is slanted to ensure that the momentum of the engine would be transferred away from the cockpit in a crash. A roll bar provides pilot and passenger protection in a crash situation that would cause the plane to flip upside down.

Another main goal of the SATS program is to make travel as affordable as possible. Cost was a large factor in the design of Ikelos. Right now, the price of Ikelos is predicted to be comparable to that of a conventional GA aircraft. The Rand Cam engine is predicted to cost less than comparable piston engines. To keep the cost low, the controls were kept fairly standard, using cables to adjust the control surfaces. The avionics on Ikelos were designed for low cost and to meet SATS goals to be compatible with an integrated information system between the pilot and the SATS infrastructure on the ground.

Finally, Ikelos not only addresses the needs and concerns of its own passengers, but also of the people around it. The Rand Cam engine produces very little noise and does not even require a muffler. The ducted fans allow for a lower tip speed, and decrease the noise to an estimated 60 dBA when flying overhead at 305 m (1000 ft) (Appendix C). The engine is also highly fuel efficient and low polluting.

Ikelos meets many of the goals of the SATS program, while also maintaining a price that is comparable to existing general aviation aircraft. Because the cost constraint was emphasized in the design, it became a limiting factor on the extent to which each goal could be met. However, Ikelos has tremendous room for adaptation and variability. With the loosening of the cost constraint, many systems could be modified to meet the demands of the higher end general aviation market or possibly even the military. For example, with a higher allowable cost, the ducted props could be rotated to vector the thrust and, when combined with an automated control system, this could allow the possibility of vertical takeoff and landing.

4. DESCRIPTION OF STUDENT WORK

Both halves of the team each began by proposing design concepts that were capable of the defined performance. These included gyroplanes, helicopters, and more conventional jet and prop designs. The groups at each university then narrowed their concepts to the three that best met the goals of the design criteria using a similar approach of rating each design. In November 2001, the team met in Loughborough, UK and evaluated these six design concepts to begin the

selection process. First, three designs were chosen for further consideration. These designs included a conventional jet, a pusher prop and a box-wing design.

A rating system was designed and implemented to evaluate these top three design concepts, comparing the designs over a range of criteria and selecting the highest rated concept. Nine broad categories of criteria were chosen to rate the designs. These consisted of performance, weight, cost, ease of operation, serviceability, manufacturability, durability, safety, and miscellaneous categories. Each of the nine categories, as well as their numerous criteria, was then weighted according to its importance. For example, the miscellaneous category was divided into noise/pollution, comfort, aesthetics, originality and adaptability (Table 4-1). The full table of criteria appears in Appendix L. As a result of the selection process, the box-wing was chosen as the base concept for the design.

Table 4-1: Sample evaluation criteria

Category	Criteria	Weight	Conventional Jet	Pusher Prop	Box Wing
Misc.	Noise/pollution	5	1	4	3
	Comfort	2	2	3	5
	Aesthetics	4	4	1	5
	Originality	4	4	2	5
	Adaptability	2	3	3	4

Once the final concept was chosen, the team was divided into sub-teams which worked on the various aspects of the design process. These sub-teams were as follows: aerodynamics, stability and control, aircraft performance, avionics and systems, structures, propulsion, weights, ergonomics, cost, and manufacturing. Each sub-team created a list of all the things that they felt were important and needed to be accomplished during the design process. The takeoff and landing performance was decided as the first area of focus because it was deemed to be the most difficult element to achieve and would most likely define other aspects of the aircraft.

The performance sub-team, with the help of others, set out to determine what was needed for the aircraft to meet the takeoff and landing requirements of the design. The calculations showed that the takeoff could be met with the existing characteristics of the aircraft, however, the landing criteria proved harder to meet. Not only was the landing distance a difficult criterion to meet, high g-forces were encountered during landing.

Different landing methods were analyzed to fulfill the landing criteria while also considering flight performance. The configurations considered included conventional Super Short Takeoff and Landing (SSTOL), the use of vertical thrust on approach and ground roll, vertical thrust on approach only, and reverse thrust on the ground roll. In all cases the basic assumptions included a speed of $1.15V_{stall}$ at touchdown, zero thrust landing, horizontal deceleration beginning immediately at touchdown, and vertical deceleration distance taken as the stroke length with no damping. Even with these assumptions, it was determined the landing requirements could not be easily met with a conventional landing configuration. Pilot comfort also had to be addressed with such strict landing constraints.

Vectored thrust offered the benefit of improved takeoff and landing performance. However, by vectoring the thrust, the aircraft could be made to takeoff and land vertically. Based on these findings, the team deliberated between SSTOL and VTOL. The team considered the advantages and disadvantages of each method and found that vertical flight involved highly

complex control systems, added weight, cost, and an increase in pilot training. A decision was made to remain with a conventional approach and landing without vectored thrust. Nevertheless, the aircraft's box-wing configuration still allows the possibility of employing vectored thrust on future versions.

In making this decision, the team had to reevaluate the initial design requirements. Due to the inability to meet the required distances, it was necessary to relax the takeoff and landing constraints. Since NASA considers a Super Short Takeoff and Landing (SSTOL) to clear a 15 m (50 ft) obstacle and land in 152 m (500 ft)[1], it was decided the takeoff and landing requirements would be relaxed by dropping the 5 m (16 ft) obstacle and restricting the ground run to 46 m (150 ft).

To be effective in the SATS environment, the cost of this design needed to be comparable to that of current general aviation aircraft. The cost and manufacturing sub-teams addressed many design features in order to keep the cost on the order of the current price of a new Cessna Skyhawk (C-172), around $180,000.[33] Some considerations included the engine, control systems, landing gear, wing structure, and noise reduction. Because cost is proportional to complexity, the design was kept as simple as possible.

The main concern for the avionics sub-team was the integration of all systems into the cockpit environment. These systems included communication equipment, navigation equipment, propulsion, and control systems. To reduce operational stress, systems like Global Positioning System (GPS), autopilot, Heads-Up Displays (HUDs), weather radar, and ground data link-traffic management were also considered. The team also looked into making the systems adaptable for upgrades and modifications. Safety and cabin conditioning systems were also taken into consideration to ensure pilot comfort and safety during flight.

With a short takeoff and landing aircraft, structural issues became very important. The structures sub-team considered the landing and takeoff loads, which were higher than for traditional aircraft. The structure was designed to withstand these extra loads with special attention paid to the landing gear. A box-wing offered more structural stability at a decreased weight. The use of composites would be necessary to further reduce the weight. Folded or detached wings were also considered to fit the aircraft on a standard trailer for ease of transportation.

The power-to-weight ratio, fuel efficiency, cost, and noise were primary considerations for the propulsion sub-team. The SSTOL design required a higher power-to-weight ratio than conventional aircraft. The propulsion team worked to keep the complexity of these systems to a minimum.

The main concern of the aerodynamics sub-team was the wing configuration. The advantages and disadvantages of the box-wing were examined. The team used a program called *Tornado*, which is a 3-D non-planar vortex lattice method that can model all aspects of the wing geometry. *Tornado* was used to study the characteristics of many wing configurations to determine which would be best for our requirements. Using *Tornado*, the sub-team studied variations in wing sweep, taper, twist, and vertical and horizontal separation.

The stability and control sub-team addressed concerns about control during slow flight. At these low speeds, the control surfaces lose some effectiveness. Devices such as longitudinal and lateral-directional control nozzles and circulation control systems were considered to increase handling capabilities. The effects of tilting ducts in flight were also analyzed to determine the control characteristics of the design. All of these factors affected the weight balance and stability of the aircraft.

The performance sub-team considered variables such as duct angle, high-lift devices, control surfaces, stall speed, thrust-to-weight ratio, wing area, and lift-to-drag ratio, which all influence the overall performance of the aircraft during takeoff and landing. The landing performance became a critical factor. It was determined what was needed to meet the landing criterion; this information was used to meet the cruise, range, and endurance specifications. This sub-team worked along with the aerodynamics sub-team to determine the best configuration.

The ergonomics sub-team's main goal was to design the cockpit of the aircraft. They had to consider the comfort of the pilot and his/her ease of operation. The team sized the cockpit and determined the placement of the control panel to accommodate a 95^{th} percentile male and a 5^{th} percentile female.

In March 2002, the two halves of the team met in Blacksburg, VA to finalize the configuration and integrate all the parts. In designing this aircraft, the whole team worked together in order to create an innovative design using the most modern technology. The large variation in backgrounds of the team members gave the team the advantage of having very different perspectives which were pulled together to create the unique design of Ikelos.

APPENDIX A

EXECUTIVE SUMMARY REFERENCES
AND
REQUIRED TEAM INFORMATION
AND
ENDORSEMENT LETTER

Appendix A-1: References for Executive Summary

1. Turnbull, A. and Martin, G., "Fixed Wing PAVE Final Report," NASA PAVE Review NASA-Langley Research Center, January 2002.

2. "Slingsby T67 Firefly," Slingsby Aviation, North Yorkshire, UK, 2002

3. "Aeris 200 Specifications," ACEAIR SA, Switzerland, www.aeris.ch, April 2002.

4. "Mission M212 Specification," Lambert Aircraft Engineering, Kortrijk, Belgium, http://www.lambert-aircraft.com/english/specifications.html, April 2002.

5. "Europa XS," Europa Aircraft Company, http://www.europa-aircraft.com/Aircraft/EuropaXS.htm, April 2002.

6. "Skyhawk Specification and Description," Cessna Aircraft Company, Wichita, KS, http://skyhawk.cessna.com/spec_perf.chtml, April 2002.

7. "Jabiru Aircraft Specification," ST Aviation Ltd., Norfolk, UK, http://www.jabiru.co.uk/kitspec.html, April 2002.

8. "STOL CH 701: Performance and Specifications," Zenith Aircraft Company, Mexico, MO, http://www.zenithair.com/stolch701/7-perf.html, April 2002.

9. Jackon, P., ed., *Jane's All the World's Aircraft 1999-2000*, Jane's Information Group Limited, Coulsdon, UK, 1999, p 718.

10. Badgley, P., "150 Horsepower Aircraft Engine," personal correspondence, REGI U.S., Inc., February 12, 2002.

11. Badgley, P., Thompson, G., Clark, N. N., Mucino V. H., Smith, J. E., "The Rand Cam Engine: A Pistonless Four Stroke Engine," SAE Paper 940518, 1994.

12. Badgley, P., Untitled and unpublished technical paper about the Rand Cam engine, Reg Technologies, Inc, 1996.

13. Badgley, P., "Rand Cam Engine Cost," personal correspondence, REGI U.S., Inc., April 2002.

14. Stinton, D., *Design of the Aeroplane*, Van Nostrand Reinhold Company, New York, 1983.

15. Davis, D. G. M., "Ducted Propulsors – Progress in the United Kingdom," SAE Paper 750534, 1975.

16. Wolkovitch, J., "The Joined Wing: An Overview," AIAA 23rd Aerospace Sciences Meeting Paper 85-0274, AIAA, 1985.

17. Kroo, I., McMasters, J., Smith, S., "Highly Nonplanar Lifting Systems," September 26-28, 1995.

18. Melin, T., Vortex Lattice Method, "Tornado1.2", http://www.flyg.kth.se/Tornado/htm/tornado.htm.

19. Marchman, J. F., "Notes on Supercritical Airfoils," Department of Aerospace and Ocean Engineering, Virginia Tech.

20. Englar, Robert J., "Numerical Simulations of the Steady and Unsteady Aerodynamic Characteristics of a Circulation Control Wing Airfoil" AIAA Paper 2001-0704, AIAA, 2001.

21. Hoerner, S. F., *Fluid Dynamic Drag: Practical Information on Aerodynamic Drag and Hydrodynamic Resistance*, Hoerner Fluid Dynamics, Midland Park, NJ, 1958.

22. Roskam, J., *Airplane Design, Part IV: Layout Design of Landing Gear and Systems*, Roskam Aviation and Engineering Corporation, Ottawa, Kansas, 1989.

23. "Flight Op 200," Op Technologies, Hillsboro, OR, http://www.optechnologies.com/products.html, April 2002.

24. "BMW Motorrad," BMW (GB) Limited, http://www.bmw-motorrad.co.uk/, April 2002.

25. "Ballistic Recovery Parachute," Ballistic Recovery Systems, Inc., St. Paul, MN, http://www.airplaneparachutes.com/, April 2002.

26. Sanders, M. and McCormick, E., *Human Factors in Engineering and Design*, McGraw-Hill, New York, 1993.

27. "Confor™ Foam," Aviation Design, California, http://www.aviationdesign.com/confor.html, March 2002.

28. Tompkins, White, Bozer, Frazelle, Tranchoco, and Trevino, *Facilities Planning*, New York, John Wiley & Sons, Inc., 1996.

29. Roskam, J., *Airplane Design Part VIII: Airplane Cost Estimation*, The University of Kansas Lawrence, Kansas, 1990.

30. "SATS Overview," NASA SATS Program Homepage, General Aviation Programs Office, NASA Langley Research Center, VA, http://sats.larc.nasa.gov/overview_sats.html, April 2002.

31. Onion, A., "The Way We'll Move," *ABC News*, http://abcnews.go.com/sections/scitech/DailyNews/futureoftransportation020219.html, February 2002.

32. Croft, J., "Small Airports: To Be Or Not To Be?" *Aviation Week and Space Technology*, April 15, 2002, pp. 58-61.

33. "Skyhawk Price List," Cessna Aircraft Company, Wichita, KS, http://skyhawk.cessna.com/pricelist.chtml, April 2002.

APPENDIX A-2

TEAM RESUME

The Virginia Tech / Loughborough University Aircraft Design Team is composed of 26 students and three faculty advisors. Fourteen of the team members are undergraduate students at Virginia Tech and twelve are undergraduate students from Loughborough University in the UK. Of the Virginia Tech students, nine are seniors in Aerospace Engineering, three are seniors in Industrial Engineering and Operations Research, and two are freshman level students in the General Engineering program. The Loughborough University students are all fourth year students in Aeronautical Engineering. All participants are listed below. Other information on each team member was included in the list of team members presented in the Introductory Material section of this report.

Virginia Tech	**Loughborough University**
Nicole Bratt *	Dave Etchells
Jillian Harper *	Matt Fletcher
Andrew Kates	Stu Frizzel
Ernest Keen	Michelle Hill *
Joseph Kehoe	Will James
John Leonard	Graham Joyce
Steve Penn	Jon Newton
Carrie Phelps *	Josh Phelps
Bryan Racine	Melissa Puran *
Adam Shuty	Greg Reid
Jessica Walker *	Paul Whitehouse
Lyndsey Wuethrich *	Jamie Wright
Michael Willemann	
Trisha Basuray *	
	Gary J. Page **
James F. Marchman, III **	*Lloyd R. Jenkinson* **

* female
** *Faculty Advisor*

Part of the work of this team is an ongoing experiment in international teamwork. The team met at Loughborough University in the UK in November during the Virginia Tech Thanksgiving break and met again in March at Virginia Tech during the Loughborough University Easter break. At other times during the academic year long project the team held weekly teleconferences using telephone, video, and internet links. Extensive use of email communications and linked web sites also proved valuable in conducting the project.

We feel that this experience in international teaming is an important part of preparing these students for future work in the international aerospace industry.

APPENDIX A-3

TEAM MEMBER UNOFFICIAL TRANSCRIPTS

The following unofficial transcripts are provided at the request of NASA. The Virginia Tech transcripts have been edited to exclude grade and GPA information in accord with University Privacy Policy. Those wishing to obtain Official Transcripts with complete grade and GPA records or unofficial transcripts with this information should request such a document directly from the individual student. These transcripts list all courses taken at Virginia Tech and college level credit transferred to Virginia Tech or earned by virtue of AP testing. The unofficial transcripts from Loughborough University consist of listings of the *modules* (courses) taken by these students during their studies at LU. Those wishing to obtain more detailed information on the academic records of the Loughborough University students should also request the relevant information directly from the individual student.

Dr. J. F. Marchman, III
Professor,
Aerospace & Ocean Engineering
Virginia Tech

THIS PAGE INTENTIONALLY BLANK

IN THE PRINTED REPORT UNNOFFICIAL TRANSCRIPTS OF PARTICIPATING STUDENTS ARE INSERTED AT THIS POINT

APPENDIX A-4

LETTER OF ENDORSEMENT

May 1, 2002

TO: NASA / SATS Design Competition

FROM: Dr. J. F. Marchman, III [SIGNATURE HERE]
Professor

SUBJECT: LETTER OF ENDORSEMENT

This report, consisting of the preceding Executive Summary section and these Appendices and supporting documentation, is a description of an Aircraft Design project done during the 2001 - 2002 academic year by an international team of students from Virginia Tech and Loughborough University in the UK. I, along with my UK faculty advisor counterparts, Gary Page and Lloyd Jenkinson, enthusiastically endorse this report as an accurate description of our students' work during the year

This work was done to fulfill requirements at Virginia Tech and at Loughborough University for a final year undergraduate aircraft design project. We would like to thank NASA and the SATS program for the opportunity to submit this work in the 2002 SATS Design Competition. This competition provides an excellent basis for giving our students and interesting and challenging design experience and for an outstanding experiment in international collaboration.

We also wish to thank Virginia Tech, Loughborough University, The Boeing Company, BAE Systems and others who have provided funding and other support for team travel and teleconferencing. Special thanks also go to Robert Hanley and Jessica Wilt of NAVAIR for providing the team an outstanding tour of the Naval Air Warfare Center in Patuxent River, MD and to Kevin Burke of BAE Systems for an equally informative tour of the BAE facilities at Wharton, UK.

Appendix B: Performance

TABLE OF CONTENTS

B-1 INTRODUCTION……..…….... B-3
B-2 TAKEOFF PERFORMANCE……..... B-3
B-3 CLIMB PERFORMANCE……..…… B-7
B-4 STRAIGHT AND LEVEL PERFORMANCE……..……... B-9
B-5 TURNING PERFORMANCE…..……..... B-12
B-6 LANDING PERFORMANCE..…….....B-13
B-7 STALL PERFORMANCE…….....…… B-16
B-8 MISSION ANALYSIS……..……... B-17
B-9 PERFORMANCE SUMMARY……..…….. B-17
REFERENCES……..... B-18

LIST OF FIGURES

Figure B-1 Takeoff Nomenclature
Figure B-2 Iteration Process for Takeoff
Figure B-3 C_L vs. Velocity, on Takeoff run
Figure B-4 Ground Roll
Figure B-5 Field Length
Figure B-6 Climb at Cruise speed and Throttle Settings
Figure B-7 Climb Integration
Figure B-8 Range at Different Cruise Speeds
Figure B-9 Cruise Integration
Figure B-10 Turn rate curves at 1000 ft
Figure B-11 Landing Nomenclature
Figure B-12 Iteration Process for Landing
Figure B-13 Field Length

LIST OF TABLES

Table B-1 Cruise Speeds for Throttle Settings
Table B-2 Mission Breakdown
Table B-3 Flight Performance Data

LIST OF SYMBOLS

S	Wing Area
AR	Aspect Ratio
D	Drag
C_{d0}	Base Drag Coefficient
C_D	Drag Coefficient
e	Oswald's efficiency Factor
L	Lift
C_{Lmax}	Maximum Lift Coefficient
C_L	Lift Coefficient

W	Weight
MTOW	Max Takeoff Weight
ρ	Density
μ	Friction Coefficient
T_{max}	Maximum Thrust
V	Velocity
s	Horizontal Distance
h	Vertical Distance
R	Radius of Transition
n	Load Factor
$\dot{\psi}$	Turn Rate

B-1 INTRODUCTION

In order for the aircraft to meet the design brief, the following criteria need to be satisfied:

- Maximum takeoff and landing ground roll of 46 m (150 ft), with a conventional flap system.
- Sea level cruise speed of greater than 140 kts (72 m/s).
- Maximum range of at least 500 nm (926 km).
- Stall speed of less than 37 kts (19 m/s).
- Sea level climb rate greater than 1000 ft/min (5 m/s).

These requirements need to be met in order for the aircraft to be competitive with STOL aircraft landing performance as well as CTOL aircraft cruise performance. Additional factors that must be considered are the fuel consumption and running costs, which must allow the aircraft to maintain a competitive edge. This section of the report analyses the performance of the baseline aircraft to establish whether it meets the prime performance requirements.

All performance calculations were performed using the following values:

Geometric:
$S = 8.65 m^2$ (93.1 ft^2)
AR = 6.47

Aerodynamic:
C_{d0} clean = 0.03
C_{d0} spoiled = 0.184
Oswald's efficiency, e = 1.46
C_{Lmax} flapped = 4.19
C_{Lmax} takeoff = 3.5
C_{Lmax} clean = 2.6
ΔCL takeoff flap = 0.24

Weight:
MTOW = 6093N (1370 lb)

Atmospheric:
$\rho = 1.225$ kg/m^3 (.00238 sl/ft^3)

Friction
μ free roll = 0.03
μ braked = 0.5

Engine:
T_{max} = 4057N (912 lb)

C_L at zero incidence established from lift curve slope.

B-2 TAKEOFF PERFORMANCE

The takeoff performance of the aircraft is constrained by JAR and FAR regulations, which define the takeoff distance as the length of the takeoff run, to the point where the aircraft is 15 m (50 ft) above the ground. This consists of:

a) Ground roll
b) Transition to climb
c) Climb

Where ground roll is limited to a maximum of 46 m (150 ft). This is shown schematically in Figure B-1.

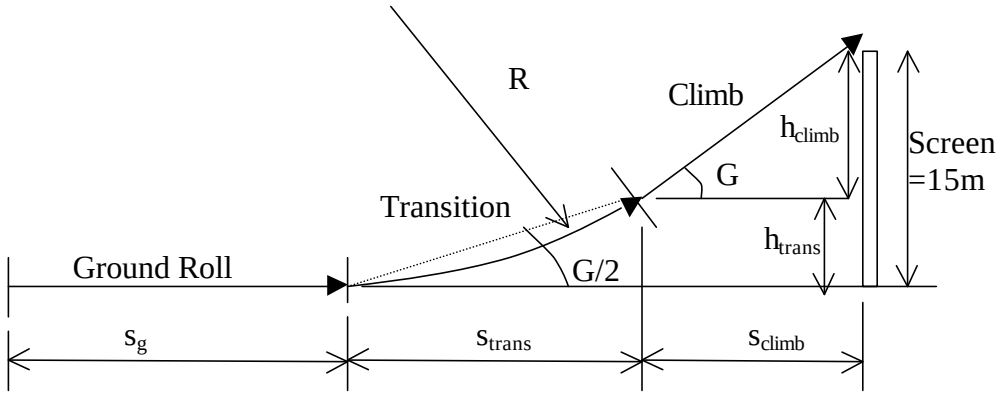

Figure B-1: Takeoff Nomenclature[1]

The takeoff calculation was performed using a time step integration process. This method takes a snapshot of the aircraft and the forces acting upon it, applies these forces for a period of time, t, to establish the velocity at that point. The forces are then re-calculated at this point and this process is continued until the desired parameter is met and the desired output can be calculated. In the landing case, the desired parameter is V=0 and the desired output is distance covered, s. Figure B-2 shows this schematically.

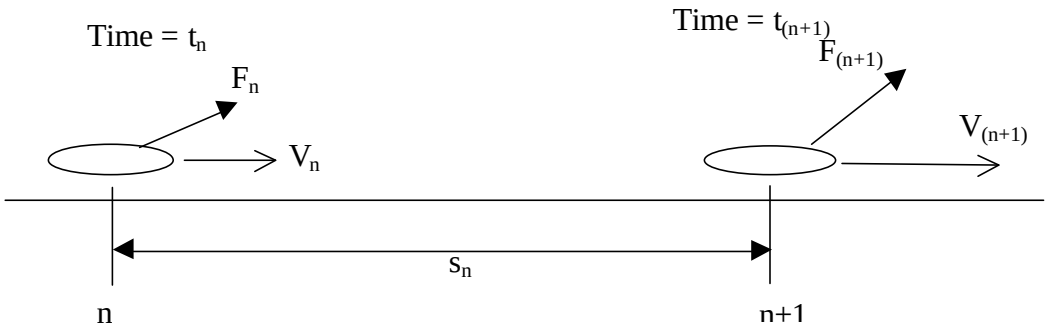

Figure B-2: Iteration Process for Takeoff

Where F is the resultant force on the aircraft, V is the resultant velocity, and s is the distance covered in the time step.

In order to gain sufficient accuracy, but to avoid superfluous calculations, a time step of 0.01 seconds was used to carry out the analysis. For the takeoff performance there are 5 forces acting on the aircraft: thrust, drag, lift, weight and rolling resistance. Where:

$$Thrust = T_{\max} = 4075N \quad \text{(B-1)}$$

$$Weight = W = MTOW = 6093N \quad \text{(B-2)}$$

$$Lift = L_n = \frac{1}{2} r V_n^2 S C_{Ln} \quad \text{(B-3)}$$

$$Rolling\ \ friction = r_n = m(W_n - L_n) \quad \text{(B-4)}$$

$$Drag = D_n = \frac{1}{2} r V_n^2 S C_{dn} \quad \text{(B-5)}$$

where

$$C_{dn} = C_{d0} + \frac{C_{Ln}^2}{peAR} \quad \text{(B-6)}$$

As Ikelos is expected to operate from paved runways predominantly, so the free rolling resistance is assumed to be $\mu = 0.03$

These equations allow the forces acting on the aircraft at any instance to be calculated and of particular interest for the takeoff performance are the resultant horizontal forces acting on the aircraft. This is given by:

$$F_{resn} = T - D_n - r_n \quad \text{(B-7)}$$

From the aircraft weight it is then possible to calculate the acceleration that is imposed on the aircraft by this force.

$$\dot{V}_n = \frac{9.81 F_{resn}}{W} \quad \text{(B-8)}$$

Now, using the time step process it is possible to calculate $V_{(n+1)}$ using:

$$V_{(n+1)} = V_n + t\dot{V} \quad \text{(B-9)}$$

Where t is the time step interval, 0.01 sec.

Knowing $V_{(n+1)}$ it is now possible to calculate the distance covered, s_n, by the simple relationship:

$$s_n = \frac{V_{mean}}{t} = \frac{V_{(n+1)} + V_n}{2t} \quad \text{(B-10)}$$

Now all the key parameters of step n have been calculated and $V_{(n+1)}$ is known it is possible to repeat the same process for step n+1.

It should be stated that the other variable with velocity is C_L, once the aircraft has exceeded V_{stall}. For the ground roll, up to V_{stall}, it is assumed that the aircraft is at zero incidence and $C_L = 1.15$. From V_{stall} to V_{to} the CL is assumed to increase linearly up to the C_L required for V_{to}.

$$\begin{aligned} V_{stall} &= \sqrt{\frac{2W}{rSC_{L\max}}} \\ C_{L\max} &= 3.5 \\ \therefore V_{stall} &= 18.13 ms^{-1} \\ Stating\ V_{to} &= 1.1 V_{stall} \\ V_{to} &= 19.94 ms^{-1} \\ \therefore C_{Lto} &= 2.893 \end{aligned} \quad \text{(B-11)}$$

These quantities are true at maximum takeoff weight

The plot of C_L with velocity at takeoff is shown in Figure B-3.

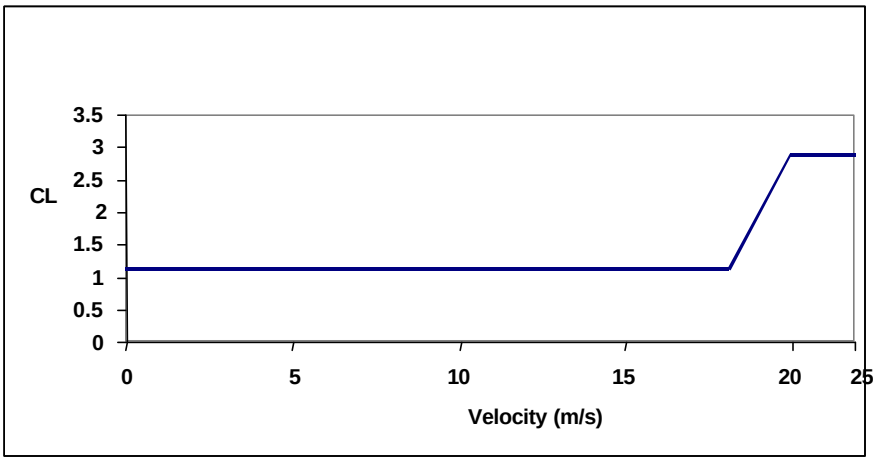

Figure B-3: C_L vs. Velocity, on Takeoff run

Applying this integration process to Ikelos over a range of weights yields the results shown in Figure B-4.

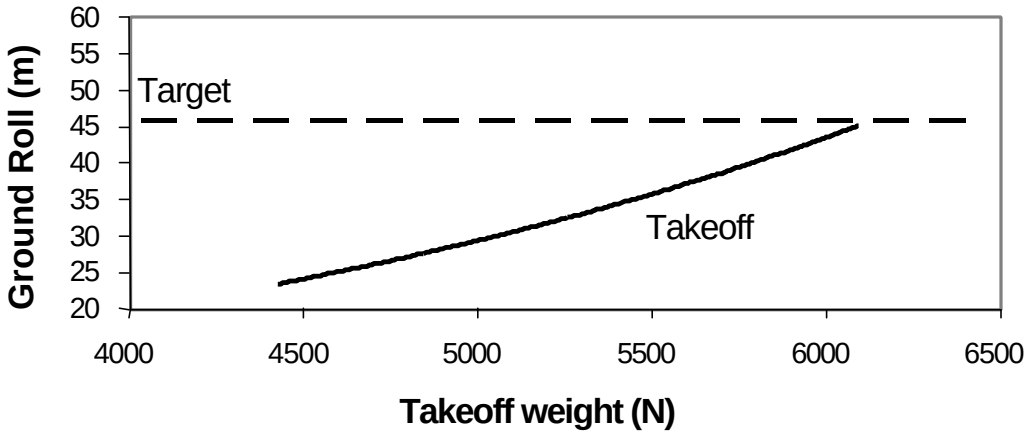

Figure B-4: Ground Roll

The next phase of the takeoff run is transition from ground roll to climb. This has been evaluated using the following equations. It is assumed that the final climb angle will be 10^o, which is assumed to be a standard climb out, evidently this could be steeper in reality. However, unless it is really necessary it is unlikely that a pilot will climb out at such a steep angle.

$$V_{trans} = \frac{V_{lof} + V_2}{2} = \frac{1.1V_s + 1.2V_s}{2} = 1.15V_{stall}$$
$$\therefore V_{trans} = 20.9ms^{-1}$$
$$n = 1.2$$
$$C_{Ltrans} \approx \frac{nC_{L\max}V_{stall}^2}{V_{trans}^2} = 3.15 \qquad \text{(B-12)}$$
$$R = \frac{V_{trans}^2}{g(n-1)} = radius\,of\ transition \quad \therefore R = 223m$$
$$s_{trans} = RG \quad G = 10^o \ \therefore S_{trans} = 38.8m$$
$$h_{trans} = s_{trans}\tan(\frac{G}{2}) \therefore h_{trans} = 3.4m$$

Leaving 11.8m to climb before the obstacle is cleared.

$$h_{climb} = 11.8m \quad G = 10^o$$
$$s_{climb} = \frac{11}{\tan 10^o} = 67m \qquad \text{(B-13)}$$
$$s_{take-off} = 45.5 + 38.8 + 67 = 151.5m$$

The same calculation was carried out at a series of weights and the results are shown in Figure B-5.

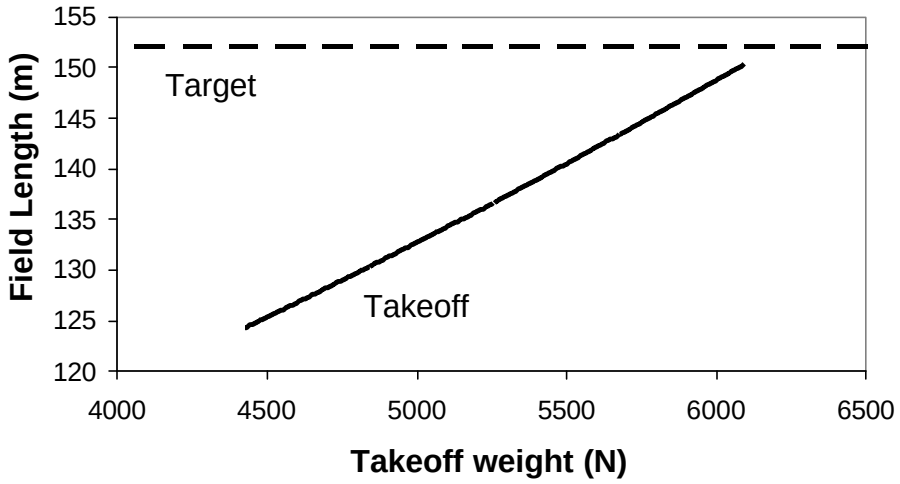

Figure B-5: Field Length

B-3 CLIMB PERFORMANCE

Stated in the design brief the aircraft needs to be capable of sea level climb rate of greater than 1000 ft per minute. The calculated climb rate has been calculated for different

throttle settings as outlined below. The maximum thrust against drag at a set speed gives the maximum rate of climb. The maximum climb gradient can be also be calculated as this gives the best angle for clearing obstacles. Using 100% throttle the maximum climb rate at max takeoff weight is 1367 ft per minute, which is in excess of the specification. The largest angle of incidence is 13.2° this has a climb rate of 762 ft per minute. Figure B-6 shows the rate of climb versus velocity for the different throttle settings. It can be seen from this that at 85% throttle and 90 knots, the aircraft can climb 10,000 feet in less than 12 minutes.

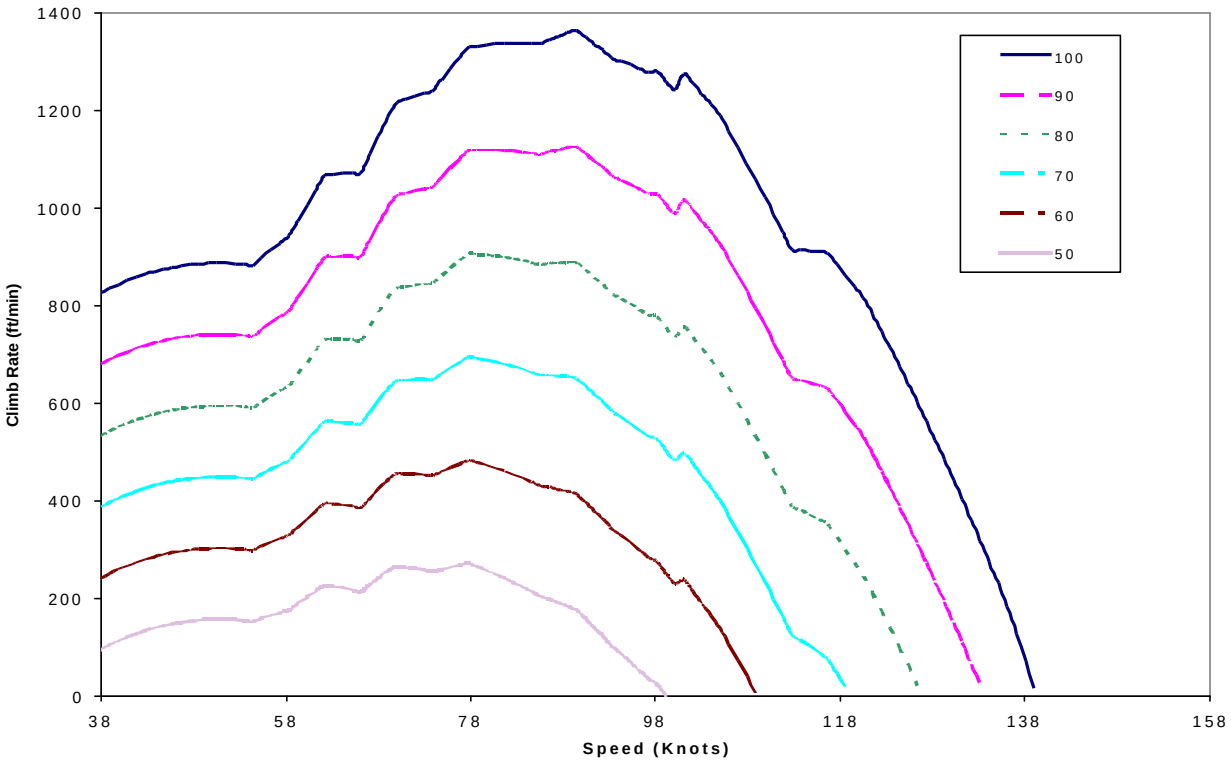

Figure B-6: Climb at Cruise speed and Throttle Settings

Equations for Climb

Firstly C_L is calculated at the investigated speed:

$$C_L = \frac{W}{\frac{1}{2} r V^2 S} \tag{B-14}$$

This value for C_L is now used to calculate the induced drag

$$C_{D_{i0}} = \frac{C_L^2}{K} \tag{B-15}$$

The profile drag coefficient is looked up from a table of aerodynamic data that states the coefficient at different velocities. This table of data was gotten from Aerodynamics.

Adding the coefficient of induced drag to the coefficient for profile drag C_{D0} gives the total drag coefficient. This can now be used to calculate the drag at any given velocity.

$$D_v = \frac{1}{2} r V^2 S C_D \tag{B-16}$$

The thrust developed by the engines is again velocity dependent. A data sheet of max thrust at varying velocities and altitudes is used. See Appendix C, section C-3.5 Figure C-7 for a plot of the thrust vs. velocity. From this the maximum thrust available is obtained.

The difference between the maximum thrust available and the total drag at a given velocity is the called the excess thrust. This can be used to accelerate the aircraft either horizontally or vertically. As aircraft do not normally climb at 100% throttle, fractions of this thrust can be used to simulate throttle settings.

The climb rate can be calculated by:[2]

$$\text{Climb} = \frac{V \times (T - D)}{W} \tag{B-17}$$

The angle of incidence this climb is achieved at is related to the forward speed of the aircraft and so can be calculated using a velocity triangle or the following equation: [2]

$$Gradient = \frac{T - D}{L} \tag{B-18}$$

For the purpose of the mission analysis (Section B-8) an analysis of the climb period is required. To achieve this, a time step integration was performed. The main characteristics of this are a constant throttle climb with a varying weight and velocity. This therefore varies the major forces acting on the aircraft.

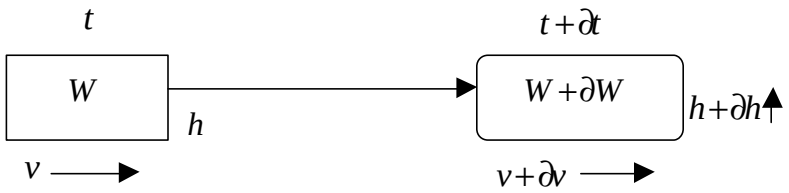

Figure B-7: Climb Integration

The mass of the aircraft is calculated each at each time step by the following equation.

$$W_2 = W_1 - (BSFC \times P \times thr \times \partial t) \tag{B-19}$$

Where: BSFC = Brake Specific Fuel Consumption
P = Power of the Engine
thr = Throttle Setting of the Engine

Using the velocity and altitude ratio the drag can be calculated. With a set throttle the excess thrust can then be calculated. From this instantaneous climb rate and a new height can be calculated for the next time step. With the throttle setting the BSFC can be looked up and the fuel used in the time step calculated. This accurate simulation of the aircraft's climb then enables the time to a set altitude to be obtained as well as the fuel used to climb.

B-4 STRAIGHT AND LEVEL PERFORMANCE

To enable the aircraft to compete with modern personal aircraft the cruise speed was specified as 140 knots at sea level. Calculation of the cruise speed involved the cruise drag coefficient C_D and the C_l for the cruise speed. This was balanced by a throttle setting to

receive a thrust equal to the drag. The equations used to calculate these forces are the same as for climb and can be seen below. A table showing throttle against cruise speed for full payload at 10,000 ft can be seen in Table B-1. Another consideration for cruise is that the weight of the aircraft decreases during the cruise so the cruise speed would increase as the lift induced drag decreased.

Table B-1: Cruise Speeds for Throttle Settings

Throttle Setting	**Cruise Speed S.L**	**Cruise Speed (10kft)**
75%	122.4 kts	118.6 kts
85%	130.2 kts	126.4 kts
100%	139.0 kts	136.1 kts

As can be seen the engine needs to be operating at 100% to meet the cruise requirement. As this is a high rating for an engine at cruise, it has been decided to run the engine at 85% for cruise for the mission mass calculations (see B-8). This means the aircraft falls short of the cruise specification by 9.8 knots.

The range and endurance of the aircraft were also important calculations. The original specifications stated that the aircraft was to have a maximum range of greater 500 nm at typical cruising speed and an endurance of greater than 2 hours. The maximum range with full payload was found to be 650 nm at 80 knots, which is greater than the specification. The 500 nm specification can be achieved at 124 knots. Figure B-8 shows the range at 10,000 ft for max takeoff weight and for one passenger and a full tank of fuel. The maximum endurance is just under nine hours (8.8 hours) at a speed of 64 knots.

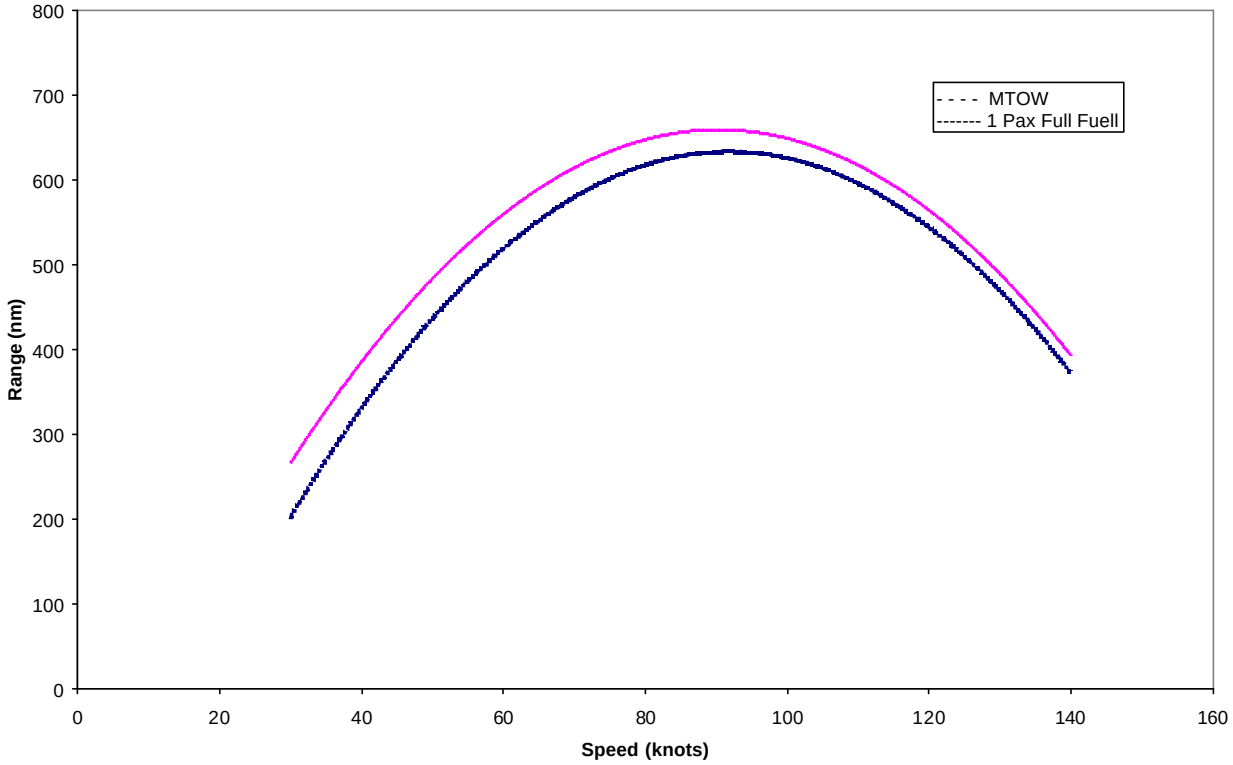

Figure B-8: Range at Different Cruise Speeds

Equations for Cruise

A cruise speed is set and using the equations above, the drag of the aircraft can be calculated. The maximum thrust at the set speed is looked up from a propulsion table.

$$thr_v = \frac{D_v}{T_{\max}} \qquad \text{(B-20)}$$

The throttle setting required to achieve the velocity can then be calculated. Using this throttle setting the fuel used can be calculated.

For the purpose of the mission analysis (Section B-8) an analysis of the cruise period is required. To achieve this a time step integration was performed (see Figure B-9). The main characteristics of this are a constant speed with a varying weight and throttle setting. This alters the induced drag and fuel consumption of the aircraft.

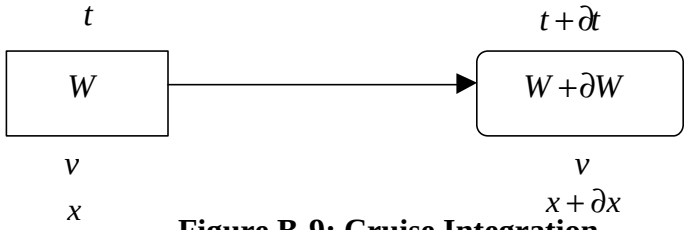

Figure B-9: Cruise Integration

Into these equations a set amount of fuel can be entered this will then calculate the maximum range for a given weight and fuel load. (Figure B-8)

B-5 TURNING PERFORMANCE

As the aircraft is expected to land in small areas it may have to maneuver to the final flight path around obstacles. For this purpose the turn performance has been calculated so any flight path can be analyzed to see if it is possible. Furthermore there could be other applications for the aircraft other than personal use and so agencies may wish for this data. Figure B-10 shows the turn rates of the aircraft at different speeds. This shows that the maximum turn rate is 70 deg/s at 57 knots.

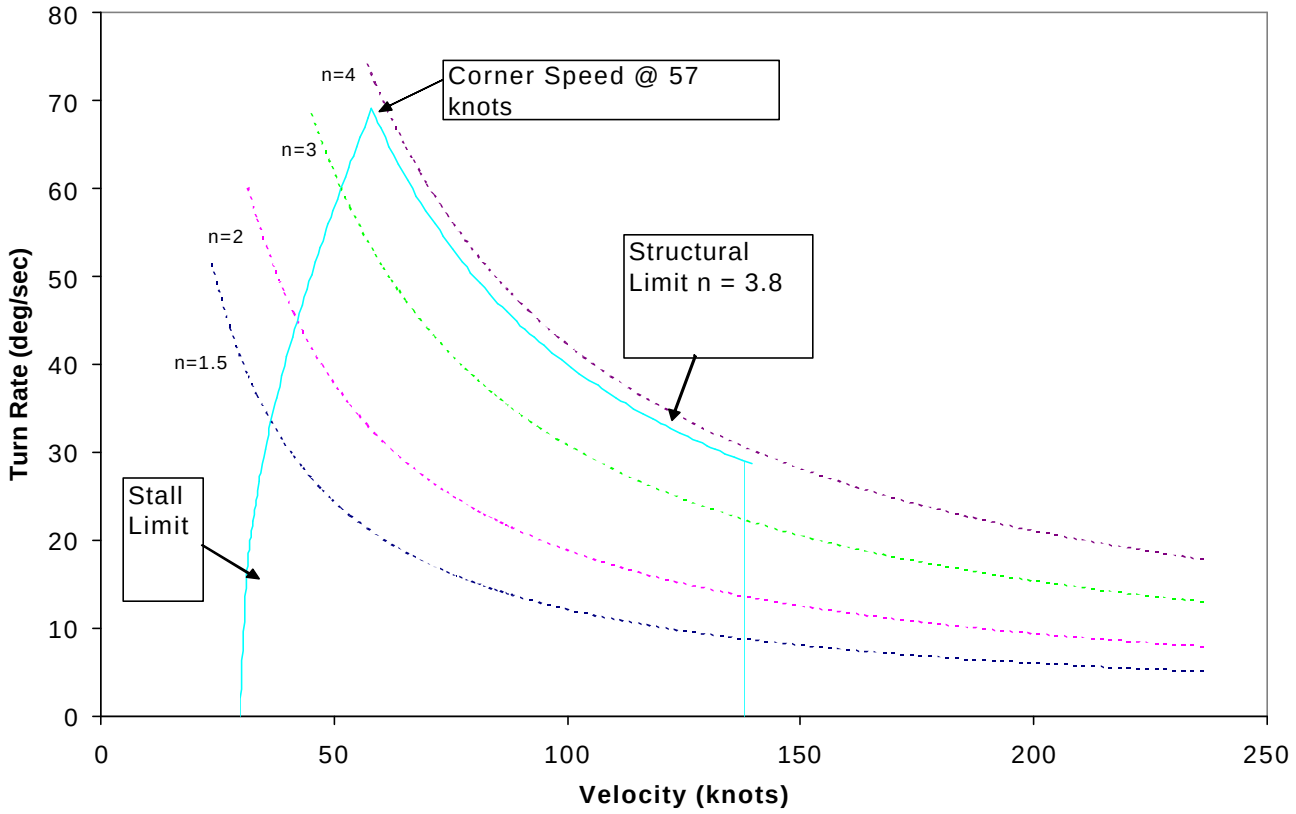

Figure B-10: Turn rate curves at 1000 ft

The turning limits of the aircraft can also be seen from this figure. The three limits are the stall limit, the structural limit and the max velocity of the aircraft.

Equations for Turns [1]

To turn the aircraft, there needs to be more lift than the weight of the plane:

$$L = nW \tag{B-21}$$

Where, n is the load factor on the aircraft.

The rate of the turn is defined as follows:

$$\dot{\Psi} = \frac{g\sqrt{n^2 - 1}}{V} \tag{B-22}$$

To find the stall limit, velocity was found by:

$$V = \sqrt{\frac{L}{0.5 r S C_{L\max}}} \tag{B-23}$$

B-6 LANDING PERFORMANCE

The landing of this aircraft is the most crucial phase of the flight and the most difficult to achieve within the criteria. The landing mode of the aircraft is to consist of:

a) Descent
b) Flare
c) Ground Roll

Where the ground roll is limited to a maximum of 46 m (150 ft). This is shown schematically in Figure B-11.

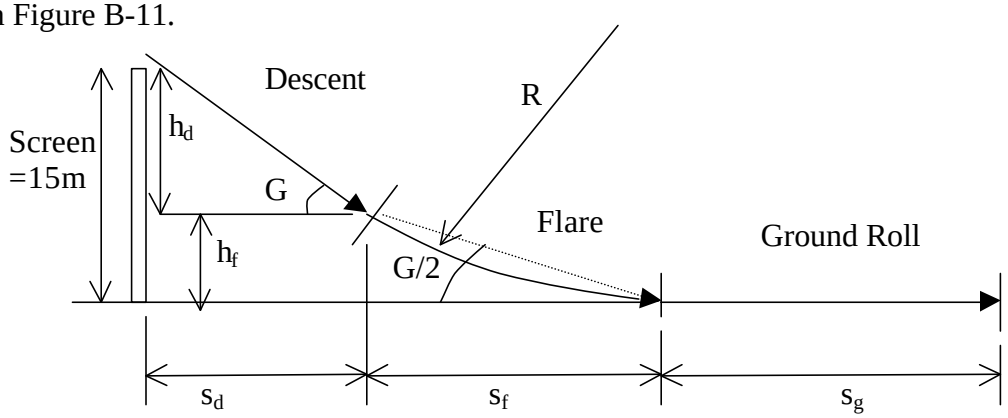

Figure B-11: Landing Nomenclature[1]

Using a time step integration process, similar to that employed in the takeoff calculation, the landing ground roll can be analyzed. Figure B-12 shows how the forces act on the aircraft

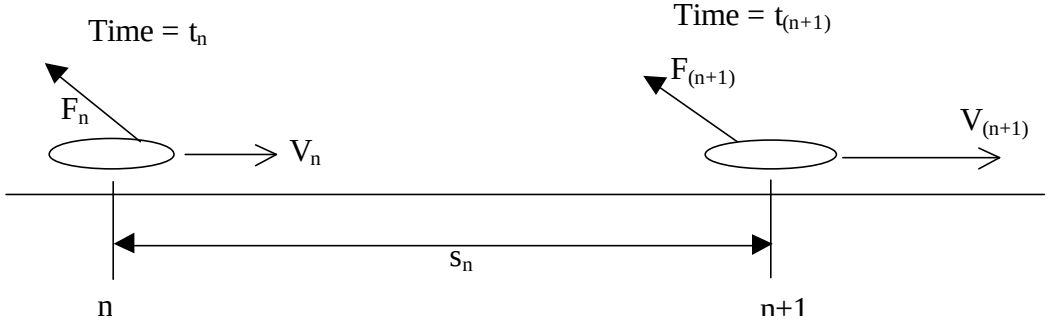

Figure B-12: Iteration Process for Landing

This is the same as the takeoff analysis, except the resultant force now retards the aircraft. The assumptions made for the analysis are that thrust reduces to zero on touchdown instantaneously, and from touchdown until the aircraft has stopped C_L remains at C_{Ltd} =1.89. The brakes are applied after 1 second of ground roll, to allow the aircraft to stabilize. It is

assumed that the rolling resistance before brakes are applied is μ=0.03 and with brakes applied it is μ=0.5, these are assuming ABS on a dry paved runway.

$$V_{stall} = \sqrt{\frac{2W}{rSC_{L\max}}}, \quad C_{L\max} = 4.19 \; at \; landing$$
$$\therefore V_{stall} = 16.57 ms^{-1} \qquad \text{(B-24)}$$
$$V_{td} = 1.15 V_{stall} \quad \therefore \quad V_{td} = 19.05 ms^{-1}$$
$$\therefore C_{Ltd} = 3.17$$

Thus the variation of C_l and μ with time is given by Figure B-13.

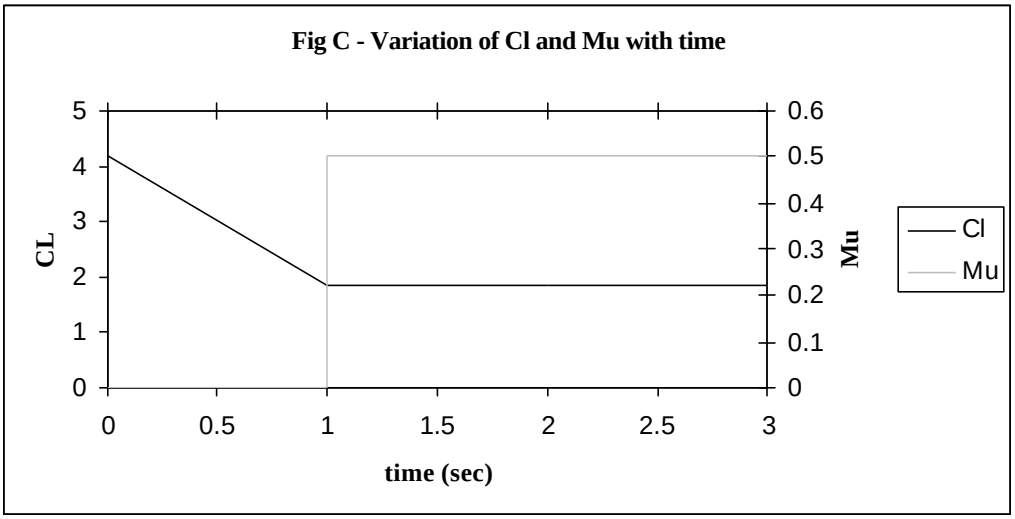

Figure B-13: Variation of C_l and m with time

The basic 4 forces acting on the aircraft during the landing phase are:

$$Weight = W = MTOW = 6093N$$
$$Lift = L_n = \frac{1}{2} r V_n^2 S C_{Ln}$$
$$Rolling \;\; friction = r_n = m(W_n - L_n) \qquad \text{(B-25)}$$
$$Drag = D_n = \frac{1}{2} r V_n^2 S C_{dn}$$

Resolving the forces and taking a time step it is possible to establish the ground roll and the resultant velocity.

$$F_{nres} = -D_n - r_n$$
$$\dot{V} = \frac{9.81 F_{res}}{W}$$
$$\textit{taking time steps } t = 0.01s \qquad \text{(B-26)}$$
$$V_{n+1} = V_n + t\dot{V}$$
$$\textit{and}$$
$$s_n = \frac{V_{n+1} + V_n}{2}$$

Conducting the integration over a range of weights gives the results shown in Figure B-14.

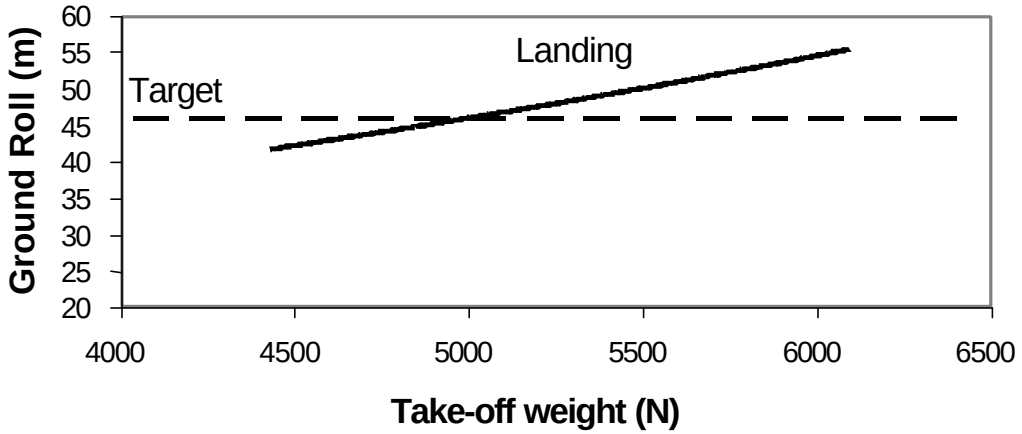

Figure B-14: Ground Roll

The remaining performance throughout the landing phase is calculated using standard results for flare and descent, as follows. The approach is assumed to be on a 9 degree glide slope to enable the aircraft to operate from SSTOL airfields.

$$V_f = \frac{V_A + V_{td}}{2} = \frac{1.3V_s + 1.15V_s}{2} = 1.225V_s$$
$$\textit{Based on MTOW}$$
$$V_s = 16.57 ms^{-1} \quad \therefore \quad V_f = 20.29 ms^{-1}$$
$$n = 1.35g$$
$$\textit{Assume } C_{Lflare} = \frac{nC_{LMax}V_{stall}^2}{V_{flare}^2} = 3.77 \qquad \text{(B-27)}$$
$$R = \frac{V_f^2}{g(n-1)} = 120m$$
$$s_f \approx SG \qquad G = 9^o \quad \therefore \quad s_f = 20.8m$$
$$h_f = s_f \tan\left(\frac{G}{2}\right) = 1.8m$$

This means that the descent over the obstacle to flare must be over a vertical distance of 13.4m

$$s_d = \frac{h_d}{\tan 9^o} = 76m$$
$$s_{total} = s_g + s_f + s_d = 152.4m \quad at\ MTOW \tag{B-28}$$

This analysis was carried out at the full range of operating weights and the results are shown in Figure B15.

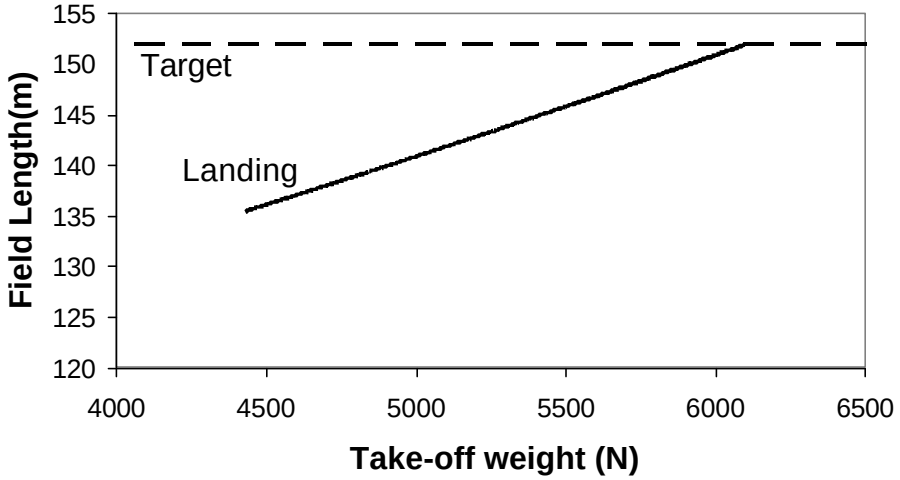

Figure B-15: Field Length

B-7 STALL PERFORMANCE

Based on the wing area of 8.65m^2 and a C_{Lmax} of 4.19 with full flaps, the stall speed at MTOW is 32.2 kts which is within the limits defined by the specification. In clean configuration at MTOW, where C_{Lmax} is reduced to 3.5, the stall speed is 35.2 kts. These calculations can be seen below.

$$V_{stall} = \sqrt{\frac{2W}{rSC_{L\max}}}$$
$$With\ \ full\ \ flaps,\ C_{L\max} = 4.19$$
$$\therefore V_{stall} = 16.6ms^{-1} = 32.2kts \tag{B-29}$$
$$In\ clean\ Config,\ C_{L\max} = 3.5$$
$$\therefore V_{stall} = 18.12ms^{-1} = 35.2kts$$

B-8 MISSION ANALYSIS

The mission analysis in Table B-2 shows an example of the break down of the aircraft and its performance through out a flight. This mission shows a full payload and full fuel. A cruise speed of 117 knots was set.

Table B-2: Mission Breakdown

Segment	Throttle (%)	Duration (hrs)	Fuel Used (kg)	Weight
Taxi/idle	10.00	0.25	0.54	6070.66
Takeoff	100.00	0.02	0.33	6067.45
Climb	85.00	0.03	0.60	6061.60
Cruise		4.02	65.30	5996.30
Descent	20.00	0.08	0.36	5992.74
Landing	10.00	0.02	0.04	5992.39
		Total w/o Reserves	67.17	
		Reserves	4.03	5952.85
		Total w/ Reserves	71.20	

Equations for Mission Analysis

The mission analysis is the combination of the cruise analysis, climb analysis, takeoff and landing. Added to this are the assumptions of taxing and descent. The taxing was assumed as 10 minutes based on light aircraft moving around a small airport and including engine checks. The descent was assumed to take the same amount of time as the climb, 12 minutes. After the total fuel required is calculated the standard 6% reserves is taken into account. Using iterations on a spreadsheet program the maximum fuel available for cruise is calculated using the mission analysis. This then inputted into the cruise simulation will give a range for the given payload and cruise speed. The maximum fuel is 71.2 Kg (707.3N) and a cruise speed of 124knots at 10,000 ft gives a cruise range of 500 nautical

B-9 PERFORMANCE SUMMARY

Table B-3 shows the performance parameters achieved by the baseline design and how these compare to the specification.

Table B-3: Flight Performance Data

Performance Parameter	Requirement	Baseline Achievement
Landing Ground Roll	<46 m	44 m
Takeoff ground roll	<46 m	38 m
SSTOL LDR	<152 m	148 m
SSTOL TODR	<152 m	146 m
Sea Level Stall Speed (full flaps)	<37 kts	32.7 kts
Sea level Range	>500nm	500nm
Sea Level Cruise Speed	>140 kts	132 kts
Sea Level maximum Speed	>140 kts	143 kts
Sea level Climb Rate	>1000 ft/min	3170 ft/min

As can be seen from this performance analysis all the objectives, with the exception of cruise speed, have been achieved. The cruise speed deficit is only 8kts below the specification so by optimizing the design this could be reached. The other area that needs careful consideration in the detailed design is the landing requirement, although the requirement has been achieved it is extremely close to the specification limit. The landing also assumes many favorable conditions, such as a high braking coefficient, that all the wing lift is spoiled on landing and that there is no thrust from the propellers on landing.

In order to more satisfactorily achieve the landing requirement it is necessary to review the following:

1) The MTOW of the aircraft - an increase in wing area may be required.
2) Braking systems available - an analysis of the brake and wheel combinations that can achieve the greatest braking coefficient.
3) The C_{Lmax} achievable with flaps and slats - if this can be increased then the landing distance can be achieved.

In order to achieve the cruise requirement it will be necessary to review the following:

1) The clean configuration profile drag of the aircraft - examine how this could be reduced in order to achieve the cruise requirement.
2) Propeller efficiency in cruise - if this could be increased to achieve the cruise requirement and if this would adversely affect takeoff performance.
3) Engine Power - it may be necessary to simply increase the power available in order to achieve the cruise speed refinements 1 and 2 cannot be achieved.

However, the baseline design is a satisfactory design, which, with the refinements described above, will be able to meet all the performance objectives that are required.

REFERENCES

1. Raymer, Daniel P. "Aircraft Design: A Conceptual Approach." AIAA, Inc. Reston, Virginia, 1999.

2. Render, Dr. P.M. “An Introduction to Fixed Wing Performance & Stability,” University of Loughborough Department of Aeronautical & Automotive Studies Departmental Publication, October 1994.

Appendix C: Propulsion

TABLE OF CONTENTS

C-1 ENGINE SELECTION…… C-2
C-2 RAND CAM ENGINE…… C-3
C-2.1 Overview…….. C-3
C-2.2 Background……...C-5
C-2.3 Operating Cycle……C-6
C-2.4 Operation……..C-6
C-2.5 Design Aspects…….C-8
C-2.6 Installation…… C-9
C-2.7 Engine Accessories…….. C-11
C-3 DUCTED FANS……...C-12
C-3.1 Why Use Ducted Fans……..C-12
C-3.2 Ducted Fan Properties…….. C-12
C-3.3 Transmission…… C-13
C-3.4 Duct Removal……...C-14
C-3.5 Calculation of thrust…….C-14
C-3.6 Fan Noise……..C-16
REFERENCES…… C-17

LIST OF FIGURES

Figure C-1 Rand Cam engine cutaway
Figure C-2 Six vane Rand Cam engine rotor/stator assembly
Figure C-3 Rand Cam engine cutaway showing intake/exhaust ports, fuel injector, and combustion chamber geometry
Figure C-4 Twelve vane Rand Cam diesel engine schematic
Figure C-5 General layout of the propulsion system
Figure C-6 Shaft spline linkage for detachable ducts
Figure C-7 Graph of thrust varying with airspeed at sea level

LIST OF TABLES

Table C-1 Engine data comparison
Table C-2 Disc loading comparison

LIST OF SYMBOLS

C_p power coefficient
D propeller diameter
DL disc loading
n rotational speed
N number of blades
P power
T thrust
V airspeed
η efficiency
ρ air density

C-1 ENGINE SELECTION

During the engine selection process, several options were considered and evaluated based primarily on power to weight ratio, cost, fuel efficiency, noise and emissions. A light weight engine was considered a necessity due to the exceptional performance needed for the aircraft. Cost was a major consideration because the propulsion system typically represents a significant portion of the total cost of an aircraft. Also, environmental criteria such as fuel efficiency, noise, and emissions were considered since in recent years there has been increased emphasis placed on aircraft that are environmentally friendly.

It was first believed that a small turboprop engine scaled down to the necessary power rating would prove to be viable option. Turboprops offer a high power to weight ratio which, as stated previously, was a very important consideration. The first engine considered was a scaled down version of the Williams International TSX-2 in development for NASA under the General Aviation Propulsion (GAP) Program. This engine has very promising performance but it was found that even if the engine were successfully scaled down to the 112 kW (150 hp) range, it would still not be able to match the fuel burn of a competing piston engine. There was also concern that the unit cost per engine would not be competitive with similar piston engines.

A piston engine was then considered as the other propulsion option due to its widespread long term use in general aviation. The Lycoming O-320 series engine was the primary piston engine studied.

Finally, an engine called the Rand Cam was considered as a third option. This rotary diesel engine features a design which is unique amongst internal combustion engines. The Rand Cam, like the GAP Turboprop, is not yet in production but boasts impressive expected performance.

Table C-1: Engine data comparison

Engine	**Lycoming O-320** [(1)]	**GAP Turboprop** [(2)]	**Rand Cam** [(3)]
Power kW (hp)	112 (150)	186 (250)	112 (150)
Bare Weight N (lbs)	-	196 (44)	245 (55)
Total Weight N (lbs)	1085 (244)	311 (70)	432 (97)
BSFC kg/kW-hr (lbs/hp-hr)	0.27 (0.45)	0.31 (0.51)	0.18 (0.30)
Fuel Type	AvGas	Jet Fuel	Diesel or Jet Fuel
Length cm (in)	78.7 (30)	70.1 (27.6)	20.3 (8)
Width or Diameter cm (in)	81.3 (32)	19.8 (7.8)	24.4 (9.6)
Cost USD	$35000	$44000	$10000[(4)]

A comparison of the three engine choices appears in Table C-1. The Rand Cam does not offer the power to weight ratio of the turboprop, but it offers an advantage in fuel efficiency and cost. It was acknowledged that the piston engine represented the lowest risk propulsion choice since the technology is well proven. Despite this fact, it was concluded that the potential benefits of the innovative Rand Cam outweighed the technological risk and it was chosen as the aircraft propulsion system.

C-2 RAND CAM ENGINE

C-2.1 Overview

The Rand Cam engine (Figure C-1) is an innovative rotary engine concept that is very mechanically simple yet capable of generating high power output. The engine's mechanical simplicity is demonstrated by the fact that it does away with pistons, piston rings, valves, valve actuation camshafts, timing gears, cylinders, cylinder liners, connecting rods, crankshafts, and rod bearings.[5]

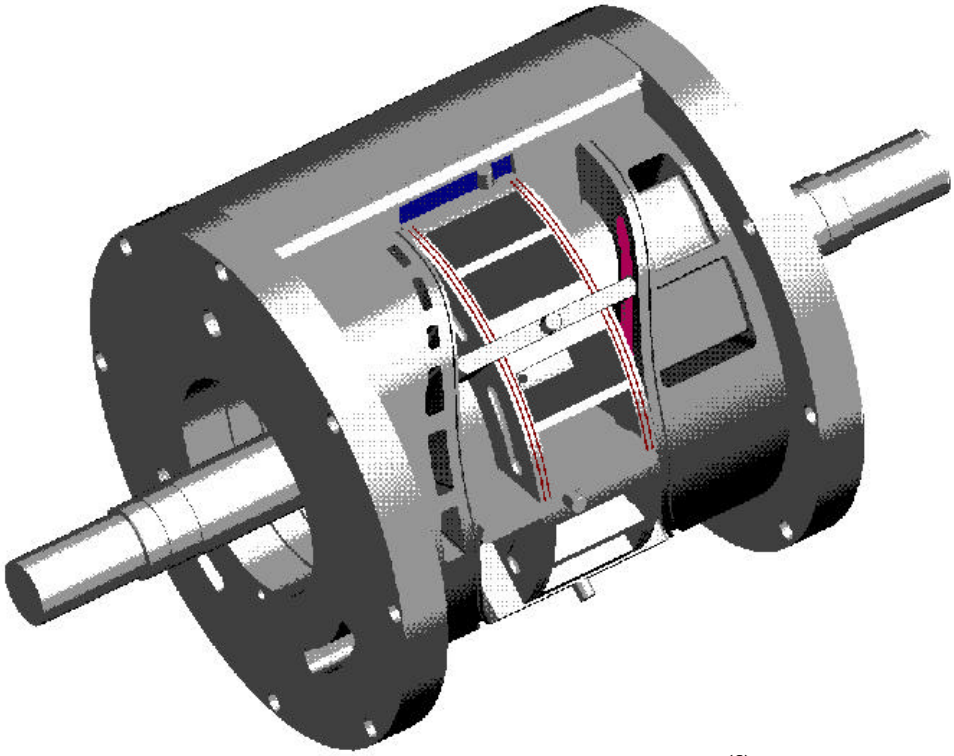

Figure C-1: Rand Cam engine cutaway [6]

The engine consists of a rotor with multiple axial vanes that rotates in a cam shaped housing. The cam shaped housing consists of two stators (front and rear), each containing a bearing that the rotor shaft is mounted on. The rotor/stator assembly is shown in Figure C-2. Each of the stators has a toroidal trough of varying depth machined into it. When the cam housing is assembled, two opposing troughs of varying depth, one in front of the rotor and the other behind, are formed. The depth distributions of the troughs are out of phase such that the maximum depth of one trough corresponds to the minimum depth of the other.[5]

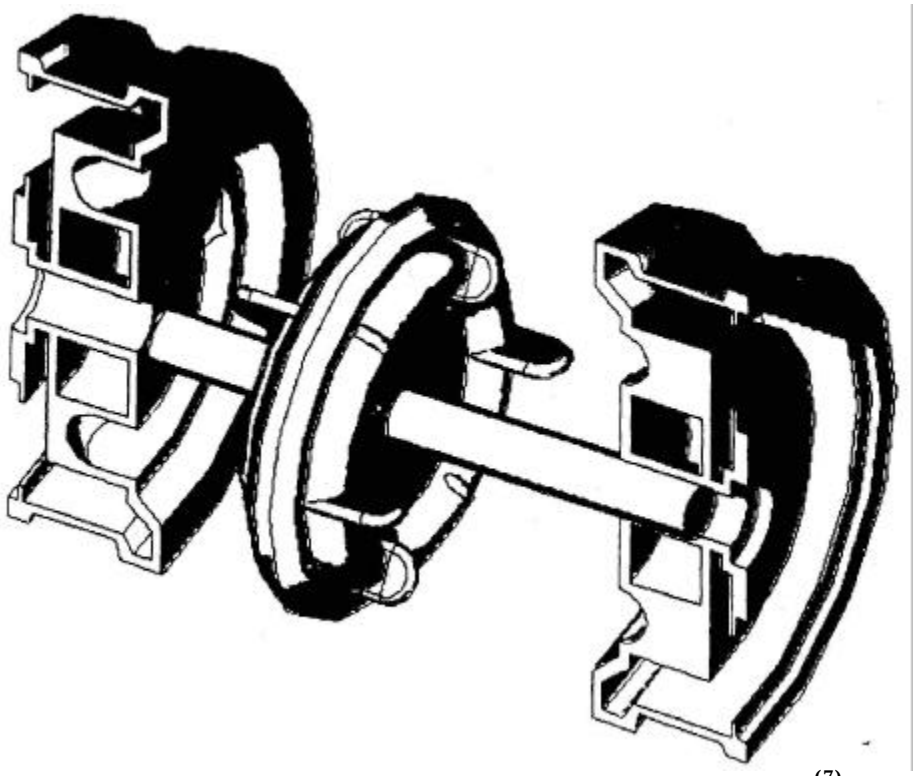

Figure C-2: Six vane Rand Cam engine rotor/stator assembly [7]

The axial vanes that protrude from the rotor span the axial distance between the troughs in the front and rear stators. The vanes are mounted in slots milled in the rotor disk so that they are free to slide in the axial direction. The vanes translate forward and backward as the rotor rotates, forming a constant seal against the sidewalls of the troughs. A sealed cavity is thus formed, bounded by two vanes, the trough sidewalls, and the rotor face. The cavities are used to trap the working fluid and serve as individual combustion chambers.[5]

The seal formed by the vanes against the trough sidewalls is critical in that it must restrict leakage between adjacent chambers. To prevent the vanes from rubbing against the trough wall, the vanes are positioned axially by a pin that rides in an oil filled groove machined into the outer housing. The path of the groove is identical to the cam shaped trough contour so that the vanes maintain constant clearance with the trough as they sweep through it. Maintaining constant clearance between the vane and sidewalls is a crucial balance of maintaining a seal and preventing rubbing.[5]

The individual cavities captured between the vanes vary in volume with circumferential location, hence providing a venue for an internal combustion engine. For this reason, the Rand Cam concept can also be adapted for other applications, such as a steam engine, pump, or air motor. Figure C-3 illustrates how each individual combustion chamber features an elongated reentrant bowl machined into the rotor face. This bowl is important feature of the combustion chamber geometry. In piston diesel engines, a reentrant bowl is machined into the top of the piston. This bowl receives the fuel spray and is where combustion actually occurs. The reentrant bowls in the Rand Cam rotor serve the same purpose.[5]

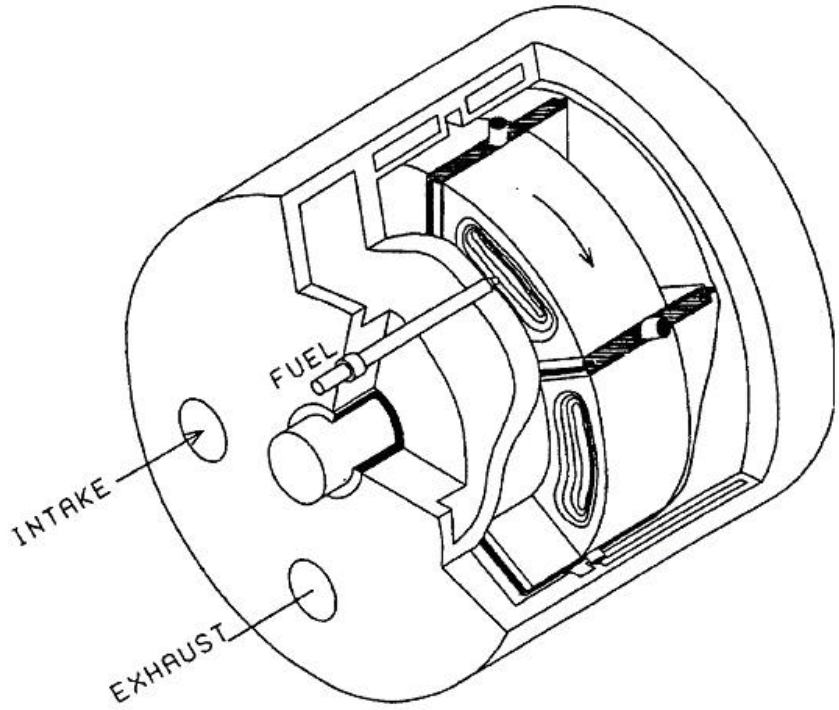

Figure C-3: Rand Cam engine cutaway showing intake/exhaust ports, fuel injector, and combustion chamber geometry [5]

Unlike a piston engine in which the entire cycle takes place in the same cylinder, the cycle processes in the Rand Cam are distributed circumferentially around the trough. Air intake occurs through ports located in the trough at locations where chamber volume is increasing. Exhaust gases are expelled through similar ports located where the trough depth is decreasing and hence chamber volume is decreasing. The use of ports for intake, fuel injection, and exhaust eliminates the need for valves, which would require an actuation mechanism.[5] Each trough has two deep points and two shallow points so four stroke operation is achieved in each individual chamber for every engine revolution. Therefore for a twelve vane configuration, there are twenty four power strokes per revolution. This is equivalent to a four stroke reciprocating engine with forty eight cylinders.[6]

C-2.2 Background

The Rand Cam engine is a relatively new and innovative propulsion concept which was patented in 1983. Reg Technologies, Inc. of Richmond, British Columbia has been involved in research and development of the Rand Cam since 1987. Since then, the engine has undergone research and development under contract from Reg Technologies at West Virginia University's Center for Industrial Research Applications and at Adiabatics, Inc. Reg Technologies' U.S. subsidiary, REGI U.S., Inc. was incorporated in 1992 and owns the U.S. marketing and intellectual rights to the engine. Reg Technologies and REGI U.S. jointly own the worldwide rights to the Rand Cam technology.[8]

Development of the Rand Cam has steadily progressed since the filing of the initial patent. More recent designs incorporate eight or more vanes while the original patent specified only two. Having eight vanes means that there are sixteen power impulses per revolution as opposed to only four for the two vane configuration.[8]

In 1998 Reg Technologies was contracted by NASA to develop a 186 kW (250 hp) diesel engine specifically designed for aircraft operation. Phase I of the program consisted of modification and testing of a 93 kW (125 hp) Rand Cam engine. It also included the preliminary design of a 186 kW (250 hp) version to be developed in Phase II. After Phase I was completed, the NASA funding was cut and Phase II of the development was cancelled. NASA apparently was concerned about the quantity of engine test data available and that the engine sealing was adequate.[8]

In January 2001, Reg Tech patented a new axial vane sealing system. The new system represents a vast improvement as it eliminates interaction problems between the rotor and stator. The latest development is the incorporation of the "winged rotor" concept. The winged rotor is intended to improve sealing, reduce friction, and omit more than 50 parts in a diesel version of the Rand Cam.[8]

C-2.3 Operating Cycle

The Rand Cam engine operates on the Miller Cycle with extended duration combustion and continuous fuel injection.[6] The Miller Cycle is very similar to the Otto Cycle with the exception that the Miller Cycle utilizes an abbreviated compression stroke and hence has a lower compression ratio. The expansion stoke remains unchanged, yielding an engine with a greater expansion ratio than compression ratio. This mismatch allows the engine to extract more energy from the combustion process without the penalty of a higher compression ratio.[9]

The Miller Cycle is well illustrated when it is applied to a piston engine by merely adjusting the valve timing. The key aspect to consider is that the compression and expansion strokes are governed by the status of the valves, and not necessarily by the position of the piston. For an Otto Cycle piston engine, the compression stroke begins when the piston is at bottom dead center and begins moving toward top dead center. This is only the case because the intake valve is closed at this instant. For a Miller Cycle piston engine, the piston is moving away from bottom dead center yet the intake valve remains open, so compression is not yet taking place. The abbreviated compression begins when the valve finally closes after the piston has moved part way up the cylinder.[9]

C-2.4 Operation

Shown in Figure C-4 is a schematic of the twelve vane engine showing the outer diameter surface unwrapped. From this schematic the axial translation of the vanes within the slots in the rotor can be observed. The cam shaped front and rear walls of the rotor chamber are shown with the relative locations of the intakes, fuel injectors, and exhaust ports. The cam shaped pin track that guides the motion of the vanes appears on the diagram as well.[6]

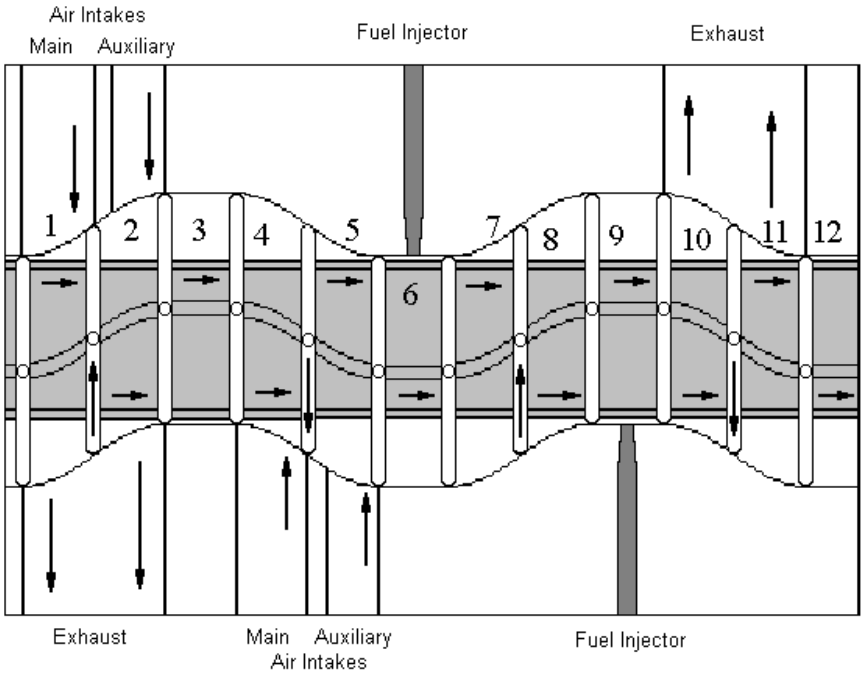

Figure C-4: Twelve vane Rand Cam diesel engine schematic [6]

The operating cycle (with reference to Figure C-4) is described by Badgley[6] as follows. "The rotor is shown moving from the left to the right. The operating cycle is explained by looking at the chambers (from left to right) at the top of the schematic. The cycle is as follows for each of the twelve chambers.

1. The first chamber (located between the first and second vanes) is drawing air in through the main intake port as the rotor rotates and its' volume increases.
2. The second chamber has just closed the main intake port and is drawing air in through the auxiliary intake port. The main and auxiliary intake ports are used to effect the Miller Cycle. When the auxiliary intake port is closed (with a throttle type valve) the intake is closed early in the cycle before the chamber achieves maximum volume. This lowers the effective compression ratio while leaving the expansion ratio unchanged. For cold starting and light load operation the auxiliary intake ports are opened thereby raising the compression ratio of the engine.
3. The third chamber is at maximum volume (the equivalent of bottom dead center on a piston type reciprocating engine) and represents the displacement of one of the chambers. Since there are twelve chambers on each side of the engine for a total of 24 chambers, the total displacement is the displacement of one chamber times 24.
4. The fourth chamber is part way into the compression cycle and
5. the fifth chamber is almost through compression.
6. The sixth chamber is at minimum volume and is equivalent to top-dead-center. The fuel injector is located in the side cams at this location and this chamber is halfway through the combustion cycle. The combustion chamber is represented by the two parallel lines on the face of the rotor and are better identified as the pockets on the face of the rotor in Figure C-1.
7. The seventh chamber is into the beginning of the expansion cycle and
8. the eighth chamber is nearly completed its' expansion cycle.

9. The ninth chamber is at maximum volume and as about to open the exhaust port.
10. The tenth chamber is exhausting through the exhaust port and
11. the eleventh chamber has nearly completed exhausting.
12. The twelfth chamber has just closed the exhaust port and is about to about the intake port. This chamber is at minimum volume and shows that the engine has zero overlap."

C-2.5 Design Aspects

C-2.5.1 Emissions

High compression ratio engines have high combustion temperatures and pressures, which lead to production of nitrogen oxides (NO_x). At high temperature, nitrogen is no longer inert, and tends to chemically react with oxygen to form oxides. Since the Rand Cam operates on the reduced compression Miller Cycle, NO_x emissions are reduced.[9]

Emissions of carbon monoxide (CO) and unburned hydrocarbons (HC) are reduced by more complete combustion, which can be facilitated by increasing the combustion residence time. The cam profile of the Rand Cam engine is shaped such that there is a dwell between each segment. The implication of this is that the volume changes very slowly at the minimum and maximum positions. This allows for an increased period of time for burning to occur at nearly constant volume before the expansion process begins.[6]

Lubricating oil that is burned in an engine combustion chamber results in higher hydrocarbon emissions, so it is advantageous for an engine to be designed to prevent this. The combustion chambers of the Rand Cam engine are designed to be free of seals and rubbing surfaces. Combustion chamber sealing is dependent on maintaining vane clearance with the walls of the troughs, so there is no need to lubricate the trough surface. The lubricated vane positioning cam track is physically separated from the combustion chambers, so oil leakage into the combustion chambers can thus be avoided.[6]

C-2.5.2 Vibration

The Rand Cam engine offers a distinct advantage in vibration levels over piston engines in that it does not have masses that are rapidly reversing direction. The Rand Cam is inherently balanced as long as its number of vanes is divisible by four. The rotor of the Rand Cam would be dynamically balanced as an assembly during manufacture in order to eliminate any potential vibration.[6]

C-2.5.3 Noise

By virtue of its unique design, the Rand Cam also has several features that make it a quiet engine. The lack of vibration in the engine assures that little noise can be expected from the engine structure. Since the fuel injection in the Rand Cam engine is continuous, the noise produced by typical diesel engine valves opening and closing is non-existent. Due to the high firing frequency of the engine, what little exhaust noise there is will consequently have a high frequency. It is expected that if a muffler were needed at all, a very small one would most likely be adequate.[6]

C-2.5.4 Cost

Due to the inherent simplicity of the Rand Cam engine, it is expected that an aircraft version of the engine rated at 112 kW (150 hp) will cost $10,000. This assumes that over 2000

units are produced per year.[4] The elimination of gears and valve actuation components as well as the use of only two bearings contributes greatly to the low cost of the engine. In addition, the basic engine assembly is comprised of low cost materials such as aluminum, iron, and steel.[6]

C-2.5.5 Maintenance

The Rand Cam is designed to operate virtually maintenance free. The engine has no valve actuation system that requires adjustment and has no spark plugs that can wear out. The engine is cooled by fan driven air circulating through the engine compartment. The oil pump is also electrically driven so that the engine can always be primed with oil to avoid wear upon start up. The lubrication system is used to remove heat from the engine and is coupled to the coolant system via a heat exchanger. The only major item of maintenance concern is changing the lubricant at regular intervals.[6]

C-2.5.6 Fuel

The Rand Cam offers some flexibility in fuel choice as it will run on either diesel or jet fuel. Diesel fuel is fairly inexpensive and can be easily obtained from most automobile service stations. If the aircraft is to be operated from an airport, the engine can run on Jet-A which is commonly found at most airports. With this flexibility comes the need for increased caution as it is not recommended that the two fuel types be mixed.[4]

C-2.6 Installation

The Rand Cam is mounted inside the fuselage, bolted to the aft face of a bulkhead which is located at approximately the same station as the ducts. A side and overhead view of the engine installation appears in Figure C-5. The bulkhead is slanted aft as a safety feature in a crash situation. If the engine should become liberated from its mounting, the slanted bulkhead will deflect the engine down and away from the cockpit as it exits the aircraft.

The engine is mounted in a transverse fashion, with the shaft running parallel the lateral axis of the aircraft. This allows the engine to be in line with both ducted fans and drive them directly. If the engine were mounted parallel to the longitudinal axis, additional gearing would be necessary to couple the engine shaft with the fan shaft.

The engine compartment is configured to allow cooling air to freely circulate. A scoop inlet is located on the bottom of the fuselage to admit cooling air. The air travels via a duct from the inlet up to the engine to cool it. The air then travels aft past the oil cooler and down a duct to be dumped overboard. The cooling air exhaust is located on the underside of the empennage where the low pressure will help draw the air through the duct when the aircraft is in flight. There is an electric fan located in the duct which is used to draw the air when there is not enough flow due to ram effect.

Air for the engine enters through a scoop inlet mounted on top of the aircraft, aft of the baggage compartment. After entering the inlet, air is directed downward to a plenum which is located above the engine compartment. Air is drawn to the engine from the plenum through two pipes which feed the two intake ports on either side of the engine.

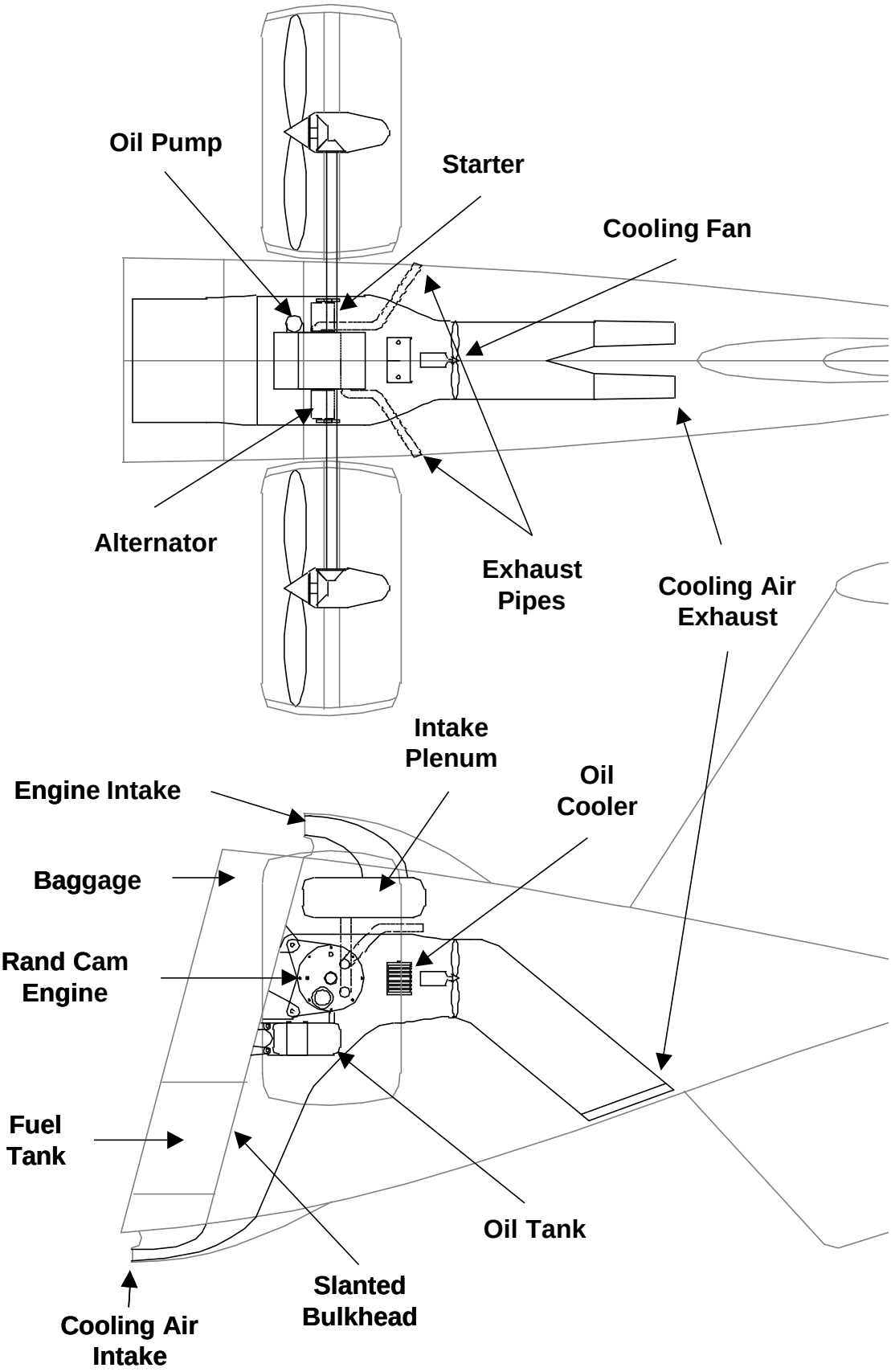

Figure C-5: General layout of the propulsion system

Exhaust air exits the engine from both sides through pipes that are similar to the intake pipes. The dual exhaust pipes protrude from both sides of the fuselage near the ducts. There are no mufflers on the exhaust pipes due to the low noise emitted by the engine.

C-2.7 Engine Accessories

C-2.7.1 Alternator

Electrical power is provided by an alternator, which is driven by the engine shaft via a belt. Electrical power is necessary to run not only the avionics, but various electrically driven engine accessories as well. The fuel pump, oil pump, and engine cooling fan are all electrically driven.

C-2.7.2 Starter

The electrical starter motor is connected to the engine shaft by a gear. The starter runs off the battery which has been placed at the front of the aircraft. To start the engine, the oil pump first runs to prime the engine with lubricant and then the starter is engaged. The intake valves are fully throttled and the fuel valves remain closed as the starter spins the engine up to operating speed. As full speed is reached, the intake valve opens, followed shortly thereafter by the fuel valve. The starter then shuts down as the engine can now sustain its own combustion.[6]

C-2.7.2 Oil System

The oil pump circulates engine oil through the oil tank, oil cooler, shaft gearboxes, and the engine. The oil pump is electrically driven to allow the engine to be primed with oil prior to startup and thus avoid wear on the engine components.[6] Oil drains from the engine through a port in the bottom to a tank below. The oil cooler was placed behind the engine in order to benefit from the same cooling air that the engine does.

C-2.7.3 Cooling Fan

A cooling fan was placed in a duct at the rear of the engine compartment in order to ensure the flow of cooling air. When the aircraft is stationary or moving slowly, intake ram air is not sufficient to cool the engine, so air must be drawn up the intake by a fan. The fan is connected to a temperature sensor which will allow it to activate when the engine compartment temperature is too high. During normal flight, the fan will be turned off and allowed to windmill.

C-2.7.4 Fuel Pump

An electrically driven fuel pump is mounted on the fuel tank. The fuel line passes through the bulkhead between the fuel tank and the engine compartment. The fuel line splits into two lines to feed the fuel ports on either side of the engine.

C-3 DUCTED FANS

C-3.1 Why Use Ducted Fans

Ducted fans are employed instead of simply using propellers as it has been shown that a ducted fan can produce the same amount of thrust as a propeller 1.4 times greater in diameter.[10] Ducted fans have not really been used in the past because it was thought impractical as the increase in weight, due to the duct, outweighed the advantage of the smaller diameter for a given thrust. However with the increase in knowledge and availability of composite materials it is now possible to produce a lightweight duct. The size reduction, therefore, now makes the ducted fan extremely useful - especially in a small transport vehicle.

Ducted fans have several advantages:

- They offer a higher thrust per horsepower for a given diameter than un-ducted fans.
- They give better performance at low speeds than un-ducted fans as flow does not separate and re-circulate at the propeller tips which can cause a conventional propeller to become inefficient at low speeds.[11]
- Ducted fans are inherently quieter than propellers because noise can be damped out using special damping material in the ducts themselves.
- Thrust vectoring can be achieved relatively easily with guide vanes in the duct or by tilting the ducts.
- The duct also provides a desirable safety feature, serving as a guard to prevent the fan from being damaged by surrounding objects and to protect people from injury by the fan.

However, a ducted fan does have its disadvantages. At a Mach number of around 0.6 and above, the duct can increase the drag of the aircraft considerably, though due to the cruise speed of Ikelos this should not be a factor. In addition, experiments have shown that when the aircraft is at high angles of attack, a duct can produce quite significant pitching moments.[12] However the Ikelos does have large control surfaces due to its wing design. These surfaces should be significant enough to be able to counteract any pitch moment that may be produced by the ducts.

C-3.2 Ducted Fan Properties

The ducted fans are 0.8 m (31.5 in) in diameter, and each consists of five rotor blades. An odd number of blades are needed, as fans are susceptible to resonance. The odd number of blades helps to counteract this resonance.[11] Five rotor blades were chosen because a comparison of disc loading was made against other aircraft that fulfilled a similar role to that of the Ikelos. However to make the comparison valid, the number of blades on the aircraft had to be taken into account as it would be unreasonable to compare for example the disc loading of a three bladed Cessna with a five bladed aircraft. Below shows the disc loading ratio that was used to compare the aircraft.

$$DL = \frac{P}{ND} \tag{C-1}$$

where

DL = disc loading
P = power
N = number of blades
D = propeller diameter

A constant chord was assumed for all blades.

A comparison of propellers for different aircraft appears in Table C-2. As can be seen from the table of results, if the fan had only three blades the disc loading would be quite high compared to the similar aircraft. If the fan had seven blades then the disc loading would be quite low however this would increase the weight of the fan and also mean that the fan was not being used to its full potential. Therefore five blades seemed the most logical configuration.

Table C-2: Disc loading comparison

	Power (W)	Propeller Diameter, D (m)	Number of Blades, N	D*N	Disc Loading
Aquilla trike Microlight	37285	1.73	3	5.19	7184
Spartan DFS trike Microlight	26010	1.68	3	5.04	5178
Kolb Fire Fly	29828	1.68	3	5.04	5918
Ikarus C42 Ultralight	59656	1.83	3	5.49	10866
Cessna 172 Skyhawk	119312	1.914	3	5.74	20780
Cessna 152	82030	1.7526	3	5.26	15601
Ikelos	55927	0.8	3	2.4	23303
	55927	0.8	5	4	13982
	55927	0.8	7	5.6	9987

Stators are also placed in the ducts directly behind the rotors. It has been found that if just over double the amount of stator blades compared to rotor blades are place directly behind the rotor blades a noise reduction of approximately 5 dB can be achieved.[14] This is due to the fact that the stator blades cut out noise produced by the rotating blades. Therefore eleven stator blades were placed behind the rotors. They were designed so that the flow exits the duct axially.

The ducted fans are also contra rotating. If they rotate in opposite directions any moment that they transfer to the aircraft is cancelled out. The rotors and stators are made from molded Kevlar, as this material is particularly good at absorbing sharp impacts. If foreign objects should hit the aircraft during take-off or landing and it hits the propellers they should be able to handle the impact without deforming. The ducts have a fiberglass skin and contain foam known as Suprafoam. This foam has extremely good noise damping capabilities therefore should further decrease the noise of the propellers.

C-3.3 Transmission

The ducted fans are attached to the engine via a shaft that is perpendicular to the blade axis requiring 90° gearing (Figure C-5). This is done with spiraled (or helical) bevel gears. These are also used as a speed reduction gear. To try to reduce the noise of the aircraft the propellers run as slowly as possible. The engine shaft turns at 5400 rpm, so the gear reduction is be 1:2 to enable the propellers to turn at 2700 rpm. As the bevel gears are used to reduce the

speed of the shaft no gearbox or additional transmission system is needed. This means that a significant reduction in the propulsion system overall weight can be achieved. Spiraled (or helical) bevel gears are used as they enter the meshing zone progressively and, therefore, have a smoother action than conventional spur gear teeth hence tend to be quieter.[15]

C-3.4 Duct Removal

To enable the aircraft to be transported by road on a trailer one of the ducts must be removable. This means that the aircraft is not be too wide to be transported on the road (provided the wings are removed as well). The drive shaft to one of the ducts therefore has to be detachable from the engine shaft. This is achieved using a spline linkage shown in Figure C-6. The two shafts simply slide together to produce a secure connection. The larger shaft's internal surface mimics that of the smaller shaft surface to produce a locked link. The two shafts are held in place due to the connection of the duct with the fuselage, as the linkage will not be able to slide out if the duct is attached firmly to the fuselage. Even though it is only required that one duct be removable, it may be easier to allow both ducts to be removed for parts commonality and therefore ease of manufacture.

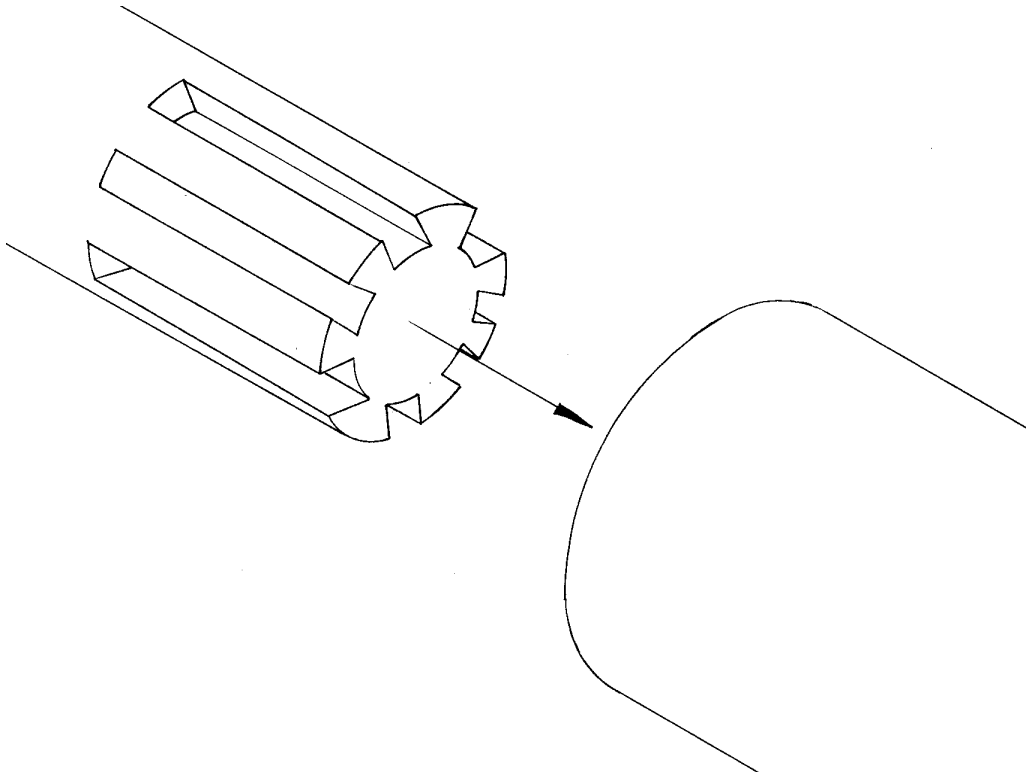

Figure C-6: Shaft spline linkage for the detachable ducts

C-3.5 Calculation of Thrust

Calculating the thrust of a propeller is a fairly difficult task. Therefore a series of estimations have been made to find the thrust of the ducted fans. Disc actuator theory was used to find the ideal theoretical case.[16] This give initial estimates of what thrust could be achieved from a conventional propeller. The calculations involved assume that the propeller was 1.4 times the size of the actual propeller that was to be used in the duct to account for the effect that the

duct has on the thrust (as already mentioned above). Following this, a worst case scenario was then calculated using the general thrust equation given below.

$$T = \frac{\eta P}{V} \tag{C-2}$$

where

T = thrust
η = propeller efficiency
P = power
V = airspeed

Since ducted fans are not widely used, very little data is available concerning their use. Therefore empirical data for a three bladed propeller was used to find the propeller efficiency.[17] First the values of advance ratio (J) and power coefficient (C_P) were calculated for the five bladed propeller. Efficiency was then determined from a plot of efficiency versus advance ratio and power coefficient for a three bladed propeller. The value of the efficiency was used in Equation C-2 to calculate thrust. This calculation was an under-estimation of the thrust that would be produced as the ducted fans had five propellers and were ducted. Therefore the final thrust that would be produced could now be estimated. It would simply lie between the two lines plotted in Figure C-7. Also shown below are the equations used to calculate C_P and J.

$$C_P = \frac{P}{\rho n^3 D^5} \tag{C-3}$$

$$J = \frac{V}{nD} \tag{C-4}$$

where

C_P = coefficient of power
P = power
r = air density
n = rotational speed
D = propeller diameter
V = airspeed

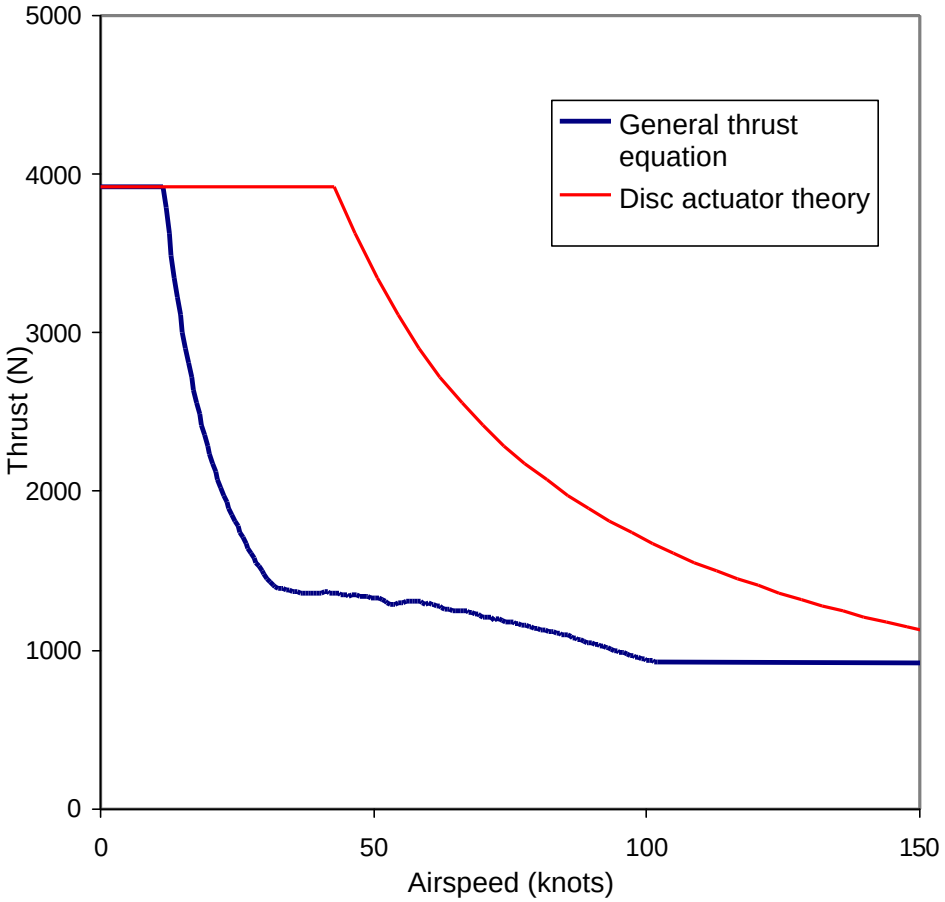

Figure C-7: Graph of thrust varying with airspeed at sea level

This means that there are not exact values for the thrust that will be produced. However the predicted thrust will lie between the two lines plotted on the graph above, as these to lines are the best and worst case scenarios.

C-3.6 Fan Noise

The noise of a propeller or a fan is determined by the tip speed. The propeller tip follows a helical path through the air, so tip speed is function of rotational speed and the axial flow speed entering the propeller. For most analyses, the axial flow speed is approximated as the aircraft forward speed. Tip speed is determined using the relations

$$V_{tip\,(static)} = pnD \quad (18) \qquad \text{(C-5)}$$

$$V_{tip(helical)} = \sqrt{V_{tip\,(static)}^2 + V^2} \quad (18) \qquad \text{(C-6)}$$

where

n = rotational speed in revolutions per second (45 rps)
D = propeller diameter
V = airspeed

For the fans on this aircraft, the static tip speed based on a rotational speed of 2700 rpm is 113 m/s (370 ft/s). The helical tip speed on takeoff and at maximum speed is 115 m/s (337 ft/s) and 134 m/s (440 ft/s).

For quiet aircraft, Raymer[18] recommends a tip speed of no more than 152 m/s (500 ft/s). According to correlations of tip speed and noise that appear in Stinton[11] and Davis[12], a tip

speed of 152 m/s (500 ft/s) corresponds to approximately 60 dBA. This speed/noise correlation applies to two ducted propulsors flying overhead at 305 m (1000 ft). Ikelos would have to fly at approximately 200 kts in order to attain tip speeds of 152 m/s (500 ft/s). The less than 60 dBA noise level of the aircraft is well within the FAR Part 36 noise requirement for propeller driven small airplanes, which stipulates a maximum level of 76 dBA.[19]

REFERENCES

1. "New Engines," Textron Lycoming, Williamsport, PA, http://www.lycoming.textron.com/main.html, April 2002.

2. Freeh, Josh, "NASA GAP Engine Data," personal correspondence, NASA Glenn Research Center, Cleveland, OH, July 2001.

3. Badgley, P., "150 Horsepower Aircraft Engine," personal correspondence, REGI U.S., Inc., February 2002.

4. Badgley, P., "Rand Cam Engine Cost," personal correspondence, REGI U.S., Inc., April 2002.

5. Badgley, P., Thompson, G., Clark, N. N., Mucino V. H., Smith, J. E., "The Rand Cam Engine: A Pistonless Four Stroke Engine," SAE Paper 940518, 1994.

6. Badgley, P., Untitled and unpublished technical paper about the Rand Cam engine, Reg Technologies, Inc, 1996.

7. Mucino, V. H., Smith, J. E., Thompson, G., "Engineering Modeling and Synthesis of a Rand Cam Engine Through CAD Parametric Techniques," SAE Paper 930061, 1993.

8. "News Releases," Reg Technologies, http://www.regtech.com, April 2002.

9. "Miller Cycle Engine," Mazda Motor Corp., http://www.mazda.co.nz/technology/1022.html, April 2002.

10. Campbell, J., *Vertical Take-off and Landing Aircraft*, The Macmillan Company, New York, 1962.

11. Stinton, D., *Design of the Aeroplane*, Van Nostrand Reinhold Company, New York, 1983.

12. Davis, D.G.M., "Ducted Propulsors – Progress in the United Kingdom", SAE paper 750534, 1975.

13. Weir, R.J., "Aerodynamic design considerations for a free-flying ducted propeller", SAE Paper 88-4377-CP, 1988.

14. Woodward, R.P., “Far field noise and internal modes from a ducted propeller at simulated aircraft take-off conditions”, NASA technical memorandum 105369, AIAA 92-0371, 1992.

15. Townsend, D.P., *Dudley’s Gear Handbook, Second Edition*, McGraw-Hill Inc., New York, 1991.

16. Theodorsen, T., *Theory of Propellers*, McGraw-Hill Inc., New York, 1948.

17. Wood, K., *Aerospace Vehicle Design Volume 1*, Johnson Publishing, Boulder Colorado, 1968.

18. Raymer, D., *Aircraft Design: A Conceptual Approach*, AIAA, Reston, VA, 1999.

19. Federal Aviation Regulations, Part 36 Sec. G36.301: Noise Standards, http://www1.airweb.faa.gov/Regulatory_and_Guidance_Library/rgFAR.nsf/CurrentFARPart, April 2002.

Appendix D: Aerodynamics

TABLE OF CONTENTS

D-1 TORNADO VORTEX LATTICE METHOD……...D-2
D-1.1 Program Description.……..D-2
D-1.2 Tornado Validation.……D-2
D-1.3 Considerations of the Box-Wing ……..D-2
D-2 BOX-WING CONFIGURATION……D-4
D-2.1 Decision Process……D-4
D-2.2 Airfoil Selection and Flap System……D-6
D-3 WING LIFT CHARACTERISTICS……..D-8
D-3.1 Lift Coefficient Calculations and Predictions……D-8
D-4 WING DRAG CHARACTERISTICS……...D-9
D-4.1 Aircraft Drag……..D-9
D-4.2 Undercarriage Design…… D-10
D-4.3 Wing Profile Drag……..D-11
D-4.4 Fuselage……. D-12
D-4.5 Vertical Surfaces……D-13
D-4.6 Ducts…….. D-13
D-4.7 Flaps…….....D-14
D-4.8 End-Plate Influence on Drag…… D-14
D-4.9 Induced Drag…….. D-14
D-4.10 Total Drag……D-15
REFERENCES……. D-16

LIST OF FIGURES

Figure D-1 Example of a preliminary box-wing configuration used for initial comparisons and decisions
Figure D-2 Basic Tandem Wing configuration used for preliminary comparison purposes only.
Figure D-3 Final wing configuration planform.
Figure D-4 C_L vs. Alpha plot for GAW-2 airfoil
Figure D-5 Flap Configuration Figure
Figure D-6 C_L vs. Alpha plot for final configuration.
Figure D-7 Profile Drag Breakdown in Cruise Configuration
Figure D-8 Profile Drag Breakdown in Landing Configuration

LIST OF TABLES

Table D-1: Form factor calculation for wings
Table D-2: Drag of Wings
Table D-3: Surface area calculations
Table D-4: Drag of vertical surfaces
Table D-5: Drag due to flap deflection
Table D-6: Drag benefits of endplates

LIST OF SYMBOLS

C_L	Lift coefficient
C_{La}	Lift curve slope
C_m	Moment coefficient
C_D	Drag coefficient
C_{Do}	Zero lift drag coefficient
a	Angle of attack

D-1 TORNADO VORTEX LATTICE METHOD

D-1.1 Program Description

Nearly all aerodynamic calculations and predictions done during the design process were done through the use of the Tornado Vortex Lattice Method[(1)] subroutine written in a Matlab file format. Tornado is a vortex lattice method that was written by Tomas Melin of the Royal Institute of Technology KTH, Department of Aeronautics, Sweden, as part of a masters thesis[(1)]. Currently, this code is not used in industry, but the source code is available as a free download over the internet for use in preliminary or conceptual design and for instructional purposes.

A main feature of Tornado is its ability to handle a wide variety of user-defined inputs for wing geometry that include wing sweep, dihedral, twist, taper, multiple trailing edge control surfaces, camber for the NACA 4 digit airfoils, and the ability to handle nonplanar wing configurations. As well as the options for wing configuration, the code also allows for a particular flight state to be set up by the user. Some examples of the input for a flight state are angle of attack, pitch rate, roll rate, yaw rate, and true airspeed. Given a particular flight state setup and wing geometry, Tornado will output the lift, drag, pitching moment, yawing moment, rolling moment, and all coefficients corresponding to the forces and moments at that particular flight state. As well as single state computations, the code has the ability to compute values of the above listed forces and coefficients over a range of angles of attack. Roll sweeps, control surface sweeps, and yaw sweeps can also be performed by the program. Use of these features was primarily in the stability and control area of the project.

D-1.2 Tornado Validation

Tornado is offered as freeware by the author, with no implied warranty or validation on the program[(1)]. To assure that the code gives accurate results, a simple validation was done with the program.

A variety of simple rectangular wings of varying aspect ratios with NACA 4 digit series airfoils were entered into the program, and the resulting C_L versus a plots were compared to results published for the 2-D NACA airfoil in Abbot and Von Doenhoff[(2)]. After several trials, it was found that the paneling scheme used on the wing is extremely important to achieving accurate results. With an inadequate paneling scheme, the primary error that was encountered was that the zero-lift angle of attack of the wing was calculated incorrectly. Increasing the number of panels in the chordwise direction on the wing solved this problem, as the finer paneling density allowed for a more accurate representation of the camberline of the airfoil, resulting in more accurate agreement with published data.

D-1.3 Considerations of the Box-Wing

With the complex setup of the box-wing configuration, it is important to keep in mind some seemingly simple factors. With a setup such as a box-wing, the rear wing, while acting as a horizontal stabilizer, contributes more to the overall lift of the wing setup than a conventional horizontal tail. This results in a larger amount of actual lift produced by the box-wing. It is important to note that even with a large amount of lift, the lift coefficient could be small or large, depending on the reference area used. Tornado uses the area of the "main wing," which is defined as the first wing defined in the program for the reference area. This would be the front wing in all of our configurations. There is an option to override this function and input any

desired reference area, but it was decided after many trials that the front wing area was the best choice.

Tornado is also limited to only "plain flap" style trailing edge devices. This creates no issues for the elevator, aileron, or rudder control surfaces, but limits our analysis of the flap system to non-fowler type flaps. The plain flap analysis provides for a good base estimation of $?C_L$ with flaps deployed, but further estimation methods must be applied to account for the use of more complex flap designs.

D-2 BOX-WING CONFIGURATION

D-2.1 Decision Process

Figure D-1 shows a typical box-wing setup, which is an extension of the joined wing proposed by Wolkovitch,[3] that was used during the initial decision making process. This simple model was used as a basis for comparison to other fairly simple configurations such as a tandem wing configuration shown in Figure D-2. Using this initial simple geometry, it was found through Tornado analysis that the box-wing gave slightly better performance than a tandem wing configuration, mainly due to the winglet/endplates connecting the tips of the front and rear wings. These endplates help reduce tip losses and improved the overall efficiency of the wing setup, giving a span efficiency factor of 1.46.[4]

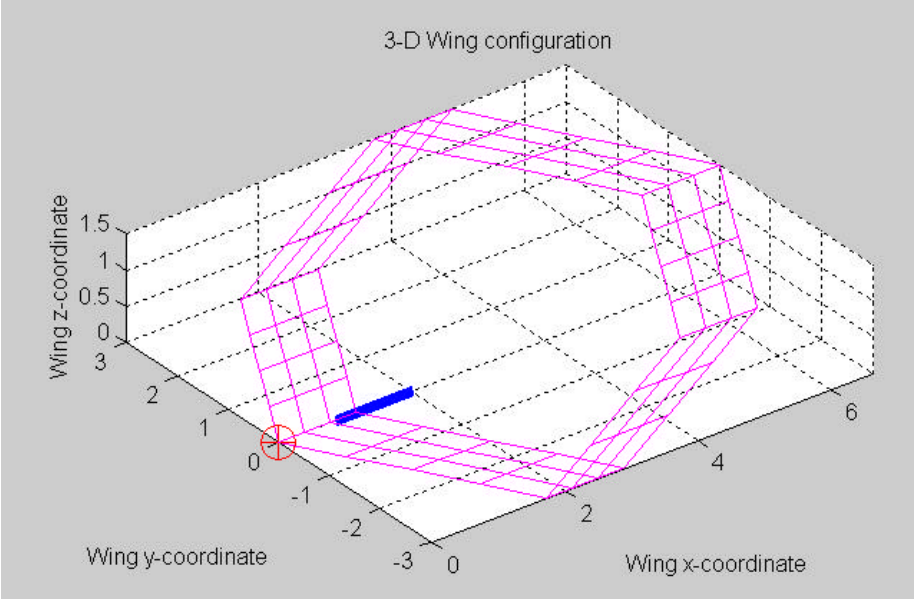

Figure D-1: Example of a preliminary box-wing configuration used for initial comparisons

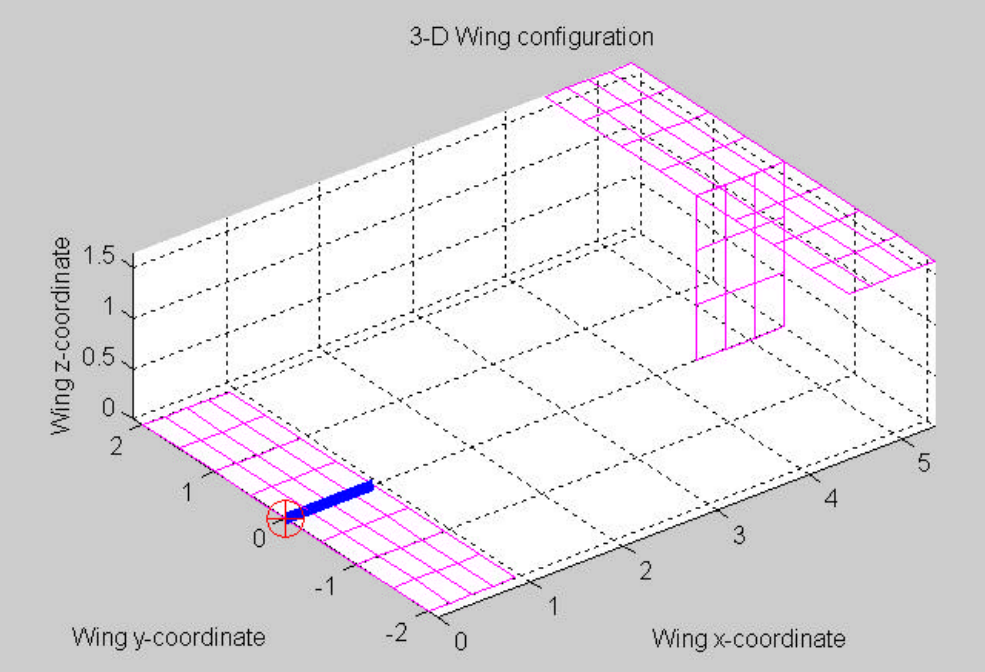

Figure D-2: Basic Tandem Wing configuration used for preliminary comparison purposes

Once the box-wing configuration was selected, modifications of the simple geometry used in the initial decision process were made. Efforts were made to make the computer model accurately reflect the designed aircraft for obvious reasons. Dihedral on the front wing and anhedral on the rear wing were added for stability and control reasons, as well as structural reasons. The anhedral and dihedral give a slightly more compact wing setup which requires slightly less structure and would be easier to manufacture.

The final wing configuration is shown in Figure D-3. The main characteristics of this wing are a larger area front wing with varying taper and a tapered rear wing. The varying taper on the front wing gives an unswept inboard trailing edge section of the wing. This straight trailing edge section was created to increase the effectiveness of the inboard flap from the swept trailing edge condition. Taper was added to the wings primarily from a structural point of view, in an effort to help reduce the structural weight of the wing. Though not obvious in the figure, the front wing has a 2.5° of washout twist, meaning that the wing is twisted 2.5° up at the root and 0° at the tip. This twist gives the aircraft a natural trim state while in the cruise configuration so that no elevator deflection is required to maintain straight and level flight.

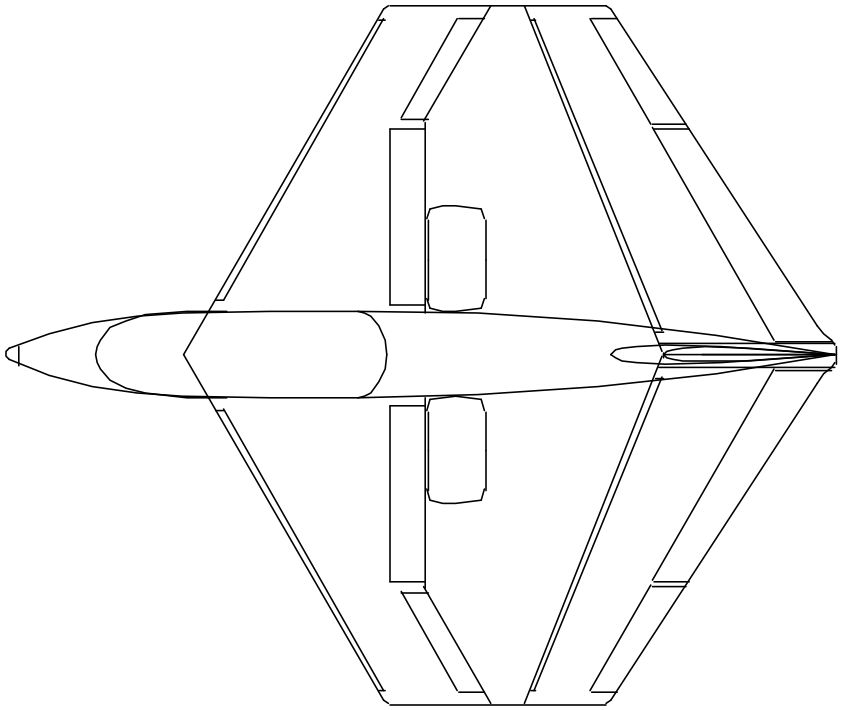

Figure D-3: Final wing planform geometry

All control surfaces for the aircraft are located on the rear wing, with elevators inboard and ailerons outboard. More detailed description of the elevator and aileron sizing and performance can be found in the stability and control appendix. The flap system for this setup consists of a straight trailing edge flap on the inboard section of the front wing as well as a trailing edge flap on the outboard section of the front wing. Automatically deploying leading edge slats are also located on the leading edge of the front wing and the rear wing has a fixed leading edge slat to ensure that the rear wing stalls well after the front wing.

D-2.2 Airfoil Selection and Flap System

Many airfoils were researched, including several 4-digit NACA airfoils, but the GAW-2 (also known as the NASA LS-1)[6] proved to have the best performance for our design. Data for this airfoil shows a high C_{Lmax} value at a fairly high angle of attack as shown in Figure D-4.[6] Another benefit of the LS-1 airfoil is its fairly thick profile. This profile gives room for supporting airframe structure and a large housing area for the flap system.

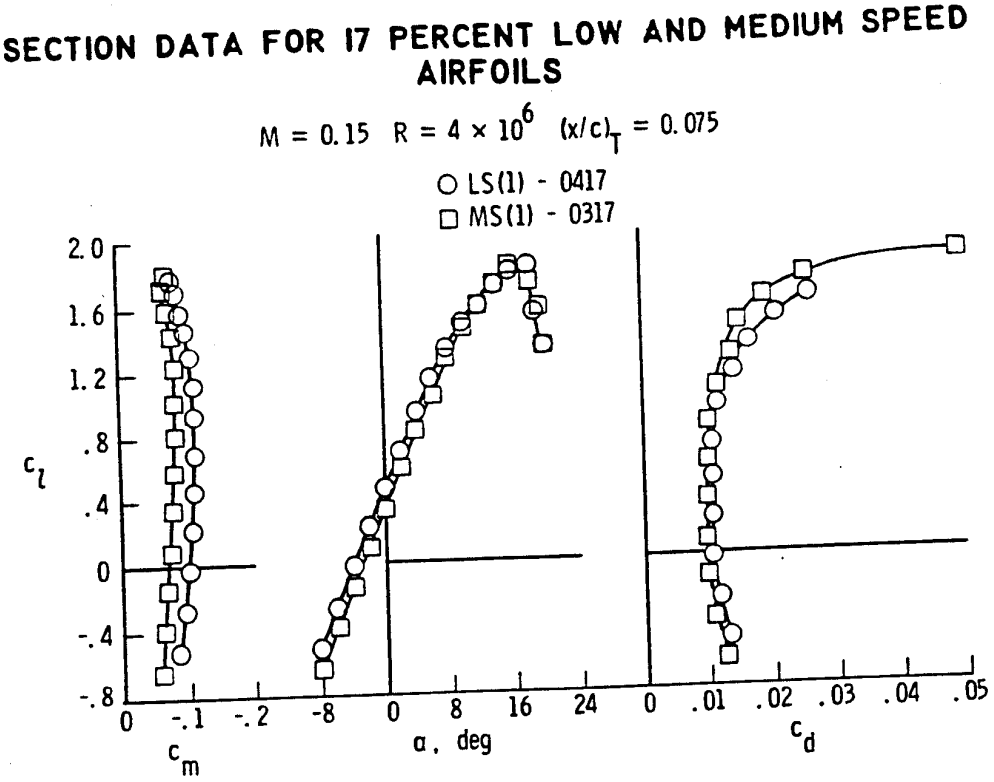

Figure D-4: C_L vs. Alpha for GAW-2 (LS-1) airfoil[6]

The flap system designed is a fixed-slot fowler type as shown in Figure D-5. This setup increases performance of a standard Fowler-type flap to nearly that of a double-slotted flap without the complex rigging required for a double slotted flap. The flap maintains a mechanical simplicity by keeping a slat fixed slightly above the leading edge of the flap. This system is employed on both the inboard and outboard trailing edge sections of the front wing, with a maximum flap deflection of 60° for each section. The leading edge of the front wing also employs spring loaded leading edge slats that deploy automatically at high angles of attack. When deployed, the stalling angle of attack is increased for the wing, allowing the wing to continue to higher lift coefficients.

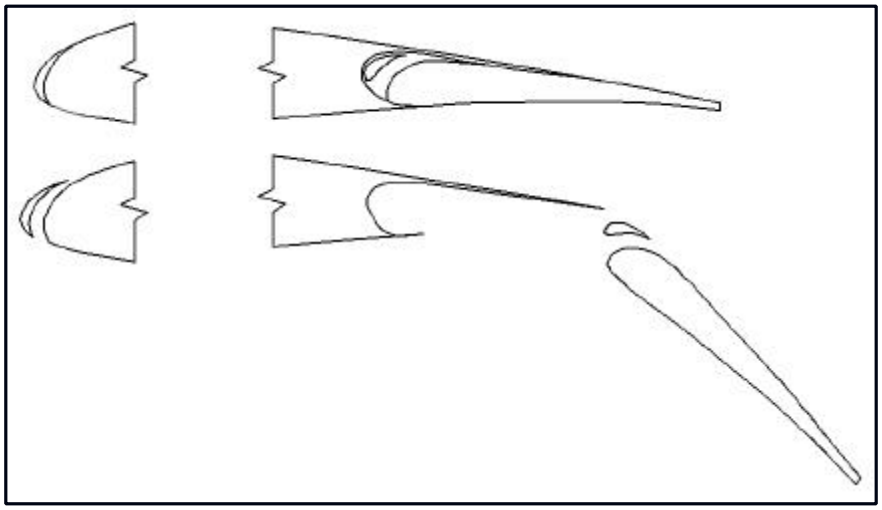

Figure D-5: Flap configuration retracted (top) and deployed 60° (bottom)

The concept of a Circulation Control Wing was examined as an alternative to mechanical high lift systems. Much research has been done on these types of systems by Robert Englar[7]. The basic principle of circulation control involves tangential blowing near the trailing and/or leading edges. Since lift is directly proportional to circulation, significant increases in lift can be obtained by increasing circulation. Research indicates that aerodynamic force augmentations of 80 to 100 can be achieved through appropriate application of this technology. The basic parameter in circulation control system is the blowing coefficient:

$$C_m = \frac{V_{jet}\,\dot{m}}{\frac{1}{2}Sr_\infty V_\infty^2} \qquad \text{(D-1)}$$

For a given lift coefficient increase, the test data collected by Englar[7] could be used to estimate the value of the blowing coefficient necessary. For Ikelos, it was estimated that a blowing coefficient of 0.2 was required. Estimations of the necessary mass flow and plenum pressure indicated that a circulation control system would pose a problem for the propulsion system. While a separate compressor could be installed exclusively to operate the circulation control system, this adds cost and complexity to the design. In addition, the issues of noise and system maintainability were also concerns. While increases in high lift performance were anticipated from the use of a circulation control system, they were outweighed by the concerns of successfully integrating such a system into the design of Ikelos.

D-3 WING LIFT CHARACTERISTICS

D-3.1 Lift Coefficient Calculations and Predictions

Tornado VLM was used to determine lift-curve slopes for the box-wing configuration. Since Tornado is limited to NACA-4000 series camberlines, a NACA airfoil profile that gave near results of an LS-1 airfoil was specified in the geometry. Results showed that a NACA-4509 gave a close approximation to the zero-lift angle of attack of the LS-1 airfoil and it was selected

for calculation purposes. Since Tornado is an inviscid vortex lattice method and hence cannot predict stall, it was not important that the NACA-4509 stall at the same angle of attack as the LS-1.

With the final wing configuration having an area distribution of 8.65m^2 (93.1ft^2) of area on the front wing and 6.62m^2 (71.3ft^2) on the rear wing, as shown in Figure D-3, Tornado analysis gave a lift curve slope (C_{La}) of 6.024 per radian (0.105 per degree), as obtained from the lift curve shown in Figure D-6. C_{LMAX} was estimated by assuming a stalling angle of approximately 15° based on published data and applying estimations to account for the effects of the auto-deploying leading edge slats[6,9]. Estimated C_{LMAX} values are 2.25 for the unflapped wing and 4.19 for full flaps, leading and trailing edge, in the landing configuration. The C_{LMAX} value for the flapped case also involved estimations from Render[9] to take into account the lift enhancements of the double slotted flap over the plain flap analyzed in the program.

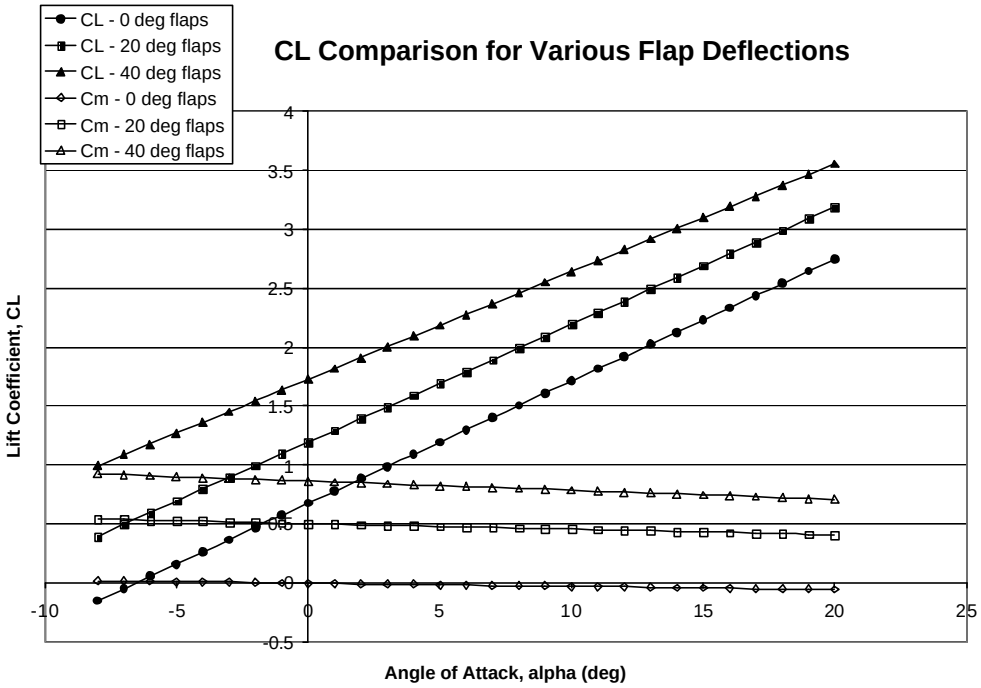

Figure D-6: Lift and moment coefficient data for final wing configuration

D-4 WING DRAG CHARACTERISTICS

D-4.1 Aircraft Drag

The following is a detailing of the calculations carried out for estimating the profile drag of the aircraft.

The following assumptions were made:

Cruise speed = 64 m/s
Landing speed = 19 m/s

All calculations use sea-level atmospheric conditions as follows:

$r = 1.225 kgm^{-3}$

$m = 1.8 \times 10^{-5} m^2 s^{-1}$

Reynolds numbers quoted are based on the length of the component and are calculated using:

$$R_l = \frac{lvr}{m} \quad \text{(D-2)}$$

Where:

R_l = Reynolds number based on length

l = Characteristic length of the component in the stream wise direction

m = Viscosity

r = Local air density

The following sections each deal with a different component of the aircraft.

D-4.2 Undercarriage Design

A comparison of the drag of retractable and fixed undercarriages was required to justify the decision to opt for a fixed system. In addition to the estimation shown below, cost and weight were also considered.

D-4.2.1 Undercarriage Drag Retractable Type

The aircraft was assumed to have a 3 wheel tricycle layout, the nose wheel having 2/3 the frontal area of the main wheels. The sizing of the undercarriage is based on data found in structures Appendix G.

From Render[9].

Based on frontal area:

$C_{d0\ strut}$ = 1.2

$C_{d0\ wheel}$ = 0.25

Assuming a wheel of diameter 0.361 m (14.2 in) and width 0.118 m (4.65 in) and a strut of total length 1 m (3.28 ft) and average diameter 0.1 m (3.94 in) for the main undercarriage a drag area can be calculated. Assume that the main undercarriage has a mutual interference factor, which increases the drag of each wheel by 1.2, and the nose is increased by 1.1.

$$C_{d0\_u/c} = C_{d0\_u/c\_wheel} S_{wheel} + C_{d0\_u/c\_strut} S_{strut}$$

$$C_{d0\_u/c\_wheel} S_{wheel} = \left(2C_{d\_front\_main\_wheel} S_{frontal\_main\_wheel}\right)\times 1.2 + \left(C_{d\_front\_nose\_wheel} S_{frontal\_nose\_wheel}\right)\times 1.1$$

$$C_{d0\_u/c\_strut} S_{strut} = \left(2C_{d\_front\_main\_strut} S_{frontal\_main\_strut}\right)\times 1.2 + \left(C_{d\_front\_nose\_strut} S_{frontal\_nose\_strutl}\right)\times 1.1$$

$$S_{wheel} = S_{frontal\_main\_wheel} + S_{frontal\_nose\_wheel}$$

$$S_{strut} = S_{frontal\_main\_strut} + S_{frontal\_nose\_strutl}$$

$$S_{frontal\_main\_wheel} = .361\times .118 = .0426$$

$$S_{frontal\_nose\_wheel} = .203\times .076 = .0154$$

$$S_{frontal\_main\_strut} = .1\times 1 = .1$$

$$S_{frontal\_nose\_strutl} = \tfrac{2}{3}\times .1 = .0667$$

$$\begin{aligned} C_{d0\_u/c\_wheel} S_{wheel} &= \left(2\times .25\times .0426\right)\times 1.2 + \left(.25\times .0154\right)\times 1.1 \\ &= .0316 \\ C_{d0\_u/c\_strut} S_{strut} &= \left(2\times 1.2\times .1\right)\times 1.2 + \left(1.2\times .0667\right)\times 1.1 \\ &= .376 \\ C_{d0\_u/c} &= \frac{.0316 + .376}{8.65} \\ &= .0469 \end{aligned}$$

D-4.2.2 Fixed Undercarriage Modification

From data provided by Hoerner the drag is reduced to 1/5 by using a well-faired fixed undercarriage[8].

$$C_{d0\_u/c} = \frac{0.0469}{5}$$

$$C_{d0\_u/c} = 0.00938$$

D-4.3 Wing Profile Drag

As previously mentioned many of the components use a combination of a flat plate skin friction calculation and factoring for interference and shape. The wing profile drag is calculated by this method:

$$C_{d0} = \frac{S_{wet}}{S} C_f QF \tag{D-3}$$

Where:

C_f = Skin friction coefficient, from equation D-2 above.
Q = Interference factor
F = Form factor of the component
S_{wet} = Wetted area of the component

For the wing the form factor is calculated using

$$F = \left[1 + \frac{0.6}{(x/c)}\left(t/c\right) + 100\left(t/c\right)^4\right]\left[1.34M^{0.18}\left(\cos\Lambda_m\right)^{0.28}\right] \tag{D-4}$$

Where:

x/c = Position of wing maximum thickness

t/c = Thickness to chord ratio

Λ_m = Sweep of point of maximum thickness

For the forward and aft wing the values estimated for this are shown in Table D-1, followed by the calculated values of *F*.

Table D-1: Form Factor Calculation for the Wings.

	Forward Wing	Aft Wing
x/c =	0.3	0.3
t/c =	0.15	0.15
Λ_m =	28^o	24^o
F – Landing	1.045	1.055
F – Cruise	1.300	1.313

A wetted area of 16.4 m^2 for the forward and 13.5 m^2 with a moderate interference factor of 1.05 assumed for both front and rear wings, giving final drag values as shown in Table D-2.

Table D-2: Drag estimations of the wings

C_{d0_wing}	Forward Wing	Aft Wing	Total
Cruise	0.0084	0.0072	0.0156
Landing	0.0084	0.0072	0.0156

D-4.4 Fuselage

The fuselage drag is estimated using a wetted area calculation as used for the wing. A form factor of 1.5 is used to account for the shape and irregularities on the surface. Calculation of the wetted area is completed using an estimation based on a number of cross sections along the length of the aircraft; this is described in more detail below.

Using the 3 view drawing of the aircraft it was possible to estimate the width and height of the fuselage at a number of positions. These were estimated to be roughly elliptical in shape and the following formula was used to find the perimeter.

$$Perimeter = p\sqrt{2\left(\left(\frac{height}{2}\right)^2+\left(\frac{width}{2}\right)^2\right)-\frac{\left(\frac{height-width}{2}\right)^2}{2}} \quad \text{(D-5)}$$

Each perimeter was then assumed to extend for a length of the fuselage based on its position. Each of these sections were added together to form the whole fuselage. Table D-3 shows the end result.

Table D-3: Surface area calculation points of fuselage.

Width	Height	a	b	Position	Length	Perimeter	Average	Area
0	0	0	0	0		0		
548.5	749.4	374.7	374.7	775.6	775.6	2354.3	1177.2	913001
736.0	1311.4	655.7	655.7	1906.2	1130.6	4119.9	3237.1	3659862
746.8	1372.8	686.4	686.4	2167.8	261.6	4312.8	4216.3	1102992
736.6	1419.3	709.7	709.7	2757.8	590.0	4458.9	4385.8	2587634
736.6	1403.9	702.0	702.0	3035.0	277.2	4410.5	4434.7	1229291
672.4	1312.7	656.4	656.4	3564.9	529.9	4124.0	4267.2	2261203
709.4	1219.4	609.7	609.7	3870.3	305.4	3830.9	3977.4	1214702
427.7	473.8	236.9	236.9	5644.7	1774.4	1488.5	2659.7	4719323
0	0	0	0	6302.0	657.3	0	744.2	489191

Summing up all the areas gives a total surface area of 18.2m^2 (195.9ft^2). Using the Fuselage length of 6.3m (20.67ft) this gives a $C_{d0\text{-fuselage}}$ of 0.0096 in the landing configuration and 0.0079 in cruise.

D-4.5 Vertical Surfaces

Drag of the vertical surfaces (including the fin and the end plates on the wing) is calculated by using a flat plate approximation. As such the form factor is assumed to be 1. Interference factors for the end plates are estimated at 1.1 and for the fin 1.2. The dimensions and final drag values are shown in Table D-4.

Table D-4: Drag of vertical surfaces.

		End Plates	**Fin**
Length (m)		0.55	1.01
Wetted Area (m^2)		2.76	3.23
C_{d0}	**Cruise**	0.0014	0.0017
	Landing	0.0018	0.0021

D-4.6 Ducts

The drag of the ducts is calculated using the same method as the wings. The ducts are assumed cylindrical and the wetted area is calculated as the outside surface of an open cylinder. The form factor is calculated using equation D-5. The duct diameter is measured to be 0.93 m and the length 0.5 m.

$$F = 1 + 0.35\left(d/l\right) \tag{D-6}$$

This gives a C_{d0} of 0.0035 in the landing configuration and 0.0028 in the cruise.

D-4.7 Flaps

The method for determining the drag caused by flap deflection is taken from Render.[9] It must be noted that this method gives only a very rough estimate of the result and further analysis will be required. Equation D-6 will determine the drag of a flap based on the wing area. The drag for the flaps are shown in Table D-5.

$$C_{d0\_flap} = 0.00023 \frac{b_{flap}}{b} \frac{S_{wing}}{S} d_{flap} \tag{D-7}$$

Where
b_{flap} = Flap span
d_{flap} = Flap deflection in degrees

Table D-5: Drag due to flap deflection.

		Forward Wing
b_{flap} **(m)**		4.16
d_{flap} **(Degrees)**		60
C_{d0}	**Cruise**	0 – no deflection
	Landing	0.0774

D-4.8 End Plate Influence On Drag

As previously discussed the end plates on the wings contribute to the profile drag of the aircraft, increasing it by 0.0014 in the cruise condition. Apart from the structural benefits of having the end plates they also have an affect on the induced drag of the aircraft. This must be calculated in order to justify their inclusion on the aircraft. To do this, two separate calculations were carried out using the Tornado code - one with the end plates and one without endplates. Table D-6 gives details of the drag penalties. It is obvious from the results that including the end plates gives an overall drag reduction, despite the extra skin friction.

Table D-6: Drag benefits of endplates.

	With End Plates	Without End Plates
Induced Drag	0.087	0.097
Profile Drag Penalty	.0014	0
Total	0.0884	0.097

D-4.9 Induced Drag

The induced drag of the aircraft is calculated by use of the *Tornado* VLM as discussed previously in this appendix. The results from the method were used to find a value of k in the drag polar equation shown below.

$$C_D = C_{d0} + kC_l^2 \tag{D-8}$$

The value of k was found to be 0.05; this is a relatively low value due to the influence of the end plates as discussed previously.

D-4.10 Total Drag

Figure D-7 shows the breakdown of the drag in the cruise condition (64 m/s, 124 knots) and Figure D-8 the breakdown in the landing configuration (19 m/s, 37 knots). Total profile drag in the landing configuration is heavily dominated by the flaps on the forward wing, constituting almost 2/3 of the total profile drag. The drag coefficient in this configuration is 0.1263. In the cruise configuration the value is reduced to 0.0458. As mentioned previously, all of the drag coefficients are based on a reference area of the forward wing area, and may appear large from the use of this small reference area.

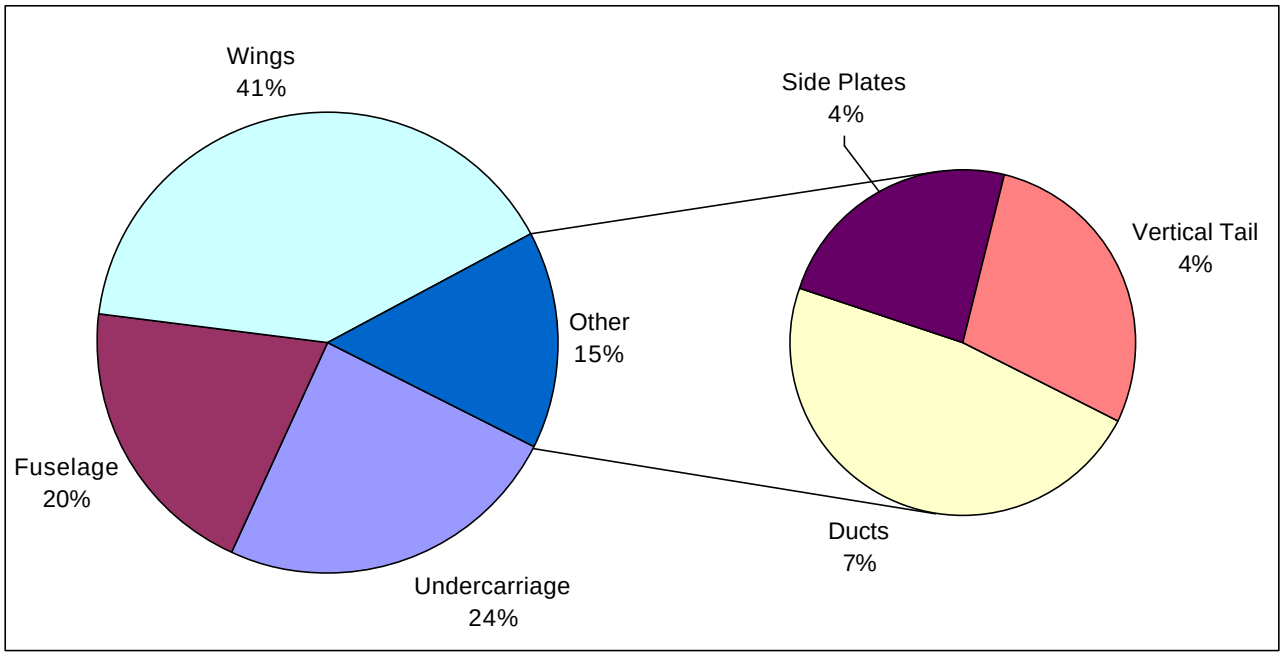

Figure D-7: Profile drag breakdown in cruise configuration

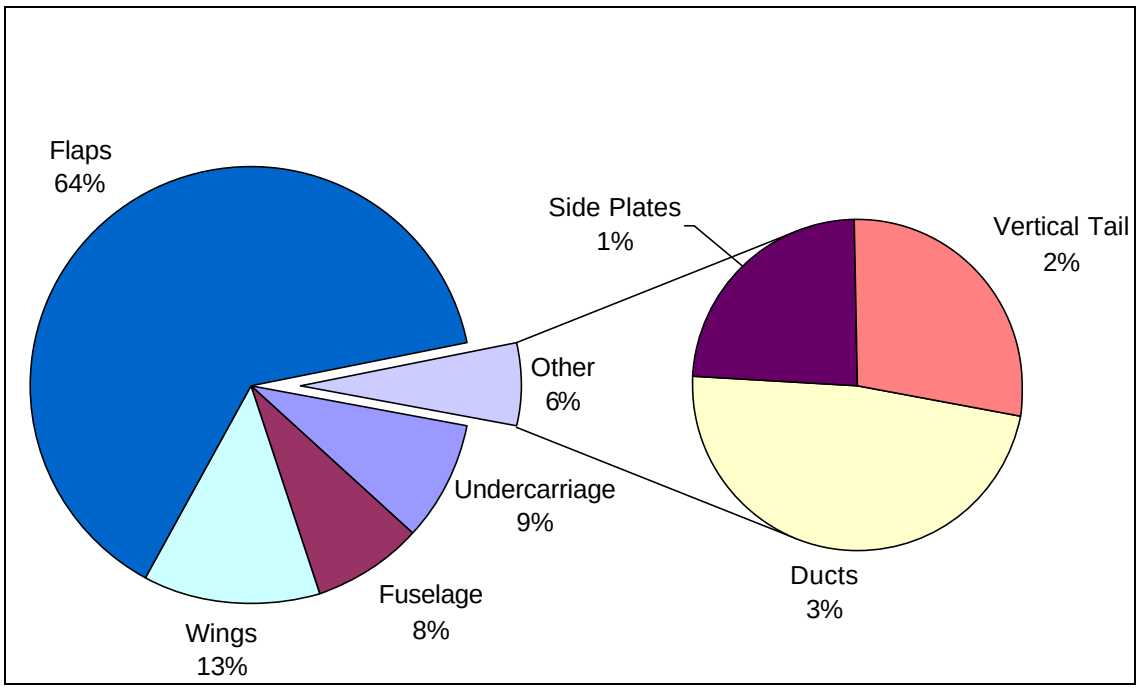

Figure D-8: Profile drag breakdown in landing configuration

REFERENCES

1. Melin, T., Vortex Lattice Method, "Tornado1.2", http://www.flyg.kth.se/Tornado/htm/tornado.htm.

2. Abbott, I. H. and Von Doenhoff A. E., *Theory of Wing Sections*, Dover Publications Inc., New York, 1959.

3. Wolkovitch, J., "The Joined Wing: An Overview," AIAA 23rd Aerospace Sciences Meeting Paper 85-0274, AIAA, 1985.

4. Kroo, I., McMasters, J., Smith, S., "Highly Nonplanar Lifting Systems," September 26-28, 1995.

5. Melin, T., Vortex Lattice Method, "Tornado1.2", http://www.flyg.kth.se/Tornado/htm/tornado.htm.

6. Marchman, J. F., "Notes on Supercritical Airfoils," Department of Aerospace and Ocean Engineering, Virginia Tech, 1990.

7. Englar, Robert J., "Numerical Simulations of the Steady and Unsteady Aerodynamic Characteristics of a Circulation Control Wing Airfoil", AIAA Paper 2001-0704, AIAA, 2001.

8. Hoerner, S. F., *Fluid Dynamic Drag: Practical Information on Aerodynamic Drag and Hydrodynamic Resistance*, Hoerner Fluid Dynamics, Midland Park, NJ, 1958.

9. Render, P. M., "Departmental Publication No. 38: An Intro To Fixed Wing Aircraft Performance," Loughborough University, Loughborough, UK, 2001.

Appendix E: Stability and Control

TABLE OF CONTENTS

E-1 INTRODUCTION……..E-5
E-2 LONGITUDINAL STATIC STABILITY AND CONTROL……... E-6
E-2.1 Stability Requirements…… E-6
E-2.2 Configuration Study…… E-8
E-2.3 Dihedral Study…… E-13
E-2.4 Twist Study……. E-15
E-2.5 Flap Study……... E-17
E-2.6 Elevator Sizing…… E-19
E-2.7 CG Location and Movement……... E-22
E-3 LATERAL STATIC STABILITY AND CONTROL……... E-24
E-3.1 Stability Requirements…… E-24
E-3.2 Dihedral Study…… E-24
E-3.3 Rudder Sizing……. E-25
E-3.4 Aileron Sizing……. E-26
E-4 CONTROL FORCES/STICK FORCES…… E-28
E-5 DYNAMIC STABILITY……... E-32
E-5.1 Stability Requirements…… E-32
E-5.2 Approach…… E-32
E-5.3 Longitudinal Dynamics……...E-37
E-5.4 Lateral-Directional Dynamics…… E-43
E-6 DESCRIPTION OF DERIVATIVES…… E-43
E-6.1 Longitudinal…… E-43
E-6.2 Lateral-Directional…….. E-44
REFERENCES…….. E-46

LIST OF FIGURES

Figure E-1 Box-Wing Configurations for Longitudinal Stability Analysis
Figure E-2 Lift Coefficient versus Alpha for the Box-Wing Configurations
Figure E-3 Pitching Moment Coefficient vs. Angle of Attack for the Box-Wing Configurations (X_{cg} = 2.95 meters)
Figure E-4 Tandem Wing Configurations for Longitudinal Stability Analysis
Figure E-5 Lift Coefficient versus Alpha for the Tandem Wing Configurations
Figure E-6 Pitching Moment Coefficient vs. Angle of Attack for the Tandem Wing configurations (X_{cg} = 2.95 meters)
Figure E-7 Base Configuration (no dihedral/anhedral, symmetric airfoils, body area modeled as a flat plate)
Figure E-8 Lift and Pitching Moment Coefficient Curves for different Dihedral Settings
Figure E-9 C_L vs. Alpha for the different Twist Configurations
Figure E-10 C_m vs. Alpha for the different Twist Configurations
Figure E-11 Configuration Plot for the Flap Analysis (units in meters)

Figure E-12 Change in Aerodynamic Coefficients as a function of Flap Deflection Angles
Figure E-13 Aileron and Elevator Location and Size in Relation to the Aircraft
Figure E-14 Trim cross-plot in cruise configuration
Figure E-15 CG Excursion for Various Weight Configurations
Figure E-16 C_n and C_Y vs. Beta for Different Dihedral Settings
Figure E-17 Rudder Location and Size in Relation to the Rest of the Aircraft
Figure E-18 Historical Data for Aileron Sizing
Figure E-19 Control Forces versus Control Deflections in Landing
Figure E-20 Control Forces versus Control Deflection in Cruise
Figure E-21 Variation of Thrust with Airspeed
Figure E-22 Aircraft Geometry Model with Fuselage Approximation

LIST OF TABLES

Table E-1 Estimated Neutral Points for Each of the Box-Wing Configurations
Table E-2 Estimated Neutral Points for Each of the Tandem Wing Configurations
Table E-3 Control Derivatives for the Front and Rear Flap Deflections
Table E-4 Elevator control derivatives in Cruise and Landing Configurations
Table E-5 CG Locations for Different Weight Configurations
Table E-6 $C_{l\beta}$ for Different Wing Dihedral Angles under the Basic Configuration
Table E-7 Required Rudder Performance
Table E-8 Calculation of the Control Surface Hinge Moments
Table E-9 Maximum Permissible Control Forces
Table E-10 *Tornado* Derived Non-Dimensional Longitudinal Stability & Control Derivatives (Cruise)
Table E-11 *Tornado* Derived Non-Dimensional Longitudinal Stability & Control Derivatives (Landing)

LIST OF SYMBOLS

(Descriptions of the coefficient derivatives listed below are located in Section E-7)

m	Mass
$\bar{c}$	Mean aerodynamic cord length
$\bar{q}_{ref}$	Reference dynamic pressure
S	Reference wing area
h	Center of gravity location (percentage of MAC from the wing apex)
h_n	Neutral point location (percentage of MAC from the wing apex)
h_{min}	Maneuverability point location (percentage of MAC from the wing apex)
K_n	Static Margin
L	Lift force
D	Drag force
Y	Side force
p	Roll-rate
q	Pitch-rate
r	Yaw-rate
C_L	Lift coefficient
C_D	Drag coefficient
C_Y	Side force coefficient
C_l	Rolling moment coefficient
C_m	Pitching moment coefficient (Pitch Stiffness)
C_{m0}	Zero lift pitching moment coefficient
C_n	Yawing moment coefficient
C_{lp}	Change in rolling moment coefficient with roll-rate
C_{Lq}	Change in lift coefficient with pitch-rate
C_{lr}	Change in rolling moment coefficient with yaw-rate
$C_{L\alpha}$	Change in lift coefficient with angle of attack
$C_{l\beta}$	Change in rolling moment coefficient with sideslip (Roll Stiffness)
C_{mq}	Change in pitching moment coefficient with pitch-rate
$C_{m\alpha}$	Change in pitching moment coefficient with angle of attack
$C_{m\delta e}$	Change in pitching moment coefficient with elevator deflection

C_{np}	Change in yawing moment coefficient with roll-rate
C_{nr}	Change in yawing moment coefficient with yaw-rate
$C_{n\beta}$	Change in yawing moment coefficient with sideslip (Yaw Stiffness)
C_{yp}	Change in side force coefficient with roll-rate
C_{yr}	Change in side force coefficient with yaw-rate
$C_{y\beta}$	Change in side force coefficient with sideslip
D_{ref}	Drag at reference conditions
I_X	Roll moment of inertia
I_{yy}	Pitch moment of inertia
I_{zz}	Yaw moment of inertia
V_{ref}	Reference velocity
V_{stall}	Stall velocity
α	Angle of attack
α_{0L}	Zero lift angle of attack
β	Sideslip angle
ω_n	Un-damped natural frequency
w_n^2 / n_a	Control anticipation parameter
ζ	Damping ratio

E-1 INTRODUCTION

For any aircraft, the stability and control analysis is vital to its success since it determines the maneuverability and effective "usefulness" of the design. In the case of a general aviation aircraft, such as Ikelos, they must be statically stable, safe to maneuver, and have good flying qualities. The following sections detail the static and dynamic stability analysis of Ikelos, and the determination of control surface type, size, and placement.

Many excellent sources were used to analyze Ikelos, including Roskam[1,2], Etkin and Reid[3], and Raymer[4]. The USAF DATCOM[5] was also used for initial estimations. Due to the unique box-wing design, many of the methods described by the above books had to be used with care since most were for monoplane configurations (one main wing and a small horizontal tail/canard). The methods could often be made relevant by re-introducing factors ignored in conventional wing-tail derivations.

Of particular use in the stability and control analysis was the MATLAB-based vortex lattice code *Tornado*. Details on this programs origins, abilities, and limitations can be found in Appendix D. The program's ability to model plain flap control surface deflections was used in most of the control power estimations. Longitudinal stability derivatives were also produced by the program, though lateral-directional stability derivatives were more difficult to obtain. This was due to the difficulty in accurately modeling the fuselage inside of *Tornado*. Ikelos was designed using a combination of this vortex lattice method and conventional methods found in the above resources.

The conventional body axis system described by Etkin[3] was used in Ikelos' stability and control analysis. The longitudinal equations of motion are:

$$C_L = a(a - a_{oL}) = \frac{2W}{rv^2 S} \tag{E-1}$$

$$C_m = C_{mOL} + C_{m,a}(a - a_{0L}) + \left(\frac{T}{qS_w}\right)(z_{thrust} - z_{cg}) = 0 \tag{E-2}$$

The lateral-directional equations of motion are:

$$C_y = C_{y,b}b + C_{y,p}p + C_{y,r}r \tag{E-3}$$

$$C_l = C_{l,b}b + C_{l,p}p + C_{l,r}r \tag{E-4}$$

$$C_n = C_{n,b}b + C_{n,p}p + C_{n,r}r \tag{E-5}$$

Equations (1)-(5) are shown without the control device effects. These will be discussed in the sections that follow.

E-2: LONGITUDINAL STATIC STABILITY & CONTROL

E-2.1: Stability Requirements

The above mentioned aircraft flying qualities and stability requirements are defined by many sources. The requirements for longitudinal static stability are simply that the pitching moment at zero-lift angle of attack, C_{m0}, must be positive and that the derivative of the pitching moment with respect to the angle of attack, $C_{m\alpha}$, must be negative.[2] These two requirements are determined mainly by the wing configuration. The following sections go into more detail on the specific effects that each part of the wing configuration has on the aircraft's static stability.

E-2.2: Configuration Study

This study is meant to give a stability and control analysis (primarily longitudinal) of the effectiveness of different box-wing designs. Four box-wing variations (Figure E-1) were tested with *Tornado* to look at the lift, pitching moment, and yawing moment characteristics for each configuration. All surfaces were modeled with flat plates to reduce processor times. Therefore, the results only show the relative differences between each configuration, not the actual values that these configurations would achieve with airfoils. Each configuration had an equal amount of lifting area (14 m^2 (150.7 ft^2)) and wingspan (6 m (19.7 ft)). All of the configurations used planar wings (no dihedral or anhedral) so that the actual planform wing layout is the only variable. Vertical surfaces were also placed at the wing tips to complete the box-wing design in every case. A flat vertical surface that extending from the apex of the front wing to the trailing edge of the rear wing with height of 0.75 meters (2.5 ft) was used to model the body of the aircraft. This modeling scheme assumed the nose of the fuselage coincided with the apex of the front wing. The fuselage is a very rough estimate since its area extends beyond the wing apex and is not a rectangle. The model was used since the error in the fuselage modeling mainly affects the lateral directional stability, which is much more dependant on the unset vertical fin size than the fuselage itself. The vertical fin in each case was 0.75 meters (2.5 ft) high with a chord length of 1.165 meters (3.8 ft). This made the vertical distance between wings 1.5 meters (4.9 ft). This sizing was only an initial guess since the vertical fin hadn't been sized yet. The primary goal of this study was to look at the longitudinal static stability inherent to each configuration, and to find a configuration with desirable lifting and static stability characteristics.

All force and moment coefficients were calculated with a reference area of 14 square meters (150.7 ft^2). There is a serious question as to the appropriate representative area for a box-wing. In other sections of this report only the area of the front wing was used in the calculation of coefficients. The use of the entire (both wings) planform area results in aerodynamic coefficients which are lower than normal, while the use of the planform area of only the front wing gives high values of most coefficients. The coefficient values cited in this portion of the report are, therefore, about half the magnitude of those used in some other sections. The CG location (moment reference) was chosen such that it would lie in the general vicinity of its final position between the pilots and the engine. The reference was set at 2.95 meters (9.7 ft) behind the wing apex (for every test) to fulfill this requirement. This way, rough estimates of static stability could be obtained. Likewise, the moment could be transferred to find a configuration's neutral point (where the pitching moment does not change with angle of attack). After deciding on the procedure for this study, the next step was to define the different configurations to be tested.

Box-Wing 1: Figure E-1 (a) shows the equally swept wings creating a diamond shape with the leading edge of the tip of the rear wing directly over the trailing edge of the tip of the front wing (overall length is 6.631 meters (21.8 ft)).

Box-Wing 2: Figure E-1 (b) shows the completely unswept front wing and forward swept back wing to connect its tip leading edge to the front wing's trailing edge (overall length is 6.33 meters (20.8 ft)).

Box-Wing 3: Figure E-1 (c) shows the swept front wing and unswept back wing configuration (overall length is 6.614 m (21.7 ft)). The sweep was determined by making the front wing's trailing edge meets up with the rear wings leading edge (at the tip).

Box-Wing 4: Figure E-1 (d) shows the slightly swept front and back wings (overall length is 6.99 meters (22.9 ft)). The sweep angles are the same for both wings creating a diamond shape similar to the first option, but with a larger horizontal separation.

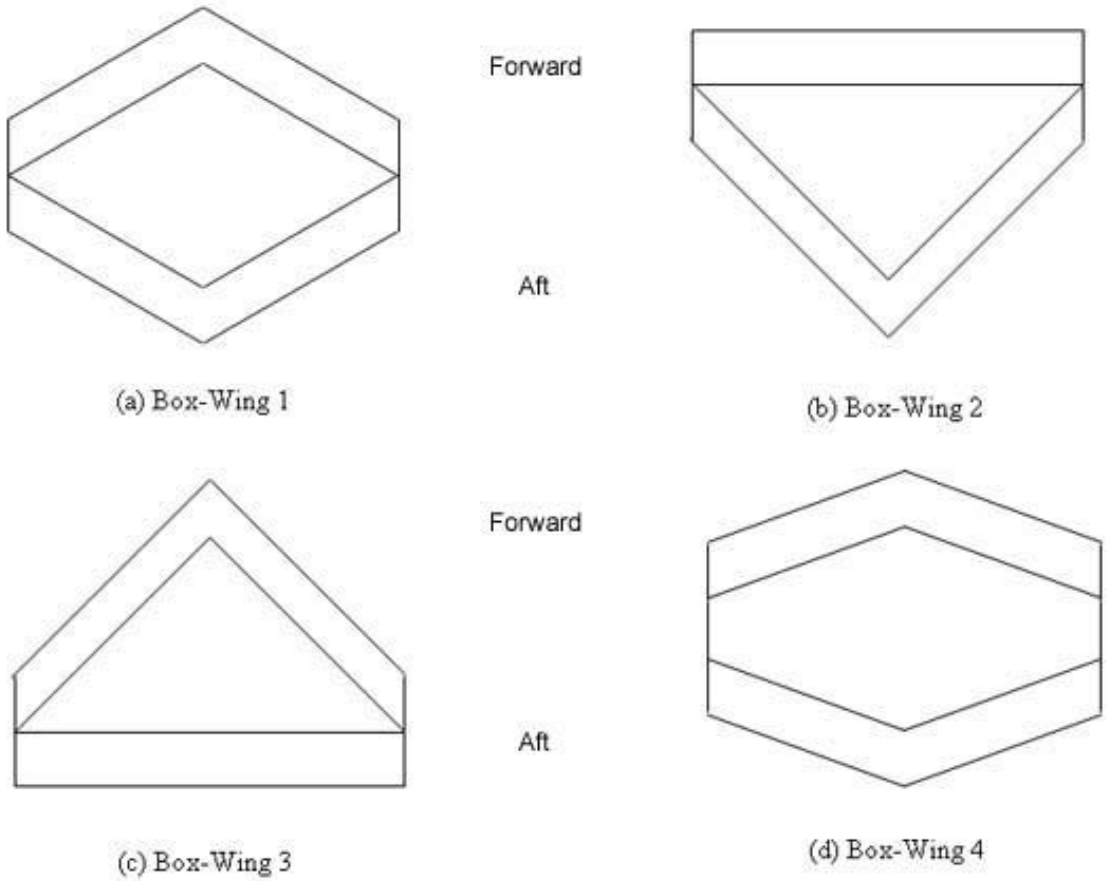

Figure E-1: Box-Wing Configurations for Longitudinal Stability Analysis

Figure E-2 shows the lift curve slopes of the four box wing configurations. The lift coefficient plot doesn't say much about a configuration's stability, but it is useful to determine their aerodynamic performance. Option 4 has a slightly higher lift curve slope due to its small amount of sweep and the wings' large horizontal separation. Since all the cases are fairly close,

the longitudinal stability will be a major deciding factor for the wing layout. Figure E-3 shows the pitching moment about the estimated CG location (2.95 meters (9.7 ft) from the wing apex). The second configuration is extremely unstable with its large positive $C_{m\alpha}$, the 3rd is overly stable (large negative $C_{m\alpha}$). Options 1 and 4 are marginally unstable assuming that the CG is in its correct location, which it's not. The point of this analysis is to show that no matter what is done, configuration 2 may never be stable, configuration 3 may be too stable for reasonable control forces, and that configurations 1 and 4 are in a reasonable envelope to work with.

A more useful interpretation of this data comes from performing a moment transfer to obtain each configuration's neutral point. This is done by examining the relationship between the moment at two points at positions x_1 and x_2 with a given C_L. When the derivative with respect to alpha is taken, the following equations are obtained [3]:

$$C_{m2} = C_{m1} + C_L (x_2 - x_1) \quad \text{(E-6)}$$

$$C_{m\alpha 2} = C_{m\alpha 1} + C_{L\alpha} (x_2 - x_1) \quad \text{(E-7)}$$

$C_{m\alpha 1}$ is the slope of the moment curve at the CG location, x_1 = 2.95 m (9.7 ft). The neutral point at x_2 can be found using the above equations so that $C_{m\alpha}$ at x_2 is equal to zero. Table E-1 presents the results of the moment transfers for each configuration.

Configuration	Neutral Point (m from apex)
Box 1	2.726 (8.94 ft)
Box 2	1.544 (5.07 ft)
Box 3	4.053 (13.3 ft)
Box 4	2.810 (9.22 ft)

Table E-1: Estimated Neutral Points for Each of the Box-Wing Configurations

A test case was run using the neutral point as the moment reference point to make sure that $C_{m\alpha}$ would indeed be zero. The moment curve about the neutral point was found to be close to horizontal, with only a very slight slope. The discrepancy could be due to lack of complex paneling scheme or error in vertical location of the reference point. Since the slope is very small, the above points were considered the neutral point of each configuration for comparison. For longitudinal static stability, the CG must be forward of the neutral point creating the negative pitch stiffness. For a reasonable static margin, the above results would place the CG behind the engine for configuration 3, ahead of the pilot for configuration 2, and slightly behind the pilot for configurations 1 and 4. Therefore, configurations 1 and 4 are the best options for maintaining static longitudinal stability during flight.

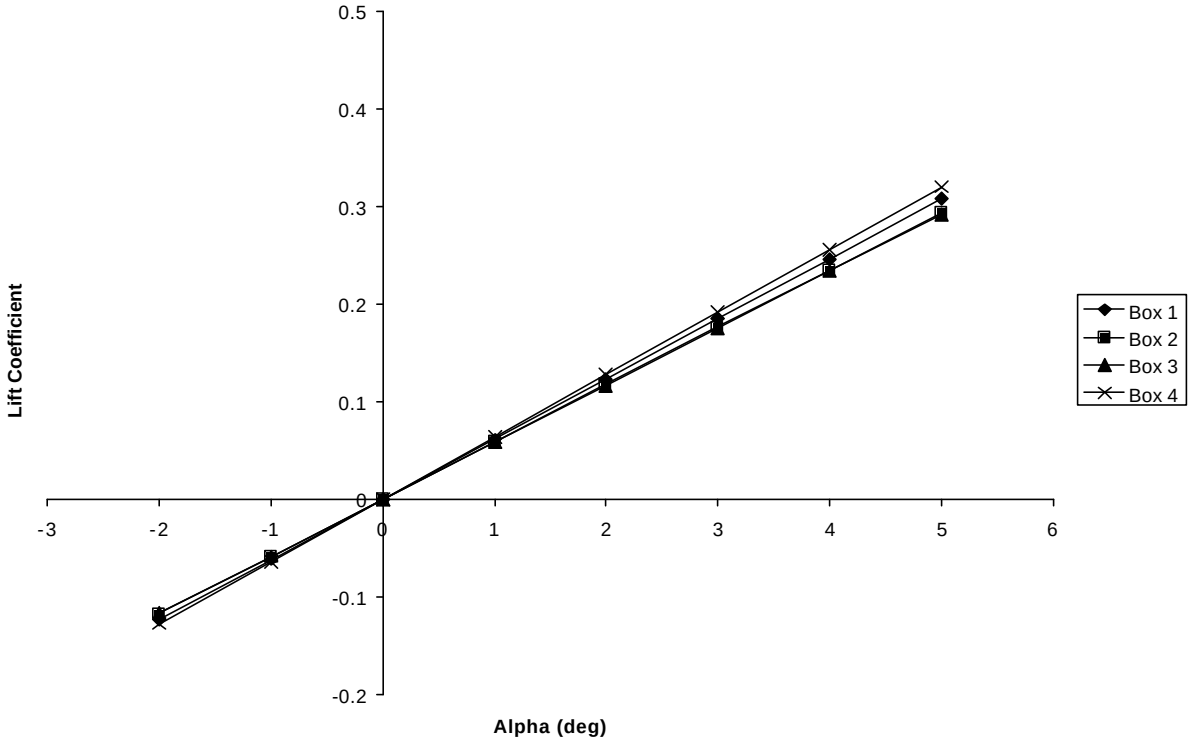

Figure E-2: Lift Coefficient versus Alpha for the Box-Wing Configurations

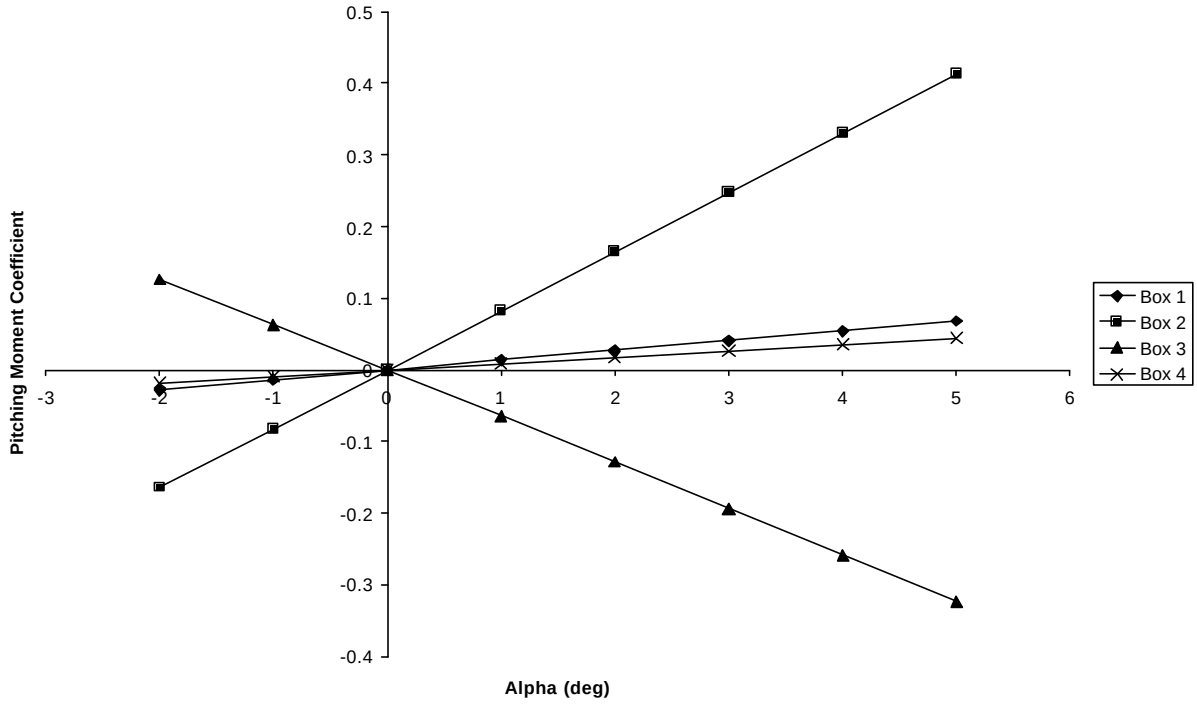

Figure E-3: Pitching Moment Coefficient vs. Angle of Attack for the Box-Wing Configurations (X_{cg} = 2.95 meters (9.7 ft)))

With the box wing results suggesting that the aerodynamic performance increased as sweep angle decreased and horizontal separation increased, it became necessary to look a tandem wing-type configuration. The tandem wing, or lifting canard, layout would be the maximum extent of this observation. Four combinations of lifting surfaces with the same wing area as the box-wing designs were examined. When a lifting canard was used, the span of the rear wing was increased to keep the area constant. All wing sections were modeled with flat plates as before with chords of 1.165 meters (3.82 ft). These configurations used the same fuselage and vertical tail design as the box-wings.

Tandem 1: Figure E-4 (a) consists of a lifting canard (4 meter (13.1 ft) span) and an unswept rear wing 1.5 meters (4.9 ft) above the front wing (8 meter (26.2 ft) span).

Tandem 2: Figure E-4 (b) consists of a lifting canard (2 meter (6.6 ft) span) and an unswept 10 meter (32.8 ft) span rear wing that is 1.5 meters (4.9 ft) above the front wing.

Tandem 3: Figure E-4 (c) is a pure tandem wing configuration with unswept front and rear wings, both with spans of 6 m (19.7 ft) and a vertical separation of 1.5 m (4.9 ft).

Tandem 4: Figure E-4 (d) is a variation of the first option with the rear wing swept forward 30 degrees. This will effectively move the CG and aerodynamic center forward to compensate for the aft positions in the first two options.

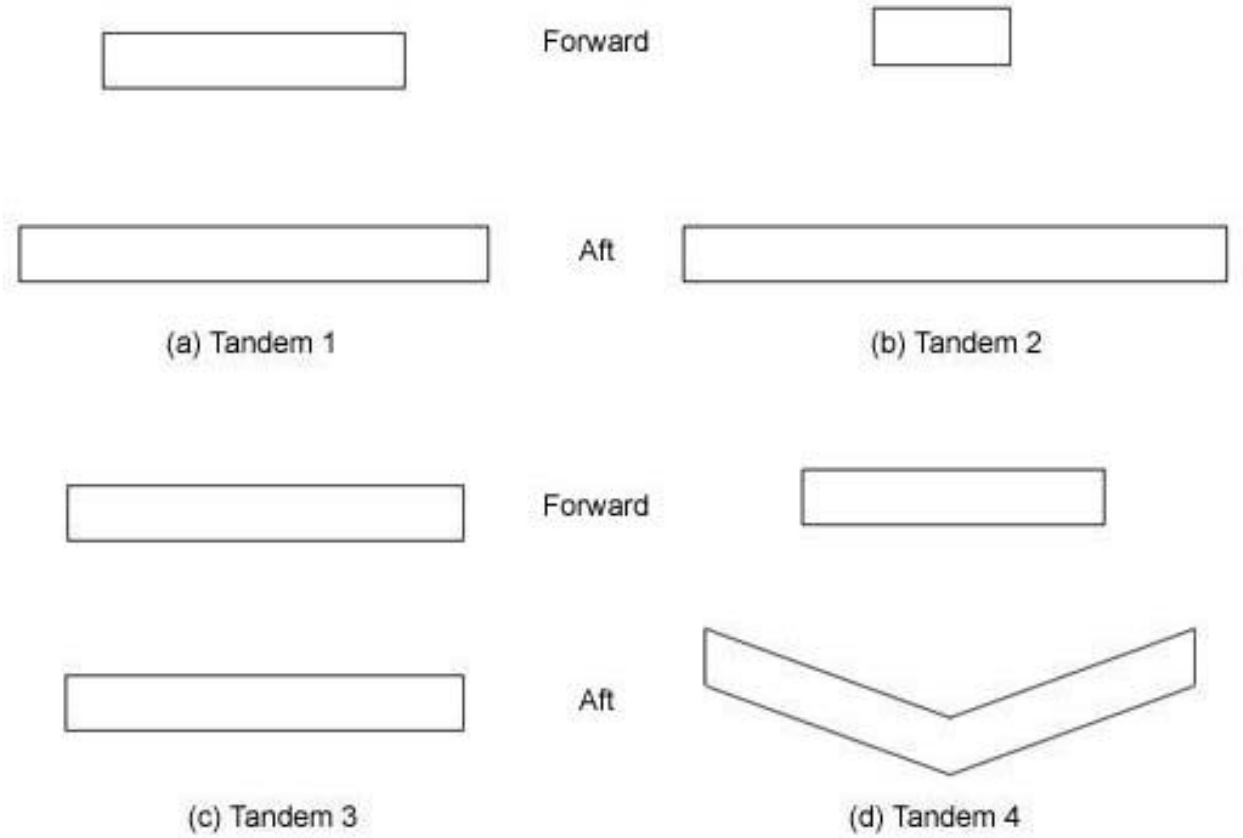

Figure E-4: Tandem Wing Configurations for Longitudinal Stability Analysis

Figure E-5 shows the lift curve slopes of the four tandem wing configurations. The highest box wing slope (box configuration 4) is included for comparison purposes. All of the lifting canard configurations have higher lift curve slopes than the highest of the box wings. As with the box-wing layouts, the lift coefficient plot is used only as a reference to make sure that stability can still play a major role in deciding the wing layout. The 1st and 2nd lifting canard configurations have notably higher slopes, but as discussed below, have a neutral point much too far aft to be used. Despite their aerodynamic benefits, these two configurations must be disregarded. Configurations 3 and 4 have more acceptable neutral points so they will continue to be compared against the box-wing designs presented above.

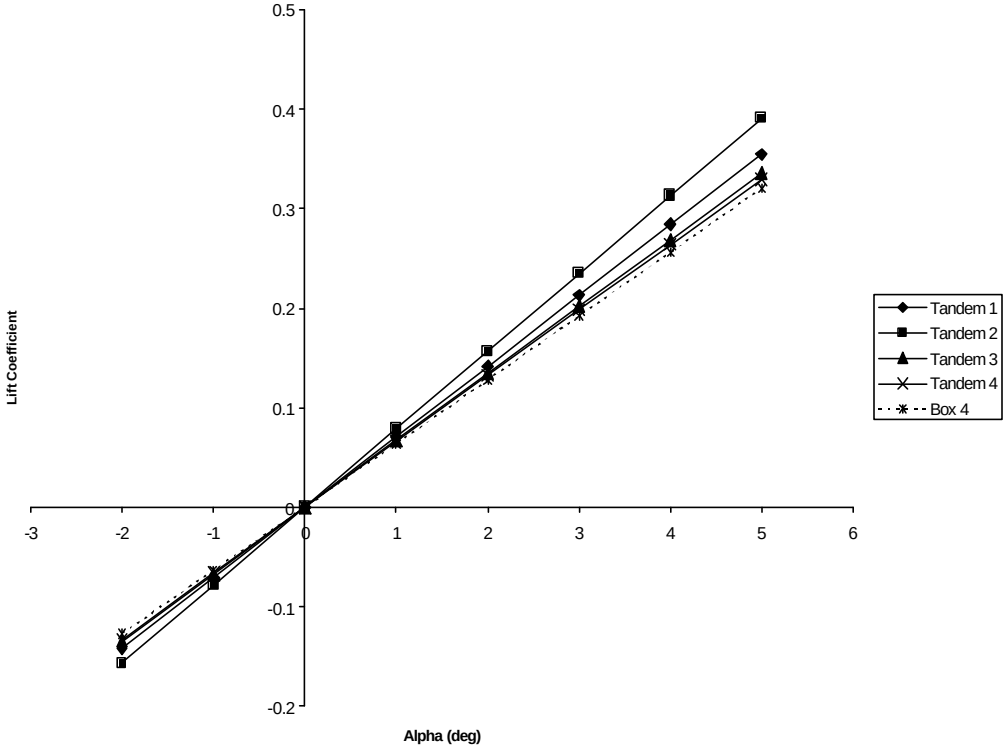

Figure E-5: Lift Coefficient versus Alpha for the Tandem Wing Configurations

Figure E-6 shows the moment curves for the tandem wing configurations as well as the fourth box-wing. From this plot, the most reasonable configuration for negative pitch stiffness is the 4th lifting canard configuration. It has the least negative $C_{m\alpha}$ because of the sweep on the back wing decreasing the lift that is farther away from the CG location (moment reference point). Using the methods presented when examining the box-wing configurations, the neutral points were calculated for these configurations and the results are in Table E-2.

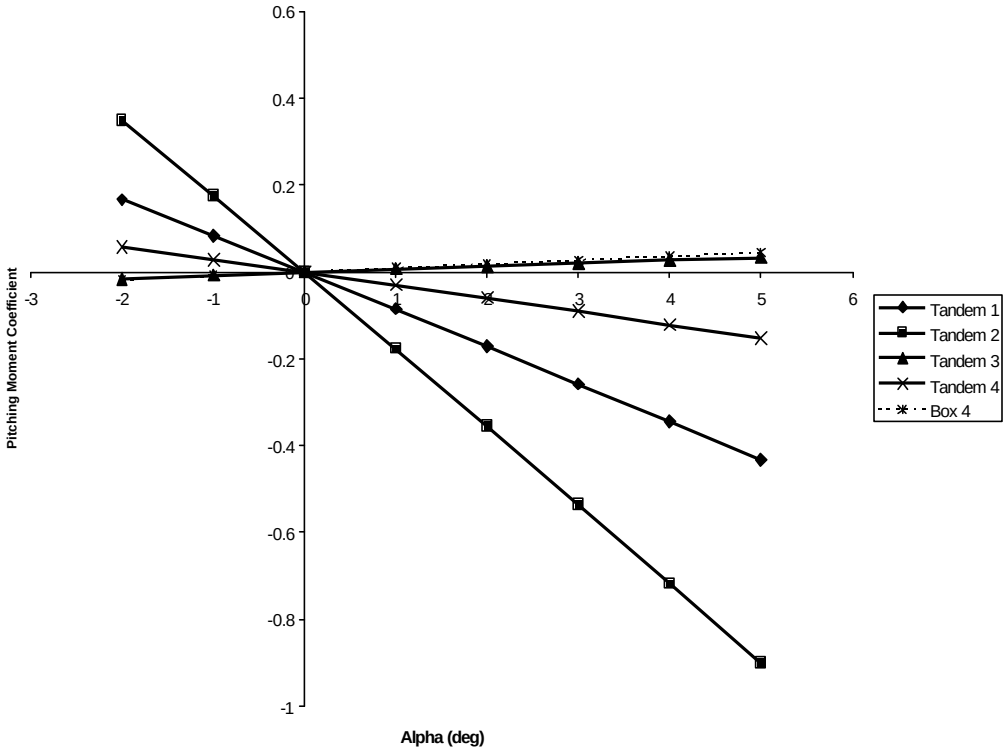

Figure E-6: Pitching Moment Coefficient vs. Angle of Attack for the Tandem Wing Configurations (X_{cg} = 2.95 meters (9.7 ft))

Configuration	Neutral Point (m from apex)
Tandem 1	4.158 (13.64 ft)
Tandem 2	5.230 (17.16 ft)
Tandem 3	2.848 (9.34 ft)
Tandem 4	3.404 (11.17 ft)

Table E-2: Estimated Neutral Points for Each of the Tandem Wing Configurations

Cases 1 and 2 are too far aft for unassisted control force requirements. The 3rd configuration has a neutral point in the same neighborhood as the realistic box wing cases (1 and 4), and the 4th configuration, which had a forward swept rear wing, has a neutral point roughly right at the engine location. The CG locations for the 3rd and 4th configurations are in acceptable locations.

Of the configurations tested, the 2nd tandem wing configuration had the most desirable lift curve slope. At the same time, it had the most undesirable neutral point (too far aft). Other than this case, all of the layouts (box and tandem wings) were aerodynamically similar, with the lifting canard slightly edging out the box wing. The discrepancy in lift curve slopes was over a range of about 0.02 /deg (1.15 /rad). Aerodynamically, it would be best to have the highest lift curve slope, but not a great deal is lost by picking a lower one. The real differences came in the neutral point locations. The CG is likely to be located between the cockpit and the engine, which would place it at around 3 m (9.8 ft) from the front wing apex. The exact CG location and analysis is presented in Section 2.7 of this Appendix.

A configuration should be picked such that the neutral point is slightly behind the CG location for longitudinal static stability. The above study shows two ways this can be done: a box wing that has more sweep on the front wing than the back wing (somewhere between box configurations 1 and 3), or with a lifting canard configuration with a forward swept rear wing (like the lifting canard configuration 4). Both had very similar lift curve slopes, and longitudinal stability can be obtained fairly easily by shifting the CG or making small tweaks to the wings. Since the two configurations are very close, the box wing will be used since it structurally stronger (Appendix G).

E-2.3 Dihedral Study

Based on DATCOM [5] methods, the CG position was estimated for the base model used (Figure E-7) and used as the moment reference center in *Tornado*. The wings were modeled as flat plates to decrease the complexity in this study by eliminating a variable: camber. Alpha sweeps were run for a variety of front and rear wing dihedral angles to determine the affects of dihedral on longitudinal static stability. Figure E-8 shows the lift and pitching moment coefficient versus alpha plots for the various configurations.

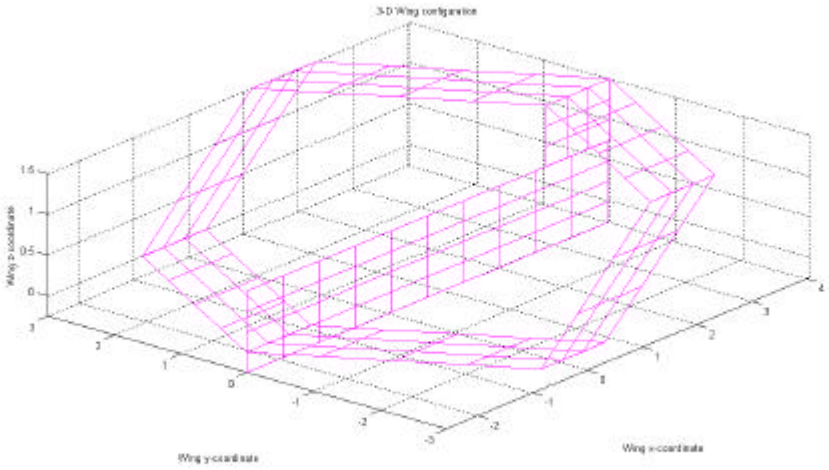

Figure E-7: Base Configuration (no dihedral/anhedral, symmetric airfoils, body area modeled as a flat plate)

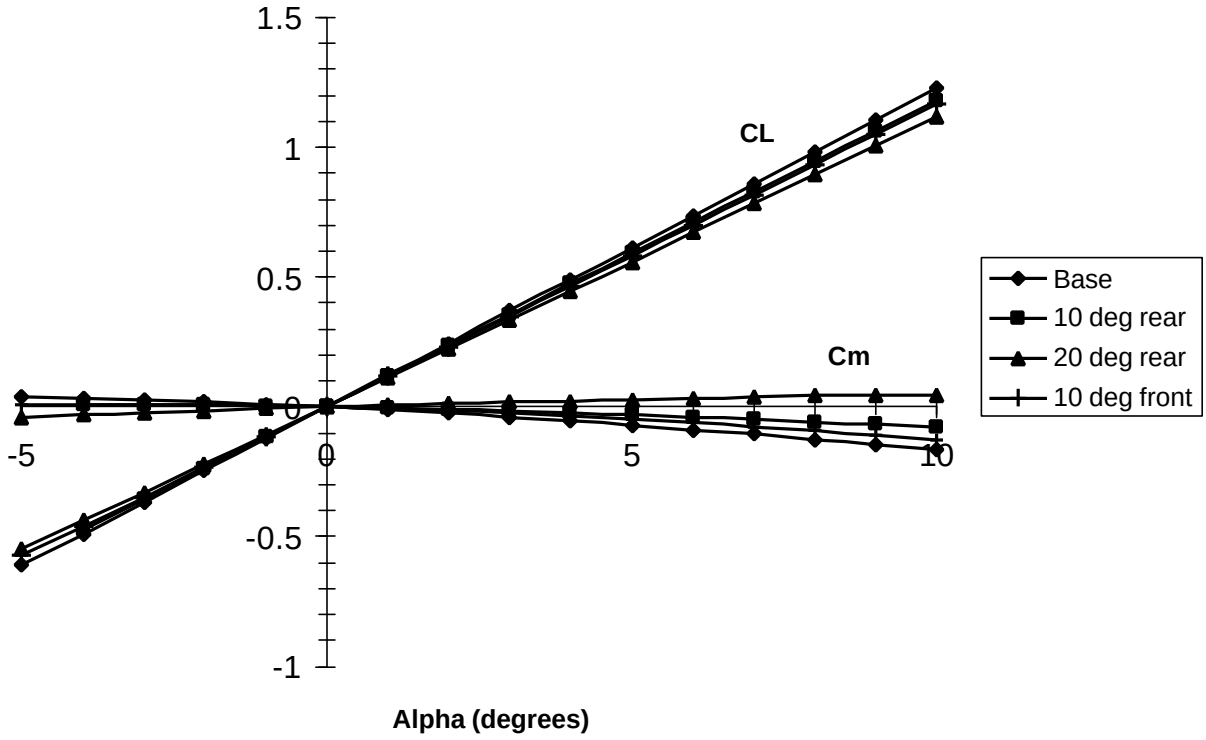

Figure E-8: Lift and Pitching Moment Coefficient Curves for different Dihedral Settings

As expected, an increase in dihedral leads to a decrease in lift curve slope. This is due to the increased immersion of the back wing in the front wing's downwash. The dihedral angles have a much larger impact on the pitching moment coefficients. Most importantly, when the anhedral angle on the back wing is increased from 10 to 20 degrees, $C_{m\alpha}$ becomes positive. This positive pitch stiffness makes the model statically unstable (longitudinally). The positive $C_{m\alpha}$ is brought about by the back wing's loss of lift and the subsequent "pitch-up" attitude. This study was used as a preliminary test to determine what angles for dihedral and anhedral would be the most appropriate for this design. The presence of rear-wing anhedral produces favorable results, but excessive angles not only diminish lift performance, but cause pitch instability. Without other changes to the wing configuration, such as twisting, the maximum rear anhedral angle was set to 10 degrees. This is a very rough limit to the angle since the process was used as an initial test to help determine the aircrafts initial design. The accuracy of this study could be increased by generating a higher density paneling scheme for the vortex lattice code. However, since the error was common to each test, it was considered negligible when comparing similar configurations.

E-2.4 Twist Study

Adding the desired GAW-2 airfoil to the once flat plate wings created a large problem: a negative C_{m0}. Having a negative pitching moment at zero lift angle of attack signifies a large imbalance in the lift distribution between the two surfaces. In this case, the lift on the back wing is too large making the pitching moment coefficient positive. For most aircraft with a positively-cambered main surface, a down-force is required on the rear surface to make C_{m0} positive [3]. With the design's CG location, it is possible to either generate a down-force on the rear wing or to redistribute the lift. The first option is very undesirable because for the slow landing speeds, the aircraft needs as much lift as it can generate. Therefore, the second option was researched further by twisting the wings. Using *Tornado* to perform quick and accurate calculations for the different twist configurations, trends were observed that would help to pick a better wing configuration. All configurations were based on the basic geometry in Figure E-7 with a CG location of 3.306 m (10.8 ft) from the nose, giving a 10% static margin. Figures E-9 and E-10 show the comparative aircraft lift curve curves and pitching moment curves respectively. The main options used in this study are:

Option 1: Uncambered, untwisted rear surface. The loss of C_{mac} from the rear wing gives a positive C_{m0}, by giving up a lot of lift. The uncambered rear wing was chosen because it is more suitable for elevators.

Option 2: Uncambered, twisted rear surface. Some of the lift can be recovered by "washing in" the wing so the inboard portion is providing a down-force at =0 degrees.

Option 3: Cambered, twisted rear surface. The camber gives better lift performance, as long as the inboard section isn't producing too much lift (that area contributes the most to moment calculations). However, elevators on the cambered sections would require more range to achieve the same pitch control as an uncambered wing would.

Option 4: Cambered, untwisted rear surface with incidence given to the front surface. Since the other options were getting fairly poor lift values, a small amount of incidence (around 2 or 3 degrees) was added to the front wing. This increased the lift ahead of the CG (front wing), allowing the back surface to be positively loaded and still have a positive C_{m0}.

Option 5: Combinations of Options 3 and 4 with incidence angles given to front and rear wings.

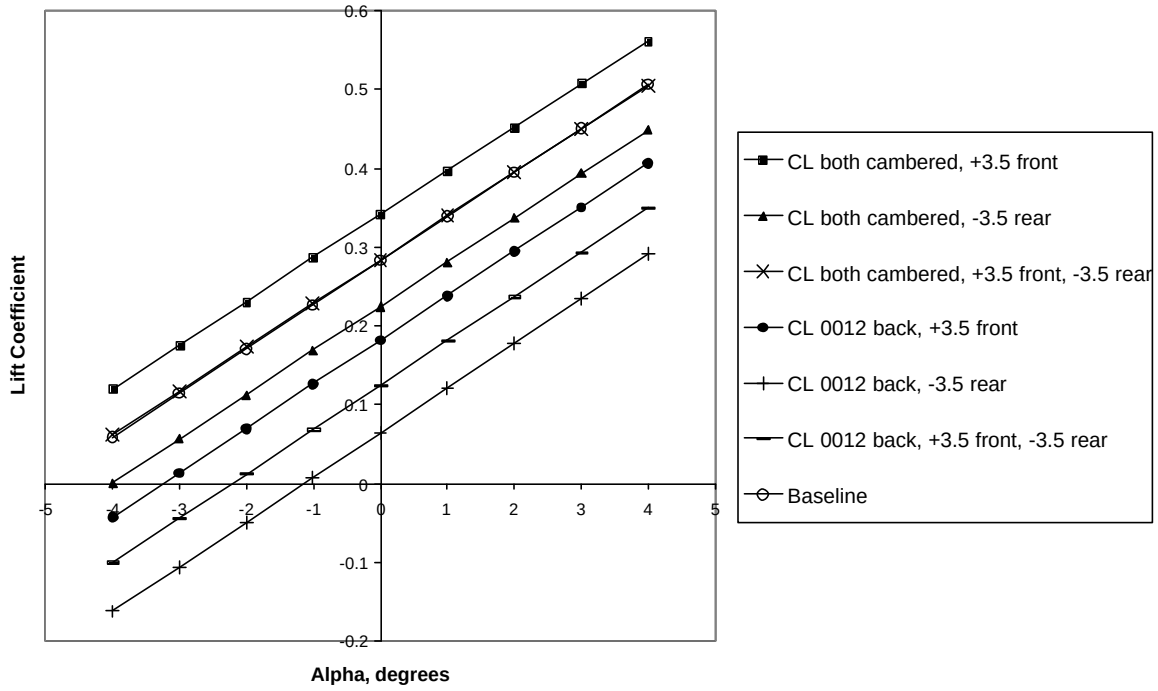

Figure E-9: C_L vs. Alpha for the different Twist Configurations

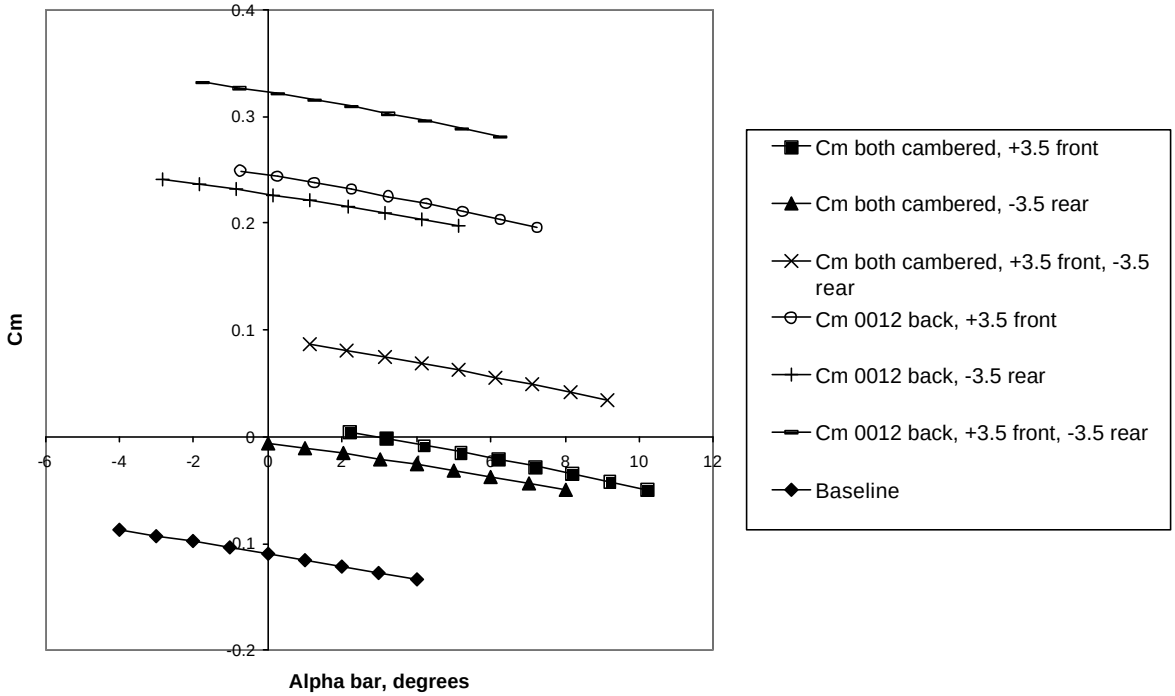

Figure E-10: C_m vs. Alpha for the different Twist Configurations

E-2.5 Flap Study

Flaps and other control surfaces add a lot of complexity to the stability and control issues for the different flight conditions (i.e. landing and cruise). In order to determine the best way to place the different control surfaces, various configurations were proposed and tested using *Tornado*. The first control surfaces analyzed were the 80% span 25% chord flaps on both the front and rear wings with the GAW-2 airfoil on the configuration in Figure E-11. Initially, flaps were desired on both wings in order to produce the needed lift for the slow landing speeds. Delta sweeps were performed for both the forward and back wing flaps (separately) by deflecting the flaps from zero degrees to sixty degrees down in five degree intervals. The zero degree deflections were used to double check the configurations for each case to make sure the lift, drag and pitching moment coefficients were all equal in the same flight conditions. All measurements were taken about the cg location of 2.92 m (9.58 ft) from the nose and 0.5 m (1.64 ft) up from the apex of the wing. In order to get data that is easily comparable with other test cases, the simulation was run at straight and level flight conditions at a speed of 25 m/s (82 fps).

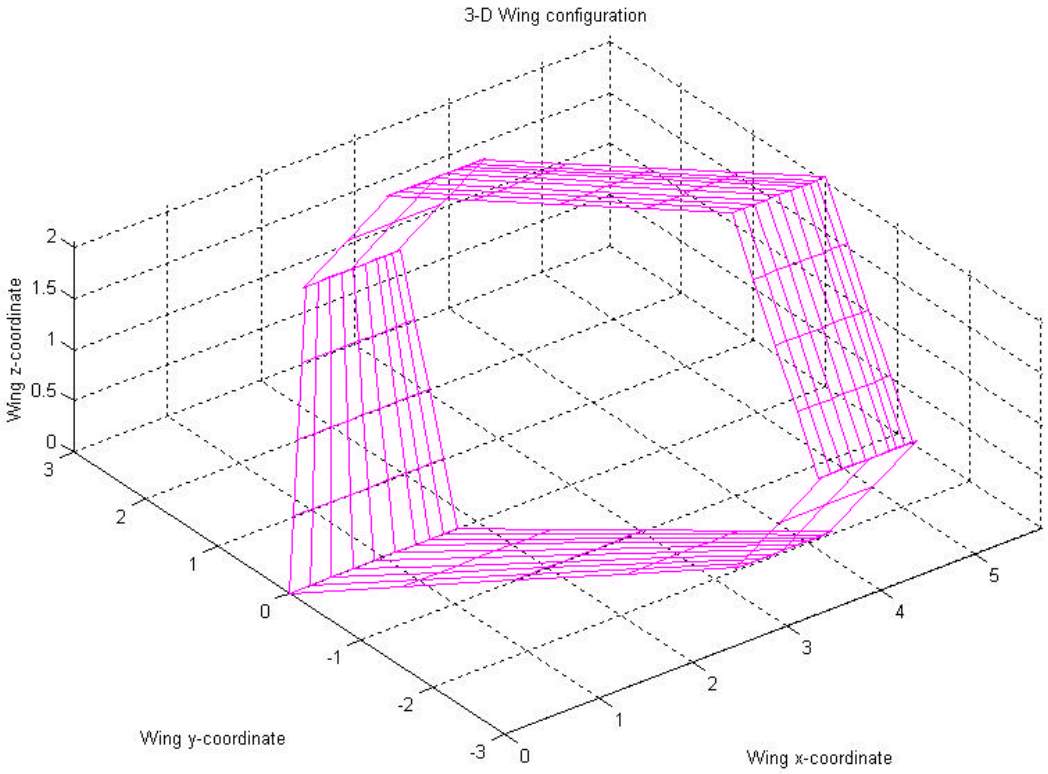

Figure E-11: Wing Configuration Plot for the Flap Analysis (units in meters)

The output generated by *Tornado* consisted of the changes in the lift, drag and pitching moment coefficients at the different deflection angles. As is expected, the coefficients increased (or decreased depending on their slopes) from their original values of no deflection. The plots in Figure E-12 represent the slightly curved relationships between the coefficients and the flap deflection. In order to maintain the simplicity of this initial approximation, linear least-square fit lines were applied to the curves to determine the control derivatives for each flap. These derivatives are presented in Table E-3 for both the front and rear wing flaps. The pitching

moment curves had the most amount of error in these approximations due to their larger curvature. Although this had the most error out of the coefficients examined, the R^2 value was only around 0.99, representing a loss in accuracy but not too dramatic.

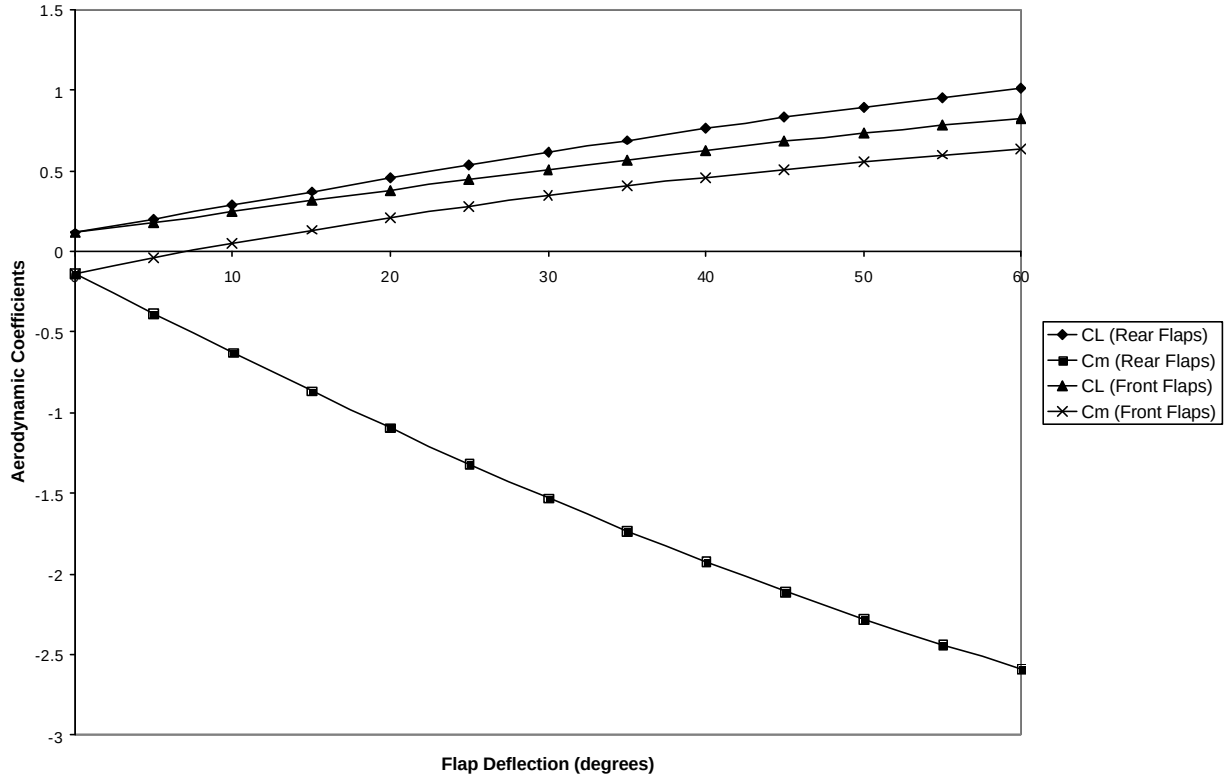

Figure E-12: Change in Aerodynamic Coefficients as a function of Flap Deflection Angles

Control Derivatives (Front)		Control Derivatives (Rear)	
CL-delta-e (per deg) =	0.012	CL-delta-e (per deg) =	0.0151
Cm-delta-e (per deg) =	0.0128	Cm-delta-e (per deg) =	-0.0411
CD-delta-e (per deg) =	0.0017	CD-delta-e (per deg) =	0.0019

Table E-3: Control Derivatives for the Front and Rear Flap Deflections

The lift and drag both increase with greater flap deflections as expected. The main cause for the increased drag is the induced drag increase from the larger amounts of lift. The rear wing is able to produce slightly more lift at a given flap deflection, so in this respect it would seem that if only one wing is used with flaps, it would be the rear wing. However, lift cannot be the only deciding factor. The pitching moment is crucial for the aircraft's longitudinal static stability. The aircraft itself is stable with the current wing configuration because the neutral point is located behind the cg location (creating a negative $C_{m\alpha}$). Unfortunately, the static margin of 0.3 is very large under in this configuration, which may make the aircraft over stable and unable to rotate on takeoff. With this in mind, the large negative pitching moment generated by the rear wing flaps would make the aircraft almost impossible to control. In order to balance this effect, the forward wings would have to generate a positive pitching moment of the same magnitude. As seen in Figure E-12, the forward flaps can only counter up to about 5 degrees of deflection of the rear flaps. This huge difference in pitching moment is caused by the large

differences in moment arms between the two wings. The forward wing is located very close to the cg whereas the rear wing is at a large distance from the cg being at the aft of the aircraft. In order to maintain control of the aircraft, the amount of lift generated under this limited deflection case, is almost entirely done by the front wing. There is no point in having flaps on the rear wing if they cannot be deflected enough to generate a significant amount of lift. Therefore flaps were set to the front wing and the rear wing would be used for other control surfaces: elevators and ailerons. These control surfaces would be sufficient to counter any pitching moment generated by the front wing. Having flaps only on the front wing can generate a change in lift coefficient of around 0.9, which should be enough to increase the aircraft's C_{Lmax} to the required value during landing of approximately 4.

E-2.6 Elevator Sizing

Ikelos trims itself longitudinally using plain flap elevators on the rear wing. Elevator deflections (through an angle, d_e) produce changes in both C_m and C_L which must be analyzed to appropriately size the control surfaces. As stated by Etkin [3], these increments are linear with elevator deflection, which is a fair assumption at high Reynolds Numbers. By adding a term to equations (1) and (2), such that in any aircraft attitude or flap setting the aircraft can be trimmed (C_m=0), the longitudinal equations become:

$$C_L = a(a - a_{oL}) + C_{L,df}d_f + C_{L,de}d_e = \frac{2W}{rv^2S} \tag{E-8}$$

$$C_m = C_{mOL} + C_{m,a}(a - a_{0L}) + C_{m,df}d_f + C_{m,de}d_e + \left(\frac{T}{qS_w}\right)(z_{thrust} - z_{cg}) = 0 \tag{E-9}$$

The pitching moment due to thrust is ignored since the line of application of the thrust nearly coincides with the vertical CG location. The high-lift device's contribution ($C_{m,df}$) was calculated by the aerodynamics group (Appendix D). The primary concern in elevator sizing is the "control power", $C_{m,de}$. Since the moment produced by the elevator is directly proportional to the tail volume, placing the elevators as far behind the CG as possible maximizes their effectiveness. The natural location for Ikelos' configuration is the inboard section of the rear wing.

Equation (9) is written for pitching about the center of gravity, which is accurate when the aircraft is in flight. However, as described by Raymer[4], the condition which generally dictates the necessary elevator control power is rotation in takeoff. This is due to the slow speeds at rotation, thus low dynamic pressures, and the fact that the aircraft is now rotating about the main landing gear, which must be aft of the CG. These factors combine to reduce the elevator's effectiveness, which requires more elevator area.

Using takeoff rotation as the constraint on elevator size, the following equation was used from Roskam[1]:

$$S_h = \left\{W\left(X_{mg} - X_{CG} + mZ_{mg}\right) - L_{wf}\left(X_{mg} - X_{ac} + m_g Z_{mg}\right) - Cm_{ac}q_{rot}S\bar{c} - I_{yy}\ddot{q}\right\} / \left\{q_{rot}\left(X_{ac} - X_{mg} + m_g Z_{mg}\right)C_{Lh\max}\right\} \tag{E-10}$$

where S_h is the elevator area, 'mg' denotes the main gear. Using a rotation speed of 19.8 m/s (65 fps), equation (9) gives the necessary area to be 2.7 m^2 (29.1 ft^2). Since some of the trailing edge space must be reserved for the ailerons, as little span length as possible was used to obtain this area. Following structural requirements, a flap chord fraction of 0.30 was selected. Using simply geometry, the elevator span was found to be 2.03 m (6.7 ft) as seen in Figure E-13. This is approximately 2/3 of the rear wing span. While this value seems high, it is not unreasonable given the difficult requirement imposed by takeoff rotation.

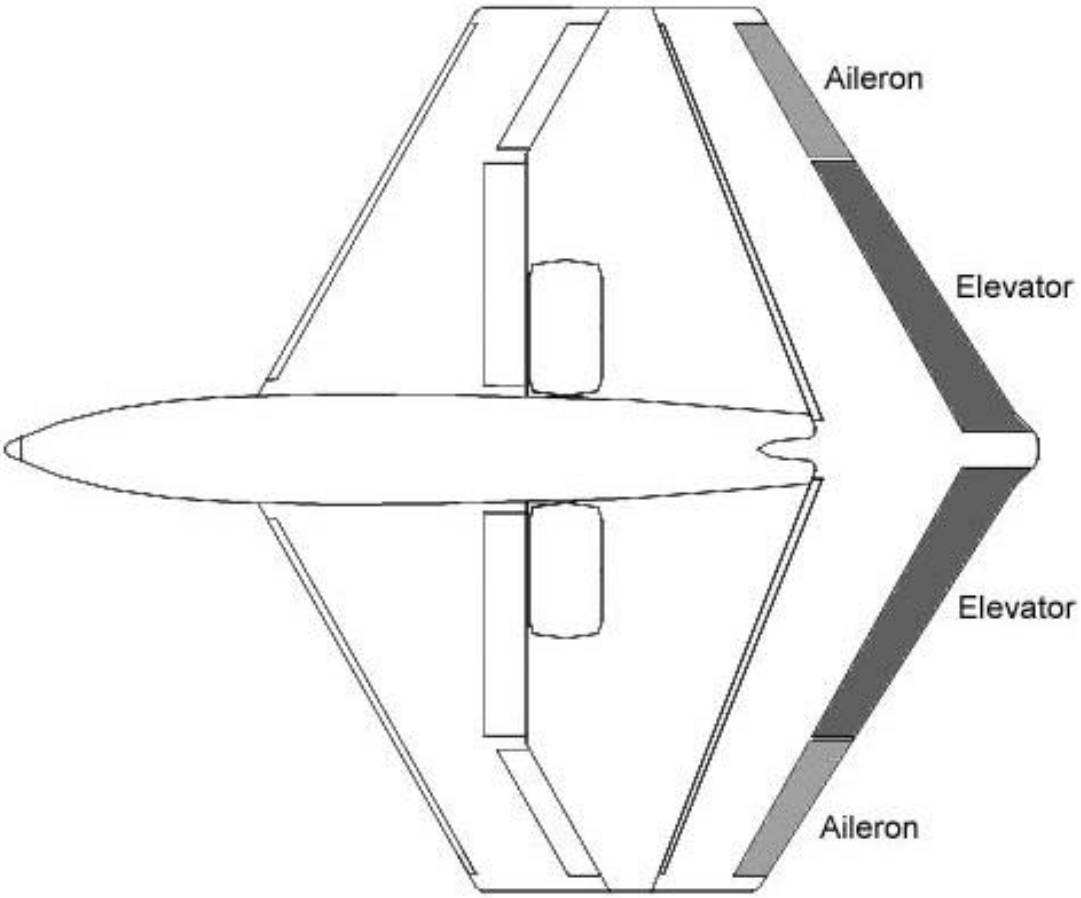

Figure E-13: Aileron and Elevator Location and Size in Relation to the Aircraft

These dimensions were used to construct elevators in Ikelos' *Tornado* vortex lattice model. Elevator sweeps were then run to determine $C_{L,de}$ and $C_{m,de}$. Since the use of high-lift devices on the front wing could degrade the performance of the elevators, the effectiveness of the elevators was also tested in a landing configuration (full flaps). The following table lists the elevator control derivatives in cruise and landing configurations:

	Cruise	Landing
CL deltaE (1/rad)	1.322	1.212
Cm deltaE (1/rad)	-1.900	-1.970

Table E-4: Elevator control derivatives in Cruise and Landing Configurations

As shown above, some change of control effectiveness is seen, but the differences are not severe. The magnitudes of these values seem slightly high, but this should be expected giving the "over-sized" nature of the elevators. Figure E-14 shows a trim cross-plot for Ikelos in cruise. In a clean configuration (no high-lift devices), very small elevator deflections are sufficient to trim Ikelos through a wide range of lift coefficients.

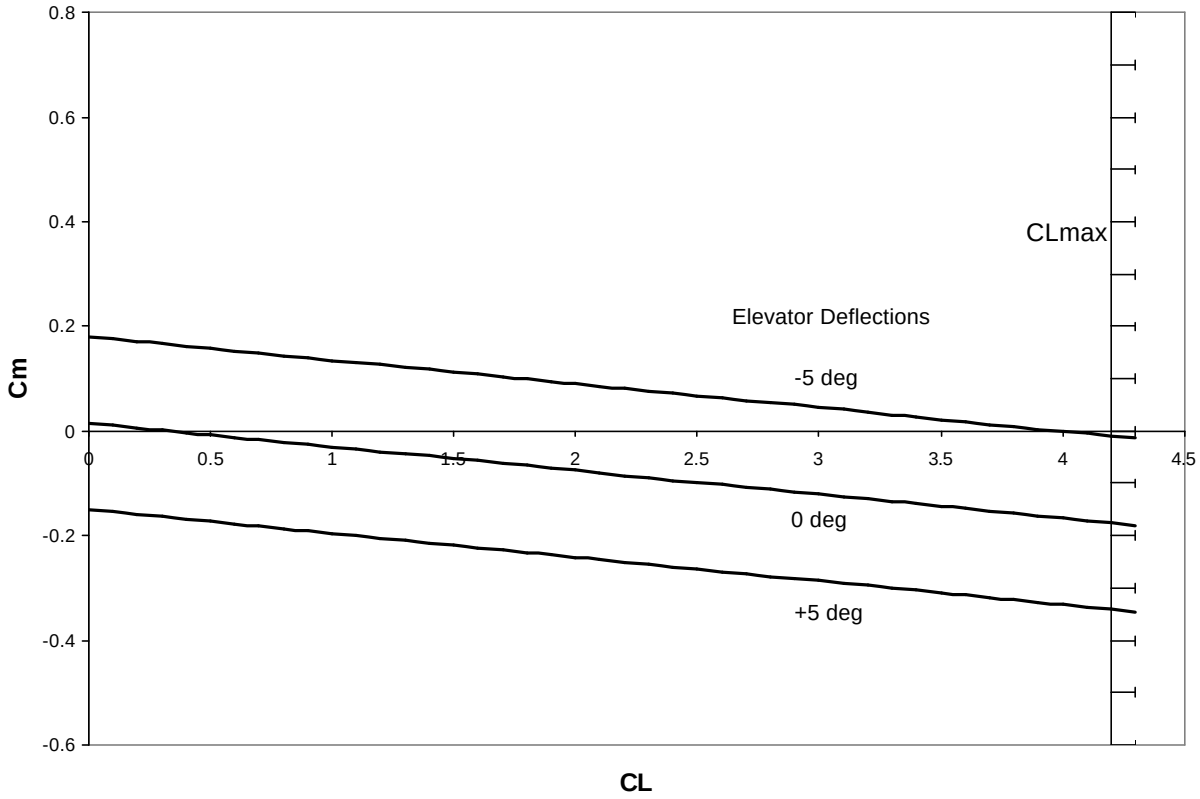

Figure E-14: Trim cross-plot in cruise configuration

Ikelos' trim situation is fundamentally different from most general aviation aircraft in that application of the high-lift devices produces a large nose-up pitching moment. Although the flaps create a strong pitching moment about the section aerodynamic center, this effect is overshadowed by the effects of increasing lift so far ahead of the aircraft CG. Thus, an application of positive elevator deflection is needed to trim when flaps are deflected. This positive increment improves the aircraft lift coefficient. A simple application of equations (3) and (4) using the values of aircraft aerodynamic characteristics listed in Appendix D, and the elevator control derivatives listed above, the elevator must be deflected +24 degrees during landing. This deflection corresponds to a ? C_L of 0.55.

The elevator control power sets the most forward location of the CG with respect to the neutral point. It is desirable to set the most forward CG position such that the limit of the elevator's ability to trim the aircraft coincides with the stall condition. Thus, having the CG located beyond this point would cause the aircraft to reach its maximum trimmed angle of attack before the aircraft reaches C_{Lmax}. The following equation can be derived from equations (1) and (2) for the case where C_L=C_{Lmax}.

$$h_{\min} = h_n - \frac{\Delta}{C_{L,a} C_{L\max}} \left[\frac{C_{m0L} C_{L,a}}{\Delta} - d_{e,\max} \right] \quad \text{(E-11)}$$

$$\Delta = C_{L,a} C_{m,de} - C_{m,a} C_{L,de} \quad \text{(E-12)}$$

With a maximum elevator deflection of 30 degrees, h_n=0.972, and the elevator control derivatives found in Table E-4, the maximum forward CG location for Ikelos is 0.74 m.a.c.

E-2.7 CG Movement and Location

Once the wing design was finalized, the Ikelos' static longitudinal stability could be further analyzed. Having the aircraft stable at full takeoff weight is important, but it must also be stable during the rest of the flight. Since, the center of gravity (CG) location determines whether or not the aircraft is statically stable in a given flight condition, the CG location was moved by changing the amount of weight in the aircraft. The forward and aft limits on the CG are defined by the wing's properties. The aft limit is the neutral point, which is set at 2.05 meters (6.73 ft) behind the apex of the wing, while the forward most point is defined by the maneuverability point (h_{min}). This is CG location at which the elevators have just enough control power to rotate the aircraft (mainly during takeoff) – determined above in Section E.2.6. With the minimum CG location at 1.695 meters (5.56 ft) behind the wing apex, the CG must be located in the 0.355 meter (1.1647 feet) range between it and the neutral point.

The approach taken to determine the aircraft's overall stability was to change the pilots, their baggage, and the amount of fuel onboard. Initially, the two pilots were assumed to weigh 756 Newtons (170 lbs), in accordance to military flight regulations. However, a large portion of the adult male population weighs more than this, so heavy pilots of 900 N (~200 lbs) were used for more weight balances. The 133 N (30 pounds) of baggage for each pilot was taken in and out of the aircraft as well. For most of these flight configurations, the amount of fuel was also varied to simulate different flight phases. The full fuel was considered the takeoff and climb configuration, 53% fuel was used to resemble cruise conditions and 6% fuel left was used as the landing case. Figure E-15 is a plot of the CG locations for different weight configurations. The two vertical lines represent the forward and aft limits for the CG, h_{min} and h_n respectively. The data points are marked with numbers 1 through 22, distinguishing the different configurations. The configurations are defined in Table E-5 with the number, the total mass, the CG location from the apex of the wing and the description of the weight configuration. The fuel variation is listed first, if there is no mention of the amount of fuel onboard it is assumed to have full fuel. Next in the description is the pilot(s) weights, where the heavy pilot indicates the 900 N (200 lb) pilot. The last portion states if the pilots' baggage has been removed. From this plot, Ikelos meets longitudinal static stability requirements for all the tested flight conditions with room to spare. The only condition that did not pass is the operational empty weight case. Since the aircraft cannot be flown without a pilot, this configuration is disregarded, leaving the aircraft overall statically stable.

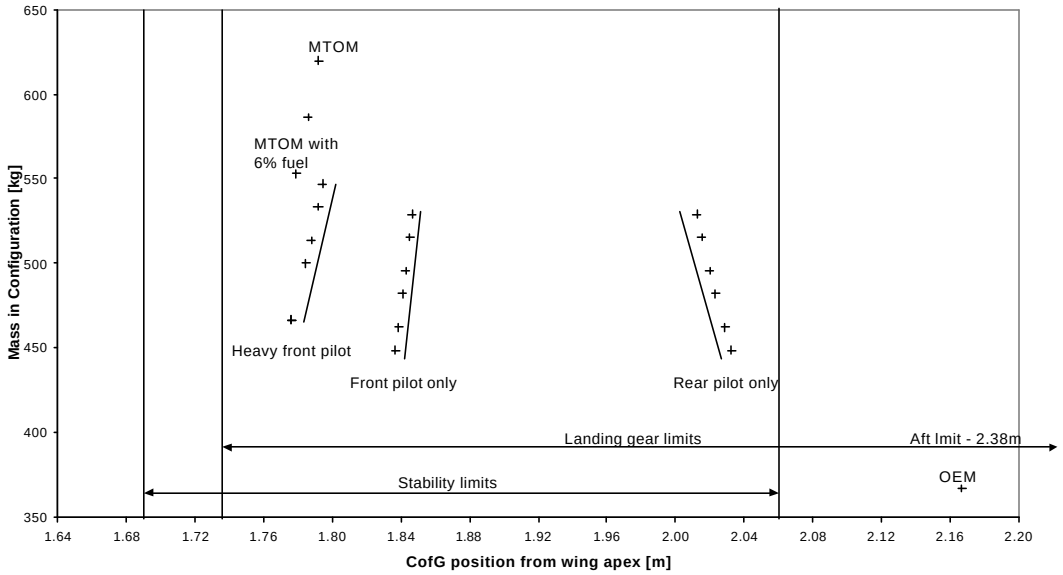

Figure E-15: CG Excursion for Various Weight Configurations (See Table E.2.7-1)

	Mass (kg)	CG Position from Wing Apex (m)	Description
1	619.8	1.792	Maximum Take-Off Weight (MTOW)
2	367.1	2.167	Operational Empty Weight (OEW)
3	586.3	1.786	MTOW: 53% Fuel
4	552.8	1.779	MTOW: 6% Fuel
5	529.1	1.846	MTOW: No Rear Pilot
6	495.6	1.843	MTOW: 53% Fuel and No Rear Pilot
7	462.1	1.838	MTOW: 6% Fuel and No Rear Pilot
8	529.1	2.012	MTOW: No Front Pilot
9	495.6	2.020	MTOW: 53% Fuel and No Front Pilot
10	462.1	2.029	MTOW: 6% Fuel and No Front Pilot
11	515.5	1.845	MTOW: No Rear Pilot and No Baggage
12	482.0	1.841	MTOW: 53% Fuel, No Rear Pilot and No Baggage
13	448.5	1.837	MTOW: 6% Fuel, No Rear Pilot and No Baggage
14	515.5	2.015	MTOW: No Front Pilot and No Baggage
15	482.0	2.023	MTOW: 53% Fuel, No Front Pilot and No Baggage
16	448.5	2.033	MTOW: 6% Fuel, No Front Pilot and No Baggage
17	547.0	1.794	MTOW: Heavy Front Pilot and No Rear Pilot
18	513.5	1.787	MTOW: 53% Fuel, Heavy Front Pilot and No Rear Pilot
19	466.4	1.776	MTOW: 6% Fuel, Heavy Front Pilot, No Rear Pilot or Bags
20	533.3	1.792	MTOW: Heavy Front Pilot, No Rear Pilot and No Baggage
21	499.9	1.784	MTOW: 53% Fuel, Heavy Front Pilot, No Rear Pilot and No Bags
22	466.4	1.776	MTOW: 6% Fuel, Heavy Front Pilot, No Rear Pilot and No Bags

Table E-5: Figure E-15 Legend - CG Locations for Different Weight Configurations

E-3 LATERAL-DIRECTIONAL STABILITY & CONTROL

E-3.1 Stability Requirements

Similar to the longitudinal stability requirements, the lateral-directional stability is based off of both static and dynamic requirements. For static stability, the aircraft's yaw stiffness, $C_{n\beta}$, must be positive and its roll stiffness, $C_{l\beta}$, must be negative. These requirements ensure that the aircraft generates a positive yawing moment and a negative rolling moment for a positive sideslip, so it will stay in controllable flight conditions. Unlike the longitudinal case, the wing only plays a minor role in the lateral directional stability. The main contributors are the fuselage and the vertical tail. The main portion of the wing that does contribute is the dihedral on the two wings and the endplates connecting them.

E-3.2 Dihedral Study

As described in Section E.2.4, the dihedral study is based off of the basic configuration in Figure E-7. This lateral directional study was performed at the same time as the longitudinal one. Beta sweeps were run in *Tornado* for a variety of front and rear wing dihedral angles to determine the affects of dihedral on lateral directional static stability. Figure E-16 shows the yawing moment and side force coefficient curves as functions of beta for the various configurations.

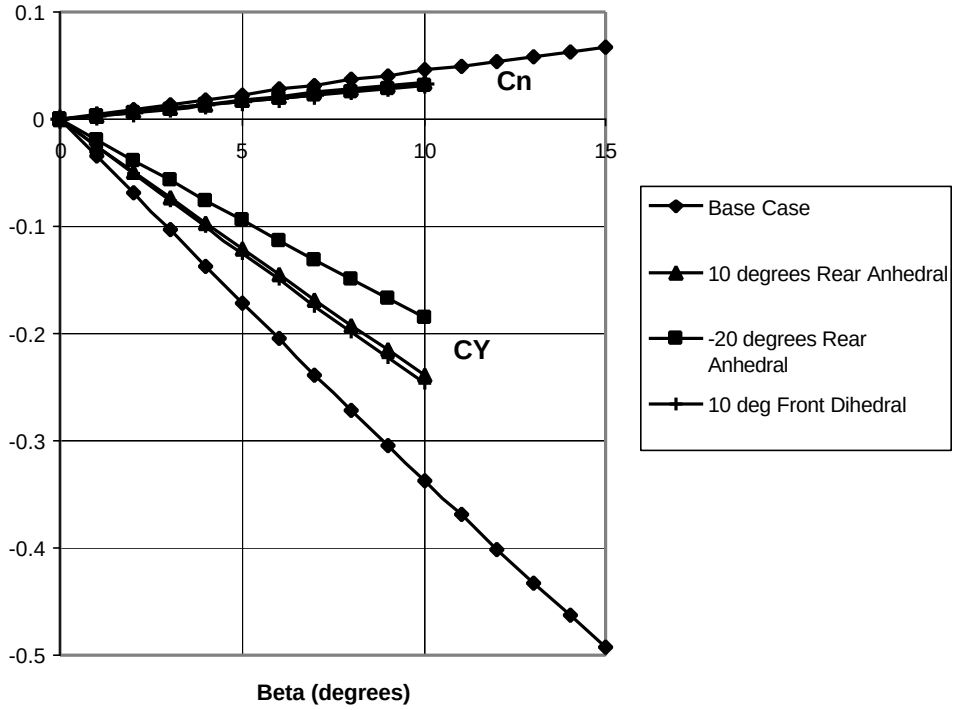

Figure E-16: C_n and C_Y vs. Beta for Different Dihedral Settings

For lateral directional static stability, $C_{y\beta}$ must be negative, which it clearly is, and it becomes less negative with increasing wing dihedral. The yaw stiffness, $C_{n\beta}$, needs to be positive for lateral static stability. This requirement is also satisfied if just barely as seen with the small slopes for C_n. The small vertical tail is the primary contributor to the small yaw

stiffness. It is worth noting that the vertical "winglets" contributed very little due to their location near the CG (lengthwise down the fuselage). Since both the winglets and the small vertical tail are almost useless, the main contributor to the yaw stiffness is the fuselage. Furthermore, the derivative $C_{l\beta}$ must also be negative, so that the aircraft generates a negative rolling moment for a positive sideslip angle. $C_{l\beta}$ is the prime beneficiary of wing dihedral, and the results for each different configuration are summarized in Table E-6.

Front Angle	Rear Angle	Clbeta
0	0	0.148
10	0	0.235
0	10	-0.023
0	20	-0.124
10	10	0.074

Table E-6: $C_{l\beta}$ for Different Wing Dihedral Angles under the Basic Configuration

The rear wing anhedral produces a configuration that is statically stable with respect to $C_{l\beta}$. The front wing dihedral does not produce the required stability. The vertical tail size has a large impact on the aircraft's lateral directional static stability. By increasing the tail size, $C_{l\beta}$ can be made negative, or driven to a greater negative value. It also is used to generate a positive yaw stiffness. The vertical tail and rudder sizing are critical in maintaining lateral directional static stability.

E-3.3 Rudder Sizing

A plain flap rudder is the primary method of yawing trim for Ikelos. Adding the rudder control power into the lateral-directional equation for yawing gives:

$$C_n = C_{n,b}\,b + C_{n,p}\,p + C_{n,r}\,r + C_{n,dr}\,d_r \qquad \text{(E-13)}$$

The rudder design constraint most often used for general aviation is the maximum cross-wing landing condition. That is, the aircraft must be able to maintain zero yawing moment (C_n=0) at a given angle, β_{max}, so that it can land straight on the runway. Due to the nature of Ikelos' propulsion system, the case of asymmetric thrust must also be considered. For the limiting case of no combined motion, i.e. the yawing moment is isolated, equation (13) can be solved for the requirement rudder control power in each case.

We first consider the maximum crosswind landing case. As discuss in the stability and control requirements, Ikelos must be able to land with a crosswind of 20 knots. This corresponds to a β_{max} of 22.2 degrees. Since the thrust due to yaw is zero in this case, equation (10) can be solved directly for $C_{n,dr}$. Similarly, if the limiting asymmetric thrust case is for one-fan-out at takeoff, we wish to hold our β at zero (no sideslip angle). Equation (10) can then be solved for $C_{n,dr}$. The results are summarized in the following table:

Crosswind Landing (20 knots)		Assymetric Thrust	
Cn,dr (1/rad)	-0.00571	Cn,dr (1/rad)	-0.029304

Table E-7: Required Rudder Performance

Thus, the case of asymmetric thrust is a considerably more stringent design requirement.

Based on space constraints produced by structural requirements, the maximum available chord percentage available for the rudder was 24%. Given the large amount of power dictated by the asymmetric thrust requirement, the rudder was sized to occupy the full vertical tail span and 24% of the chord as shown in Figure E-17.

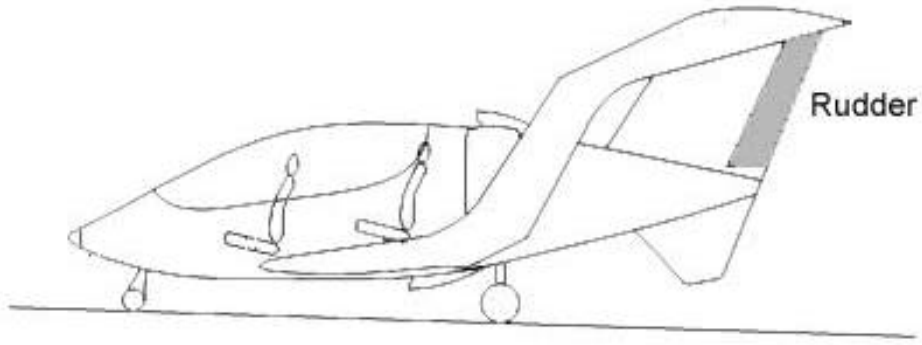

Figure E-17: Rudder Location and Size in Relation to the Rest of the Aircraft

Tornado was used to give a value of the rudder control power for a given flap size. Our rudder power, $C_{n,dr}$, was found to be –0.00375 1/deg. Comparing this value with those in Table E-7, Ikelos clearly has enough control power to handle a 20 knot crosswind landing. Although it falls short of desired performance in an asymmetric thrust case, two important notes can be made: (1) Aircraft designed for short-field operations typically have very high thrust capabilities, which make full throttle asymmetric thrust situations hard to deal with, and (2) Reducing the throttle setting to around 75% would allow Ikelos to maintain straight flight with asymmetric thrust.

E-3.4 Aileron Sizing

Rolling control on Ikelos is accomplished by use of ailerons located on the outboard section of the rear wing. For general aviation aircraft, the restrictions imposed by roll control are generally not severe. Due to the use of a cambered airfoil on the rear wing, the elevators function slightly differently than those on a symmetric horizontal tail. The "throw" of the elevators must be greater when deflecting upward to counter the effects of camber. This makes the design slightly more complex, but the aerodynamic benefits provided by cambering the rear wing far outweigh this complexity.

At first glance it might appear that locating ailerons on the rear wing would improve the pitching moment problem; however since ailerons deflect in opposite directions the net Cm due to aileron deflection is zero. Due to the size of the elevators on the trailing edge of the rear wing, the space for conventional roll control methods such as ailerons was somewhat limited. The maximum space available, with a 2.03 m (6.7 ft) elevator span, semi-span being 3.0 m (9.8 ft), and allowing for a small separation between control surfaces, was 0.95 m (6.2 ft). The following figure was taken from Raymer [4], and demonstrates the aileron size of comparable aircraft.

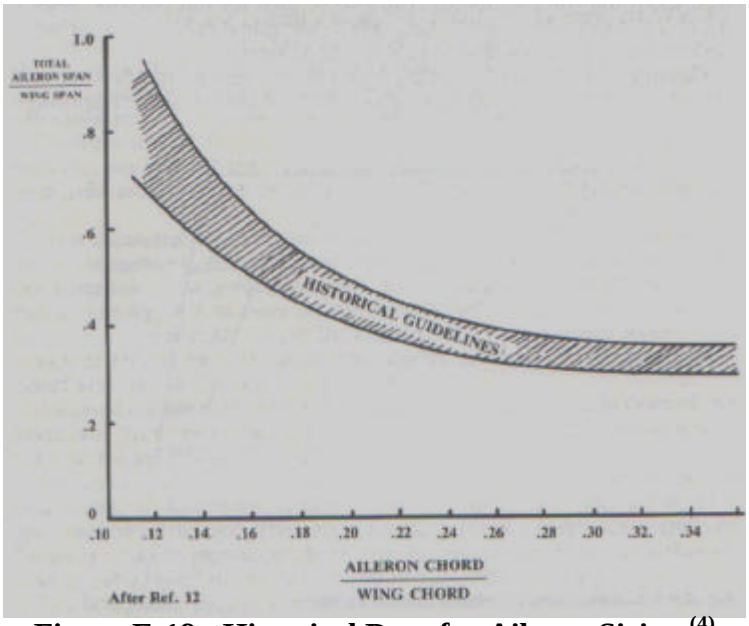

Figure E-18: Historical Data for Aileron Sizing [4]

Based on the above figure, it was seen that for an aileron chord fraction of 30%, the span fraction should be around 30%. For a 6.0 m (19.7 ft) span, this corresponds to 1.8 m (5.9 ft) of total aileron span, which would naturally be 0.9 m (2.95 ft) span for each aileron. Thus, the available space corresponds very nicely will historical guidelines for aileron size. Refer to Figure E-13 for a drawing of Ikelos' roll control system.

Using *Tornado*, the control power was found for both cruise and landing configurations. The results are presented in Table E-8.

	Cruise	Landing
Cl delta A (1/rad)	-0.139	-0.157
Cn delta A (1/rad)	0.004	0.051
CY delta A (1/rad)	0.000	0.000

Table E-8: Aileron Control Power for Cruise and Landing Configurations

As shown above, following the standard convention using in stability analysis, a positive aileron deflection produces a negative rolling moment (C_l). Also, as is the case with ailerons, a positive deflection produces adverse yaw. The magnitude of the derivatives with respect to yawing moment is relatively small however, as are the derivatives with respect to the side force which are effectively zero. More details on the performance of these ailerons such as steady-state roll rate and dynamic analysis can be found in Section E.3.5.

Other methods were considered for roll control in the design of Ikelos. Due to the space constraints presented by the need for powerful rear-wing elevators and full front-wing span high-lift devices, the use of spoilers was considered. This option would be feasible if higher roll performance were required. Spoilers can be very difficult to analyze, however, due to their very non-linear response. The use of the outboard flaps on the front wing in conjunction with the ailerons is also an option. Due to the complexity this introduces into the control system, this

option would be less feasible. These options are only for increasing the roll performance, which is adequate with the current aileron configuration.

E-4 CONTROL FORCES / STICK FORCES

The control surface forces were calculated using a method from Roskam Part VII[1]. First the control surface hinge moment, HM, representing the force per radian of deflection of the control surface was calculated for each of the different flight configurations using Equation 11.

$$HM = C_h (S \cdot \bar{c}) \bar{q} \tag{E-14}$$

where C_h is the control surface hinge moment coefficient. The hinge moment coefficient depends on the detail design of the control surfaces of the aircraft. For this aircraft the hinge moment coefficients were estimated about the control surface hinge line using hinge moment derivative charts in Roskam Part VI[2]. The calculations of the three control surface hinge moments are summarized in Table E-8.

	Aileron	Elevator	Rudder
Hinge Moment Coefficient	- 0.134	- 0.419	- 0.106
Control Surface Areas (m^2)	0.586 (6.3 ft^2)	1.496 (16.1 ft^2)	0.41 (4.4 ft^2)
Control Surface Mean Aerodynamic Chord (m)	0.32 (1.0 ft)	0.37 (1.2 ft)	0.33 (1.1 ft)
Landing Hinge Moment (N/rad) ($q_{landing}$ = 221.113 N-m)	30.88 (0.12 lb/deg)	92.59 (0.36 lb/deg)	23.48 (0.09 lb/deg)
Cruise Hinge Moment (N/rad) (q_{cruise} = 2330.209 N-m)	325.40 (1.28 lb/deg)	975.75 (3.83 lb/deg)	247.43 (0.97 lb/deg)

Table E-8: Calculation of the Control Surface Hinge Moments

The control surface forces were then calculated using Equation 12.

$$F_{control\_surface} = HM \cdot d_{control\_surface} \tag{E-15}$$

The variation of the control surface forces with deflection angles in the landing and cruise configurations are plotted in Figures E.4-1 and E.4-2 respectively. With the FAR [7] requirements in Table E-9.

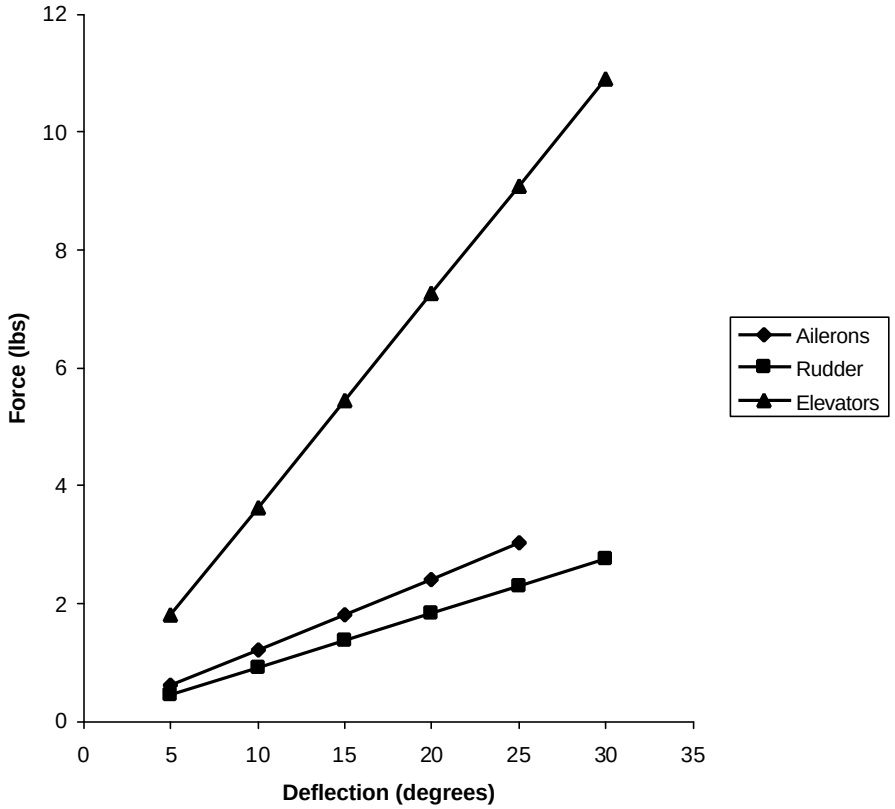

Figure E-19: Control Forces versus Control Deflections in Landing

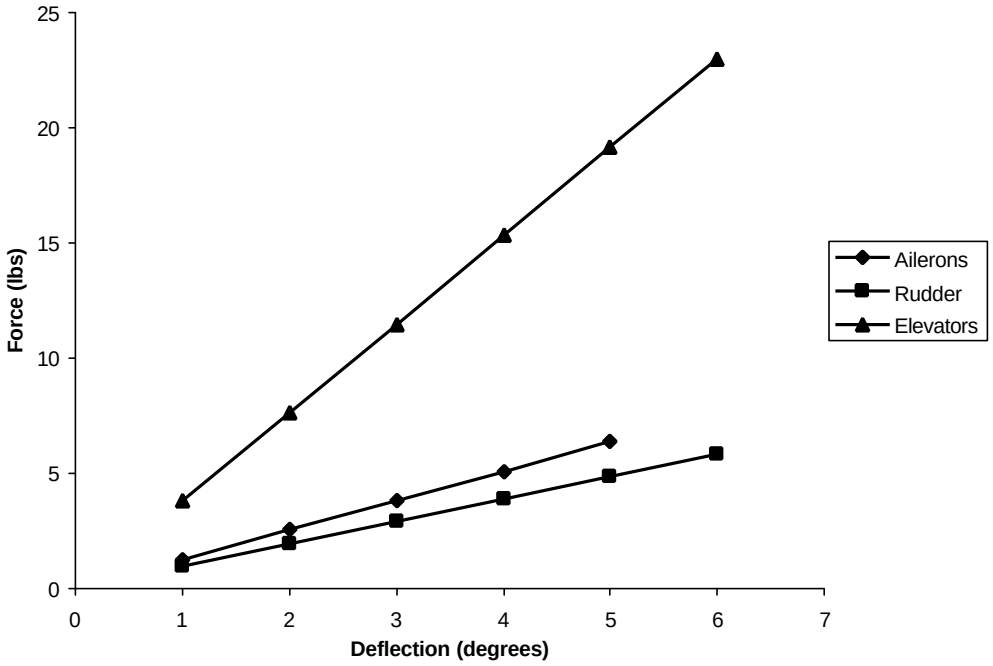

Figure E-20: Control Forces versus Control Deflection in Cruise

Table E-9: Maximum Permissible Control Forces[7]

Control	Maximum Force
Stick Force (Roll)	135 N (30 lbs)
Stick Force (Pitch)	270 N (60 lbs)
Rudder Pedal Force (Yaw)	670 N (150 lbs)

From Figures E.4-1 and E.4-2, it is observed that all the control forces corresponding to the maximum deflections of each control surface during landing and a deflection of 6 degrees during cruise meet the requirements outlined in Table E-9. The variation of cockpit control forces with deflection during take-off is expected to be similar to that for landing since the dynamic pressures are the same for both conditions.

E-5 DYNAMIC STABILITY

E-5.1 Stability Requirements

Ikelos must not only be statically stable but it also needs to meet the Level 1 Flying Quality requirements set by the military specification document, MIL-F-8785C[6], for Class 1 (light-weight) aircraft at cruise (Category B) flight conditions. The longitudinal dynamic stability requirements are:

Phugoid (P) Damping Ratio	$z_P > 0.04$
Short Period (SP) Damping Ratio	$0.3 \le z_{SP} \le 2.0$
Short Period Natural Frequency, ω_{SP}	$0.085 \le \frac{w_{SP}^2}{n/a} \le 3.6 rad/\sec$

The following lateral-directional dynamic stability requirements for the Level 1 flight qualities were also obtained from the MIL SPEC document:

Dutch Roll (DR) Damping Ratio	$z_{DR} > 0.08$
Dutch Roll Natural Frequency	$w_{DR} > 0.4 rad/\sec$
Dutch Roll Requirement	$z_{DR} w_{DR} > 0.15 rad/\sec$
Roll Mode Time Constant	$t_R < 1.4 \sec$
Spiral Mode Time to Double Amplitude	$T_{2SP} > 20 \sec$
Maximum Crosswind Landing	20 knots

E-5.2 Approach

The approach taken in analyzing the dynamic behavior of the airplane was to use the solutions to the uncoupled, linearized equations of motion. To obtain the equations, a MATLAB function *Lin*[8] was used. Once the equations were set up, it remained a simple exercise in extracting the system eigenvalues, which could be used to determine the dynamic properties of the system.

Lin takes three vectors as an input, all in English units. The first contains six elements that describe the reference flight condition:

$$Ref = [\ \rho,\ V_{T,}\ M,\ C_L\ ,\ C_D\ ,\ \gamma\ ]$$

The above are determined by the flight condition picked. Depending what phase of flight was being examined, a certain altitude and airspeed were chosen. This would set the density (ρ), airspeed (V_T), and Mach number (M). The reference lift and drag coefficients were determined by running a simple state solution in *Tornado* at the given flight condition. The flight path angle, γ, would be determined by the flight condition.The second vector contains nine elements, all physical characteristics of the aircraft. Since all elements are physical characteristics, this vector should remain constant for any flight condition being examined, with the exception possibly being the weight due to configuration/fuel burnoff. The vector is set up as follows:

$$Phys = [\ Weight,\ I_{xx}\ ,\ I_{yy}\ ,\ I_{zz}\ ,\ I_{xz}\ ,\ S,\ b,\ c\text{-}bar,\ \varepsilon_T\ ]$$

In the above vector, the aircraft weight, reference area (S), span (b), and mean aerodynamic chord (c-bar) were known physical data. The reference area used was the planform area of the front wing. The moment of inertia about the y-axis, I_{yy}, was calculated using information from the weights and balance appendix (Appendix F). A spreadsheet kept tabs on the weight and location of everything that went into the airplane. With the weight and longitudinal distance from the CG known, I_{yy} could be estimated by summing up the moments of inertia of each individual piece. In other words, since the moment of inertia about the y-axis is defined as:

$$Integral[(x^2+z^2)^{1/2}\ dm] \qquad \text{(E-16)}$$

where dm is simply an elemental mass and $(x^2+z^2)^{1/2}$ is the perpendicular distance from the element to the y-axis, the moment of inertia was estimated using:

$$Summation[(x^2+z^2)^{1/2} * m] \qquad \text{(E-17)}$$

where m is the mass of a particular piece of the aircraft. The moments of inertia about the x and z axes, I_{xx} ad I_{zz}, were calculated using methods quoted from Raymer[(4)]. The cross product of inertia, I_{xz} , was assumed/estimated to be zero. The final element of the Phys vector left uncalculated was ε_T, which is the angle the thrust vector makes with the x-axis. This was assumed to be zero, making the Phys vector:

Phys = [1366 lb, 469 slug-ft^2, 717 slug-ft^2, 685 slug-ft^2, 0 slug-ft^2, 93.11 ft^2, 19.69 ft, 4.996 ft, 0 rad]

The third vector *Lin* takes as input is a 29-element vector containing all the non-dimensional derivatives needed to calculate the dimensional linear equations of motion. This vector is where the aerodynamic properties of the aircraft come into play, and contains the main information needed. A description of the non-dimensional derivatives can be found in section E-7. The vector is stated as follows:

$$D = [C_{L\alpha}, C_{D\alpha}, C_{m\alpha}, C_{L\alpha\text{-dot}}, C_{m\alpha\text{-dot}}, C_{Lq}, C_{mq}, C_{LM}, C_{DM}, C_{mM}, C_{L\delta e}, C_{D\delta e}, C_{m\delta e}, C_{TV}, C_{T\delta T}, C_{Y\beta}, C_{l\beta}, C_{n\beta}, C_{lp}, C_{np}, C_{Yp}, C_{lr}, C_{nr}, C_{Yr}, C_{l\delta a}, C_{n\delta a}, C_{l\delta r}, C_{n\delta r}, C_{Y\delta r}]$$

Most of the above could be estimated using *Tornado* through angle, rate, and control sweeps.

The first two derivatives that could not be found with *Tornado*, but needed to be estimated, were the damping derivatives associated with rate of change in angle of attack, $C_{L\alpha\text{-dot}}$ and $C_{m\alpha\text{-dot}}$. These were estimated using methods proposed by Roskam[2].

The derivatives of lift, drag, and pitching moment with respect to mach number, C_{LM}, C_{DM}, and C_{mM}, were assumed to be zero. The justification for this lies in the fact that Ikelos' maximum speed is 140 kts, making the mach regime at altitude:

$$0 \leq M \leq 0.2$$

This is a relatively small range of mach numbers, meaning that changing the mach number enough to significantly alter the lift or drag would involve changing the flight condition from reference drastically enough for the linear assumption to no longer hold valid. Therefore, it was decided that the assumption of these derivatives to be zero was justified.

The thrust derivatives, C_{TV} and $C_{T\delta T}$, required some estimation and assumptions as well. C_{TV} is a measure of how thrust is affected by variations in velocity. Ikelos' ducted fans are variable pitch, and were assumed to act like propellers. Constant-speed (variable pitch) propellers are usually approximated as constant-power propulsion. According to Etkin[3], for this case C_{TV} can be assumed to be $-3C_{TREF}$. For each flight condition examined, the thrust was found from figure E-21.

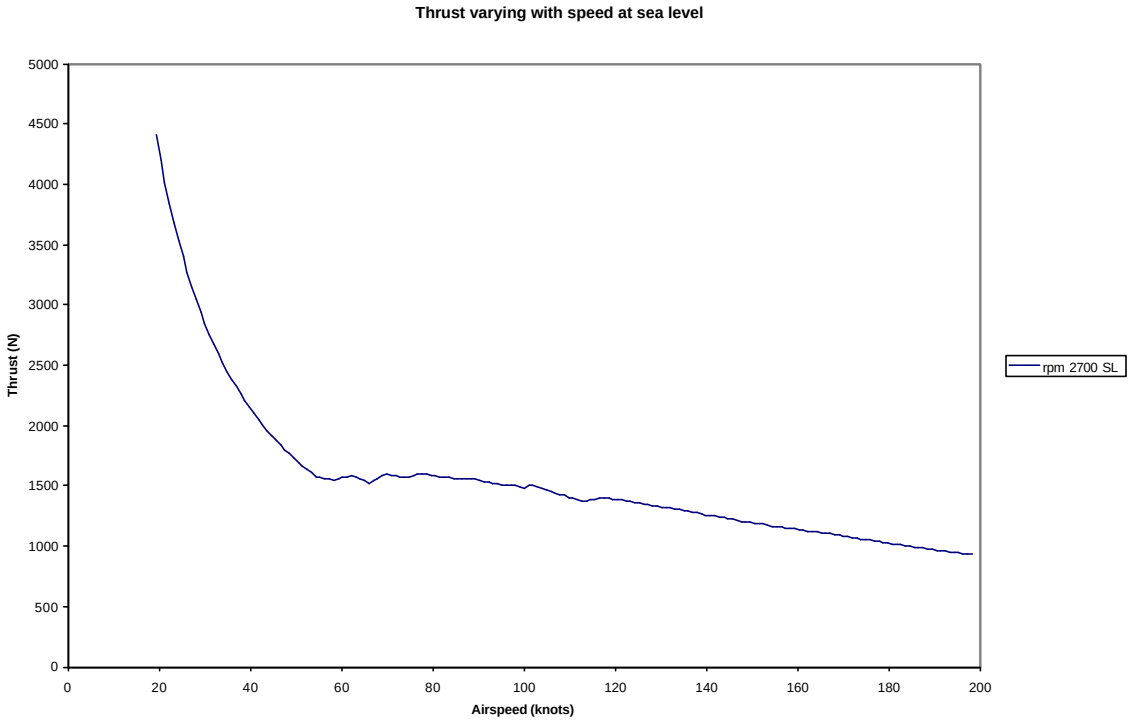

Figure E-21: Variation of Thrust with airspeed

The reference coefficient of thrust was then calculated using:

$$C_{TREF} = T_{REF} / (1/2\ \rho V^2 S) \qquad \text{(E-18)}$$

This number was multiplied by -3 to determine C_{TV}. $C_{T\delta\Gamma}$ is a control derivative which is a measure of the change in thrust due to throttle input, and therefore would only affect the longitudinal B matrix. This would not be necessary to extract the system eigenvalues. Therefore it was left as zero in the input to the *Lin* function. This is not implying that it can be assumed zero; the actual number would be far from it. To assume this control derivative to be zero would be saying that thrust is not affected by throttle setting. It was merely left as zero because it was not needed for this analysis, but something needed to be inserted into the D[ ] vector in its place.

With the above three vectors as inputs, *Lin* calculates the dimensional, linearized equations of motion for a rigid aircraft, and outputs them in matrix form. The function conveniently separates the longitudinal states from the lateral directional states, allowing for de-coupled analysis. For small perturbations from reference, the assumption that the longitudinal and lateral directional modes are de-coupled tends to be a good one[8]. The one thing left to note is that *Lin* outputs the matrices using the velocity states of u, v, and w as opposed to V_T, α, and β. Simple matrix transformations were employed to convert the matrices into the more familiar and useful form. Since, for small disturbances, the aerodynamic angles can be estimated by:

$$\alpha = w / V_T \qquad \text{(E-19)}$$

$$\beta = v / V_T \qquad \text{(E-20)}$$

The transformation matrices were given by[8] :

$$\begin{bmatrix} V_T \\ \alpha \\ q \\ \theta \end{bmatrix} = \begin{bmatrix} 1 & 0 & 0 & 0 \\ 0 & 1/V_{Tref} & 0 & 0 \\ 0 & 0 & 1 & 0 \\ 0 & 0 & 0 & 1 \end{bmatrix} \begin{bmatrix} u \\ w \\ q \\ \theta \end{bmatrix}$$

$$\begin{bmatrix} \beta \\ p \\ r \\ \phi \end{bmatrix} = \begin{bmatrix} 1/V_{Tref} & 0 & 0 & 0 \\ 0 & 1 & 0 & 0 \\ 0 & 0 & 1 & 0 \\ 0 & 0 & 0 & 1 \end{bmatrix} \begin{bmatrix} v \\ p \\ r \\ \phi \end{bmatrix}$$

The transformation of a matrix is then simply $A_2 = T * A_1 * T^{-1}$, where A_1 is the original matrix, T is the transformation matrix, and A_2 is the result of the transformation[8]. The matrices obtained from performing the above transformation on the *Lin* output were the system matrices of the aircraft in terms of V_T, α, and β. The eigenvalues of these could be obtained using MATLAB. Executing the 'damp' MATLAB command on the eigenvalues would then yield the natural frequency and damping ratio of the oscillatory modes. From this, the period, time to half/double, and time constants could also be calculated. Then these numbers could be compared to the specifications for acceptable flying qualities and the aircraft's dynamic performance could be rated.

E-5.3 Longitudinal Dynamics

E-5.3.1: Modes Explained

Phugoid

The phugoid mode is a longitudinal mode that tends to get excited with change in throttle. A throttle pulse causes a change in airspeed, which begins a very lightly damped oscillation in pitch attitude. Meanwhile, the angle of attack remains fairly constant, meaning the flight path angle oscillates with the pitch attitude. The result is a long period, lightly damped cycle of the aircraft pitching up, gaining altitude while losing speed, then pitching down, losing the gained altitude but regaining the lost airspeed. It can be viewed as an exchange between potential and kinetic energy[9].

Short Period

The short period mode is another natural mode of the aircraft dynamics, and tends to affect the angle of attack and pitch rate more heavily than the other longitudinal states. When the aircraft is given an elevator pulse as an input, a pitch rate is generated, which causes the angle of attack and pitch angle to vary. The airspeed remains fairly constant, and the angle of attack and pitch angle tend to vary in unison, which keeps the flight path angle ($\gamma = \theta - \alpha$) nearly constant[9]. The period of this mode is characteristically much shorter than the phugoid mode, hence the descriptive name. The short period mode tends to damp out fairly quickly, and usually appears only as a small ripple on plots showing the time history for which both longitudinal modes were excited[8].

E-5.3.2: Cruise Condition

As cruise is the longest phase of flight, it was deemed necessary to evaluate the dynamic longitudinal stability at this condition. The following condition was considered cruise:

$$V = 65 \text{ m/s } (126 \text{ kts})$$

$$\alpha = 0.25 \text{ deg}$$

$$\gamma = 0 \text{ deg}$$

Since *Tornado* was being used for a large part of the analysis, the reference altitude was considered to be zero, as *Tornado* treats all cases as flight at sea level. The flaps were set to zero degrees deflection. From the simple state solution at this flight condition:

$$C_L = 0.3$$

$$C_D = 0.008$$

This comprised the first of the three input vectors to the *Lin* MATLAB function. The second input vector, Phys[ ], contained the same information proposed in section E.5.2, as these are physical properties of the aircraft.

The elements of the third vector, D[ ], which contains all the stability and control derivatives for the current flight condition, were obtained through a combination of analysis with *Tornado* and estimation through hand calculations. Since the longitudinal behavior was being examined, and the linear equations were assumed to be completely uncoupled, all derivatives pertaining to lateral-directional states/variables were set to zero. This simply meant that the lateral-directional system matrices output by *Lin* would be matrices of zeros, which was of no consequence because they were not being used at this time. The mach derivatives were assumed zero as discussed in section E.5.2.

An alpha sweep was run in *Tornado* to obtain the alpha stability derivatives, a pitch rate sweep was run to obtain the pitch damping derivatives, and an elevator sweep was run to obtain the pitch control derivative. These are shown in table E-10.

Table E-10: *Tornado* Derived Non-Dimensional Longitudinal Stability & Control Derivatives (Cruise)

$C_{L\alpha}$	6.041
C_{Lq}	10.588
$C_{L\alpha\text{-dot}}$	3.041
$C_{L\delta e}$	1.322
$C_{D\alpha}$	0.00694
C_{Dq}	0.0
$C_{D\delta e}$	-0.004
$C_{m\alpha}$	-0.328
C_{mq}	-14.67
$C_{m\alpha\text{-dot}}$	-3.898
$C_{m\delta e}$	-1.9

As discussed in section E.5.2, estimates of several of the stability and control derivatives could not be found through the use of *Tornado* and had to be estimated through hand calculations. $C_{L\alpha\text{-dot}}$ and $C_{m\alpha\text{-dot}}$ were estimated using methods proposed by Roskam[2] to be:

$$C_{L\alpha\text{-dot}} = 3.041$$

$$C_{m\alpha\text{-dot}} = -3.898$$

Using the methods discussed in section E.5.2, C_{TV} was estimated to be:

$$C_{TV} = -0.18$$

With all three input vectors complete, *Lin* was run to obtain the longitudinal system matrices. The required transformation from [u, w, q, θ] to [V_T , α, q, θ] was performed, and

the eigenvalues were extracted. These were used to obtain the dynamic longitudinal properties of Ikelos. A MATLAB script was written to perform the above commands, and is shown below:

```
Ref = [0.00238; 213.25; 0.196; 0.3006; 0.008; 0];
Phys = [1366;469;717;685;0;93.11;19.69;4.996;0];
D=[6.041; 0.00694; -0.328; 3.041; -3.898; 10.588; -14.67;
  0; 0; 0; 1.322; -0.004; -1.9; -1.4012; 0.3418;
  0;0;0;0;0;0;0;0;0;0;0;0;0;0];
[aLong,bLong,aLD,bLD] = Lin(Ref,Phys,D)
T=[1 0 0 0; 0 1/213.25 0 0; 0 0 1 0; 0 0 0 1];
TI = T^(-1);
A=T*aLong*TI
eigs = eig(A)
damp(eigs)
```

N/alpha was found to be:

$$n/\alpha = 22.28$$

The results for the phugoid damping ratio, natural frequency, period, and time to half amplitude were as follows:

$$\zeta_P = 0.044$$

$$\omega_{nP} = 0.137 \text{ rad/sec}$$

$$T_P = 45.86 \text{ sec}$$

$$t_{1/2\,P} = 115 \text{ sec}$$

The results for the short period damping ratio, natural frequency, period, and time to half amplitude were as follows:

$$\zeta_{SP} = 0.979$$

$$\omega_{nSP} = 5.51 \text{ rad/sec}$$

$$T_P = 1.14 \text{ sec}$$

$$t_{1/2\,SP} = 0.128 \text{ sec}$$

The above met the requirements of the MIL-F-8785C for level one flying qualities in the cruise flight condition, which is considered a class B flight phase by the specification. Notice that the period of the short period mode is much shorter than that of the phugoid mode. This is due to the fact that the short period mode is much more heavily damped than the phugoid mode. Also of note is the time to half of each mode. The short period is extremely short-lived relative to the long, lightly damped oscillations of the phugoid mode.

E-5.3.3: Landing Condition

With landing being a terminal flight phase in which control and dynamic stability are crucially important to pilot safety, it was deemed necessary to evaluate the dynamic longitudinal stability at this condition as well. The following condition was considered landing:

$$V = 18.6 \text{ m/s } (36.2 \text{ kts})$$

$$\alpha = 14 \text{ deg}$$

$$\gamma = -9 \text{ deg}$$

Again, since *Tornado* was being used for a large part of the analysis, the reference altitude was considered to be zero, as *Tornado* treats all cases as flight at sea level. As for the configuration, both inboard and outboard flaps were set to thirty degrees deflection. From the simple state solution at this flight condition:

$$C_L = 2.97$$

$$C_D = 0.56$$

This comprised the first of the three input vectors to the *Lin* MATLAB function. The second input vector, Phys[ ], mainly contained the same information proposed in section E.5.2, as these are physical properties of the aircraft. The weight was changed to 1221.25 lb, however, to account for fuel burn. This is the weight with 6% fuel remaining.

The elements of the third vector, D[ ], were again obtained through a combination of analysis with *Tornado* and estimation through hand calculations. The lateral-directional derivatives were set to zero, as in the cruise analysis. The mach derivatives were assumed zero as discussed in section E.5.2.

An alpha sweep was run in *Tornado* to obtain the alpha stability derivatives, a pitch rate sweep was run to obtain the pitch damping derivatives, and an elevator sweep was run to obtain the pitch control derivative. These are shown in table E-11.

Table E-11: *Tornado* Derived Non-Dimensional Longitudinal Stability & Control Derivatives (Landing)

$C_{L\alpha}$	5.637
C_{Lq}	10.17
$C_{L\alpha\text{-dot}}$	3.041
$C_{L\delta e}$	1.212
$C_{D\alpha}$	0.882
C_{Dq}	0.0
$C_{D\delta e}$	0.282
$C_{m\alpha}$	-0.131
C_{mq}	-13.68
$C_{m\alpha\text{-dot}}$	-3.898
$C_{m\delta e}$	-1.97

As discussed in section E.5.2, estimates of several of the stability and control derivatives could not be found through the use of *Tornado* and had to be estimated through hand calculations. As above, $C_{L\alpha\text{-dot}}$ and $C_{m\alpha\text{-dot}}$ were estimated using methods proposed by Roskam[2] to be:

$$C_{L\alpha\text{-dot}} = 3.041$$

$$C_{m\alpha\text{-dot}} = -3.898$$

Using the method discussed in section E.5.2, C_{TV} was estimated to be:

$$C_{TV} = -3.9$$

With all three input vectors complete, *Lin* was run to obtain the longitudinal system matrices. The required transformation from [u, w, q, θ] to [V_T , α, q, θ] was performed, and the eigenvalues were extracted. These were used to obtain the dynamic longitudinal properties of Ikelos. A MATLAB script was written to perform the above commands, and is shown below as:

```
Ref = [0.00238; 61.02; 0.056; 2.97; 0.56; -0.1571];
Phys = [1221.25;469;717;685;0;93.11;19.69;4.996;0];
D=[5.637; 0.882; -0.131; 3.041; -3.898; 10.17; -13.68;
  0; 0; 0; 1.212; 0.2816; -1.97;-9.46; 0.3418;
  0;0;0;0;0;0;0;0;0;0;0;0;0];
[aLong,bLong,aLD,bLD] = Lin(Ref,Phys,D)
T=[1 0 0 0; 0 1/61.02 0 0; 0 0 1 0; 0 0 0 1];
TI = T^(-1);
```

```
A=T*aLong*TI
eigs = eig(A)
damp(eigs)
```

N/alpha was found to be:

$$n/\alpha = 1.9$$

The results for the phugoid damping ratio, natural frequency, period, and time to half amplitude were as follows:

$$\zeta_P = 0.5$$

$$\omega_{nP} = 0.391 \text{ rad/sec}$$

$$T_P = 16.1 \text{ sec}$$

$$t_{1/2\,P} = 3.55 \text{ sec}$$

The short period was non-oscillatory. MIL-F-8785C allows for this while still retaining level one flying qualities. Even though the response is non-oscillatory, a damping ratio and natural frequency can obtained by putting the characteristic equation in the standard form[8]:

$$s^2 + 2\zeta\omega_n s + \omega_n{}^2 = 0 \qquad \text{(E-21)}$$

This is done by multiplying out the eigenvalues, as follows:

$$\lambda_1 = -2.09$$

$$\lambda_2 = -0.637$$

$$(s - \lambda_1)(s - \lambda_2) = 0 \qquad \text{(E-22)}$$

$$(s + 2.09)(s + 0.637) = 0 \qquad \text{(E-23)}$$

$$s^2 + 2.728s + 1.331 = 0 \qquad \text{(E-24)}$$

This could then be solved for:

$$\zeta_{SP} = 1.182$$

$$\omega_{nSP} = 1.538 \text{ rad/sec}$$

$$t_{1/2SP} = 0.38 \text{ sec}$$

The above short period damping ratio met the requirements of the MIL-F-8785C for level one flying qualities in the landing flight condition, while the calculated natural frequency failed to meet the requirement. Although the short period natural frequency did not meet the requirement for level one flying qualities, it is considered level two and was very close to the level one boundary. This was considered acceptable.

E-5.4 Lateral-Directional Dynamics

E-5.4.1: Modes Explained

Dutch Roll

The dutch roll mode is an oscillatory mode involving both roll and yaw rates, and producing both bank angle and sideslip effects[9]. Dutch roll can be seen as the airplane rolling one way while yawing the other. The result is a lightly damped, snake-like motion with a fairly short period[8]. Since the rudder affects both roll and yaw, the dutch roll can be excited most easily with a simple rudder pulse. With the nose of the aircraft moving left while the wings are banking right, followed by the same motion in the opposite direction, an extremely lightly damped dutch roll mode can cause difficulty in landing for the pilot, while being a sickening experience for passengers.

Roll Mode

The roll mode is seen as simple rotation about the body x-axis. It is non-oscillatory, and can be modeled with a first order system. The roll rate most heavily affects the roll mode. A low roll mode time constant is desired, as this results in a fast roll rate response. A slow roll mode response causes the controls to feel sluggish and sloppy.

Spiral Mode

The spiral mode is another non-oscillatory mode like the roll mode, except that it involves the bank angle and yaw rate to a much greater extent. It involves almost no roll rate. A stable spiral mode can be seen as an airplane returning to wings level from a small initial bank angle through a combination of roll moment dependencies on sideslip and yaw rate. The sideslip and yaw rate are generated by the nose dropping slightly due to unbalanced lift when the airplane is in a bank. An unstable spiral mode works in just the opposite way: an initial bank angle results in a steeper and steeper bank angle. The spiral has a time constant characteristically smaller than the roll mode. So the motion is very slow and steady, such that the pilot may not even notice. The origin of the name lies in the unstable spiral mode, as the airplane gradually falls into a steeper and steeper bank, eventually resulting in a spiral dive.

E-5.4.1: Fuselage Model/Discussion

To be consistent with the rest of the analysis, it was decided to use *Tornado* for the lateral-directional dynamics. However, it was necessary to create a model of the fuselage, since it has such a large effect on the lateral-directional states and the associated dynamics. The fuselage can be viewed as an extremely inefficient airfoil. Therefore, a model of the fuselage was created in *Tornado* by using a combination of flat plate airfoils of 90° dihedral, as shown in figure E-22. The airfoils were of varying sweep and chord lengths, in an attempt to accurately portray the projected area.

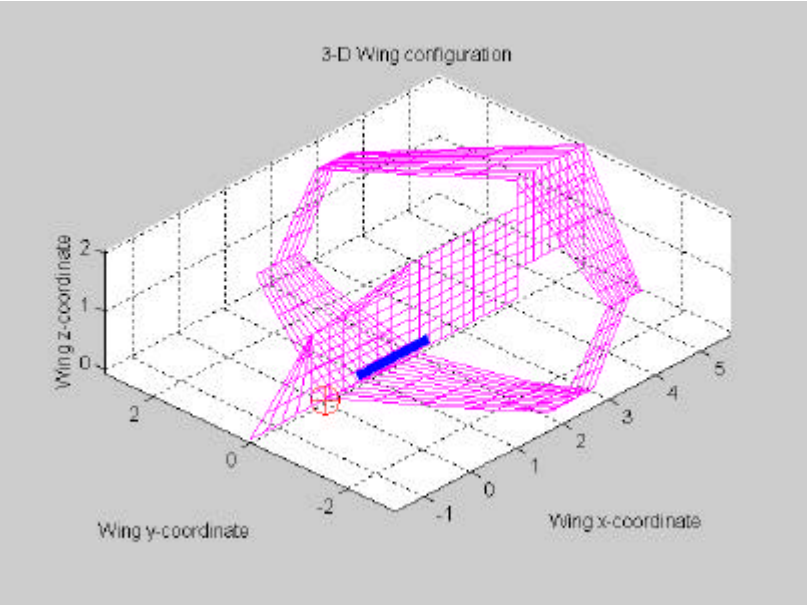

Figure E-22: Aircraft Geometry Model with Fuselage Approximation

Once the fuselage geometry was set, it was a simple matter of running angle, rate, and control sweeps to obtain the stability and control derivatives necessary for dynamic analysis. Unfortunately, the numbers obtained failed a 'common sense' check. For example, a positive roll damping derivative, C_{lp}, was obtained. This derivative measures the resistance of the air to a rolling motion, therefore C_{lp} will always be negative, regardless of the configuration. Similar results were obtained for other derivatives.

The reason for these poor results most likely had to do with the fact that *Tornado* uses an inviscid vortex panel method. The forces and moments are all calculated based on relative panel strengths over the entire model. The fact that five flat plate airfoils were placed adjacent to one another could cause some strange interaction effects.

With unusable results from *Tornado* and a highly non-planar wing configuration, it became impossible to perform accurate analysis without wind tunnel tests. Testing a scale model in a wind tunnel would allow the angle, rate, and control sweeps to be run manually, while measuring the actual forces and moments as opposed to calculating them with a vortex lattice method. As with the longitudinal example, the derivatives would then be passed to the *Lin* function to obtain the system matrices. The eigenvalues and dynamic properties could then have been easily calculated.

Based on the fact that Ikelos met all static stability requirements as well as requirements for level one longitudinal flying qualities (in most cases), a preliminary assumption that the lateral-directional dynamics would be satisfactory was made, pending wind tunnel test data.

E-6 DESCRIPTION OF DERIVATIVES

The derivatives used in this Appendix show how the states and controls affect the non-dimensional force and moment coefficients. This information can be used to determine the level of both static and dynamic stability present as well as the effectiveness of the controls.

E-6.1 Longitudinal

Angles:

- $C_{L\alpha}$ (Lift Curve Slope)
  This derivative describes how the lift varies with angle of attack. For the majority of the lift curve, it can be assumed linear ($C_{L\alpha}$ = constant). It becomes nonlinear near the stall condition, or in other words at high angles of attack and very low speeds.
- $C_{M\alpha}$ (Pitch Stiffness)
  The pitch stiffness is the longitudinal static stability parameter. For longitudinal static stability, C_{M0} must be positive and $C_{M?}$ must be negative.
- $C_{D\alpha}$
  The drag coefficient is usually thought of as being a function of the lift coefficient according to $C_D = C_{d0} + kC_L^2$ to the extent that C_L is linear in α. This means that C_D is a function of α^2.

Rates:

- C_{Lq}
  When a pitching moment is present, a non-zero pitch rate results. The rotary motion of the aircraft through the air causes a "relative wind" to be imposed particularly on the horizontal tail, changing the effective angle of attack, and thus changing the lift.
- C_{Mq}
  As stated above, a non-zero pitch rate causes a "relative wind" in the opposite direction of the pitching moment. This in effect damps the motion and acts against the direction of the pitching moment.
- $C_{L\alpha dot}$
  As the angle of attack is changed, the flow field does not adjust instantaneously. Some time is needed before the lift begins to act according to the lift curve slope. The alpha-dot derivative is a contrived attempt to account for this.
- $C_{M\alpha dot}$
  See $C_{L\alpha dot}$, substitute "pitching moment" for "lift."

Controls:

- $C_{L\delta e}$
  Any application of pitch control results in an unbalanced lift force on the airplane, therefore lift coefficient is dependent on pitch control
- $C_{M\delta e}$ (elevator power)
  Controls are generally considered moment generators, this derivative measures the effectiveness of the pitch control. In other words, for a given elevator deflection, this

derivative is a measure of the resulting change in pitching moment for a given flight condition.

- $C_{D\delta e}$
  Since drag is a function of lift, and lift is a function of pitch control, drag is also a function of pitch control.
- $C_{T\delta T}$
  This derivative measures the change in thrust for a given throttle change.

Velocity:

- C_{LM}
  This derivative is a measure of the change in lift coefficient due to Mach effects.
- C_{DM}
  This derivative is a measure of the change in drag coefficient due to Mach effects.
- C_{mM}
  This derivative is a measure of the change in pitching moment coefficient due to Mach effects.
- C_{TV}
  This derivative is a measure of the variation in thrust with airspeed.

E-6.2 Lateral-Directional

Angles:

- $C_{Y\beta}$
  This derivative is synonymous to the lift curve slope except sideways. In the presence of sideslip the fuselage and vertical tail act together to produce a sideways aerodynamic force. The curve is similar to that of the lift curve, except that (due to inefficiency of the fuselage as an airfoil) the slope is less and stall occurs earlier.
- $C_{l\beta}$ (dihedral effect)
  The most obvious contributor of rolling moment due to sideslip is the presence of off-CG vertical surfaces (such as the vertical tail). The vertical tail generates an aerodynamic force in the presence of sideslip, which in turn generates a rolling moment due to it being off-center. Other more subtle contributors result from wing dihedral, wing sweep, and wing vertical location.
- $C_{n\beta}$ (? ? Weathercock stability parameter)?
  The generation of yawing moment in the presence of sideslip is analogous to the generation of pitching moment in the presence of angle of attack. The weathercock stability parameter should be positive for static stability due to the direction in which β is defined (positive sideslip is nose left and positive yaw moment is nose right).

Rates:

- C_{Yp}
  Coefficient representing the dependency of side force on roll rate.
- C_{lp}
  A roll rate damps the roll moment in a similar fashion to the damping of the pitch moment discussed above. A roll rate causes an increased angle of attack on one wing, which increases the lift on that wing, negating some of the rolling moment.

- C_{np}
  As lift is increased on one wing due to the roll rate, the drag is also increased, usually causing some level of adverse yaw (meaning roll right will cause a slight yaw left).
- C_{Yr}
  This is analogous to C_{Lq} except sideways.
- C_{lr}
  The yaw rate causes an induced angle of attack on the rudder, changing the aerodynamic force that acts off-center, causing a rolling moment.
- C_{nr}
  This is the vertical equivalent of the above example of pitch rate affecting the horizontal tail.

Controls:

- $C_{Y\delta a}$
  This derivative is usually very small if not negligible for conventional airplanes, as the ailerons produce a moment very close to a pure couple.
- $C_{l\delta a}$
  This derivative measures the effectiveness of the ailerons, which directly cause a rolling moment.
- $C_{n\delta a}$
  Ailerons generate a moment by increasing the lift on one wing while decreasing the lift on the other. As mentioned above, adverse yaw results from the increase in induced drag on one wing.
- $C_{Y\delta r}$
  A change in rudder deflection causes a change in the aerodynamic force on the vertical stabilizer, directly affecting the side force.
- $C_{l\delta r}$
  A rudder deflection causes a change in the aerodynamic force on the vertical stabilizer, which acts off-center and causes a rolling moment.
- $C_{n\delta r}$
  This derivative measures the effectiveness of the rudder. In other words, for a given rudder deflection, this derivative is a measure of the resulting change in yawing moment for a given flight condition.

REFERENCES

1. Roskam, J., *Airplane Design Part VII: Determination of Stability, Control and Performance Characteristics: FAR and Military Requirements*, Roskam Aviation and Engineering Corporation, Ottawa Kansas, 1991

2. Roskam, J., *Airplane Design Part VI: Preliminary Calculation of Aerodynamic, Thrust and Power Characteristics*, Roskam Aviation and Engineering Corporation, Ottawa Kansas, 1990

3. Etkin, B. and L. Reid, *Dynamics of Flight: Stability and Control*, John Wiley & Sons, Inc. New York, 1996

4. Raymer, Daniel P., *Aircraft Design: A Conceptual Approach*. American Institute of Aeronautics and Astronautics Inc., Reston, VA, 1992

5. USAF, *Stability and Control DATCOM*, Air Force Flight Dynamics Lab, U.S. Air Force, 1960 (revised 1978)

6. "Military Specification Flying Qualities of Piloted Aircraft." MIL-F-8785C, 1980

7. "The Code of Federal Regulations," United States Government Printing Office, Washington D.C., http://www.access.gpo.gov/nara/cfr/cfrhtml_00/Title_14/14tab_00.html, April 25, 2002.

8. Durham, W., "AOE 4144 and AOE 5214 Course Notes," Virginia Polytechnic Instituteand State University, 2001.

9. Stevens, B. and F. Lewis, *Aircraft Control and Simulation*, John Wiley & Sons, Inc., New York, 1992.

Appendix F: Weight and Balance

TABLE OF CONTENTS

F-1: MASS CALCULATIONS…… F-3
F-2: MASS/WEIGHT BREAKDOWN…… F-5
F-3 CONFIGURATION SCENARIOS…… F-6
F-4 CG EXCURSION…….. F-7
REFERENCES ……..... F-8

LIST OF FIGURES

Figure F-1 CG Excursion
Figure F-2 MTOW CG Movement

LIST OF TABLES

Table F-1 Component Mass/Weight Breakdown
Table F-2 CG Location for various configuration scenarios

LIST OF SYMBOLS

M_{wing}	Wing mass, lb
M_{tail}	Tail mass, lb
S_w	Trapezoidal wing area, ft^2
M_{fw}	Mass of fuel in wing, lb
A	Aspect Ratio
λ	Taper ratio
t/c	Thickness/chord ratio
Λ	Wing sweep at 25% MAC, deg
N_z	Ultimate load factor, g
M_{dg}	Design gross mass, lb
H_t	Horizontal tail height above fuselage, ft
H_v	Vertical tail height above fuselage, ft
S_{vt}	Vertical tail area, ft^2
Λ_{vt}	Tail sweep, deg
S_f	Fuselage wetted area, ft^2
L_t	Tail length: wing quarter MAC to tail quarter MAC, ft
L/D	Lift to drag ratio
N_l	Ultimate landing load factor, g
M_l	Landing design gross mass, lb
L_m	Length of main landing gear, in
L_n	Length of nose landing gear, in
V_t	Total fuel volume, gal
V_i	Integral tanks volume, gal
N_t	Number of fuel tanks

N_{en}	Number of engines
L	Fuselage structural length, ft
B_w	Wing span, ft

F-1 MASS BREAKDOWN FORMULA

A crucial part of any aircraft design development is the weight and balance analysis. This section is closely related to the stability and control of the aircraft by determining the location of the center of gravity and the movement of the CG during any given flight scenario. A great deal of data exists for mass estimations for general aviation aircraft. For Ikelos, the methods presented by Raymer[1] were used. The equations used in the analysis are shown below. It should be noted that the input values in the following equations are in English units, as dictated by Raymer's empirical methods. These are converted to SI for use in later analysis.

The mass of the wing:

$$M_{wing} = 0.036 S_w^{0.758} M_{fw}^{0.0035} \left(\frac{A}{\cos^2\Lambda}\right)^{0.6} q^{0.006} \lambda^{0.04} \left(\frac{100t/c}{\cos\Lambda}\right)^{-0.3} (NzMdg)^{0.49} \quad \text{(F-1)}$$

The mass of the tail:

$$M_{vertical\ tail} = 0.073 \left(1 + 0.2\frac{H_t}{H_v}\right) (N_z M_{dg})^{0.376} q^{0.122} S_{vt}^{0.873} \left(\frac{100t/c}{\cos\Lambda_{vt}}\right)^{-0.49}$$
$$\times \left(\frac{A}{\cos^2\Lambda_{vt}}\right)^{0.357} \lambda_{vt}^{0.039} \quad \text{(F-2)}$$

The mass of the fuselage:

$$M_{fuselage} = 0.052 S_f^{1.086} (N_z M_{dg})^{0.177} L_t^{-0.051} (L/D)^{-0.072} q^{0.241} \quad \text{(F-3)}$$

The mass of the main landing gear:

$$M_{main\ landing\ gear} = 0.095 (N_l M_l)^{0.768} (L_m/12)^{0.409} \quad \text{(F-4)}$$

The mass of the nose gear:

$$M_{nose\ landing\ gear} = 0.125 (N_l M_l)^{0.566} (L_m/12)^{0.845} \quad \text{(F-5)}$$

The mass of fuel system:

$$M_{fuel\ system} = 2.19 V_t^{0.726} \left(\frac{1}{1 + V_i/V_t}\right)^{0.363} N_t^{0.242} N_{en}^{0.157} \quad \text{(F-6)}$$

The mass of the flight control system:

$$M_{flight\ controls} = 0.053 L^{1.536} B_w^{0.371} (N_z W_{dg} \times 10^{-4})^{0.80} \quad \text{(F-7)}$$

F-2 WEIGHT/MASS BREAKDOWN

From equations F-1 through F-7, the aircraft weight or mass can be calculated in a component-by-component manner. Given the aircraft geometry and placement of key aircraft systems, the distribution of this weight can also be modeled. By considering the components to be point masses at a fixed location within a fixed reference system, the center of gravity can easily be calculated. The reference point used in this analysis was the front wing apex location. The following Table lists the component, component weight/mass, and location within the reference frame for the maximum takeoff weight case (MTOW):

Table F-1: Weight/Mass breakdown by aircraft component

Component	Weight (lb)	Mass (kg)	CG from wing apex (m)	%MTOW
Front Wing	117	53	1.4	8.6
Rear Wing	100	45	4.3	7.3
Wing tips	37	17	2.7	2.7
Tail	32	15	4.5	2.3
Fuel systems	23	11	2.1	1.7
Fuselage1 (10%)	7	3	-1.2	0.5
Fuselage2 (60%)	44	20	0.5	3.2
Fuselage3 (30%)	22	10	2.7	1.6
Front gear	25	11	-0.9	1.8
Rear gear	79	36	2.3	5.8
Structure	486	221	19.1	35.6
Engine	55	25	2.4	4.0
Prop/fan	146	66	2.4	10.7
Eng sys	45	20	2.4	3.3
Propulsion	246	112	7.2	18.0
Controls (cockpit)1	8	3	-0.4	0.6
Controls (cockpit)2	8	3	0.9	0.6
Avionics	25	11	-0.9	1.8
Battery	22	10	1.5	1.6
Equipment	62	28	1.1	4.5
OEW	794	360	27	58.1
Person1	170	77	0.3	12.4
Person2	170	77	1.4	12.4
Baggage1	30	14	1.9	2.2
Baggage 2	30	14	1.9	2.2
Payload	400	181	5.5	29.3
Zero Fuel Weight	1194	542	33	87.4
Fuel	157	71	1.9	11.5
Oil	15	7	2.0	1.1
Fuel+oil	172	78	3.9	12.6
MTOW	1366	620	37	100.0
	CG		**1.792 m (5.88 ft) from apex**	

As shown, the CG location is 1.792 m (5.88 ft) from the apex of the front wing. The neutral point is located at 2.05 m (6.73 ft) front the wing apex. With a mean aerodynamic chord of 1.523 m (5.0 ft), this corresponds to a static margin of 17% at our maximum takeoff weight. Thus, static longitudinal stability is well satisfied in this configuration.

F-3 CONFIGURATION SCENARIOS

It is important in any weight analysis to consider all configuration scenarios an aircraft might face. This is especially true for multi-place tandem pilot designs such as Ikelos. If balance problems occur in any given configuration, efforts must be made to correct them or to provide the operator(s) with specific guidelines for avoiding these problems. The following configuration scenarios were studied in a manner similar to that described above:

Table F-2: Weight and CG location for various configuration scenarios

Config.	Description	Mass (kg)	CG position from apex, m (ft)
1	MTOW	619.8	1.792 (5.88)
2	OEW	367.1	2.167 (7.11)
3	MTOW less 47% fuel	586.3	1.786 (5.86)
4	MTOW with 6%fuel	552.8	1.779 (5.84)
5	MTOW with rear pilot out	529.1	1.846 (6.06)
6	MTOW less 47% fuel, rear pilot out	495.6	1.843 (6.05)
7	MTOW with 6% fuel, rear pilot out	462.1	1.838 (6.03)
8	MTOW, front pilot out	529.1	2.012 (6.60)
9	MTOW less 47% fuel, front pilot out	495.6	2.020 (6.63)
10	MTOW with 6% fuel, no front pilot	462.1	2.029 (6.66)
11	MTOW, rear pilot out, no bags	515.5	1.845 (6.05)
12	MTOW, less 47% fuel, no rear pilot, no bags	482.0	1.841 (6.04)
13	MTOW, 6% fuel, rear pilot out, bags out	448.5	1.837 (6.03)
14	MTOW, no front pilot, no bags	515.5	2.015 (6.61)
15	MTOW, less 47% fuel, no front pilot, no bags	482.0	2.023 (6.64)
16	MTOW, 6% fuel, no front pilot, no bags	448.5	2.033 (6.67)
17	MTOW, no rear pilot, heavy front pilot	547.0	1.794 (5.88)
18	MTOW less 47% fuel, no rear pilot, heavy front pilot	513.5	1.787 (5.86)
19	MTOW, heavy front pilot, no bags, rear pilot out, 6% fuel	466.4	1.776 (5.83)
20	MTOW, rear pilot out, bags out, heavy front pilot	533.3	1.792 (5.88)
21	MTOW, less 47% fuel, no bags, heavy front pilot, rear pilot out	499.9	1.784 (5.85)
22	MTOW, heavy front pilot, no bags, no rear pilot, 6% fuel	466.4	1.776 (5.83)

As shown above, the aircraft has static longitudinal stability in any operational takeoff configuration. The minimum static margin is approximately 2%, which is fairly small. This small margin, coupled with the decrease in visibility from the rear seat, is the reason that the front seat is the "primary pilot". If the aircraft is to carry just the pilot, he would sit in the front seat. In a 2-person configuration, the aircraft can be flown from the front or rear seats.

F-4 CG EXCURSION

As expendable mass is lost, the center of gravity for an aircraft can change quickly. An analysis was done for Ikelos with the only expendable mass being that of fuel. Figure F-1 shows the movement of the CG for various configurations.

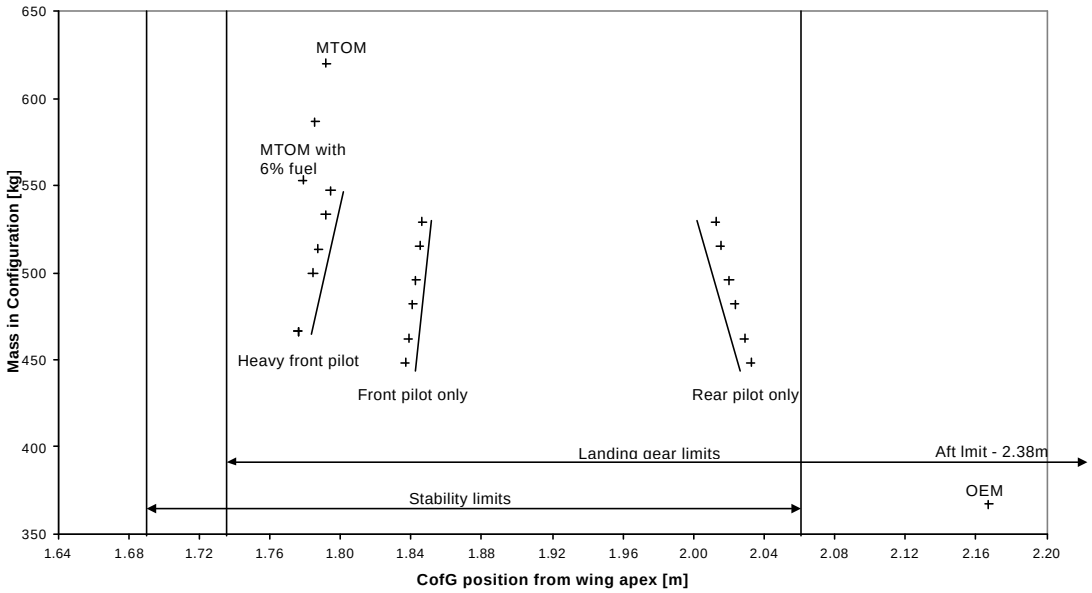

Figure F-1: CG Excursion

Since the center of gravity of the fuel was placed as close as possible to the aircraft empty center of gravity, this motion is minimized. The basic constraints on this movement are the aircraft neutral point and the elevator-limited forward limit. The neutral point is the division between static stability/instability, and the forward limit is placed at the point where the limit of elevator control coincides with the angle of attack for C_{Lmax}. The most extreme cases are depicted in Figure F-1. All other cases would lie near the center of the chart.

Ikelos is seen to be within stability limits for any aircraft configuration. For cases with front pilot only, the CG travels forward with fuel burn, which makes the aircraft more stable. The cases with only a rear pilot, which were described in the previous section as restricted for this design, show an aft movement of the CG. This trend towards decreasing static stability reinforces the descision to make the front pilot the primary pilot. In cases where there are 2 people in the aircraft, the CG location moves approximately 0.01 m (0.033 ft). Figure F-2 shows

the CG location with respect to flight segment. This chart is for the MTOW case, with 6% reserve fuel at landing.

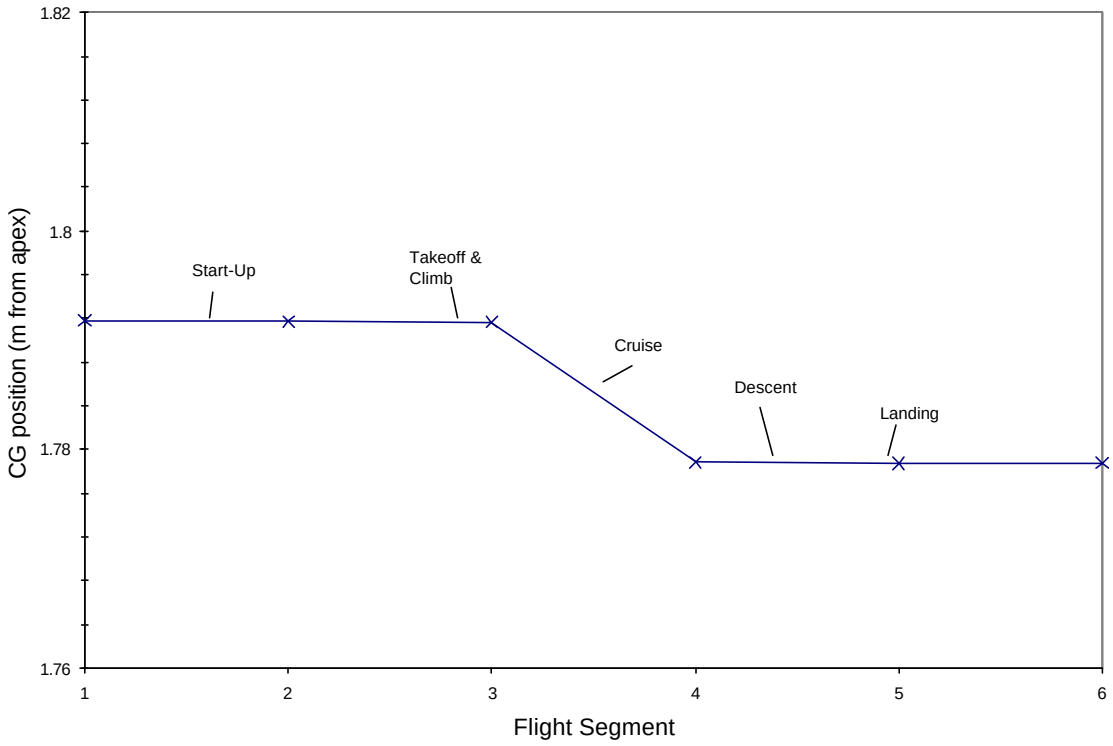

Figure F-2: MTOW CG Movement

REFERENCES

1. Raymer, D., *Aircraft Design: A Conceptual Approach*, AIAA, Reston, VA, 1999.

Appendix G: Structures

TABLE OF CONTENTS

G-1 FUSELAGE AND WING…….. G-3
G-1.1 Materials…….. G-3
G-1.2 Structural Layout……. G-5
G-2 STRUCTURAL LOADS……....G-9
G-2.1 Flight Envelope……G-9
G-2.2 Structural Analysis…….. G-11
G-3 COMPOSITE LAY UP…….. G-16
G-3.1 Composites…….. G-16
G-4 WING DETACHMENT AND TRANSPORTATION…….. G-17
G-4.1 Transportation Issues……... G-17
G-4.2 Wing Folding vs. Detachment……. G-18
G-4.3 Detachment Method…….G-20
G-5 LANDING GEAR DESIGN……...G-22
G-5.1 Static and Dynamic Loads…….. G-22
REFERENCES…….. G-27

LIST OF FIGURES

Figure G-1 Materials Used and Locations
Figure G-2 Structural Layout
Figure G-3 Bulkhead Positioning
Figure G-4 V-n Diagram with End Supports
Figure G-5 Mass Distribution
Figure G-6 Mass Distribution with End Supports
Figure G-7 Lift Distribution
Figure G-8 Illustration of the Shear Force and Bending Moment Distribution for the Front Wings
Figure G-9 Proposed Wing Folding Connection
Figure G-10 Front Wing Connection
Figure G-11 Rear Wing Connection
Figure G-12 Vertical Wing End Connections
Figure G-13 Main Landing Gear Design
Figure G-14 Nose Landing Gear Design
Figure G-15 Overturn and Tailscrape Angles

LIST OF TABLES

Table G-1 Material Properties
Table G-2 Bulkhead Functions and Materials

LIST OF SYMBOLS

σ = stress
CG = center of gravity
C_{Lmax} = maximum lift coefficient
S = wing area
ρ = density of air
α = lift curve slope
M_w = wing bending moment
V_{td} = vertical velocity on touchdown

G-1 FUSELAGE AND WING

G-1.1 Materials

The main goals in designing the structure of Ikelos were to keep it as light and inexpensive as possible. The first decision was in choosing the structural materials. For the fuselage and wing skins, many different materials were considered. Table G-1 below shows the various properties for the materials used.

Table G-1: Material Properties[(1)]

Material	Density kg/m³ (sl/ft³)	S_{1t} MPa (ksi)	S_{2t} MPa (ksi)	S_{1c} MPa (ksi)	S_{2c} MPa (ksi)
HS Carbon Epoxy	1400-1550 (2.72-3.01)	2860 (415)	57 (8.3)	1875 (272)	246 (36)
E-glass Epoxy	1900 (3.69)	1080 (157)	39 (5.6)	620 (90)	128 (18)
Kevlar Epoxy	1380 (2.68)	1280 (186)	30 (4.4)	335 (49)	158 (23)
Aluminum Alloy	2600-2900 (5.04-5.63)	~ 400 (58)	~ 400 (58)	---	300-500 (44-73)

**subscript 1 denotes the fiber direction and subscript 2 orthogonal to the fiber*

The composite materials have large ultimate and tensile strengths compared to their light densities. Even though they are generally more expensive than traditional aluminum alloys, it was decided that the low weight and strength of the composites was more important in the design of Ikelos than the slightly higher cost. Therefore, it was decided to make the skins for Ikelos from glass epoxy, which is easier to form, better impact resistant, and somewhat less expensive than the usual alternative of carbon epoxy.

In order to reduce the amount of internal reinforcing needed for the skins, a Nomex honeycomb core is designed to sandwich between a very thin inner and outer skin of the glass epoxy. This honeycomb core has a density of 144 kg/m³ (0.279 sl/ft³), and a bare compressive strength of 14 MPa (2030 psi) [(1)]. The honeycomb layer provides enough stiffness that it replaces much of the necessary internal stiffening found in traditional aircraft. The honeycomb/glass-epoxy sandwich construction is used on all of the skins of the fuselage and wings. On the bottom of the fuselage and on the lower wing surfaces, the skins are reinforced with Kevlar to provide extra toughness to places where the skins will be subjected to more damage from ground debris. The inboard sections of the upper wing skins are also reinforced with Kevlar, as the skins in this region have to withstand the impact of people stepping onto the wing when entering the aircraft. Figure G-1 shows the locations where materials were used on Ikelos.

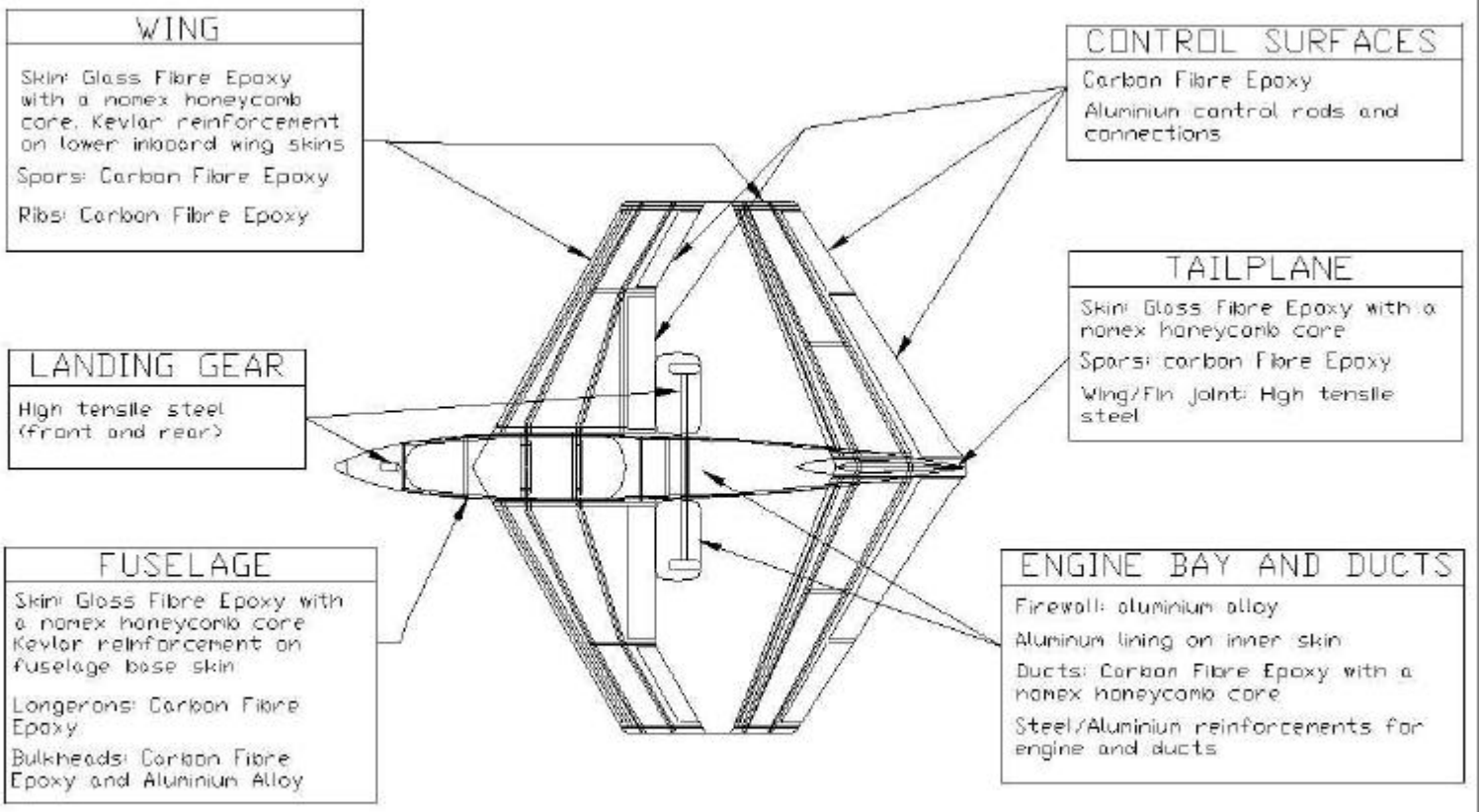

Figure G-1: Materials Used and Locations

The internal structural framework of Ikelos is constructed using carbon fiber because of its increased tensile and compressive strength over glass fiber. The high strength is required because the internal structure of the wings provides the main shear-loading path from skin to skin. The internal structure consists of the main I-section spars, C-section spars, vertical support spars, and ribs. In some places of very high loads, metal reinforcements were used. Metal reinforcements are necessary in high multi-directionally loaded regions because composites are not isotropic like metals. The firewalls are also made out of aluminum alloy to protect the passengers in a fire situation.

G-1.2 Structural Layout

G-1.2.1 Wing Design

As seen in Figure G-2, the forward wing consists of two I-section main spars, a C-section spar and 3 ribs. I-section spars are used as the main load bearing members because they have a high second moment of area for their weight and, thus, have higher critical stresses. The I-section spars start at 23% and 63% of the tip chord but are unable to extend at a constant percentage chord due to the change in planform of the wing and due to the detachable wing considerations. The pilot and passenger of the aircraft need to be able to reach the spar section under their seats in order to attach and remove the wings.

A rib is placed at the bend in the wing, to share the load as reinforcement becomes critical at corners. The C-section also attaches to this rib and extends to the inboard rib. The main advantage of having this C-section is for the attachment of the inboard flaps. A C-section also runs along the leading edge from the tip rib to the inboard rib for the connection of the slat.

The forward wing main I-section spars become solid rectangular box sections at the wing-fuselage junction for detachment and attachment purposes. The starboard and port spars run into a box section, which acts as a guide to insert and hold the wings before fixing them from inside the cockpit. The box sections are also fixed to a frame to transfer the shear loads from the wing into the fuselage. (Figure G-10)

The rear wing contains two main I-section spars at 20% and 60% constant percent chord. The leading edge slat attaches to the forward spar and the trailing edge flaps attach to the rear spar. There are three ribs, one at the inboard section where the loads are high due to the wing attachments, one midway and one at the tip of the wing. The rear wing's I-sections attach to the tail via two, three-way brackets. The brackets are permanently attached to the forward and rear fin spars.

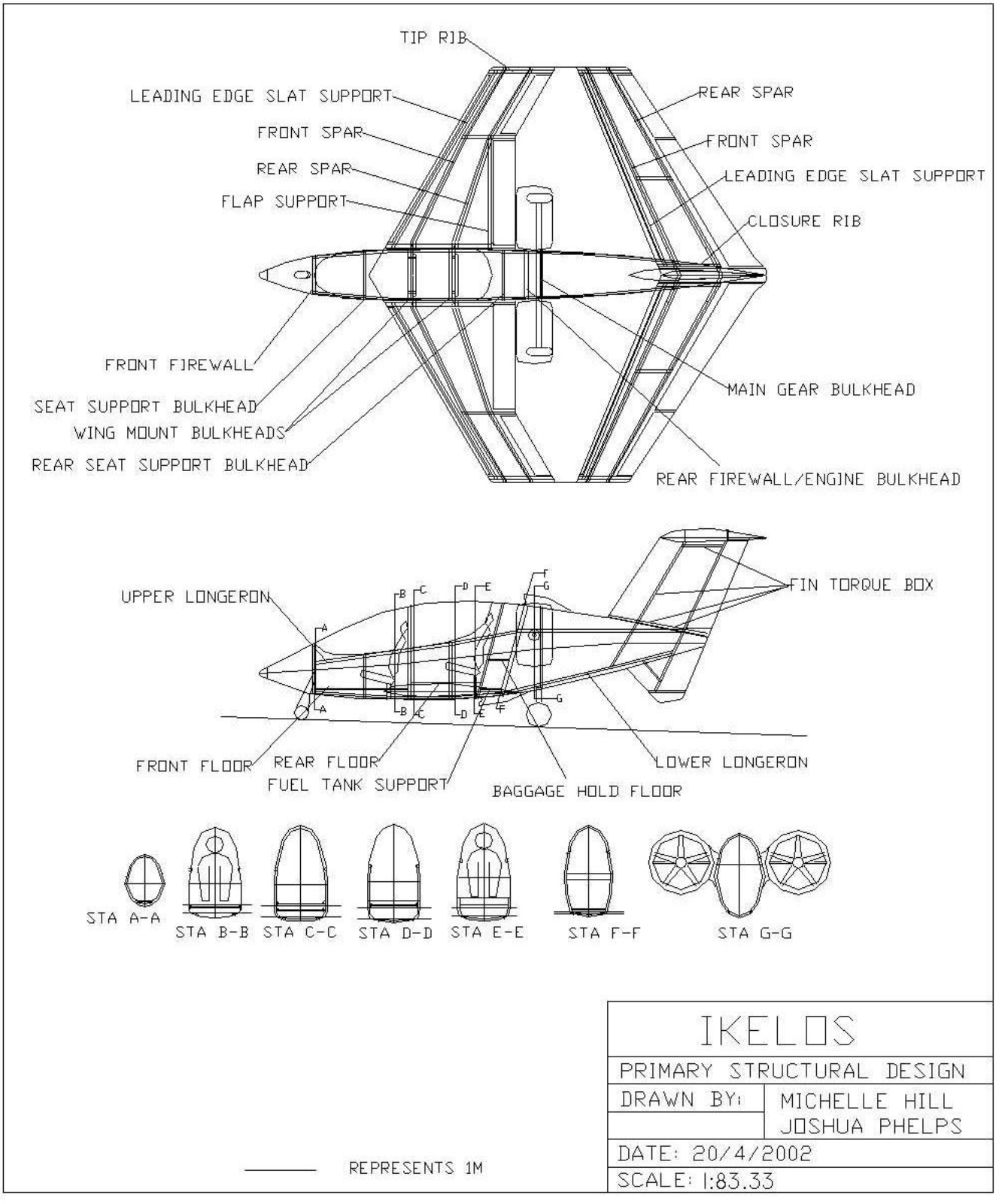

Figure G-2: Structural Layout

G-1.2.2 Fuselage Design

To help meet the performance requirements, the aircraft's overall mass needs to be kept to a minimum. Consequently, the fuselage was designed with as little structure as possible. The majority of the fuselage structure is made of composite materials. This helps to keep the structural weight of the aircraft to a minimum while also allowing a complex but smooth external shape to be produced. Due to the tandem seating arrangement and narrow fuselage width, the cross-sectional shape of the fuselage is generally oval, though flatter at the point where the front wing joins the fuselage to allow for a solid connection point to be incorporated into the structure. This can be seen in the fuselage cross-sectional views shown in Figure G-2.

The fuselage structure consists of four, carbon fiber, top-hat section longerons, positioned in a box shape, running the entire length of the fuselage and through seven bulkheads. The bulkheads are located at points of high loading and connect to each of the four longerons. This allows the loads on the aircraft to be distributed throughout the entire structure. The Nomex honeycomb structure reduces the need for any more structural stiffeners.

The actual position of each structural component is highly dependent on the location of the internal components. This is particularly true in regions such as the cockpit and engine bay. To keep the structure at a minimum, each of the major structural members supports as many internal components as possible. This happens naturally in the center/rear of the cockpit where the wing carry through structure naturally aligns with the central roll bar between the two pilots. It also provides structure underneath the rear pilot, which is good for crash protection purposes. Because there is little structure beneath the front pilot, a small bulkhead and thick floor have been added to provide a seat connection point and to offer some crash protection.

The other key area in the fuselage design is the engine bay. Since the engine and the main landing gear are located in the same region, it was hoped that one bulkhead could be used to support both components. This, however, was not possible due to CG and balance requirements placing them slightly too far apart. The engine bulkhead also acts as a firewall and, unlike the majority of components, is made out of aluminum alloy. It also has been positioned at an angle so that, in the event of a crash, the engine will be deflected downwards, away from the cockpit. A layer of fire resistant paint has been added to the structure around the engine and fuel tank. This paint is used to stop any fuel or oil coming in contact with the composites, since fuel products will destroy the composite structure. The landing gear bulkhead provides a natural connection point for the ducts and other engine related components.

A picture and table showing the position and function of each bulkhead is shown in Figure G-3 and Table G-2 below.

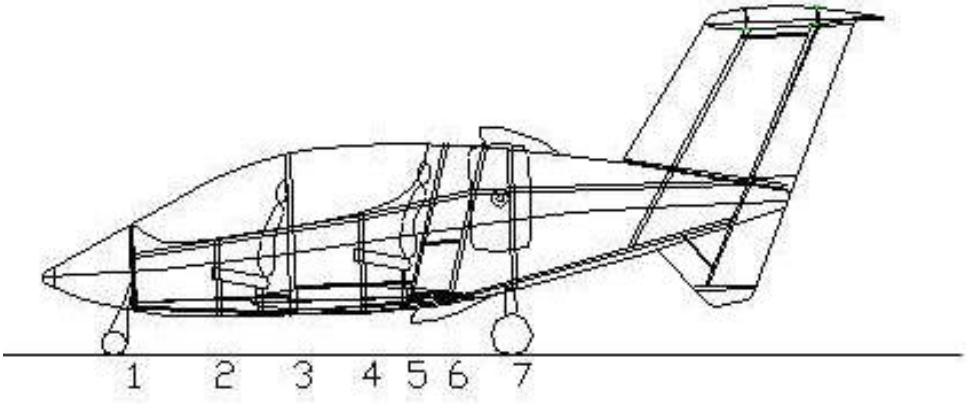

Figure G-3: Bulkhead Positioning

Table G-2: Bulkhead Functions and Materials

Bulkhead	Function	Material
1	Nose gear connection point, front connection point for avionics in nose	Aluminum Alloy
2	Front seat connection point, floor connection	Carbon Fiber Epoxy
3	Front wing spar mounting, roll bar connection, floor connection, avionics connection	Carbon Fiber Epoxy
4	Rear wing spar mounting, rear seat connection point, floor connection	Carbon Fiber Epoxy
5	Rear seat connection point, fuel tank mounting, floor connection point (cockpit and baggage hold)	Carbon Fiber Epoxy
6	Rear firewall, engine mounting, oil and fuel tank mounting	Aluminum Alloy
7	Main gear connection point, duct connection point, engine component connections	Carbon Fiber Epoxy

G-1.2.3 Fin Design

Due to the box wing design, the fin has significantly more force acting on it than that for a conventional wing layout. The two, three-way metal brackets, which join the fin to the rear wing, are bonded to the two carbon fiber I-section spars running vertically through the fin. These

spars are then joined to the four longerons in the fuselage. Two carbon fiber ribs are added at the root and tip of the fin to form a strong torsion box. Like the wing, the fin skin is made from glass fiber with a Nomex honeycomb core and is designed to be load bearing.

G-2 STRUCTURAL LOADS

G-2.1 Flight Envelope

While in flight, Ikelos encounters many different structural loads. To analyze these loads, a V-n diagram was constructed using the load limit guidelines found in JAR-VLA 301-341[(2)]. These guidelines are very similar to the restrictions in FAR23 for general aviation aircraft. Figure G-4 shows the V-n diagram for Ikelos in different flight conditions, and also shows the overall flight envelope.

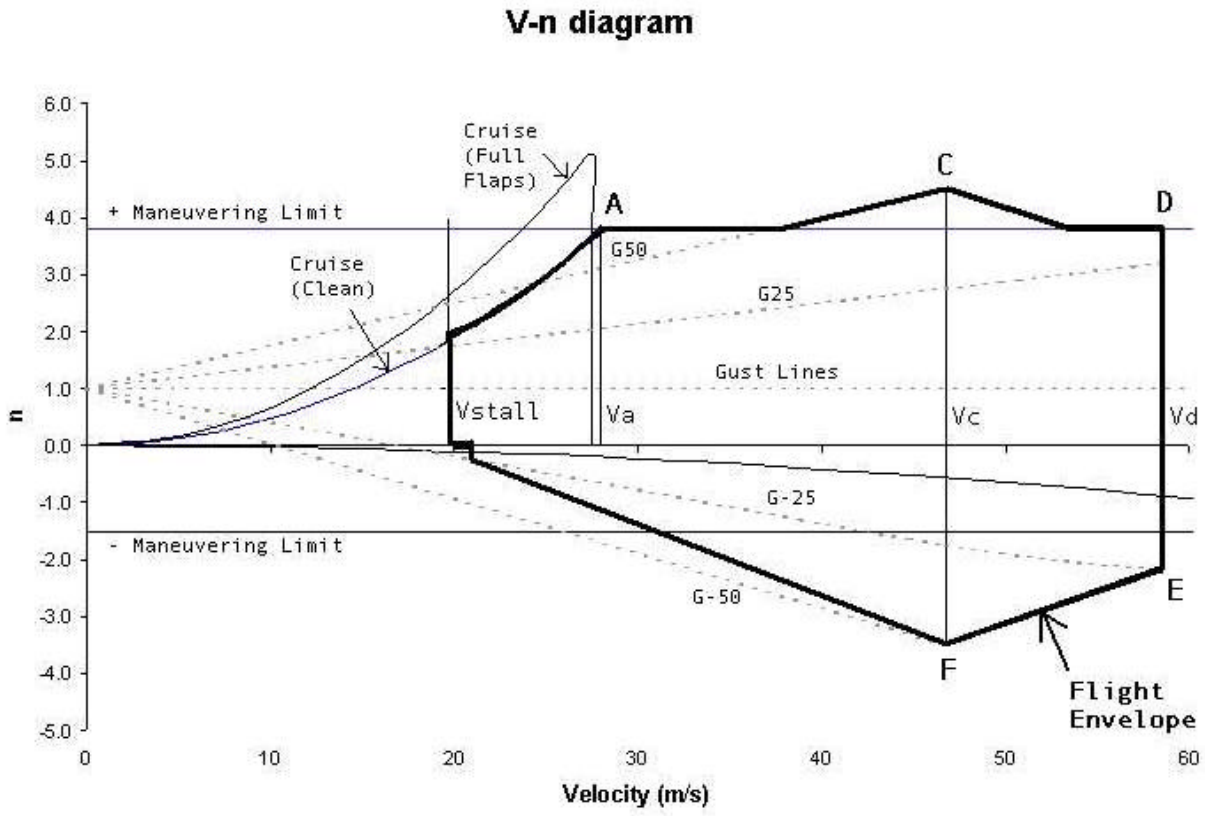

Figure G-4: V-n Diagram with Flight Envelope

The following equations and limits were used to produce the V-n diagram:

Constants:

Density = 1.225 kg/m³ (0.002377 sl/ft³)

Weight = 6200 N (1390 lbf) estimated as a maximum design weight

C_{Lmax} clean = 2.95

C_{Lmax} flaps = 4.19

C_{Lmax} clean neg = -0.16

S_{total} = 15.27 m² (164.4 ft²)

$S_{reference}$ = 8.65 m² (93.1 ft²)

(1) Positive Limit Maneuvering Load: n = 3.8 (JAR 337) (G-1)

(2) Negative Limit Maneuvering Load: n = -1.5 (JAR 337) (G-2)

(3) V_{cruise}: $V_{cruise} = \frac{1/2 * \rho * V^2 * C_{L\max, clean}}{W / S_{total}}$ (G-3)

(4) $V_{full\ flaps}$: $V_{flaps} = \frac{1/2 * \rho * V^2 * C_{L\max, flaps}}{W / S_{total}}$ (G-4)

(5) V_c: $V_C \geq 2.4\sqrt{W / S_{total}}$ (G-6)

(6) V_d: $V_d \geq 1.25 * V_C$ (G-7)

(7) V_{stall} = 19.64m/s (64.4 ft/s) (from performance calculations)

(G-8)

(8) V_a: $V_a \geq V_{stall} * \sqrt{n}$

(G-9)

(9) Calculating Gust Loads:

Gust loads were calculated using the following formula:

$$n_{gust} = 1 + \frac{0.5 * \rho_o V K_g U de}{W / S_{total}}, \quad \text{(G-10)}$$

where,

$$K_g = \frac{0.88 m_g}{5.3 + m_g}$$

$$m_g = \frac{2 * (Mass / S_{total})}{r * \bar{c} * C_{La}} \qquad \text{(G-11)}$$

$$a = 6.35 / rad$$

$$\bar{c} = mean\ geometric\ chord = 1.566\ m\ (5.14\ ft)$$

$$Ude = 15.54\ m/s\ at\ V_c\ (50.0\ ft/s)$$

$$Ude = 7.62\ m/s\ at\ V_d\ (25.0\ ft/s)$$

Values for gust loads were found at V_d and V_c, and then the lines were connected for gusts corresponding to 7.62 m/s (25ft/s) and 15.54 m/s (50ft/s).

G-2.2 Structural Analysis

Figure G-4 shows the maximum loads that the airplane is likely to see. The combination of the maneuvering envelope and the gust diagram produce a maximum load of 4.5 g. This is what the aircraft will be designed to initially with the intention of checking that the structure withstands all other load cases on the diagram eventually. The maximum take off weight of the aircraft is 6076 N (1366 lb), but the maximum design weight is assumed slightly higher at 6500 N (1461 lb) to allow for a safety margin if the weight increases.

G-2.2.1 Wing Structural Analysis

Because of its truss-like structure, the box wing has some structural advantages to that over a normal wing. However, the analysis of the box structure is complicated and is simplified in the following calculations. A complete finite element method analysis would be required for more detailed calculations.

In order to simplify the analysis for calculations, the front and rear wings are assumed to be separate and not joined. That is, the vertical tip supports are removed and the shear force and bending moments calculated. A second analysis attempts to take into account the vertical end supports. Half of the length of the support is effectively added onto the 3m (9.8 ft) span of each front and rear wing and the bending moment at the position the support begins is calculated. This gives an idea of what forces and moments are transferred through the vertical columns helping to size them.

To determine the shear forces and bending moments along the span of the wing, it is necessary to obtain the distribution of weight and aerodynamic loads across the span. An expression for the distribution of the mass of the wings may be determined using the diagram below, Figure G-5. The x distance is from the tip of the wing. This is used instead of the distance, y, from the centerline of the aircraft for ease of integration later. The equation does not include an exact representation of how the chord varies, particularly for the front wing, but the distribution of mass should not be too dissimilar. M_w is the mass of the wing and b_w is the gradient.

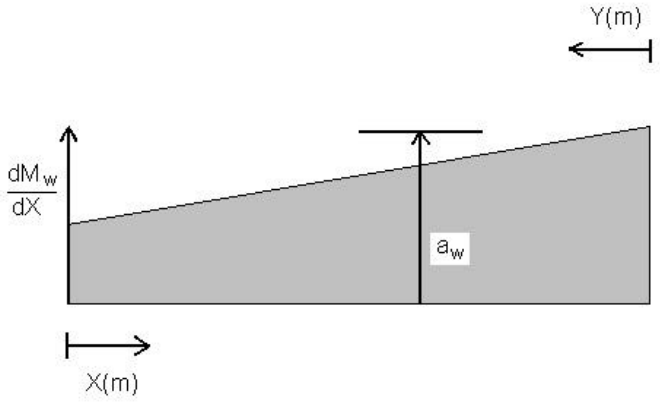

Figure G-5: Mass Distribution

Front wing mass equation development

$$dM_w/dx = a_w + b_w x \qquad \text{(G-12)}$$

$$At\ x=b/2, \quad dM_w/dx = a_w + b_w b/2,$$

$$M_w = a_w b + b_w b^2/4 = 6a_w + 9b_w = 53\ kg \qquad \text{(G-13)}$$

$$And\ at\ x=0,\ dM_w/dx = a_w$$

The mass per unit length at the root is some factor greater than the mass per unit length at the tip of the wing. This number is usually taken to be 3.7.
Thus,

$$a_w + b_w b/2 = 3.7\ a_w$$

$$2.7\ a_w = 3b_w \qquad \text{(G-14)}$$

Solving equation G-2 and G-3 yields $a_w=3.758$, $b_w=3.383$

Thus,

$$dM_w/dx = a_w + b_w x = 3.758 + 3.383x \qquad \text{(G-15)}$$

As a check, the mass of the wing may be determined using Equation G-13.
In order to include the load the aircraft is subjected to, this equation for the distribution of mass may be converted into a force distribution including the load factor n and the acceleration due to gravity.

$$dF/dx = ng(dM_w/dx)$$

$$= 4.5(9.81)(3.758 + 3.383x)$$

$$dF/dx = 166 + 149x$$

Integrating the above, gives a force distribution of $F=166X + 74.5X^2$

Inclusion of end supports

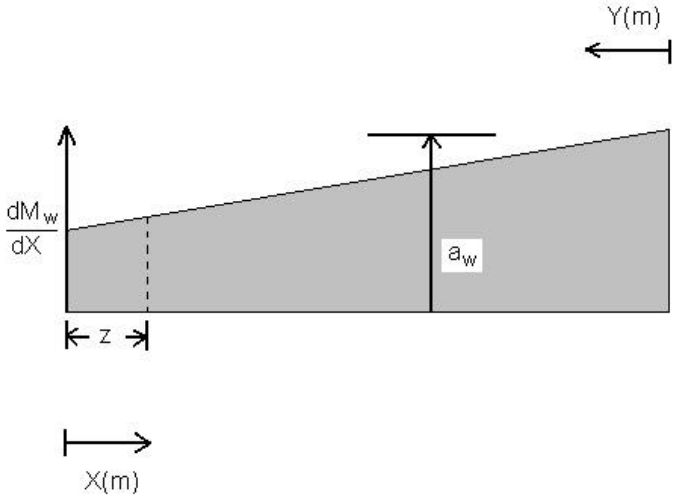

Figure G-6: Mass Distribution with End Supports

Z-Half height of vertical supports

With the inclusion of the tip section, a slightly different mass distribution produces a force distribution of

$$dF/dx = 155 + 113x$$

Using the same method, the rear wing force distribution may be determined with and without the inclusion of the vertical supports.

Rear wing without tip supports: $dF/dx = 141 + 127x$

Rear wing with tip supports: $dF/dx = 135 + 98x$

Lift distribution

The maximum load multiplied by the maximum weight determines the maximum lift of the total aircraft:

$$n_{max}mg=L_{max}=0.5(r_0)(V_{EAS})^2S(C_{LMAX}) \quad \text{(G-16)}$$

Assuming that the maximum weight is used for the calculation, a total lift of 29250 N (6576 lb) is produced. If the lift were spread across the front and rear wings according to the area distribution, the forward wings would produce 57% and the rear 43% of the total (assuming the wings provide all the lift). However, the pressure distribution suggests that the front wing is loaded more heavily per unit area because it is closer to the center of gravity. The front wings providing a lift of 70% of the total is used in the following calculations.
The lift distribution is determined for both the front and rear wings.

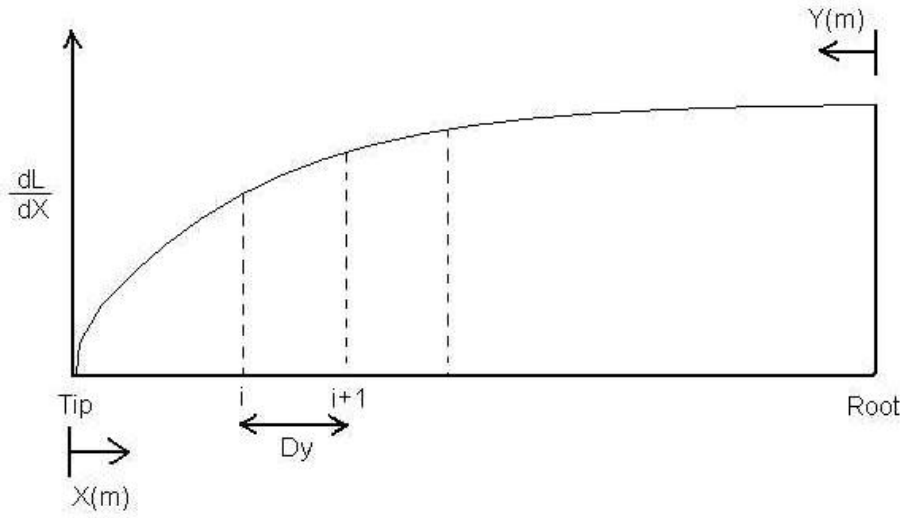

Figure G-7: Lift Distribution

The distribution of lift along the wing is given by

$$dL/dx=1/2(r)(V^2)(C_L)C$$

where all symbols have their usual meanings.
The shear force distribution may be obtained using the trapezoidal method represented by the following equation:

$$S.F.=S\,[(dL/dx)_i + (dL/dx)_{i+1}]Dy/2$$

Noting that the chord for the front wing varies approximately linearly as $C= 0.91 + 0.363X$, allows the above shear force distribution due to lift to be determined for the front wing.

$$S.F.=2154X + 431X^2$$

The rear wing distribution is $S.F.= 968X + 170X^2$

The shear force distributions when including the vertical supports horizontally are:

Forward Wing $S.F.=2154X+347X^2$

Rear wing $S.F.=968X+138X^2$

The total shear force for the front wing including the lift and weight is

$$S.F.=1988X+356.5X^2$$

Integrating to obtain the bending moment yields:

$$B.M.=994X^2+119X^3 \qquad \text{(G-19)}$$

The distribution of shear force and bending moment for each half of the forward wing without the end supports is given below in Figure G-8. Note that y=0 is X=3 m.

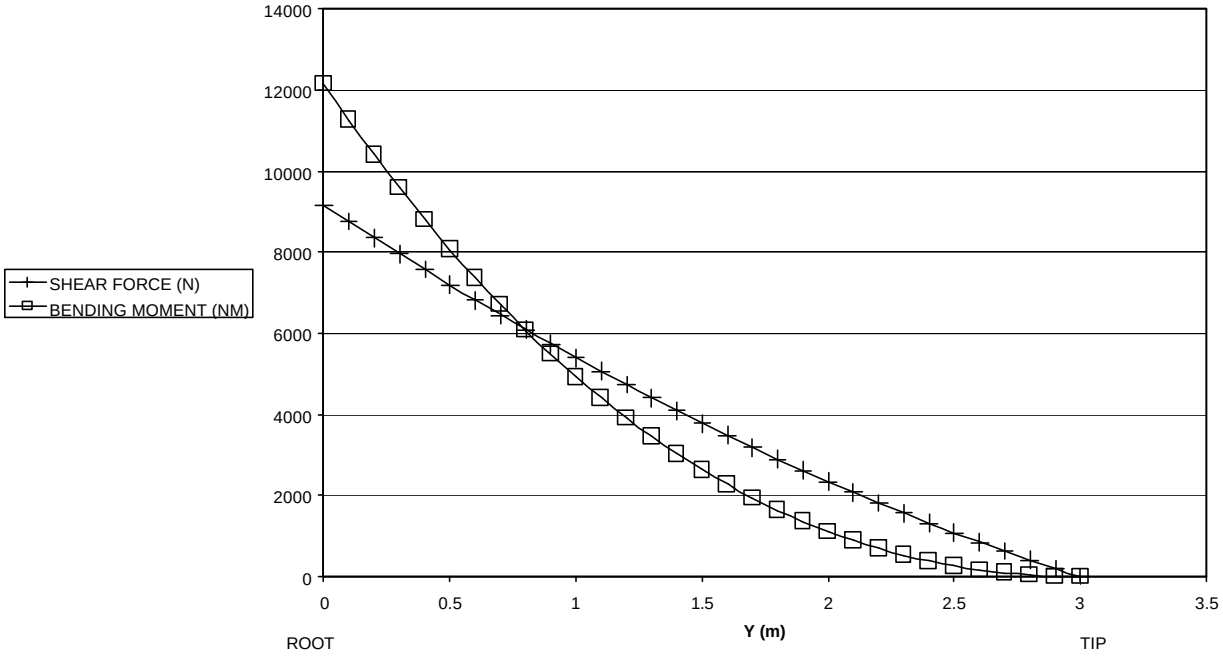

Figure G-8: Illustration of the Shear Force and Bending Moment Distribution for the Front Wings

Results

The bending moments for the rear wing were found in the same manner as for the forward wing. The root (y = 0.375 m (1.23 ft)) bending moment on the forward wing is 9002 N-m (6643 ft-lb), and that for the rear wing root is 3504 N-m (3586 ft-lb). The sum of the bending moment divided by the shear force total at the centerline yields the aerodynamic center as being at y=1.33 m (4.36 ft), which seems reasonable. The bending moment at the point at which the vertical support length begins is 554 N-m (409 ft-lb) contributed by the forward wing and 227 N-m (168 ft-lb) contributed by the rear. These results will need to be validated in future computational analysis.

Now that the moments are known, sizing of the structure can take place. This should be done using the bending stress equation and theory of composite materials. The properties of the materials used in the aircraft are given in Table G-1.

Using the bending equation G-20, an I-section with a web of 15 mm (0.59 in) and top and bottom flanges of 10mm (0.39 in) thick, with an overall height of 161 mm (6.34 in), the required height at the root of the front wing yields a maximum bending stress of 15 MPa (2176 psi). The minimum or governing ultimate stress is the ultimate tensile stress for carbon epoxy. The root stress above is within the safe region by a factor of safety of 3.85. A similar analysis may be carried out for the rest of the wing and as the bending moment becomes less towards the tip, the smaller the spars will become.

$$s_X = My/I \qquad \text{(G-20)}$$

G-3 COMPOSITE LAY-UP

The lay-up of composite materials can have a large influence on its mechanical behavior. The suggested lay-up makes use of a quasi-isotropic lay-up using +45, -45, 0, and 90 degree fiber directions. If the aircraft is loaded in any direction not predicted by the designers, then there is a fiber in the vicinity to pick up the load. Initial calculations were for a skin of solid thickness and no sandwich. Calculations suggested that the skin thickness at the root of the wing would be approximately 3 mm (0.12 in), thinning out toward the tip to 1 mm (0.04 in).

G-3.1 Composites

Research has been carried out into the usage of an all-composite airframe structure. From this, a number of advantages and disadvantages have been identified.[3]

Advantages

1. Low weight, typically around 60% of the weight of aluminum.
2. High strength, a typical carbon fiber/epoxy composite is about 5 times stronger than aluminum.
3. High stiffness, composites are about twice as stiff as aluminum.
4. Ease of manufacturing complex shapes, such as found on the fuselage. Consequently larger and fewer components are required.
5. Continuous construction means fewer fasteners are required and therefore the amount of stress concentrations from drilled holes is greatly reduced. Also the wing and fuselage external surfaces will be smoother.
6. Manufacturing process allows wing skins to be manufactured with integrally bonded stringers helping to increase the stiffness.
7. Manufacturing process is well suited to small, light aircraft.
8. Composites have longer fatigue lives than aluminum, reducing long term maintenance costs.

Disadvantages

1. Overall material cost is more expensive than aluminum.
2. Since composites are a relatively new type of material, more higher factors of safety need to be used for certification purposes than for conventional materials such as aluminum.
3. Manufacturing costs are higher than for standard metal aircraft.
4. Structure needs to be cured in an autoclave taking time and space.
5. More defects are likely to occur during manufacture - time taken to test the structure for defects is much longer than for metal constructions.
6. If a defect is found or a manufacturing mistake is made, the material is wasted as it cannot be recycled or used for another purpose.
7. Molds made for manufacturing of a certain component cannot be modified of reused for other components. Therefore design modifications and the ability to have different variations could become costly.
8. Material properties are affected by temperature with high temperature resistant composites being expensive to manufacture.

9. Material properties can be affected by moisture, which can penetrate and degrade some composites.
10. Composites are more susceptible to impact damage that can lead to material fracture or cracking.
11. Repair of damaged components can be more difficult and expensive as they are expensive to replace due to their size and are not as simple to patch as aluminum.
12. Composites do not offer any protection against lightning strikes as they cannot conduct electricity. Therefore additional aluminum meshes have to be built into the structure adding to the overall weight.

G-4 WING DETACHMENT AND TRANSPORTATION

G-4.1 Transportation Issues

The original specification for the aircraft stated that the aircraft must be able to be transported in the back of a truck or on a small trailer. Research on the feasibility of this was carried out, and it was concluded that although it is difficult it is possible.

The most sensible option would be to transport the aircraft on a specially designed trailer similar to that used for transporting gliders (i.e. all enclosed). However there are a number of regulations in force regarding the size and weights trailers. For the UK they are:[4]

1. The total width of the trailer must not exceed 2.3 m (7.5 ft) (including the wheels and trailer sides).
2. The total length of the trailer must not exceed 7m (23 ft) (excluding the drawbar).
3. There are no height restrictions but it is advised the overall height does not exceed 3m (9.8 ft) for stability reasons (for a height greater than 3m a warning sign must be displayed).
4. The overall combined mass of the trailer and load must not exceed the empty mass of the towing vehicle (typically 1250kg for a car) (weight of 2750lb).
5. For an overall trailer and load mass exceeding 750kg (weight of 1650lb) the trailer must be fitted with wings, springs, and brakes.

The regulations in Virginia, USA are: [5]

1. The total width of the trailer must not exceed 2.59 m (8 ft 6 in) (including trailer and load).
2. The total length of the trailer must not exceed 12.19m (40 ft 0 in).
3. Height of vehicle must not exceed 4.11 m (13 ft 6in) .
4. Single axle weight must not exceed a mass of 9080 kg (weight of 20,000 lb).

The regulations in the US are much less stringent than those in many other countries. However, Ikelos is designed to be used all around the world, so it has been designed to the tighter requirements of the UK, but elements like the ducts may not need to be removed for tailoring in all countries.

As well as meeting all of the legal requirements for transportation the following factors must also be considered when designing the aircraft for transportation:

(1) Even though the aircraft has the room to take two people, it can be flown solo. Therefore the methods used to prepare the aircraft for transportation need to be mechanically quick and simple such that any one person (male, female, tall, short, strong, weak, old or young) can carry out this task unaided. The height of the wing/fin connection will probably be too high to reach from the ground for the average person so a ladder may have to be used, restricting where the aircraft can be disassembled.
(2) The mechanisms used for folding/detachment must be cheap and light.
(3) The overall effect on the aircraft with respect to the possibility of damage to components must be considered. The wings are quite delicate so how will they be affected by constant removal and reconnection? Also, how their separation will affect the strength of the box wing design?

G-4.2 Wing Folding vs. Detachment

To allow the aircraft to be transported the wings with have to be either folded or detached. Both options have been considered.

Folding

Wing folding has many advantages over actual removal of the wings. First, there is no need for storage of the wing sections, and the actual folding can be done by one person, rather than the possible two people needed to carry removable wing sections. The folding, however, would require quite a lot of bending and hinging throughout the wings, making more wing structure and heavy hinging and locking mechanisms a necessity. Figure G-9 shows an example of a possible wing folding scheme.

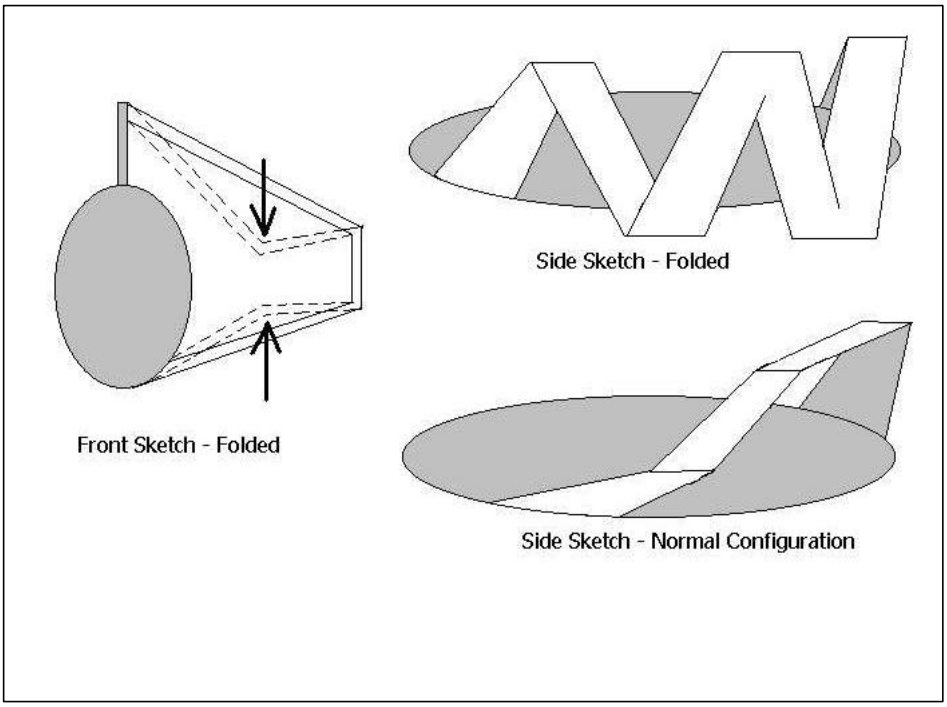

Figure G-9: Proposed Wing Folding Design

Detachment

The main reason for complete removal of the wings concerns the use of composites, especially since almost all of the aircraft is to be made from composites. Some of the benefits of using composites over conventional materials come from the reduction in the number of joints and components required and the increased strength to weight ratio comes from continuous construction. If the aircraft is to have folding wings there will have to be folding joints across the wing span breaking the wing in to parts and therefore reducing the overall strength to weight saving. Additionally it has been found that there are a number of problems with connecting metal and composite parts, due to the difference in the thermal expansion coefficients. Therefore the number of joints needs to be minimized to allow the full benefits of using composites to be realized.

Two methods of detaching the wings were identified: removing each wing at the fuselage and separating at the wing tips, so the wing is in 6 pieces for transportation, or removing the rear and front wings as two whole pieces to aid connection at the fin and nose. The vertical connections will still have to be removed for transportation.

Upon further consideration, it was decided that most owners of Ikelos would only need to trailer it once or twice a year, so the advantages in convenience of wing folding would not outweigh the price in extra weight, cost and complexity. Additionally, since a special trailer will have to be made to transport the aircraft, a method for safely transporting the detached wings can be incorporated into the design at no extra cost. Therefore the complete removal of the wings is the preferred option.

G-4.3 Detachment Method

The wings of Ikelos detach from the fuselage in six sections – a forward right and left wing, a rear right and left wing, and two vertical connectors.

The forward wings connect into the front lower part of the fuselage (Figure G-11). Each main I-spar on the leading edge of the wings becomes a solid rectangular section at the wing root/fuselage junction. These spars slide into the fuselage into a hollow box-like structure where the right and the left spar overlap. At this overlap, the spars are bolted to each other and to the box structure using two bolts. The bolts are accessible through the cockpit of the plane. The box structure is connected to the bulkhead and has fairings on either end to transfer any shear forces into the fuselage skin.

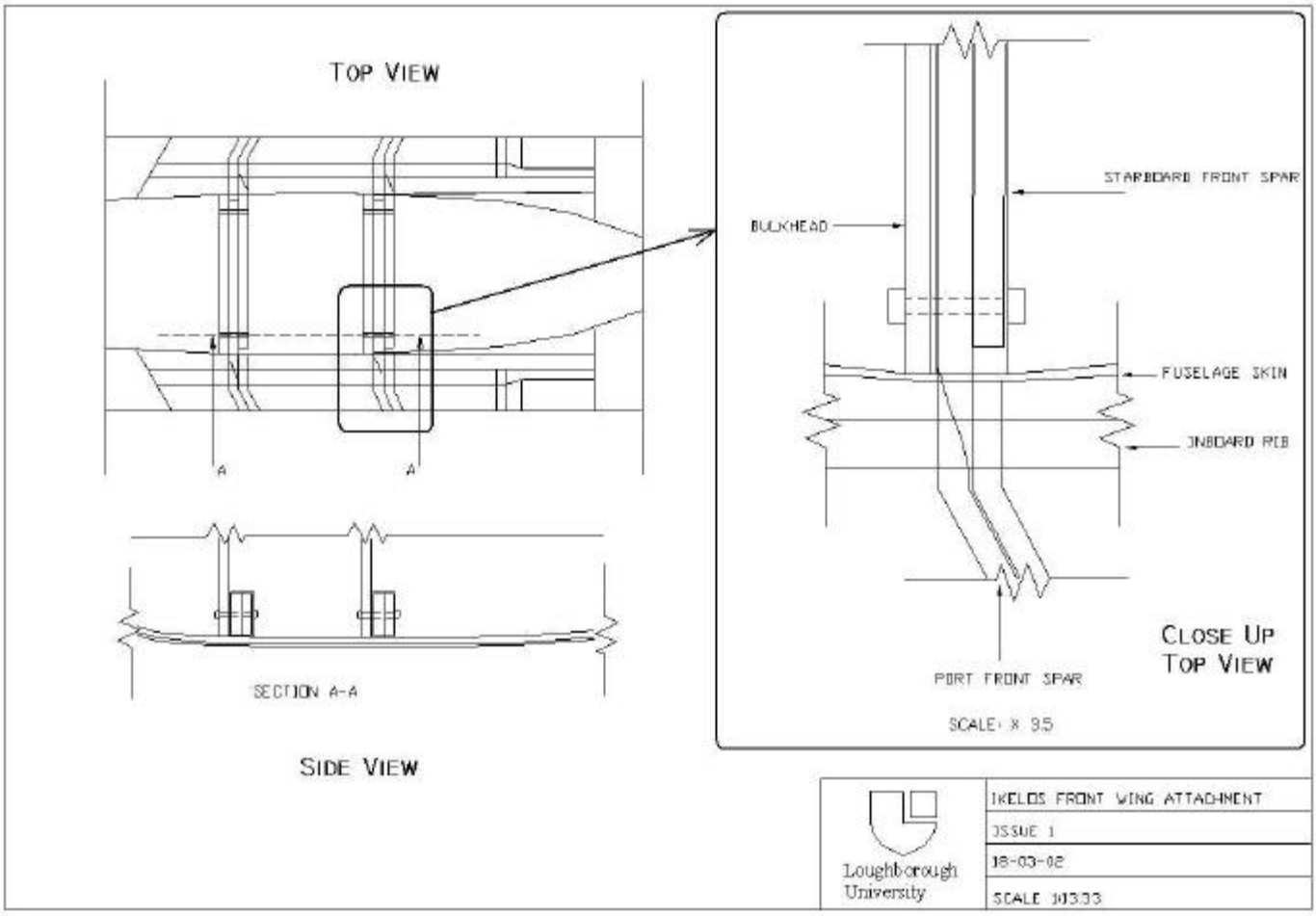

Figure G-10 : Front Wing Connection

The rear wings attach to the top of the tail using two "three-way brackets" (Figure G-11). The brackets are bolted into the fin spar, and the wings slip into the brackets where they are bolted through the wing root rib. The brackets are constructed from wrought aluminum and can be replaced if necessary. In order to reach the rear wing detachments, a person will need the help of a stepladder. However, since the plane will not be disassembled very often, it should not be too much of an inconvenience.

The vertical wing tip sections connect to the outer ribs on the forward and rear wings. (Figure G-12). Two rods are connected to these ribs, and these rods fit into either end of a hollow tube that runs through the vertical wing section. Then, the rods and tube are bolted together to keep the vertical wings in place. The ducts are also designed to be removed for towing. The shafts of the ducts are splined together outside of the fuselage, and are held in place with locking rings.

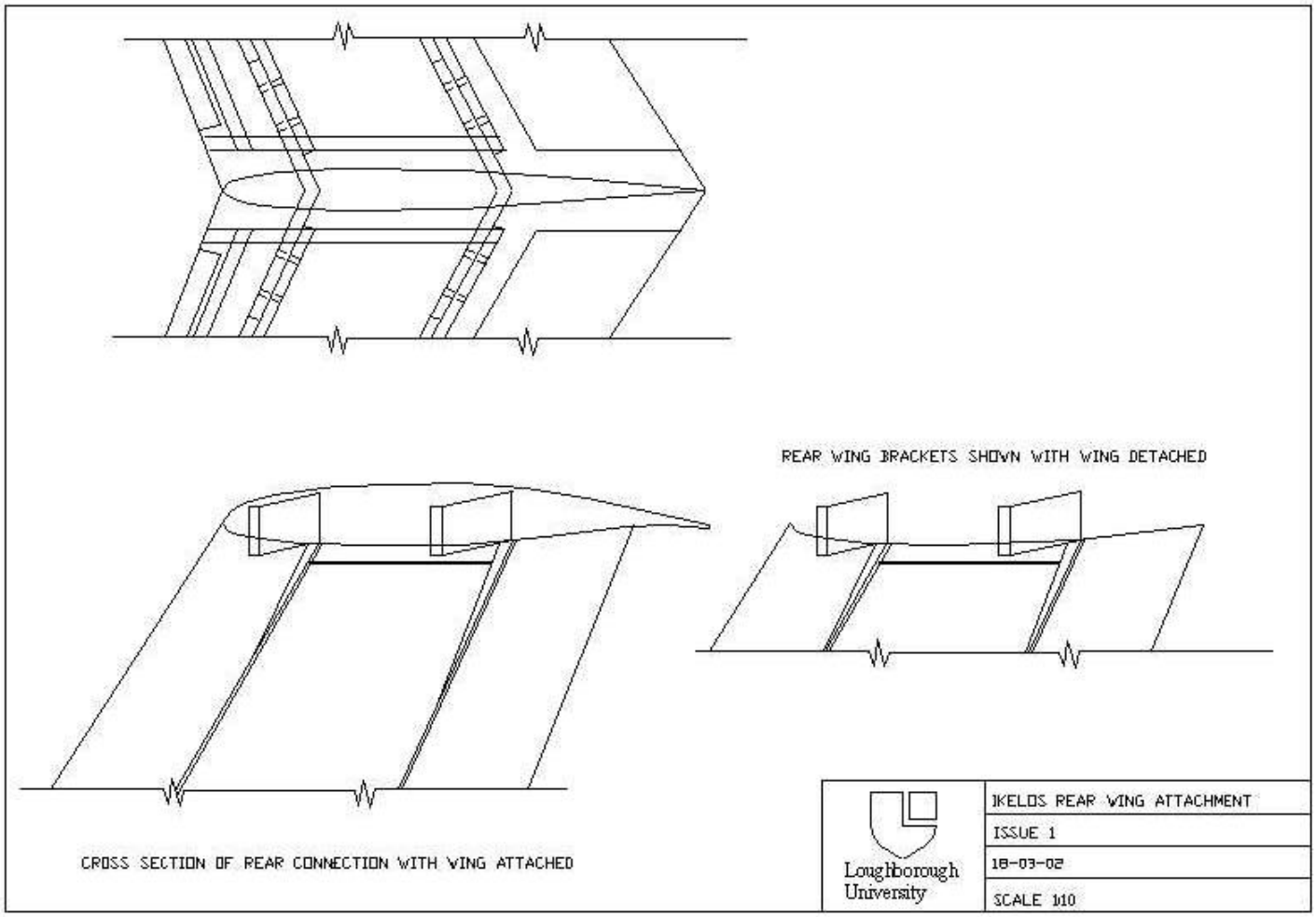

Figure G-11: Rear Wing Connection

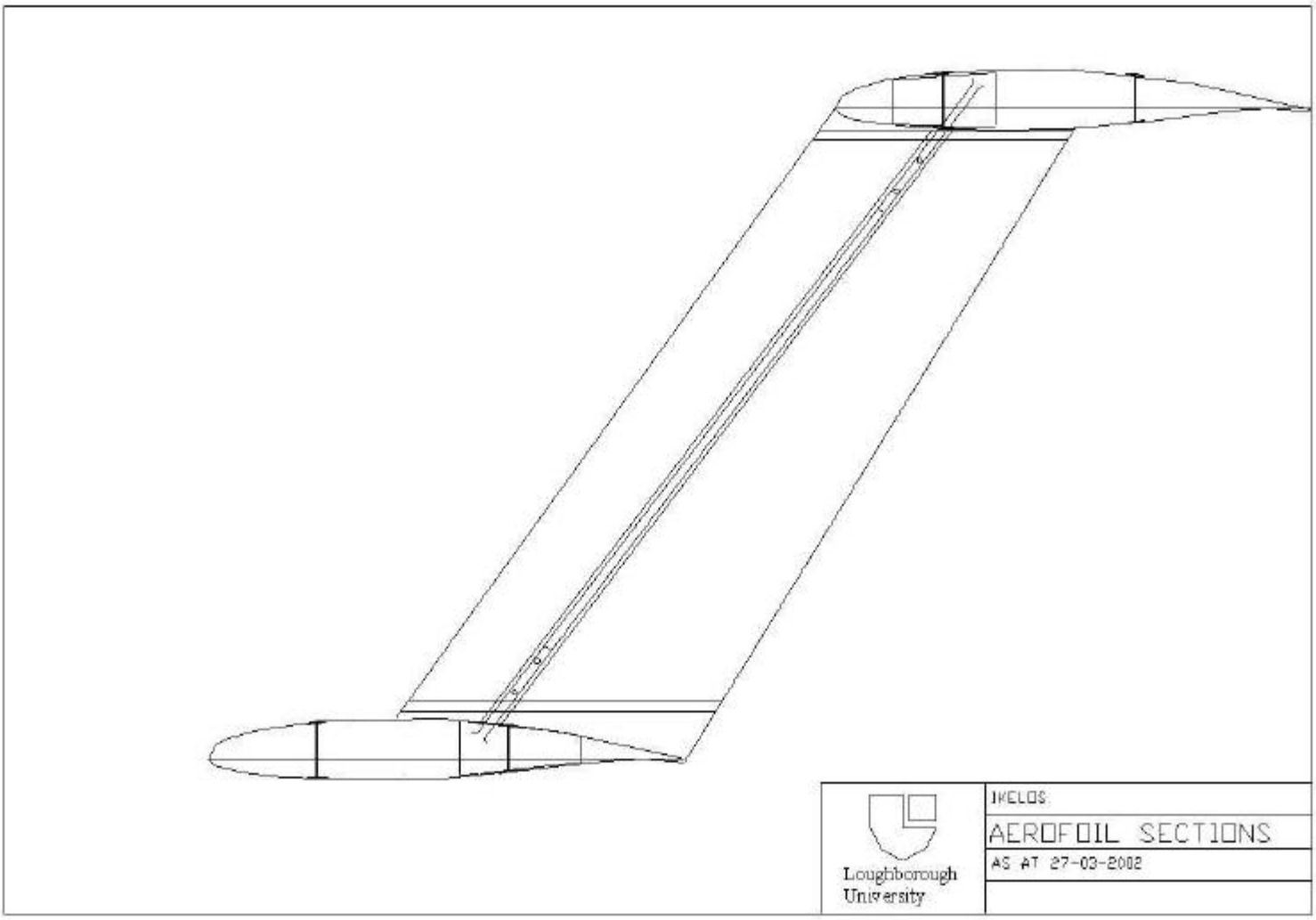

Figure G-12: Vertical Wing End Connections

G-5 LANDING GEAR DESIGN

G-5.1 Static and Dynamic Loads

In the design of the landing gear, simplicity was the main objective in order to keep weight and cost as low as possible. One of the first decisions was whether to make the gear fixed or retractable. The fixed landing gear is much lighter, less expensive to build and maintain, and requires no space in the fuselage for storage. The fixed gear does, however, create a lot of drag while the aircraft is in flight. It was decided that for a light airplane, the savings in drag is not worth the extra cost of weight and complexity involved in retractable gear.

With the fixed gear selected, the actual design of the landing gear could be started. Because Ikelos is designed for STOL flight, the landing gear needs to be slightly stronger than the gear of many traditional general aviation planes. However, since Ikelos has untraditional wings, it is difficult to attach landing gear so that an in-line shock absorber can be used. Instead, the main landing gear is similar to that used by the DHC-Twin Otter aircraft (Figure G-13) that is

basically a spring tube strut attached to the fuselage through a compressed rubber shock absorber. The rubber shock absorber helps to cushion some of the impact that is not absorbed by the cantilever spring action of the spring tubes.[6] The nose gear is similar to that used on the Cessna 172 and other small planes. (Figure G-14) It consists of a strut assembly with a liquid spring shock absorber to cushion loads on landing and take-off, especially if used on dirt or turf airstrips or fields.[6]

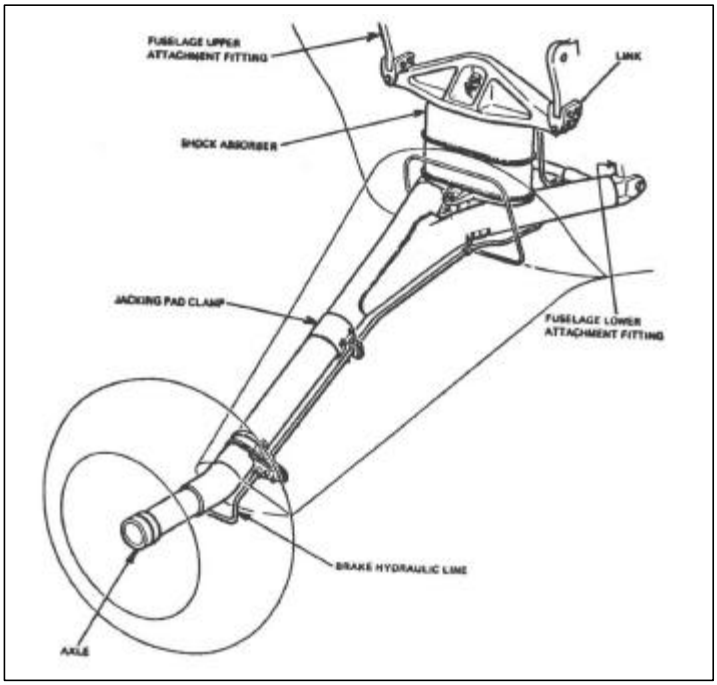

FIGURE G-13: Main Landing Gear Design [6]

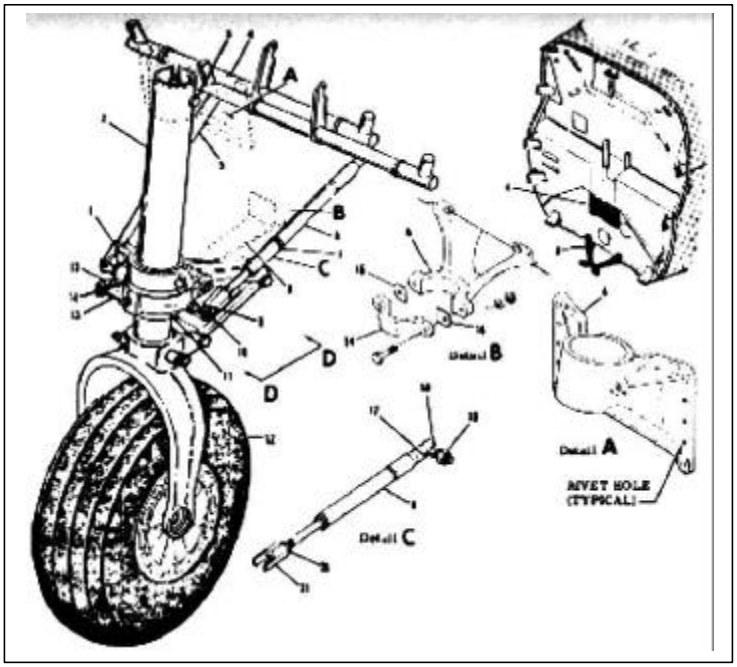

FIGURE G-14: Nose Landing Gear Design [6]

With the landing gear configuration chosen, it was necessary to size the gear, and to calculate the loads on landing needed to be absorbed with the landing gear. The first step is to locate the maximum aft location of the CG, and to place the landing gear so that the turnover angle and the tail scrape angle are acceptable. The turnover angle must be less than 60° for stability and a good ride. The tail scrape angle should be between 10° and 15°.[7] Figure G-15 shows the landing gear locations and angles for Ikelos meeting the general requirements for stability.

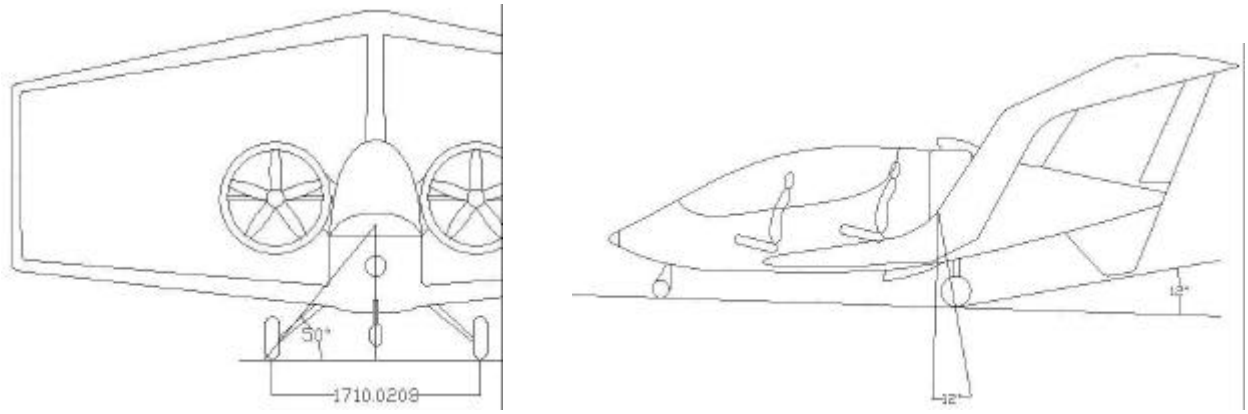

Figure G-15: Overturn and Tailscrape Angles

Once the gear is in position, and the turnover and tail scrape angles are met, the static forces on the landing gear can be calculated, and the tires sized. The nose gear is estimated to carry approximately 10% of the static load of the plane at most times on the ground. With this estimate, each main gear strut carries 45% of the total maximum take-off weight, or 2734N (615lbf). The nose gear will carry, on average, 608N (137lbf). Using these values for weight, the tire sizes could now be determined. The tires were sized to be as small as possible to keep the weight and drag lower, but large enough to carry the static weight plus an added weight margin, as well as be able to absorb some of the force on landing. The tire sizes below were chosen for each gear:

Main Landing Gear [8]

Goodyear, Do 13.7 – 14.2", W 4.65 – 4.95, Type III, 1200 lb Rated Load, 1740lb Max. Braking Load, 3200lb Max. Bottoming Load, 120 Mph speed, 0.916AR, Weight 4.3lbs, Loaded Radius 5.65".

Nose Gear [6]

B.F. Goodrich, Do 8.00", W 3.0", Type I, 450 lb Max. Loading, 55psi, smooth tread pattern, 120 Mph maximum speed, 0.85AR, Weight 1.5lbs.

With the tires sized and the configuration chosen, the loads on landing need to be calculated in order to determine how much energy needs to be absorbed by the gear upon landing. Since Ikelos will land primarily on the main gear, the main gear is designed to absorb all of the energy on landing. Most general aviation and commercial aircraft are designed to land at a usual 0.6-1.2m/s (2-4ft/s) with a maximum of 3.0m/s (10ft/s) vertical descent speed. However, since Ikelos is a short landing aircraft, the performance calculations show that in order to make the 46m (150ft) landing goal, Ikelos will land with a 9° descent slope at a descent speed of around 3m/s. The following equation was used to determine the maximum kinetic energy of Ikelos upon a usual short landing: [6]

$$KE = \frac{1}{2} W * Vtd^2 \div g = 2862J \tag{G-21}$$

where,

$$W = 6076N$$

$$V_{td} = 3.04m/s$$

$$g = 9.81m/s^2$$

This is the total kinetic energy the plane must absorb on impact. The following calculations show the absorption of the energy by the tires, struts, and shock absorbers. For these calculations, it was determined that a pilot can comfortably withstand a g-loading of 3g's for short periods of time in landing.

$$KE = n_S P_m N_g (h_t s_t + h_s s_s) \tag{G-22}$$

the kinetic energy absorbed by tires, struts, and absorbers.
n_s = number of main gear struts = 2
P_m = maximum static load per main gear strut = 2734N
N_g = g-loading = 3
η_t = tire efficiency = 0.47
s_t = maximum tire deflection = Do – 2*(loaded radius) = 0.07m (2.7in)
η_s = efficiency of shock absorber = 0.5 for cantilever spring
= 0.6 for spring tube and rubber blocks (estimated)
s_s = strut deflection necessary to absorb energy

With all of the values known, the necessary strut deflection necessary for energy absorption was calculated: [6]

$$s_S = \frac{1/2 * W/g * (V_{td})^2}{n_s * P_m * N_g * h_s} - \frac{h_t * S_t}{h_s} = \frac{2862}{2 * 2734 * 3 * 0.6} - \frac{0.47 * 0.07}{0.6} = \mathbf{0.236m\ (9.2in)}$$

This deflection was determined acceptable enabling Ikelos to completely absorb the energy of the short landing impact without too much force on the pilot and passenger.

REFERENCES

1. Isaac, D., Ori, I., *Engineering Mechanics of Composite Materials*, Oxford University Press, Inc, New York, 1994.

2. "JARs" Joint Aviation Authorities, Europe, the Netherlands, http://jaa.nl/jar/jar/355000/355325/355325.pdf, 4/23/2002.

3. Hoskin, B. and Baker,A. *Composite Materials for Aircraft Structures*, American Institute for Aeronautics and Astronautics, New York, 1986.

4. "National Trailer and Towing Association," NTTA, Warwickshire, England, www.ntta.co.uk, 2/1/2002.

5. "Virginia Department of Transportation," Richmond, VA, http://virginiadot.org/infoservice/faq-hauling.asp#how, 4/23/2002.

6. Roskam, J., *Airplane Design Part 3: Layout design of cockpit, fuselage, wing and empennage: cutaways and inboard profiles*, Roskam Aviation and Engineering Corporation, Ottawa, KA, 1989.

7. Stinton, D., *Design of the Aeroplane*, Van Nostrand Reinhold Company, New York, 1983.

8. "Goodyear Tire Data Book," Goodyear, Akron, OH, http://www.goodyearaviation.com/tiredatabook.html, 1/25/2002.

Appendix H: Avionics & Systems

TABLE OF CONTENTS

H-1 AVIONICS EVOLUTION..... H-2
H-1.1 Initial Avionics Suite..... H-2
H-1.2 Avionics Development to Baseline Level..... H-2
H-1.3 Final Avionics Suite..... H-3
H-2 INSTRUMENT PANEL AND SUPPLEMENTARY EQUIPMENT..... H-4
H-2.1 Instrument Panel Layout..... H-4
H-2.2 Supplementary Equipment..... H-6
H-2.3 Estimated System Requirements..... H-6
H-3 BRAKING SYSTEM..... H-8
H-3.1 The benefits of anti-lock brakes..... H-8
H-3.2 How anti-lock brakes work..... H-10
H-4 BALLISTIC RECOVERY SYSTEM..... H-11
REFERENCES..... H-11

LIST OF FIGURES

Figure H-1 Instrument Panel Layout
Figure H-2 Avionics Component Weights
Figure H-3 Avionics Component Cost
Figure H-4 Avionics Power Requirements
Figure H-5 Stopping distances in wet and dry conditions
Figure H-6 Variation in relative braking forces with different load distributions

LIST OF TABLES

Table H-1 Baseline Avionics Requirements
Table H-2 Final Avionics Requirements
Table H-3 Braking results in wet conditions
Table H-4 Braking results in dry conditions

H-1 AVIONICS EVOLUTION

H-1.1 Initial Avionics Suite

Initial avionics research was performed on the basis that the design objective was a light, single seat aircraft mainly for sport use. In terms of on-board equipment, this definition makes the aircraft comparatively similar to current-day gliders and ultralights and these were the categories of aircraft in addition to FAR/JAR requirements that defined the avionics package that would be required.[1,2]

Strictly speaking, in the most relaxed airspace the only obligatory avionics equipment required is an airspeed indicator, an altimeter and a magnetic direction indicator. This would be considered a minimalist approach and would severely limit the operational capabilities of the aircraft. A more rational approach was taken and the equipment listed above was supplemented by an artificial horizon, a climb/descent indicator, a Very High Frequency (VHF) Communication (COMM) radio and a Mode A (identification return) transponder. This widened the flight envelope to encompass limited Instrument Flight Rules (IFR) flying and Visual Flight Rules (VFR) in controlled airspace, which takes into account most flight regimes undertaken by light general aviation (GA) aircraft.

H-1.2 Avionics Development to Baseline Level

As aircraft concept evolved, it became clear that the role of the vehicle was changing from a light sport-aviation aircraft to a more commuter-based GA machine and this put more emphasis on all-weather (or certainly more-weather) operations than previously being considered. The result was an updated, more comprehensive avionics package, which would provide the pilot with full Instrument Flight Rules (IFR) capabilities. This revised specification was set as the Baseline Avionics Requirements, as shown in Table H-1.

Table H-1: Baseline Avionics Requirements

Avionics	Required under JAR 23 ?
Flight and navigation instruments (JAR 23.1303)	
Airspeed indicator	Yes
Altimeter	Yes
Non-stabilised magnetic direction indicator	Yes
2x COM & NAV Radio combo	Yes (NAV only required for IFR)
Transponder	Yes
VOR 1 indicator	No (Required for IFR)
VOR 2 indicator	No (Required for IFR)
ADF indicator	No (Required for IFR)
ADF radio	No (Required for IFR)
DME indicator	No (Required for IFR)
DME receiver	No (Required for IFR)
Attitude indicator	No (Required for IFR)
Vertical Speed Indicator	No (Required for IFR)
Turn Co-ordinator	No (Required for IFR)
GPS navigation system	No
Powerplant instruments (JAR 23.1305)	
Fuel quantity indicator for each tank	Yes
Oil pressure indicator	Yes
Oil temperature indicator	Yes
Oil quantity indicator for each tank	Yes
Tachometer	Yes
Fuel flow meter	Yes
Fuel pressure indicator	Yes

Powerplant instrumentation was included in the specification for completeness, as these instruments would require space on the instrument panel and would be competing for the pilot's attention alongside the flight and navigational equipment.

The GPS system was introduced due to their increasing popularity for GA use, and the resulting decreasing prices both now and in the future. The system provides the pilot with navigational accuracy far greater than can be achieved with standard radio equipment, and can present the information in a more intuitive manner. It is not required by regulations but does supply the pilot with greater flexibility and the reliability combined with the ease-of-use are what factors which pilots want where navigational systems are concerned.

Other than the addition of the GPS system, the main supplementary instrumentation comprised of radio navigation receivers and transmitters, needed for IFR navigation. Vari-Omni Range (VOR) indicators were installed at this stage as they are the most common ground-based navigational beacon in use around the world today and for the foreseeable future. The techniques involved in obtaining the directional and range information required are simple and can be quickly performed by a pilot who has basic experience in navigational techniques. This, combined with the reliability of the equipment – Mean Time Between Failures (MTBF) of approximately 5000 hrs – makes the inclusion of a VOR system virtually mandatory on IFR-capable aircraft. Automatic Direction Finder (ADF) receivers are a more basic version of VOR instrumentation, providing bearing-only information to the pilot. This equipment is not superfluous however, as it widens the number of navigational beacons available to the pilot, allows the aircraft to operate in less developed countries, is relatively inexpensive and also offers redundancy in case of other navigation instrumentation failure. Distance Measuring Equipment (DME) gives the pilot distance and speed information relative to VOR transmitter sites.

H-1.3 Final Avionics Suite

The final avionics requirements (Table H-2) saw a major change in philosophy behind the avionics package. The in-service date projected for the aircraft was to be in five to ten years time, and with the prices of newly developed technology reducing rapidly it was decided to replace the main flight and navigational instrumentation with an Electronic Flight Instrument System (EFIS) – this provides the pilot with much improved situational awareness, and an integrated package which monitors aircraft and engine performance from multiple sources. This makes the aircraft safer, more enjoyable and easier to fly than most existing light aircraft as the flight computer can monitor all parameters all of the time, in comparison to the pilot who can only monitor certain parameters some of the time. The EFIS selected for Ikelos is the Flight Op 200, manufactured by Op Technologies.[3] The Flight Op 200 features a Liquid Crystal Display (LCD) screen with all the basic flight and engine instruments, while also acting as a single cue flight/navigation director. The Flight Op 200 is driven by a powerful computing unit which contains map/chart information and is integrated with an internal GPS receiver. This combination allows for a continuously moving map display with current position readout. The onboard database contains all public, military and private airfield information. The internal GPS system also integrates fully with other aircraft data such as fuel quantity, and can therefore provide the pilot with a better picture of the aircraft's health and performance capabilities. It was decided these benefits outweighed the cost and added weight of the system. This removed the requirement for VOR, DME or ADF gauges.

Table H-2: Final Avionics Requirements

Avionics	Required under JAR 23 ?
Flight and navigation instruments (JAR 23.1303)	
EFIS Display	No
COMM & NAV Radio combo	Yes (NAV only required for IFR)
Transponder	Yes
Backup Airspeed indicator	Yes
Backup Altimeter	Yes
Backup Attitude indicator	No (Required for IFR)
Backup Vertical Speed Indicator	No (Required for IFR)
Non-stabilised magnetic direction indicator	Yes
Free air temperature indicator	Yes
Powerplant instruments (JAR 23.1305)	
Fuel quantity indicator for each tank	Yes
Fuel flow meter	Yes
Fuel pressure indicator	Yes
Oil pressure indicator	Yes
Oil temperature indicator	Yes
Oil quantity indicator for each tank	Yes
Tachometer	Yes

Despite the fact the EFIS displays all information required during a flight, there are still requirements for backup instrumentation. Dexter Turner, President of Op Technologies who manufacture the EFIS detailed previously states that "I [don't] see any of the certification authorities changing their position on [the provision of mechanical backups]. I think that at the very least, we will be delivering systems with either: backup attitude, airspeed and altitude gauges, or dual-redundant EFIS (which means 2 of everything, including AHRS and air data) and a backup mechanical attitude."(4) This leaves the option open – either provide mechanical backups for the primary flight instruments, or supply the aircraft with a dual-redundant EFIS. As the target market for this aircraft is light GA, the cost of a second EFIS could not be justified for the benefits of having a complete computer-based instrument panel. Mechanical backups are used on Ikelos, occupying the left-hand side of the panel while the right hand side is reserved for the EFIS display. Future reductions in price or changes in regulations could allow the removal of the mechanical backups and replacement with another EFIS display.

H-2 INSTRUMENT PANEL AND SUPPLEMENTARY EQUIPMENT

H-2.1 Instrument Panel Layout

Figure H-1 shows the proposed instrument panel layout for Ikelos, with all the major instrumentation detailed.

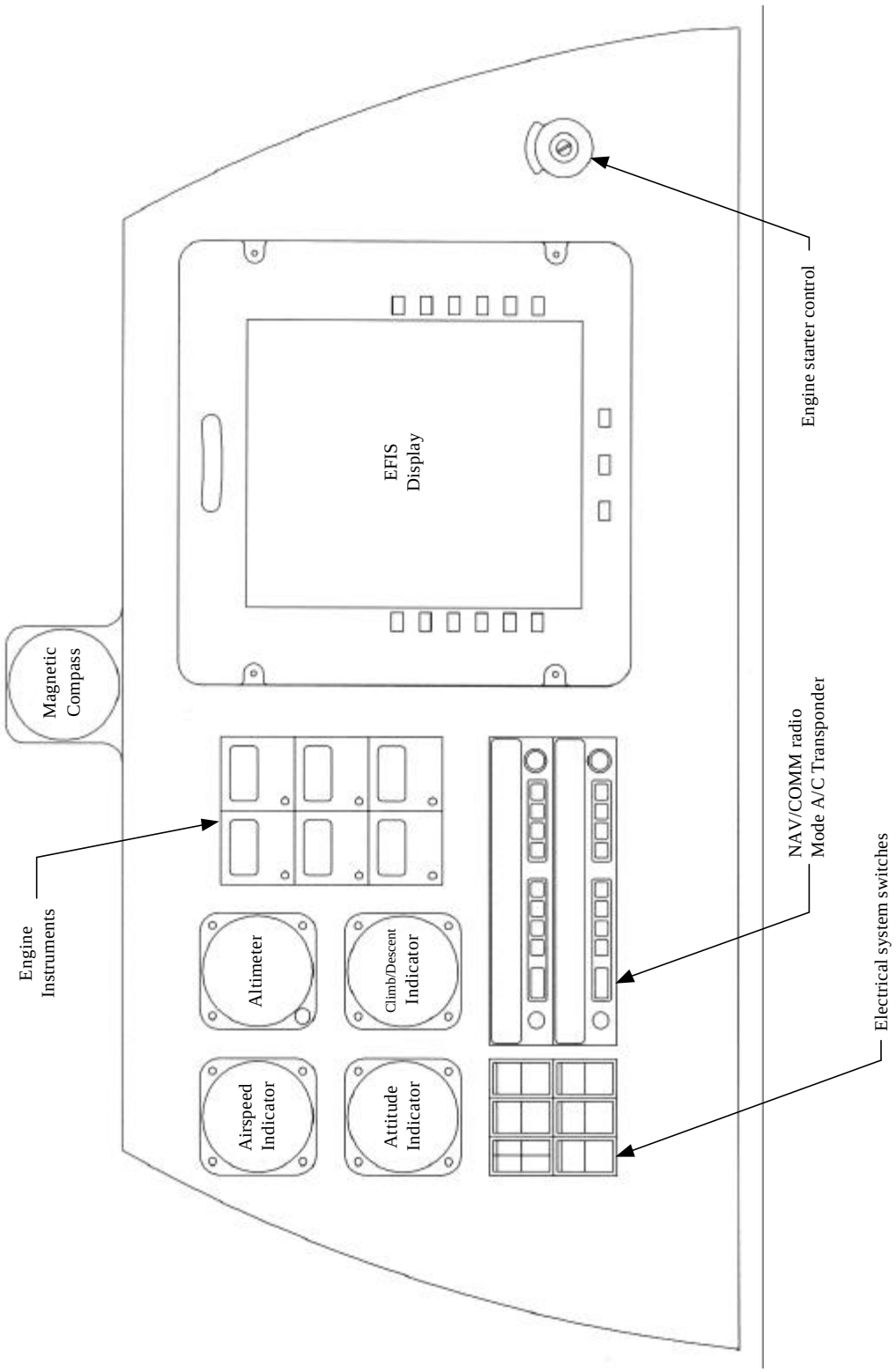

Figure H-1: Instrument Panel Layout

H-2.2 Supplementary Equipment

Several items of equipment not seen on the Figure H-1 are required in order for the avionics to function correctly. A pressure system, fed by a pitot tube positioned on the outside skin of the aircraft reads the surrounding static and dynamic pressure, and feeds this information to the backup instrumentation and the EFIS. The attitude indicator also requires a vacuum source to propel the internal gyroscopes – this will be supplied by a vacuum pump driven as an auxiliary device by the engine. The EFIS requires two extra devices, an Attitude Heading Reference System (AHRS) and a Flight Data Computer. The AHRS determines the aircraft's position in the sky via solid state sensors, this device sits just in front of the instrument panel in the nose-cone section of the aircraft. Alongside it is the Flight data computer, which reads inputs from the pitot system and the GPS system, converts the information into the relevant performance data which it then transmits to the EFIS for display.

The aircraft also requires several aerials. Due to its composite construction, the aircraft will require several aerials where conventional all-metal aircraft only require one due to the lack of reflecting surfaces on the structure to aid in transmission and reception of electromagnetic signals. Aerials will be required for the NAV/COMM radio and the GPS system, and will be duplicated on the upper and lower surfaces of the fuselage.

H-2.3 Estimated System Parameters

Figures H-2, H-3, and H-4 show the estimated weight, cost, and power needs of the selected instrumentation.

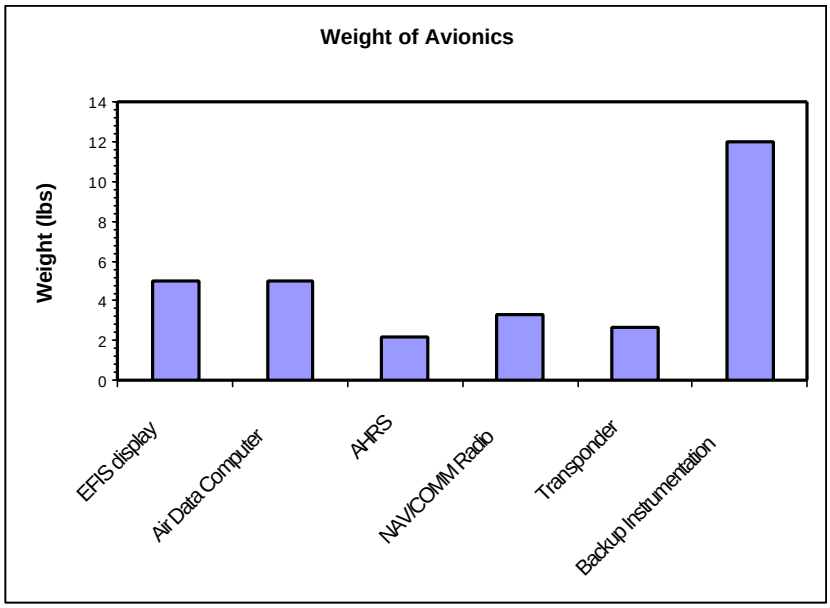

Figure H-2: Avionics Component Weights

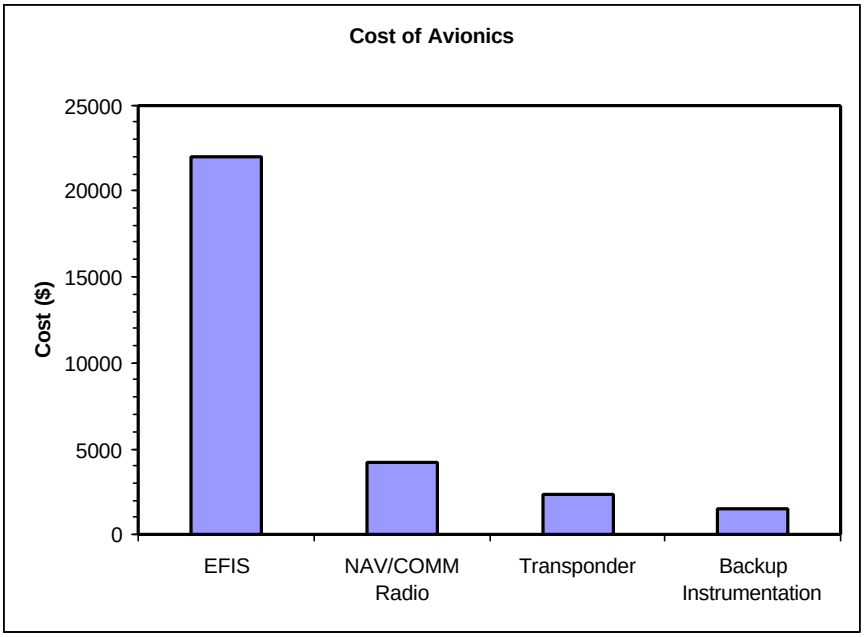

Figure H-3: Avionics Component Cost

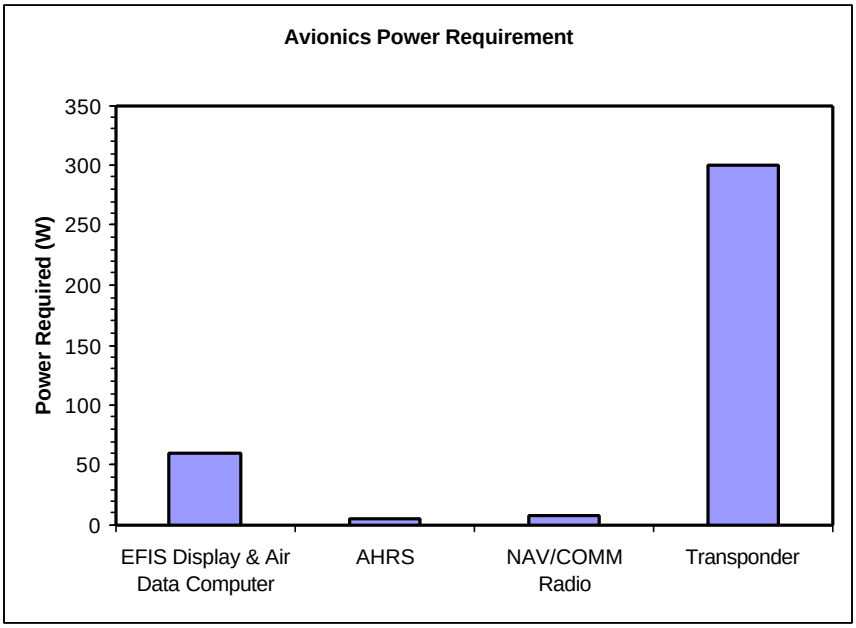

Figure H-4: Avionics Power Requirements

These give the following totals:

$$\text{Total Avionics Weight} = 30.2\,\text{lb}$$

$$\text{Total Avionics Cost} = \$29{,}950$$

$$\text{Total Avionics Power Requirement} = 375\,\text{W}$$

H-3 BRAKING SYSTEM

H-3.1 Benefits of anti-lock brakes

Of current general aviation aircraft there are very few with a full anti-lock braking system (ABS), especially on lower priced models. However, this is somewhat surprising considering it is now standard on most mid-range cars or better, and also available on upper-range of motorbikes. The advantages of ABS are well known, especially for motorbikes, as highlighted by research done by The Institute for Vehicle Safety in Munich, Germany. These results show[(5)]:

- In 93% of the cases analyzed, a fall could have been avoided by ABS.
- 10% of all fatal motorcycling accidents could be avoided if ABS were a standard feature on all motorcycles.

Although these results are for motorbikes, which are inherently more prone to a loss of stability and control than cars following a skid, the results are still useful. Aircraft too suffer from poor stability and handling characteristics when on the ground. This may be due a high center of gravity, relatively small wheel base, and the tricycle arrangement of wheels. Stopping distances of a motorbike with and without ABS in wet and dry conditions are shown in Tables H-3 and H-4 respectively, and highlighted graphically in Figure H-5.

Table H-3: Braking results in wet conditions[(6)]

Wet Pavement Braking over Sewer Cover*		
Professional	non-ABS	90m (298 ft)
	Full ABS Control	59m (193 ft)
Beginner	non-ABS	100+m (350+ ft)
	Full ABS Control	64m (210 ft)

Table H-4: Braking results in dry conditions[(6)]

Dry Pavement Braking over Sewer Cover*		
Professional	non-ABS	48m (158 ft)
	Full ABS Control	51m (166 ft)
Beginner	non-ABS	55m (180ft)
	Full ABS Control	51m (166 ft)

* Tests carried out using Yamaha FJ1200 at 60 mph.

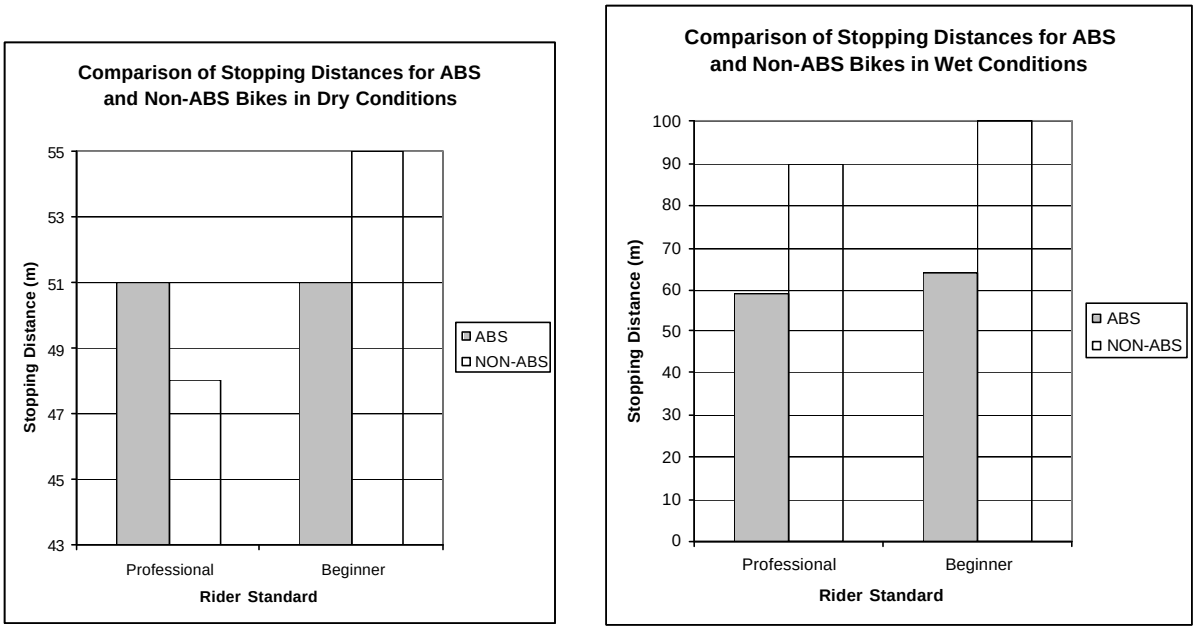

Figure H-5: Stopping distances in wet and dry conditions

It can be seen that in dry conditions an expert rider can out brake the ABS by 3 m (9 ft), but this is clearly vastly outweighed by the performance of ABS in wet conditions, cutting the stopping distance of even an expert by over a third.

H-3.2 How anti-lock brakes work

The coefficient of friction between to surfaces occurs just prior to one surface sliding over the other. The coefficient of friction, a braking effect, is reduced during the slide. The basic ABS involves sensing when the wheel has locked and then reducing the brake pressure to allow the wheel to rotate. The brakes are then re-applied at a lower pressure, hence maximizing the coefficient of friction and also preventing a loss of control. However, this is only a very basic overview. Modern ABS involves complex load distribution analysis to determine the optimum braking allocations for each wheel, maximizing the braking effort. This is highlighted by Figure H-6, which shows how the braking distributions change for different load conditions on a BMW motorbike.[7]

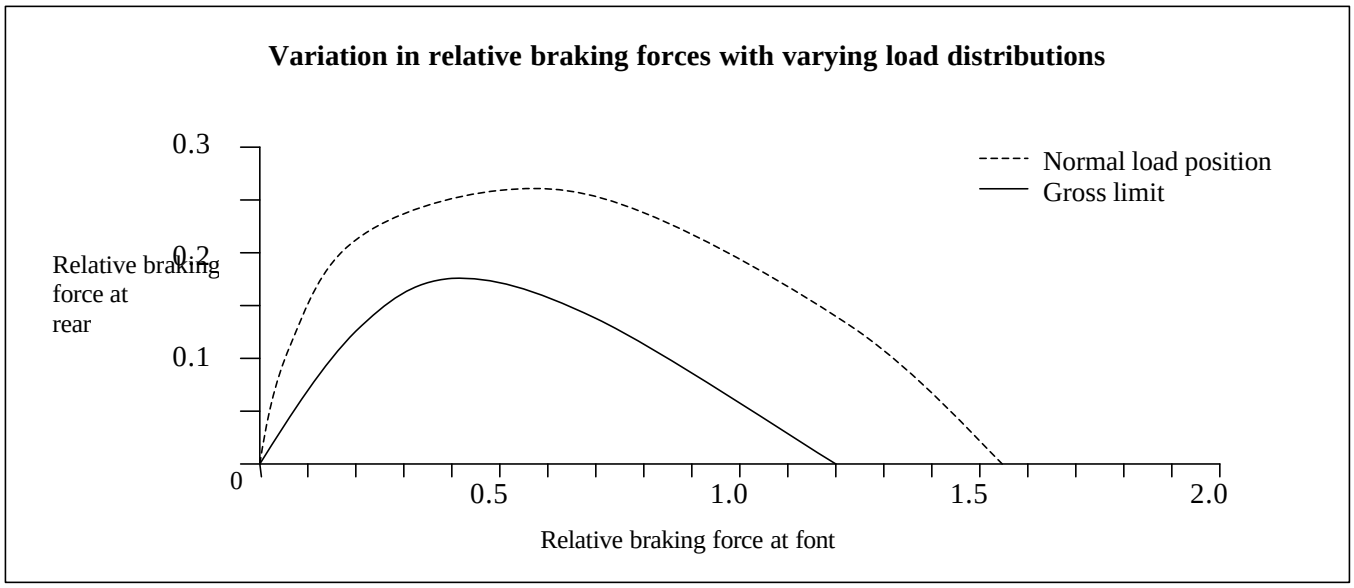

Figure H-6: Variation in relative braking forces with varying load distributions

As the braking force at the front is varied, the normal reaction between the ground and tires varies, as does the maximum braking force available prior to loss of traction. The relative braking force carried out by each wheel therefore needs to be optimized to achieve a maximum overall breaking effort. This optimum braking distribution also needs to vary with vehicle loading conditions.

The brakes themselves use wheel speed sensors to indicate to a processor the rotational speed of each wheel. Using a combination of this and the riders input the processor controls the pressure in the brake lines via electro-hydraulic valves. Pistons on the ends of the lines push the brake pads onto the brake discs, and slow the vehicle. In the event of a processor failure the ABS will be disabled but braking will still occur. The effort required by the rider will simply be increased to produce a given braking output.

The drawbacks to ABS are additional weight and cost. The additional cost quoted for a BMW Sport-Tourer R1100S is $1035[7] and the additional weight is 43.5 N (9.6 lbs).[8] To scale these values to a tricycle type aircraft of increased mass is somewhat presumptuous but conservative estimates of $1650-2100 and 70-80 N (15.4-17.6 lbs) do not seem unreasonable.

Based on these values, Ikelos has been equipped with a full Anti-Lock Braking System for the extra safety benefits that it brings at relatively low cost in terms of the total aircraft cost.

H-4 BALLISTIC RECOVERY SYSTEM

The option of having a ballistic parachute recovery system (BPRS) onboard Ikelos provides a reassuring failsafe to any nervous pilot or passenger. There are many scenarios in which having the BPRS could prove a very sensible investment. These can include:

- Mid-air collision and resulting loss of control
- Power loss during night operations – loss of visibility and awareness
- Power loss while crossing hostile terrain such as mountains
- Pilot incapacitation – including passenger safety
- Stall/spin on approach
- Loss of control or icing

One important question is the minimum deployment height. FAA certified tests have shown that full parachute inflation can occur as low as 91.4 m (100 ft) although this is from straight and level flight. Clearly the velocity and attitude of the aircraft just prior to launch can make a big difference.

Overall the inclusion of the BRPS as an option extra would offer the potential customer increased piece of mind and safety, and considering the additional cost and weight may well be a popular choice. Information on one available ballistic parachute from Ballistic Recovery Systems, Inc.[9] is given below:

Model	1500 Canister
Price	$3995
Max a/c weight	6800 N / 1500 lbs
Max deployment speed	126 kts
Re-pack cycle	6 years
Mass of system	180 N / 39 lbs
Dimensions	Cylinder 59.7 cm (23.5 in) long x 20.3 cm (8 in) Ø

REFERENCES

1. European Joint Aviation Authorities, “Very Light Aeroplane Regulations”, JAR-VLA, 2002.

2. European Joint Aviation Authorities, “Normal, Utility, Aerobatic, and Commuter Category Aeroplane Regulations”, JAR-23, 2002.

3. “Flight Op 200,” Op Technologies, Hillsboro, OR, http://www.optechnologies.com/products.html, April 2002.

4. Turner, D., “Backup requirements for EFIS”, personal correspondence, Op Technologies, Hillsboro, OR, March 2002.

5. Sporner, Dr. A., "Braking as the Cause of Fatal Accidents", (MOTORRAD, Vol. 13, June 9, 2000): , www.bmw.motorrad.co.uk, April 2002.

6. Kneebone, M., "ABS Comparison Tests", Motorcycle Consumer News, http://www.ibmwr.org/prodreview/abstests.html, April 2002.

7. http://www.bmw-motorrad.co.uk/, BMW Integral ABS – Dynamic brake force distributor, April, 2002.

8. "http://www.bmwmotorrad.co.za/motorcycles/bikenews", BMW South Africa, http://www.bmwmotorrad.co.za, April 2002.

9. "Ballistic Recovery Parachute," Ballistic Recovery Systems, Inc., St. Paul, MN, http://www.airplaneparachutes.com/, April 2002.

Appendix I: Cockpit

TABLE OF CONTENTS

I-1 INITIAL DESIGNS…….. I-2
I-1.1 Single Person……...……I-2
I-1.2 Two People with Side-by-Side Seating……...……I-2
I-2 FINAL DESIGN……...……..…… I-3
I-2.1 Two People with Tandem Seating……..……..…… I-3
I-2.2 Controls……...…… I-4
I-3 SAFETY FEATURES……...……. I-4
I-3.1 Landing Protection……...…… I-4
I-3.2 Canopy……..……... I-4
REFERENCES……...I-5

LIST OF FIGURES

Figure I-1 Single Person Cockpit
Figure I-2 Two People with Side-by-Side Seating
Figure I-3 Two People with Tandem Seating

I-1 INITIAL DESIGNS

I-1.1 Single Person

The original design constraints for Ikelos called for a single person aircraft capable of short or vertical take-off and landing. A single person cockpit was designed using ergonomic principles and existing cockpit dimension data. The seat area and head space was designed for a 95th percentile male with features that make it adjustable down to a 5th percentile female. These human dimensions are applicable to a male with a stature height of 1.8 m (6 ft) and a female with a stature height of 1.52 m (5 ft).[1]

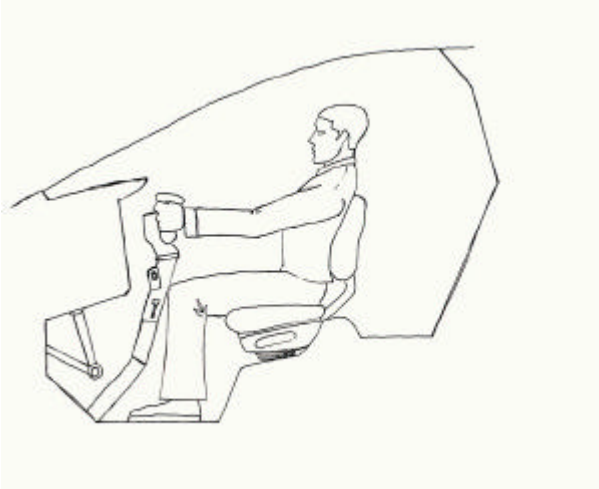

Figure I-1: Single Person Cockpit

I-1.2 Two People with Side-by-Side Seating

As work began on the design aspects of Ikelos, the team discussed adding a second seat to make the aircraft more attractive to potential buyers. It was decided that the ability of the aircraft to carry two people, pilot and passenger, would make it more competitive with other aircraft in similar markets. Most two place general aviation aircraft use side-by-side seating and it was decided that Ikelos would follow this trend. Pilot comfort, communication, and equal visibility were the main reasons for choosing this side-by-side arrangement. The cockpit was redesigned and a second seat was added and placed beside the pilot. Again, both seats were designed for a 95th percentile male with adjustability features such as seats and rudder pedals.

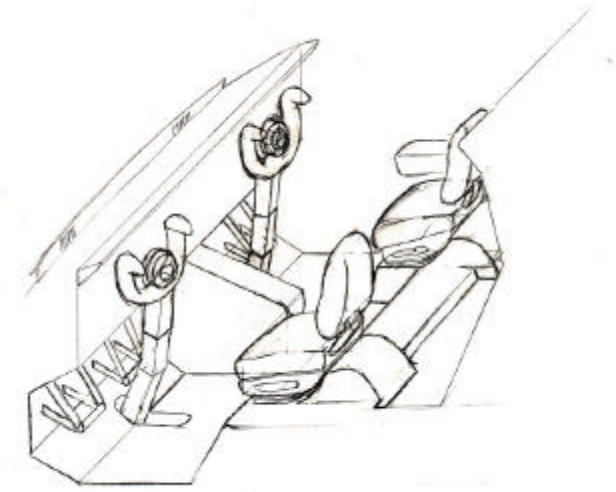

Figure I-2: Two People with Side-by-Side Seating

I-2 FINAL DESIGN

I-2.1 Two People with Tandem Seating

With further study, it was discovered that adding the second seat to the cockpit using the side-by-side arrangement made the fuselage unacceptably wide. First, the side-by-side cockpit arrangement made the aircraft too wide to fit on a trailer. Secondly, the increased width raised concerns about blocking the duct intakes and causing excess drag due the larger fuselage cross-section and wetted area. The team discussed different ways to decrease the width of the cockpit and decided to either take the second seat out or use a tandem seating arrangement. The pilot's desire to carry a person with him/her and pilot training accommodation were the main factors driving the decision to keep the second seat. The cockpit was redesigned for a third, and last, time with a tandem seating arrangement.

The pilot and passenger seat is designed for a 95^{th} percentile male that has a standing height of 1.8 m (6 ft).[(1)] The seats are adjustable, along with adjustable rudder pedals, to accommodate the shortest of females. The pilot seat leaves 0.15 m (6 in) of head room above the pilot when he/she is seated. The passenger seat leaves approximately 0.08 meters (3 inches) of head room above the passenger when he/she is seated. The total height of the cockpit is 1.18 m (47 in), the total length is 2.35 m (93 in), and the width is 0.66 m (26 in).

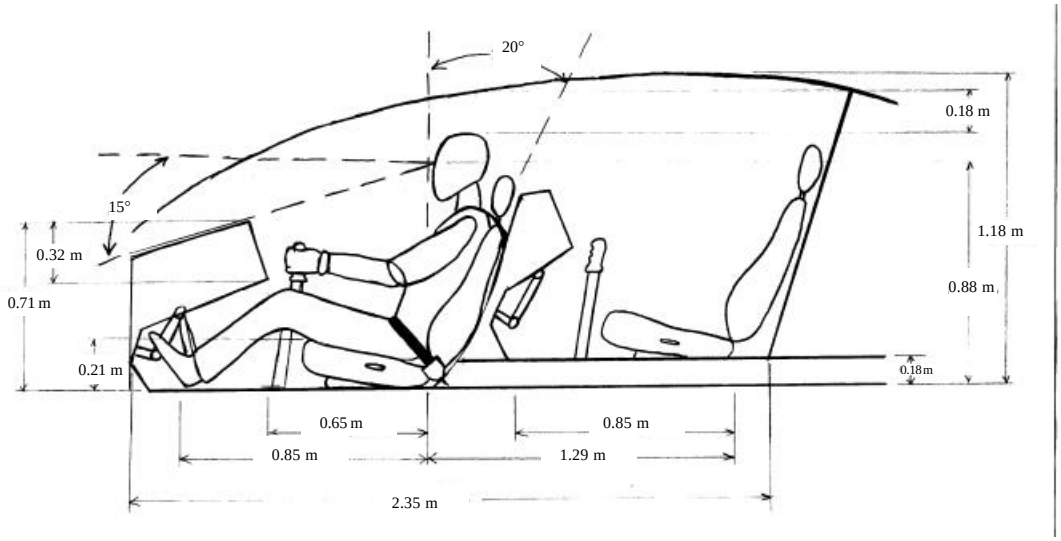

Figure I-3: Two People with Tandem Seating

I-2.2 Controls

The seating and space in the cockpit was designed so that the entire pilot population could fit and operate the controls and maintain the designed eye position. The rudder pedals are adjustable so that every pilot, regardless of size, is able to fully depress the upper part of both pedals in a comfortable flying position. The pilot and passenger center stick is adjustable and positioned so that every pilot can apply the throttle in the farthest position. The primary control stick was placed in the center to be comparable with similar aircraft, and to allow both right and left hand people to have equal control. All other controls, instruments, equipment and displays are located on the instrument panel. Duplicate instrument panels and controls exist for both front and rear seat pilot.

I-3 SAFETY FEATURES

I-3.1 Landing Protection

Since Ikelos is calculated to land in such a short distance, abrupt and hard landings are a possibility. To keep the occupants safe from heavy g-loading, the pilot and passenger seats are made out of a shock absorbing foam material called CONFOR™ FOAM.[(2)] This special foam material is also used in military pilot ejection seats, and aids in dissipating the impact energy that will be experienced during landing. There exist different foam thickness options for the aircraft owner to choose from. To further protect the occupants from potential harsh landing conditions, both seats are equipped with five point harness style seatbelts to provide maximum safety and protection. Since the aircraft will go from touchdown to full stop in a second or two, the design also includes anti-lock brakes for added safety. A ballistic parachute is also installed for emergency braking purposes.

I-3.2 Canopy

A right-side hinged canopy was chosen for the entrance/exit to the cockpit. The lightweight clear acrylic canopy is equipped with gas struts for maximum ease during opening

and closing. The canopy is split in the center into two separate sections to allow for a roll bar to be placed between the two seats for safety purposes.

REFERENCES

1. Sanders, M. and McCormick, E. *Human Factors in Engineering and Design*. McGraw-Hill, New York, 1993.

2. "Confor™ Foam," Aviation Design, California, http://www.aviationdesign.com/confor.html, March 27, 2002.

Appendix J: Manufacturing

TABLE OF CONTENTS

J-1 OVERVIEW...……..J-2
J-1.1 Just In Time……...J-3
J-1.2 Total Quality Management……....J-3
J-1.3 Total Employee Involvement ……...J-3
J-1.4 Computer Integrated Manufacturing (CIM)…… J-3
J-2 MATERIALS……...J-4
REFERENCES……...J-4

LIST OF FIGURES

Figure J-1 Facility Layout

J-1 OVERVIEW

When one walks into the facility, one sees 10 planes facing the walls at various stages of their assembly. Rather than assembly using lines, each plane will be manufactured in its own stationary bay (See Figure J-1). Adjustable lifts will position workers on either side as the plane is assembled. One team will assemble each aircraft. This system was seen on a trip to BAE Systems when the design team traveled to England. Ikelos will be produced with a selling cost competitive to other personal aircraft and a design superior to other aircraft in its class. Therefore, the manufacturing of Ikelos must be efficient and satisfy the customer.

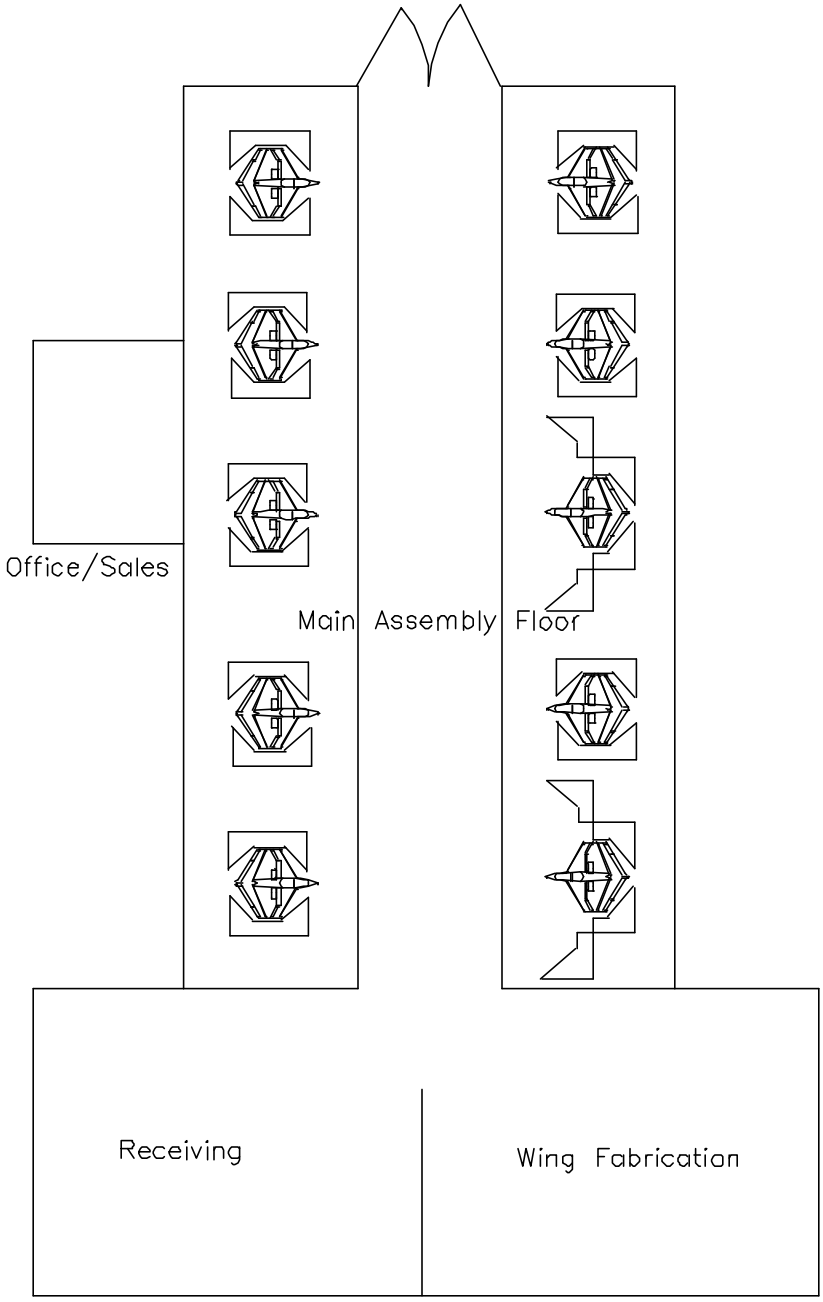

Figure J-1: Facility Layout

This goal will be achieved through continuous improvement of product design, and delivery, as well as all stages from acquisition to conversion of raw material. This will be accomplished using the contemporary methods available used to create an environment where the highest level of quality can be produced while giving the consumer the highest priority. By using the principals, procedures, techniques, and technology of *just-in-time* (JIT), *total quality management* (TQM), *total employee involvement* (TEI), and *computer integrated manufacturing* (CIM) continued aerodynamic, propulsion, and design modifications may be made during the production of Ikelos.

J-1.1 Just In Time

The American Production and Inventory Control Society defines JIT as a philosophy of manufacturing excellence based on the pursuit of planned elimination of all waste and constant improvement of productivity and quality.[1] This definition will guide the design of the manufacturing process and the facility layout.

Assembly will begin with the fuselage. Most of the complex components will come from outside sources. Based on the size of our first production run the manufacturing facility will draw up requests for proposals and submit these to the respective material vendors. For example, the manufacturing facility will purchase the propulsion system, the guidance system, and all of the airframe materials from outside vendors. Upon gaining contracts the vendors will agree to set shipping quantities and delivery schedules. These quantities and times will be optimized using simulation and/or linear programming models. Next, in a process similar to the way in which the Eurofighter is constructed, the airframe and control systems will be assembled. Then, the Rand Cam engine will be installed, linked to all of the controls. Finally, a set of wings will be attached and the plane will be ready to ship to the customer.

J-1.2 Total Quality Management (TQM)

TQM searches constantly for "continuous process improvement" through involvement of everyone in the organization, managers and workers alike in an integrated effort to improve performance.[1] In efforts to continuously improve Ikelos, manufacturing must seek out feedback from employees and customers on a regular basis. These reports will be documented, then analyzed by the management, and used for decision making and planning purposes.

J-1.3 Total Employee Involvement

"The design implementation, and operation of JIT, TQM, and CIM techniques are supported by teams and require employee empowerment, flexibility, and multifunctionality."[1] Engineers, electronics specialists, and manufacturing people will be assigned to each production bay. This will allow for a great deal of coordination during production as well as giving each member of the team a better appreciation for the others' purpose, pit-falls, and responsibilities.[2] Recommendations are encouraged from any member of the team. So when a better way to perform an action is found, changes will be made across the plant.

J-1.4 Computer Integrated Manufacturing (CIM)

To remain competitive a company must use information technology to its fullest potential. CIM uses technology to integrate all components involved in the design, manufacturing planning and control, and production process.[1] With a well-structured CIM system one reduces the time to complete work in process by maintaining high worker utilization.

One or several networked computers will serve each bay. These computers will contain the software and hardware to interface with the manufacture of each plane. Here the workers will place orders for tools and parts, perform diagnostic testing on the plane, document the results, as well as view production deadlines, and enter problems, comments, and suggestions. All collected data will then be stored on a network and be made available as information that can give both the managers and employees almost immediate feedback on their daily performance. Quality improves within this team atmosphere, as do tracking of defects in reports. In other words, a digitally continuous record will exist containing information on who assembled each plane, when it was assembled, and what problems (if any) were encountered during assembly. This high level of type of control will be important due to the complexity of production and precision required to make each individual Ikelos safe for civilian flight.

J-2 MATERIALS

Composites are used wherever possible to take advantage of their lighter weight and greater strength. Because composites are made out of molds, the different parts of the airplane can be made at different locations and then joined together at the end. The ribs, longerons, and spars of the aircraft are constructed from layers of carbon fiber, bonded together with adhesive, and allowed to cure. Likewise, the spars are created from layers of carbon fiber and then are cured in spar molds to attain their strength and shape. The wing and fuselage skins are made from sheets of glass fiber bonded with epoxy in molds. Ikelos features an inner and outer skin that sandwich a layer of Nomex honeycomb core. The honeycomb provides much needed stiffness and strength, allowing less internal structure to be used. After both halves of the wing or fuselage are made, they are fused together at the joints for a tight bond. At this point in the manufacturing, all of the pipes, cables, and controls are inserted into the structure pieces. Then the pieces are brought together and assembled in the bays. Finally, the rest of the avionics, controls, and cockpit furnishings are installed. Then the aircraft is painted, and the landing gear and engine components are installed. Now the aircraft is ready for flight testing, and eventually, certification.

REFERENCES

1. Tompkins, White, Bozer, Frazelle, Tranchoco, Trevino, *Facilities Planning*. New York, New York, John Wiley & Sons, Inc., (1996).

2. Wimpress, Jojn K., *The YC-14 Prototype: Its Design Development, and Flight Test*, American Institute of Aeronautics and Astronautics, Inc., Reston, VA, (1998).

3. "Nomex," Dupont, Wilmington, DE, http://www.dupont.com/nomex/index.html, March, 2002

4. "Kevlar," Dupont, Wilmington, DE, http://www.dupont.com/nomex/index.html, March, 2002

Appendix K: Cost

TABLE OF CONTENTS

K-1 RESEARCH, DEVELOPMENT, TEST, AND EVALUATION COST……..…….... K-2
K-2 MANUFACTURING AND ACQUISITION COST…..……. K-3
REFERENCES……..…….. K-4

LIST OF FIGURES

Figure K-1 Cost per Aircraft vs. Number of Aircraft Manufactured

LIST OF TABLES

Table K-1 RDTE inputs
Table K-2 Manufacturing Inputs
Table K-3 Key Costs for varying numbers of aircraft manufactured

LIST OF SYMBOLS

C_{aedr} Airframe Engineering and Design Cost
C_{dstr} Development Support and Testing Cost
C_{ftar} Flight Test Airplanes Cost
C_{ftor} Flight Test Operations Cost
C_{tsfr} Test and Simulation Facilities Cost
C_{pror} RDTE Profit
C_{finr} Cost to finance the RDTE phases

K-1 RESEARCH, DEVELOPMENT, TEST, AND EVALUATION COST (RDTE)

Employing methods outlined by Roskam[1], an estimation of the research, development, test, and evaluation cost (C_{RDTE}) is outlined below. The RDTE costs are broken down into seven cost categories:

1. Airframe Engineering and Design Cost: C_{aedr}
2. Development Support and Testing Cost: C_{dstr}
3. Flight Test Airplanes Cost: C_{ftar}
4. Flight Test Operations Cost: C_{ftor}
5. Test and Simulation Facilities Cost: C_{tsfr}
6. RDTE Profit: C_{pror}
7. Cost to finance the RDTE phases: C_{finr}

The total RDTE cost for the airplane program is estimated from:

$$C_{RDTE} = C_{aedr} + C_{dstr} + C_{ftar} + C_{ftor} + C_{tsfr} + C_{pror} + C_{finr} \quad \text{(K-1)}$$

Expressions for estimating these seven categories of RDTE cost are outlined in Roskam[1], whereby coefficients are employed to weight the varying aspects of the design according to the influence that they have upon the total cost. The costing analysis operates by the input of design characteristics such as weight and maximum speed, alongside factors incorporating material qualities and design complexity. The inputs are given in table K-1.

Table K-1: RDTE inputs

W_{ampr}	418.87 lb (Aeronautical Manufacturers Planning Report weight)
V_{max}	134 kts (maximum speed)
N_{rdte}	2 test aircraft
F_{diff}	1 (difficulty factor)
F_{cad}	0.8 (CAD factor)
R_{er}	84.00 US$ per hour (engineering man-hour rate)
CEF	4.20 (cost escalation factor)
C_{er}	10,000 US$ (engine cost)
N_e	1 engine
C_{pr}	2711.00 US$ (propeller cost)
N_p	2 propellers
$C_{avionicsr}$	20,000 US$ (avionics cost)
N_{st}	1 static test aircraft manufactured
R_{mr}	45.44 US$ per hour (manufacturing man-hour rate)
F_{mat}	1.5 (material factor = 1.5 for composites)

N_{rr}	0.33 units manufactured per month
R_{tr}	59.21 US$ per hour (tooling man-hour rate)
F_{obs}	1 (observation factor =1 for civil aviation)
F_{pror}	10% profit
F_{finr}	10% cost to finance project

The results are such that the RDTE cost is:

C_{aedr}	US$ 631,218
C_{dstr}	US$ 90,593
C_{ftar}	US$ 5,316,364
C_{ftor}	US$ 4,742
C_{tsfr}	US$ 0
C_{pror}	US$ 755,365
C_{finr}	US$ 755,365
C_{RDTE}	**US$ 7,553,646**

K-2 MANUFACTURING AND ACQUISITION COST

The manufacturing cost C_{MAN} and acquisition cost C_{ACQ} for the aircraft program are obtained in a similar fashion to the RDTE costs, they are given by:

$$C_{MAN} = C_{aedm} + C_{apcm} + C_{ftom} + C_{finm} \quad \text{(K-2)}$$

$$C_{ACQ} = C_{MAN} + C_{PRO} \quad \text{(K-3)}$$

The terms are the same as before, with the ‘m’ subscript denoting manufacturing stage, as opposed to ‘r’ previously referring to RDTE stage. An estimate of the unit price per airplane can then be obtained from:

$$AEP = [(C_{MAN} + C_{PRO} + C_{RDTE}) / N_m] \quad \text{(K-4)}$$

Where N_m is the number of airplanes manufactured. Similar analysis to that previously conducted is then used to calculate the above terms, thus obtaining the unit price per airplane, the inputs are given in table K-2 (those not stated are the same as for the RDTE stage).

Table K-2: Manufacturing Inputs

N_m	500 aircraft produced (sample figure)
F_{int}	500 US$ interior cost per passenger
N_{pax}	2 passengers (pilots)
$C_{ops/hr}$	100 US$ per hour operations cost
t_{pft}	2 hours flight testing per aircraft before sale

The results are as follows for a typical production run of 500aircraft:

C_{MAN} US$ 112,356,320
C_{ACQ} US$ 123,591,952
AEP US$ 293,432 per aircraft

With the RDTE cost being fixed, and the obvious economies of scale achievable, the inevitable reduction in cost with increase in production number is attained, key values are shown in table K-3, with the overall trend illustrated in figure K-1.

Table K-3: Key Costs for varying numbers of aircraft manufactured

Number of Aircraft Produced	Cost per Aircraft (US$)
500	293,432
5,000	155,504
50,000	101,114

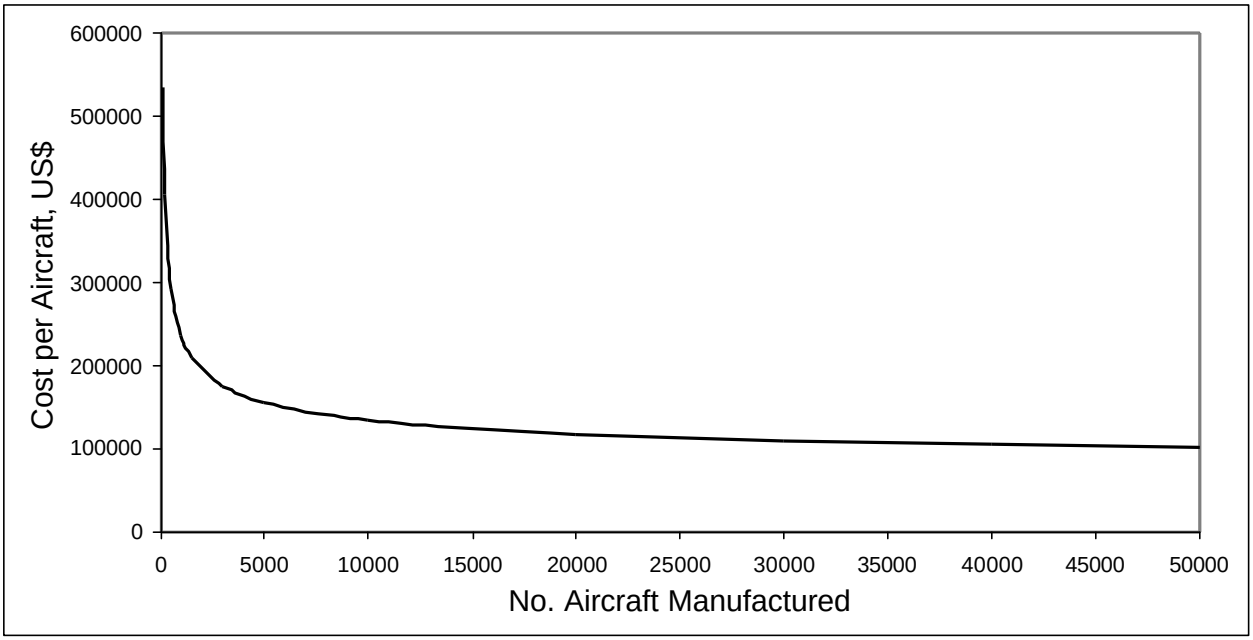

Figure K-1: Cost per Aircraft vs. Number of Aircraft Manufactured

REFERENCES

1. Roskam, J., *Airplane Design Part VIII: Airplane Cost Estimation*, The University of Kansas Lawrence, Kansas, 1990.

Appendix L: Design Selection

TABLE OF CONTENTS

L-1 COMPARATOR STUDIES……...……... L-2
L-2 STARTING DESIGN CONCEPTS…….……..L-2
L-2.1 Virginia Tech Original Concepts…… L-2
L-2.2 Loughborough University Original Concepts……L-18
L-3 SELECTION PROCESS……L-22
REFERENCES.……...…….....L-26

LIST OF FIGURES

Figure L-1 Sketch of Single Propeller-driven STOL
Figure L-2 Sketch of Tail-dragger Single Propeller Concept
Figure L-3 Sketch of Dual-Propeller Concept
Figure L-4 Sketch of Vectored Thrust Jet
Figure L-5 Sketch of the Pleasurecraft: Jet STOL
Figure L-6 Sketch of Propeller-driven Gyroplane
Figure L-7 Sketch of Ducted Propeller Concept
Figure L-8 Sketch of STOL Jet with V-tail
Figure L-9 Sketch of Initial Jet-driven Gyroplane
Figure L-10 Sketch of Revised Jet-Driven Gyroplane
Figure L-11 Sketch of Loughborough's Gyroplane Concept
Figure L-12 Sketch of Coaxial Helicopter
Figure L-13 Sketch of Joined-Wing Concept
Figure L-14 Selection Chart
Figure L-15 Example Ratings of V-tail Jet
Figure L-16 Design Concept Chosen for Further Development

LIST OF TABLES

Table L-1 Noise Production Table in EPNdB[23]

L-1 COMPARATOR STUDIES

An important step in the early stages of any design process is the retrieval and understanding of previous efforts in the field of interest. In this case, the process involves performing comparator aircraft studies. Due to the unique nature of our design, it was necessary to look at proposed aircraft that would meet our design requirements as well. Among the broad array of aircraft proposals and productions we examined were kit planes, ultralights, gyroplanes, "flying cars", vectored thrust vehicles, and common light aircraft. Each member performed an independent study and followed ideas that looked promising. New findings and problems were discussed at regular team meetings.

One design looked at was the CarterCopter which is a gyroplane equipped with a powered rotor for takeoff and landing. This design has been in progress for quite some time, and a significant amount of information exists for it.[1] Other gyroplane aircraft were studied, such as the Groen Brother Aviation Hawk IV. This craft is currently on the personal, commercial, and military markets. It also features a rotor that can be powered for super short takeoff and landing (SSTOL) capabilities.[2]

Another craft that performed a very similar task to ours was the Moller Skycar, shown in Figure 3.[3] Like the CarterCopter concept, this design has been in progress for quite some time, and is a VTOL aircraft using ducted fans and thrust vectoring. Another VTOL aircraft examined was the light, multipurpose VTOL "Krechet". While this vehicle is intended for several people, the concepts involved apply to this project. A separately powered lift fan is used for VTOL capability, and exhaust deflectors contribute to forward thrust. Two ducted propellers mounted in the rear of the aircraft produce the bulk of the forward thrust.[4]

Some other more conventional aircraft already meet some of the design requirements. The short takeoff requirements were met due mainly to the very low weight and large wing area. Such aircraft include the VSTOL Pairadigm, the Freebird Freebird, the Flying Flea, and the STOL CH 701. These small planes are capable of takeoff within 46 m (150 ft),[5-8] but do not necessarily fulfill all of the key features of the proposed design requirements.

L-2 STARTING DESIGN CONCEPTS

Team members at Virginia Tech and Loughborough University began work on the project independently, developing several initial concepts before combining in November 2001 to select a single final design concept for further development and analysis.

L-2.1 Virginia Tech Original Concepts

The Virginia Tech team split into three groups each consisting of three Aerospace engineers and one Industrial/Systems engineer. A total of nine original concepts were developed and analyzed, and eventually three of these designs were chosen to continue further development.

L-2.1.1 Single Propeller-Driven STOL

The first design considered was a small, propeller driven aircraft with a large engine and high-lift wing capable of taking off in the designated distance (Figure L-1). This design is based on the CH701 STOL aircraft already in production. This aircraft is already capable of fulfilling all of the design requirements with the exception of the max cruise velocity.[8]

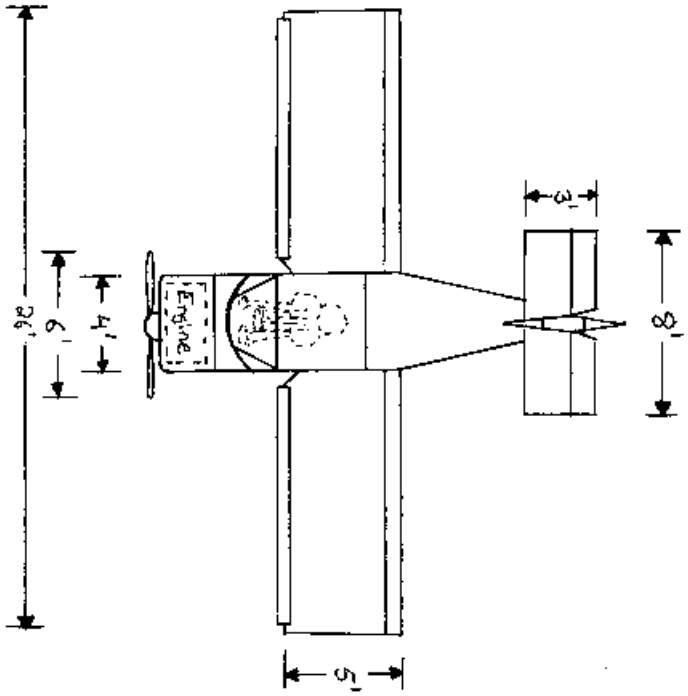

Figure L-1: Sketch of Single Propeller-driven STOL

Some features of this design are full span, fixed, leading edge wing slats and full span flaperons to increase lift and give more control. An inverted horizontal stabilizer helps pitch the plane up during takeoff rotation in order to maximize the take-off angle of attack. A large elevator and full flying rudder help to control the aircraft at the low takeoff and landing speeds. Hoerner wing tips are used to minimize the effect of tip vorticies in the flow. A thick cambered airfoil also helps to increase the lift.

While a STOL airplane with a high C_L is great for short takeoffs and low stall speeds, there are some drawbacks. Due to the increased lift coefficient, the drag is also much higher on this type of aircraft. The Hoerner wing tips also lead to increased drag. With such an increase in drag, the maximum cruise speed for this aircraft is fairly low, even though it would fulfill the design requirement. While there are several drawbacks to this design, it still does a very good job of satisfying the design requirements for this project.

L-2.1.2 Tail-Dragger Single Propeller Concept

The single engine, high-wing design (Figure L-2) is based on similar current designs from Avid Aircraft[9] and Cessna[10]. The main features of the aircraft include variable leading edge slats, inboard trailing edge flaps, outboard flaperons, and a wing flow fence. All the

devices, with the exception of the wing fence, serve to change the geometry of the airfoil to create more lift at lower speeds. The main purpose of the wing fence is to provide a more uniform flow over the flaps when deployed by limiting span-wise flow on the wing due to the varying angles of the flaps and flaperons.

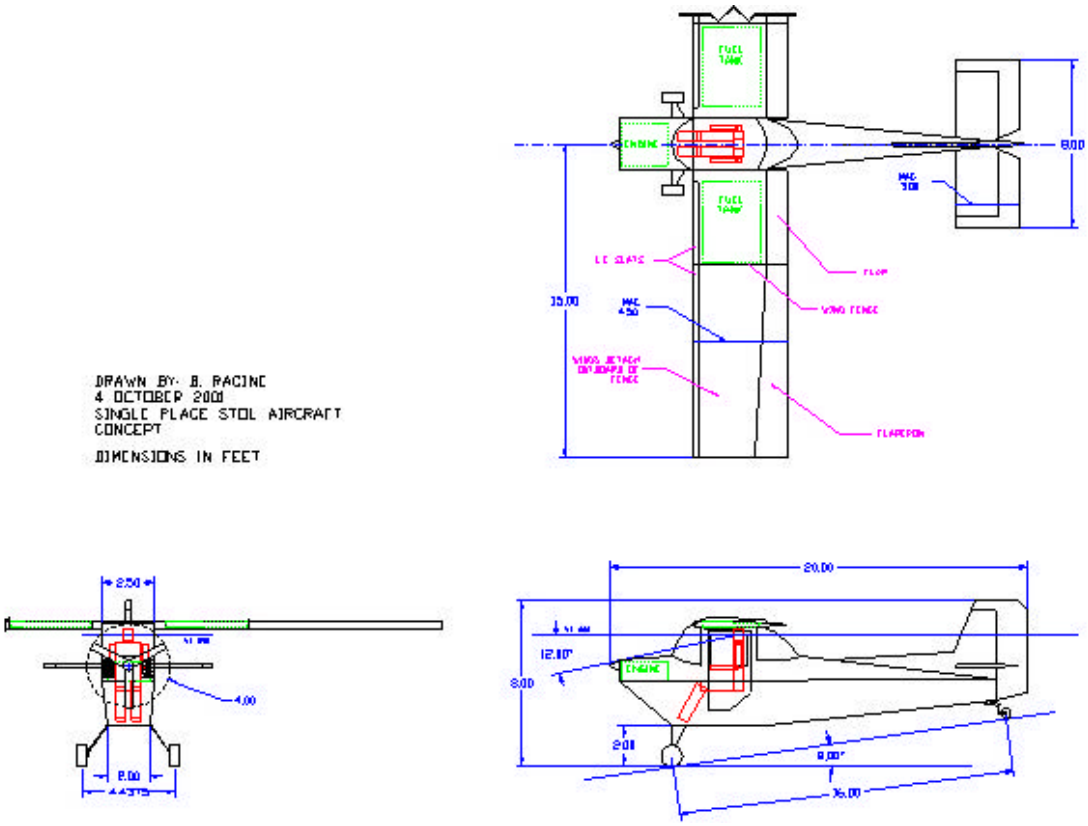

Figure L-2: Sketch of Tail-dragger Single Propeller Concept

For ease of transportation on the ground, the wings are detachable outboard of the wing fence. Detachment of the wings outboard of the wing fence leaves the fuel system intact, as the fuel tanks are contained within the wing inboard of the wing fence. Fuselage size was kept as small as possible without sacrificing pilot comfort, structural requirements, or stability issues. The smaller overall size of the fuselage allows for easier ground handling of the aircraft.

Using a weight estimation procedure outlined in Brandt[11], the estimated basic empty weight of the aircraft is 840 pounds. With a maximum gross weight specified at 5340 N (1200 lbs), and at a maximum fuel capacity of 400 N (90 lbs) (15 gal), this leaves 1200 N (270 lbs) available for pilot and cargo. A takeoff ground run distance of 38 m (125 ft) at maximum gross weight of 5340 N (1200 lbs) requires a thrust of 3870 N (870 lbs). Range is estimated at 275 nm, and endurance is estimated at 3 hours.

L-2.1.3 Dual Propeller Concept

The plane shown in Figure 3 is powered by two propellers, one at the end of each wing, which tilt during takeoff to give it added lift. The propellers would begin the takeoff run in a horizontal position and immediately before takeoff would tilt up to decrease the amount of lift needed to get off the ground.

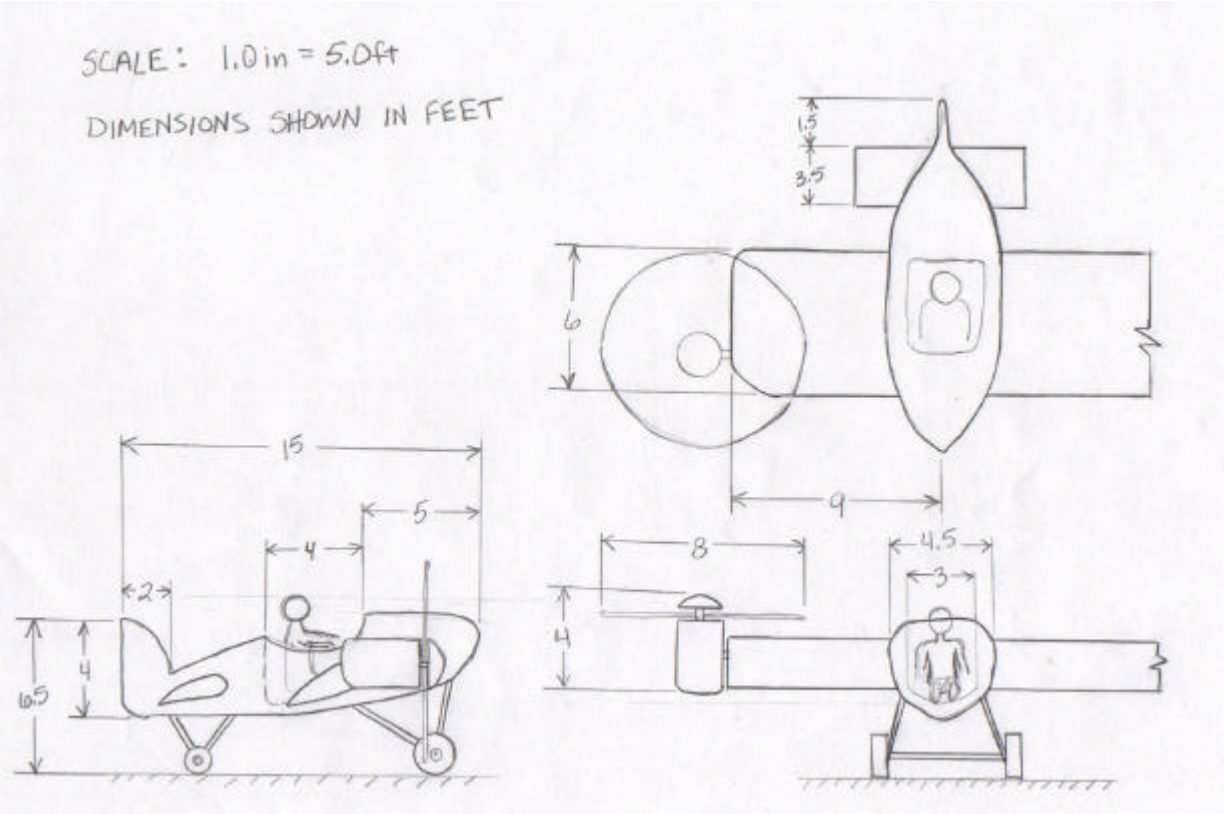

Figure L-3: Sketch of Dual-Propeller Concept

The cabin size, chosen to be 1 m (3 ft) wide by 1.2 m (4 ft) long by 1.1 m (3.5 ft) deep, is just enough to fit the body dimensions of a 95th percentile male. The plane was then sized around the cabin. The front wing was given a large planform area to create high lift, and the horizontal tail has a high-lift airfoil to keep the plane level in cruise flight. The location of the wheels were chosen simply by what appeared to be good positioning to keep the plane stable while on the ground.

Since the dimensions and materials of this plane were similar to that of the Flying Flea[(7)], the approximation of the empty weight is based on it and taken to be about 1000 N (225 lbs). Using two four-stroke, 13 kW (18 hp) engines add about 365 N (82 lbs)[(12)], and two 2-blade, 2.4 m (96in), wooden propellers with its hub add about 265 N (60 lbs).[(13)] With 890 N (200 lbs) of fuel and a 780 N (175 lb) pilot, the total weight of the plane is 3290 N (740 lbs).

For the calculation of the takeoff ground run distance, a horizontal thrust of 351 N (79 lbs) was assumed until the point of takeoff. At this point, the tilted thrust would essentially decrease the weight of the plane, which requires a smaller takeoff speed. Assuming a total takeoff run with horizontal thrust, the takeoff distance was calculated to be 56 m (183 ft). With a smaller takeoff speed needed from the tilted thrust, the takeoff distance decreases, but probably will not meet the required short takeoff distance. The plane also fits the criteria for range with a distance of 275 nm and for endurance with a time of 4.0 hours.

L-2.1.4 Thrust Vectored Jet

The first design considered using thrust vectoring was the tilt-rotor concept in Figure L-4. This design was a VTOL aircraft that used two turbine engines to power the rotors on either side of the aircraft. The aircraft would lift off with the rotors at a 90° angle. Once the aircraft was in the air, the rotors would tilt slightly to provide forward thrust while still supplying enough lift to keep the aircraft in the air.

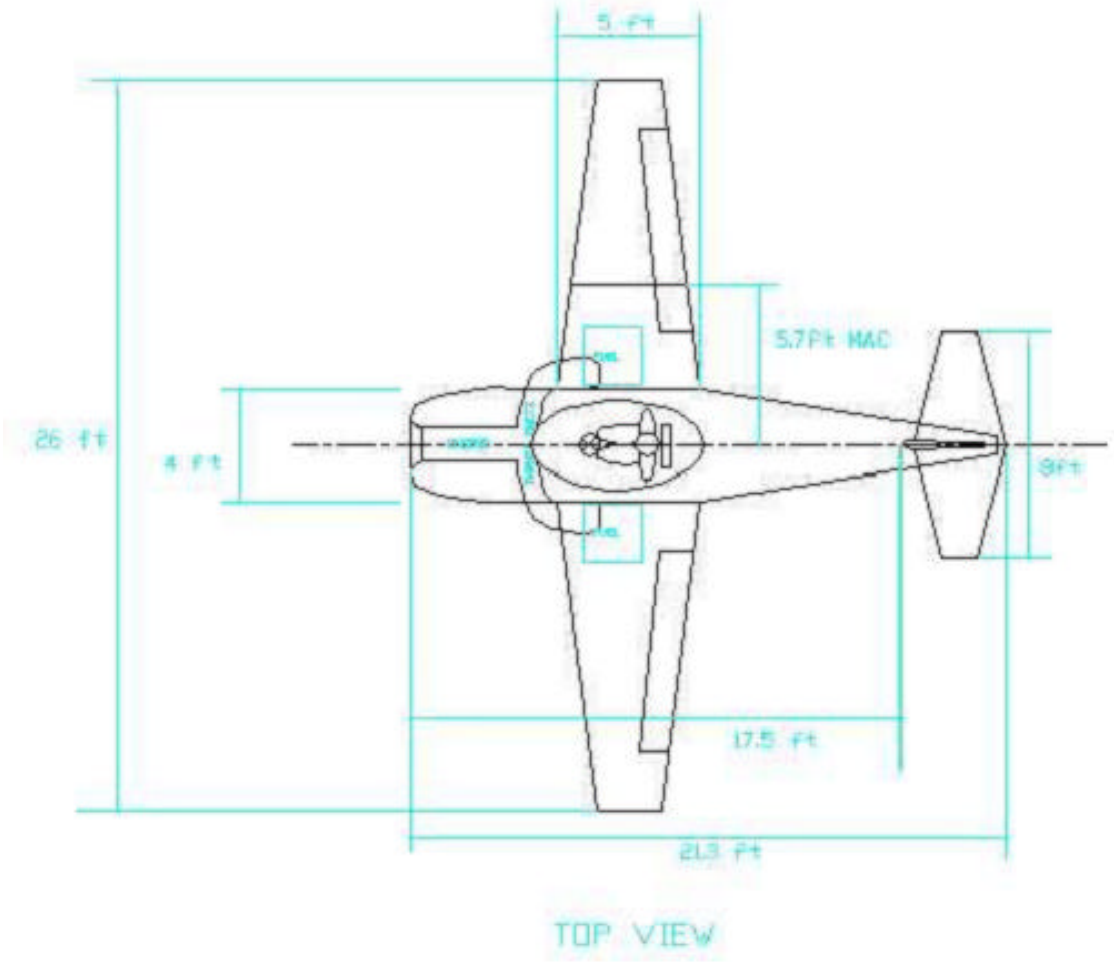

Figure L-4: Sketch of Vectored Thrust Jet

The thrust vectoring design is essentially a small airplane that runs off of the William's jet[14] and ducts the exhaust of the jet so that it can be vectored through the CG of the airplane. This will allow the plane to take off in a very short distance but will have much more stability than the VTOL tilt-rotor concept. Once at altitude, the exhaust can be vectored straight back so that the wings produce all of the lift and the engine can be used only for forward thrust.

A weight analysis estimated a total weight of 5609 N (1261 lbs) which included a fuel weight of 867 N (195 lbs). Takeoff distance was calculated to be 37 m (122 ft) with the thrust vectored at 35°.

L-2.1.5 Pleasurecraft: Jet VTOL/STOL

One solution to our design goals could be a VTOL aircraft. Of course, there are many types of VTOL aircraft, with many different ways of achieving vertical takeoff and landing. A drawing of the concept can be found in Figure L-5. Propulsion is a key consideration in any aircraft of this type. For this reason, a Williams FJX-2 Fanjet was selected for this concept due to its very high thrust and small weight and size. This power plant weighs less than 445 N (100 lbs), but produces 3114 N (700 lbs) of thrust.[14] The inlet for the engine is located on the underside of the fuselage, with the inlet duct running beneath the cockpit. A minimal turning angle is needed for the ingested air to reach the engine.

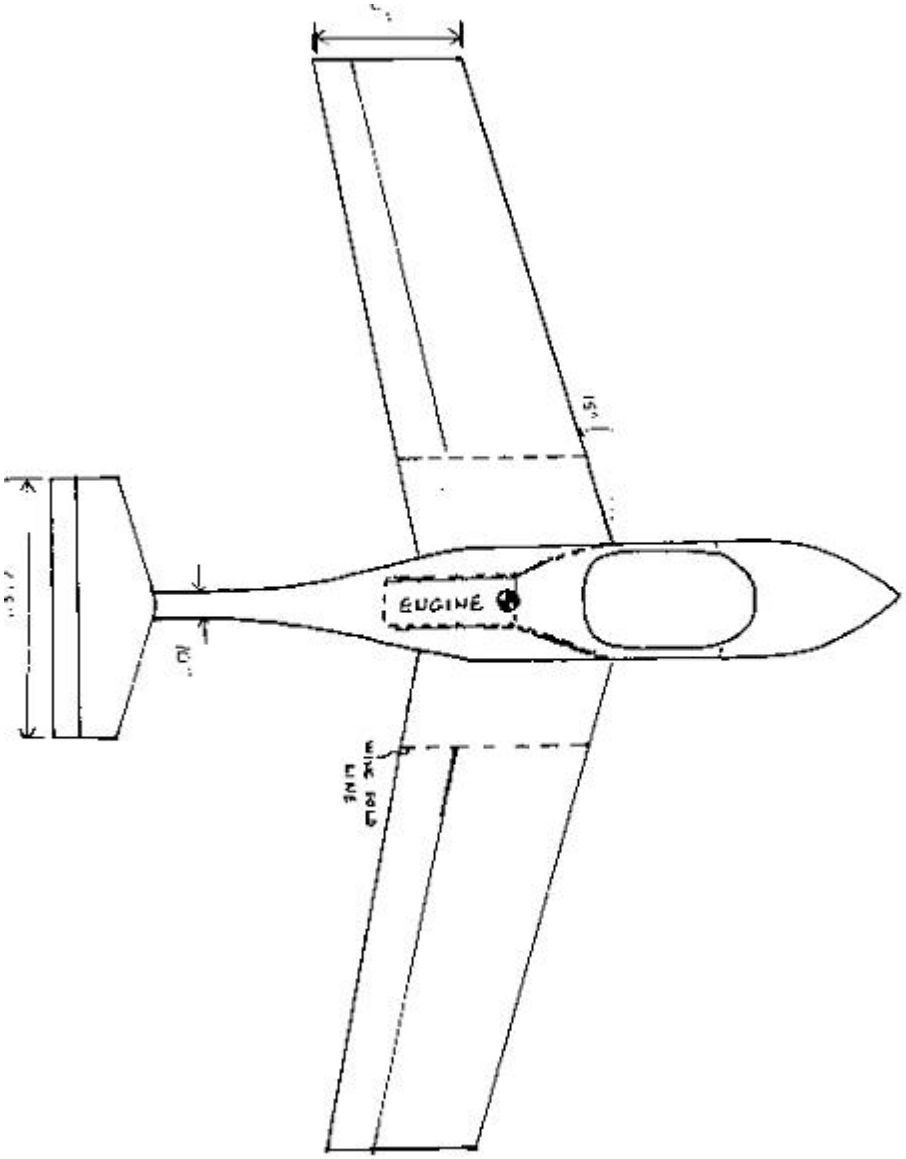

Figure L-5: Sketch of the Pleasurecraft: Jet STOL

The initial configuration used a "bucket nozzle" vectoring system to obtain vertical thrust from the turbofan engine. The "bucket nozzle" was selected due to its relatively small percentage of thrust loss from vectoring, which was around 2-3 percent. In addition, a forward lift fan was necessary to supplement this lift and provide a balanced lifting force. Due to the high degree of complexity, however, this feature was dropped, and the fanjet was moved close to the center of gravity in much the same way as used by most current VTOL/STOVL aircraft. In addition, it was found that the aircraft could take off within 46 m (150 ft) without thrust vectoring given sufficient wing area and C_{Lmax}. Thus the "bucket nozzle" vectoring system was removed entirely while the concept still meets performance goals.

Other key features of this conceptual design are its boom-like tail structure for the horizontal/vertical tail surfaces. This feature was necessitated by the placement of the fanjet engine low and near the center of gravity, and allows the tail surfaces to be far enough aft but still out of the engine exhaust flow. It is a mid-wing design with the engine located beneath the wing crossover. The fuel tank is located coincident with the center of gravity and lies primarily within the wing crossover area and the fuselage. The wing has nearly full-span "flaperons" (ailerons can act in unison with flaps), with the wing fold line being the constraint on their size. The tail has a rudder and elevators for control.

Cabin sizing was based on average numbers found in Raymer[15]. Given that the aircraft should be moderately comfortable, the fuselage width was increased to 91 cm (36 in.). There is moderate room behind the seat for luggage or recreational equipment. A firewall would separate the cabin from the fuel, fuel system, and engine. For transport, the wings can be folded upward. This provides a vehicle width of just over 2 m (6 ft.) during transport. Engine maintenance is simplified by having the engine at the bottom of the fuselage. Panel doors would provide access to the engine bay. The landing gear is in a bicycle configuration and is retractable, although it has not been verified that this idea is feasible given the limited space.

Performance calculations were based on methods outlined by Raymer[15], and Marchman[16]. Following their methods, a rough estimate of aircraft takeoff weight is 5053 N (1136 lbs). This is slightly high, but still within proposed "Sport Aircraft" limits. The fuel fraction used was 0.18, which included 5% reserve. Based on the takeoff weight, this means that approximately 890 N (200 lbs) of fuel is needed. This large amount of fuel is primarily due to having a turbine engine. The preliminary design wing loading is 508 Pa (10.6 psf), with a thrust to weight ratio of 0.67. It was found that the strict takeoff requirements could be met with a wing area of 12 m^2 (130 ft^2), and a maximum lift coefficient of 2.4. The craft had a takeoff ground run of 38 m (125 ft), and a maximum climb angle of over 33 degrees.

L-2.1.6 Propeller Driven Gyroplane

The next design considered was a gyroplane (Figure L-6). This design appears to fulfill the design requirements. Gyroplanes are a type of aircraft very similar in design to helicopters. The main difference is that helicopters have engine-powered rotors and gyroplanes have auto-rotating rotors. Gyroplanes also have controls very similar to that of an airplane including a stick, a rudder and a throttle.[17]

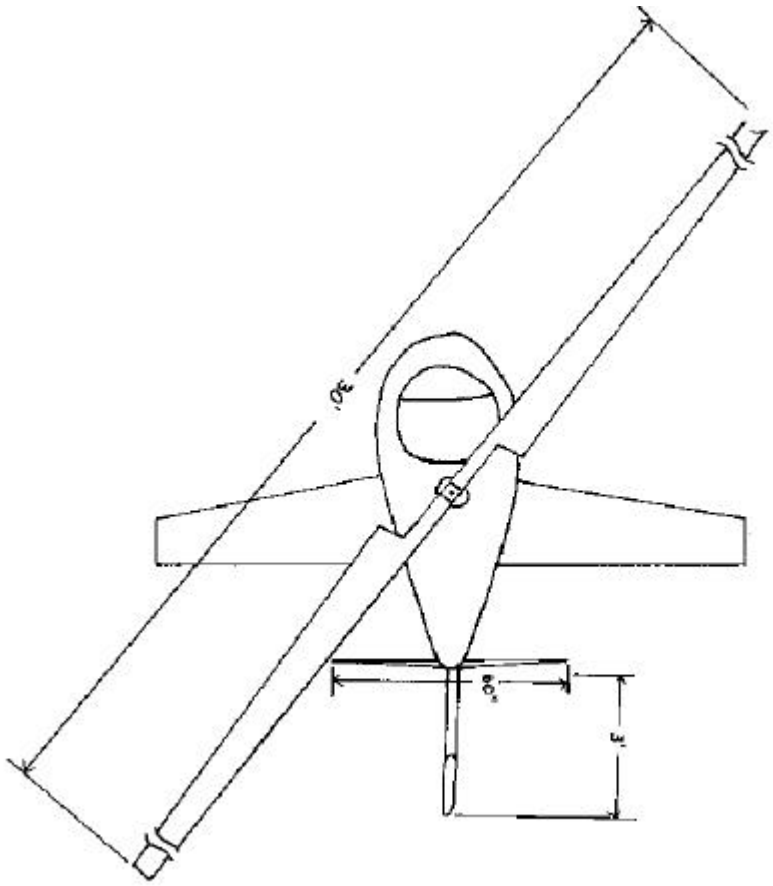

Figure L-6: Sketch of Propeller-driven Gyroplane

This gyroplane design uses a 97 kW (130 hp) engine to power a 1.73 m (68 in) diameter propeller. There will be a clutch that will allow the pilot to pre-spin the 9 m (30 ft) diameter rotor before taking off. Once the rotor has reached the desired RPM, only the propeller will be powered by the engine. This idea of pre-rotating the rotor has been used effectively in other gyroplanes allowing for shorter takeoff. The rotor blades are detachable to make it easier to transport.

Wings were added to this design to give the aircraft more lift during flight. They will also allow for easier control during cruise and landing. The wings are also a safety measure in case the engine power is lost. The gyroplane will then be able to glide similar to a conventional airplane. The wings will also have the capability to carry some of the lift so that the motion of the rotor may not be as important during cruise as it would be on a gyroplane that has no wings. The wings can also be detached at the fuselage for ease of transportation.

The design allows for the pilot to carry some baggage during flight. Allowances were made for additional payload during sizing considerations. The useful load on the airplane was estimated to be 300 lbs.

In sizing the cockpit, anthropometric data was used in order to fit the 95th percentile of a population of half males and half females.[15] A few inches were added in each direction in order to add comfort for the pilot and space for some baggage. This makes the cockpit about 1 m (3 ft.) wide, 1.1 m (3.75 ft.) long and 1.5 m (5 ft.) high.

Allowing for the added useful load, the gyroplane was approximated to weigh about 5338 N (1200 lbs). Pre-rotating the rotor allows the gyro to create lift before beginning down the runway. The rotor would produce approximately 50% of the takeoff weight, leaving only 2670 N (600 lbs) of lift to be produced by the wings during takeoff. This makes the aircraft take off in approximately 9.4 m (31 ft) not including the 5 m (16.4 ft) obstacle. Going over the obstacle would take approximately 7.6 m (25 ft), for a total takeoff distance of about 17 m (56 ft).

This design seems to work well in meeting the requirements, however, there are a few limitations and disadvantages. The performance of a gyroplane is greatly affected by wind. They are also very noisy and would probably not be suited for use in neighborhoods.

L-2.1.7 Ducted Propeller Concept

The conventional STOL concept is a ducted propeller driven, high wing, canard configuration airplane (Figure L-7). It was decided to pursue a propeller driven design based on consideration of noise, cost, and fuel efficiency. The aircraft was designed for comfort but it receives its stubby look as a result of limiting the overall size for ease of transport.

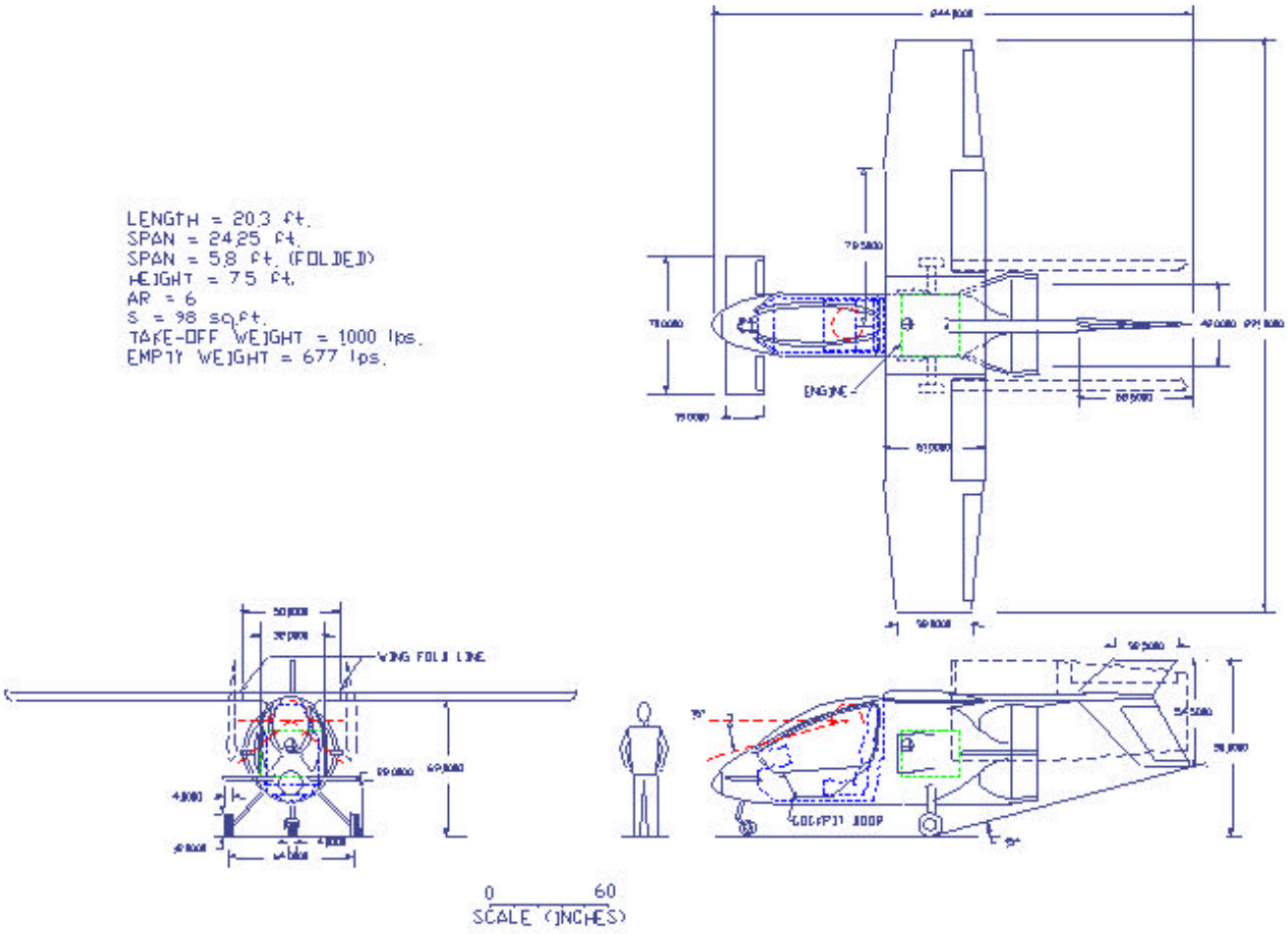

Figure L-7: Sketch of Ducted Propeller Concept

A ducted pusher propeller was chosen as the arrangement of the propulsion system. The pusher prop was chosen in order to give the pilot maximum visibility and also to place the engine near the center of gravity as is commonly seen on many ultralight aircraft. The thrust force from a pusher propeller is applied to a rather robust section of the airframe, so additional structural strengthening to accommodate the engine is not very extensive. If the engine were mounted at the nose, the forward fuselage of the aircraft would require a heavier structure to accommodate the weight and thrust of the engine. Pusher propeller driven aircraft also tend to exhibit a slight stabilizing tendency in pitch and yaw in comparison to a tractor configuration.[18] The pusher propeller has an aerodynamic advantage over a tractor in that it can reduce skin friction drag because the part of the aircraft in front of the propeller flies in undisturbed air. A shorter fuselage can also be accommodated because the propeller inflow allows for a steeper fuselage contour without flow separation.[15]

There are also disadvantages to the pusher propeller configuration. The propeller is in the disturbed wake of the fuselage so it will typically suffer from reduced efficiency. Also, the pusher propeller is vulnerable to damage by objects kicked up by the main landing gear wheels. The main landing gear has a wide track in order to alleviate this to a degree.[15] Engine placement behind the cockpit is also less desirable from a safety standpoint in a crash situation. Engine mounting will have to be carefully considered so that the engine will not enter the cockpit during a crash or collision.[19]

A pusher propeller tends to be noisier than a tractor propeller, but by the use of a duct and a multi-bladed propeller with a low rotational speed, it is possible to alleviate some of the additional noise. In addition to the external noise reduction gained by ducting the propeller, cabin interior noise is reduced by the use of the pusher configuration. The engine exhaust can be directed away from the cabin and the windscreen is not buffeted by the propwash.[15] An added safety advantage of the ducted propeller is that it is very difficult for people outside of the aircraft to be inadvertently injured by a spinning propeller that is shrouded by a duct and is not readily accessible.[19]

The disadvantages of the ducted propeller are increased weight and complexity. Also, if duct is used a reduced propeller rotational speed is desired, the added weight, complexity, and cost of a gearbox and drive shaft must also be considered.

For the purposes of dimensionally sizing a conceptual sketch, the Lycoming O-235 series piston engine was assumed.[20] Originally thrust vectoring on takeoff was considered but it was decided that a more powerful engine would be a better alternative. Thrust vectoring would have added weight and complexity to the propeller duct. Since the difference in power required between vectored thrust takeoff and not vectoring was only 19 kW (25 hp), it was decided the additional weight and complexity of vectoring was not worth the slight gain. Conventional short takeoff was calculated to require about 93 kW (125 hp), which is not an unreasonable amount. Cooling air inlets for the engine are located on either side of the fuselage. If a turboprop powerplant were chosen, a similar inlet configuration could also be used. Engine exhaust could be routed to exit the aircraft either above or below the propeller duct.

A high cantilever straight wing was chosen. A cantilever wing was chosen over a strut-braced wing due to the wing fold requirement. External bracing would have made the wing structure lighter, but also would have required extra complexity to allow the wing to fold.[21] A high wing was also chosen based on the location of the engine and the propeller. A mid wing was ruled out due to the complication of wing spars running through the engine compartment and the effect of the wake on the propeller. In a mid wing configuration, the propeller is

immersed in both the wake from over the wing and under the wing. The differences in pressure acting on the propeller could develop into a vibration problem.[15] A high wing was chosen mainly based on engine accessibility, which would be much more difficult with a low wing. A high wing also typically exhibits less interference drag and better lateral stability than a low wing configuration.[18]

The wing planform chosen was unswept and rectangular with tapered outer panels. This planform is similar to that found on many Cessna single-engine general aviation aircraft. This combination type planform offers both the desired inboard stall characteristics of a rectangular wing as well as the reduction in induced drag due to a more elliptic lift distribution.[22] This planform is more expensive to manufacture than a comparable rectangular planform, but wing performance is very important to this aircraft. The wing also has large single slotted trailing edge flaps as well as ailerons, which could be used in conjunction with the wing to achieve high lift at take-off and landing. The wings fold along a chord line inboard of the trailing edge flaps. Folding wings were chosen over detachable wings due to the difficulty in lifting the wings since they are mounted high on the fuselage. A simple manual pivot system in which the wings pitch down and then swing backward was adopted. With this type of folding scheme, the wing height does not change very much, so very little effort is required from the person folding the wings.

A canard was chosen over a conventional horizontal tail mainly due to aerodynamic considerations. Conventional horizontal tail effectiveness is reduced due to the effect the propwash has on the downwash seen by the tail.[15] The canard also might offer a structural weight advantage. Since the tail does not have horizontal surfaces, the tail experiences less loading and can therefore be built lighter. Also, if a conventional tail were chosen, the structure would have to be designed to withstand buffeting associated with being immersed in the propwash. A T-tail was considered to deal with the propwash problems, but was eliminated because of the heavier structure required and for maintainability considerations.

In keeping with the maintainability requirement, it was decided to keep the vertical tail at an accessible height. This allows for the pilot to inspect the rudder while standing on the ground without a stepladder. The vertical tail was therefore designed so that it was mounted below the tail boom, directly behind the propeller. Both the tail and rudder have large surface areas to make up for the short moment arm. The tail length was kept short in order to make transport easier.

The cockpit for the concept aircraft was sized based on data provided in Raymer.[15] The cockpit has large space allowances and can comfortably accommodate the pilot. The cockpit was also designed for maximum forward and side visibility. Forward vision is enhanced since the engine and prop are both behind the pilot. High wings can sometimes be an obstruction to pilot visibility but that is not the case in this design since the wing is located behind the cockpit. There is a large door on the left side of the aircraft that provides a low step over height so that the pilot can easily enter and exit. A traditional windscreen and door configuration was chosen instead of a bubble canopy mainly for safety reasons. Not only does the large door provide an easier exit in case of emergency, but with that configuration there is support structure above the pilot's head which could prove to be important in the case of an inverted crash.[18]

The fuel tank is located in the section of the wing inboard of the fold line. No fuel is stored in the portions of the wings that fold. If extra fuel tank volume is necessary, some of the space in the join region between the wing and fuselage could be utilized as well.

Like many general aviation aircraft, the landing gear is in a non-retractable tricycle arrangement with solid spring type struts. The tricycle arrangement allows for easy ground

handling and this aircraft will need to be maneuverable on the ground since space is assumed to be limited. Tricycle gear also allows for more pilot visibility than a taildragger arrangement for example. The solid spring type struts were chosen for their simplicity. There is a drag penalty associated with this type but they are cheap to produce and do not require maintenance. Also, with non-retractable landing gear, the possibility of the pilot forgetting to extend them for landing is eliminated.[18]

Weight estimation for the STOL concept was done using the method detailed in Raymer.[15] Weight estimation was based primarily on meeting the requirements for a minimum stall speed of 37 kts and a take-off distance of 46m (150 ft). The takeoff weight was calculated to be 4450 N (1000 lbs). This includes a 1110 N (250 lb) payload and 325 N (73 lbs) of fuel, so the empty weight of the aircraft is 3010 N (677 lbs). The empty weight fraction of the final propeller STOL concept is slightly higher than similar aircraft, but it is predicted that this aircraft will be slightly heavier due to the ducted propeller propulsion system.

L-2.1.8 Vectored Thrust Jet with V-tail

The conventional jet design in Figure L-8 is built for the 380 N (85 lb) Williams International EJ22 turbofan engine. A single engine generates 3425 N (770 lbs) of thrust and is only 37 cm (14.5 in) in diameter and 1.04 m (41 in) long. This engine's light weight and small size make it ideal for the short takeoff and lightweight requirements. Williams International has gathered noise data for this engine through the NASA noise program.[14] Predicted noise levels correlate well with actual noise levels have previously been achieved with Williams International's FJ44-1 used on a Cessna CJ1.[23] The noise data for the EJ22 is presented in Table L-1.

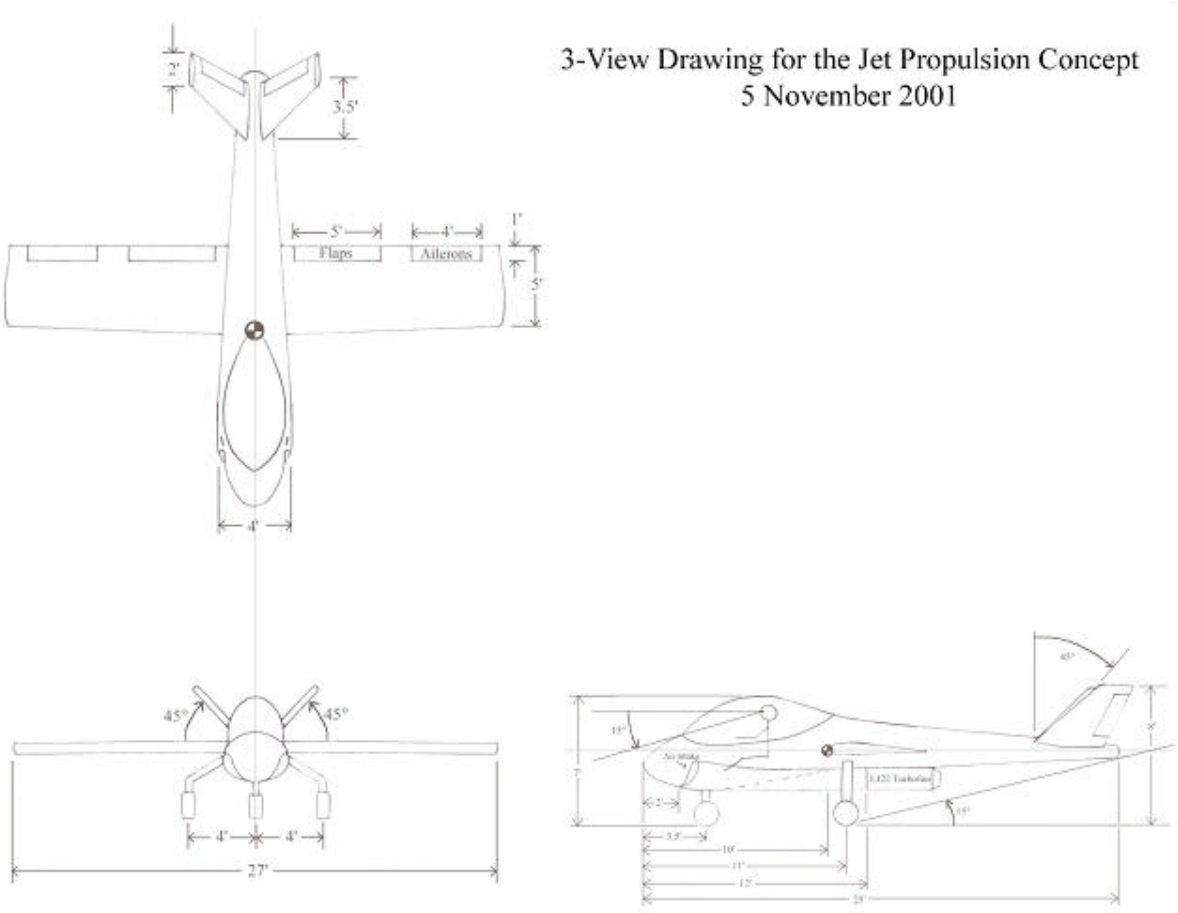

Figure L-8: Sketch of STOL Jet with V-tail

Table L-1: Noise Production Table in EPNdB[23]

	Takeoff	Sideline	Approach	Delta Stage 3
Stage 3 Requirements	89.0	94.0	98.0	
Stage 4 (Proposed)	86.0	91.0	95.0	-9.0
Cessna CJ1 Predicted	75.9	86.0	94.9	-24.2
Cessna CJ1 Actual	73.4	83.7	92.1	-31.8

The engine's thrust is deflected downward to increase the lift during takeoff and then returned to the horizontal position once after liftoff. The engine is located on the bottom of the fuselage so that the vectored thrust is directed through the center of gravity. An air intake duct is molded around the bottom of the fuselage where the engine is mounted. The intakes are located directly behind the nose of the aircraft so that the S-curve is smooth and gradual to help prevent flow separation. The shortest ground-run takeoff distance of approximately 35 m (115ft) for the given 3115 N (700 lb) thrust is achieved with a deflection of thirty degrees. A C_{Lmax} of 2.0 was assumed using an average value for a single-seat plane and current airfoil data[24]. Using this C_{Lmax} and known takeoff and stall conditions, the wing area was sized to 12.1 m^2 (130 ft^2) for a maximum takeoff weight of 5340 N (1200lbs) which is slightly lower than the maximum for the

sport aircraft group. The vectored thrust during takeoff allows the aircraft to clear a 5.8 m (19 ft) obstacle in the remaining 10.7 m (35 ft) using maximum climb angle conditions.

An aspect ratio of 8 was used because it produces good flight performance characteristics and enables the wingspan to be small enough to fit space requirements for storage. The basic weight analysis showed the aircraft could hold 1335 N (300lbs) of fuel giving it a range of 350 nautical miles and an endurance of 2.3 hours at cruise. A worst-case scenario TSFC of 0.75 was used in these calculations. The aircraft has a 1785 ft/min maximum rate of climb which almost doubles the maximum rate of climb requirement. However, these calculations showed that the range and endurance surpass the given requirements. Since the cruise speed is only 90 kts, the swept wings exist for purely aesthetic reasons. The V-tail eliminates the need for a separate horizontal and vertical tail system; a V-tail incorporates both the elevator and rudder into each tail. The cockpit area is large enough for an average man to sit comfortably with controls and instrumentation, and a small luggage area sits behind the pilot's seat. The nose wheel is mounted under the pilot and between the two intake openings on the bottom of the fuselage. At that point the intakes are separate so that the nose wheel has enough structure to resist large impacts on landing and the strut does not interrupt the airflow through the S-ducts. The intakes join together behind the wheel mount and continue back towards the engine. The two back wheels mounted to the fuselage and angled out to the side. In this configuration, the struts will act as springs to absorb the landing impact without requiring shocks installed in the landing gear.

L-2.1.8 Jet-powered Gyroplane

The concept shown in Figure L-9 examined the use of a gyroplane to meet the initial design criteria. The main problem to tackle in the design of this aircraft was considered to be the takeoff distance. Most existing gyroplane designs easily meet the range, endurance, and climb criteria, and the faster designs approach the required max cruise speed. However, few gyroplanes can get off the ground and over an obstacle in less than 46 m (150 ft).[25] In an attempt to account for this, the rotor could be pre-spun to save the time and runway distance that it would take for a full autorotation mode to develop naturally. There are many existing methods used to pre-spin the rotor. For example, the CarterCopter uses a clutch to the engine drive shaft that supposedly produces enough torque to the rotor to give the aircraft VTOL capability.[1] In addition, wings could be used to provide extra lift that might get the aircraft off the ground more quickly.

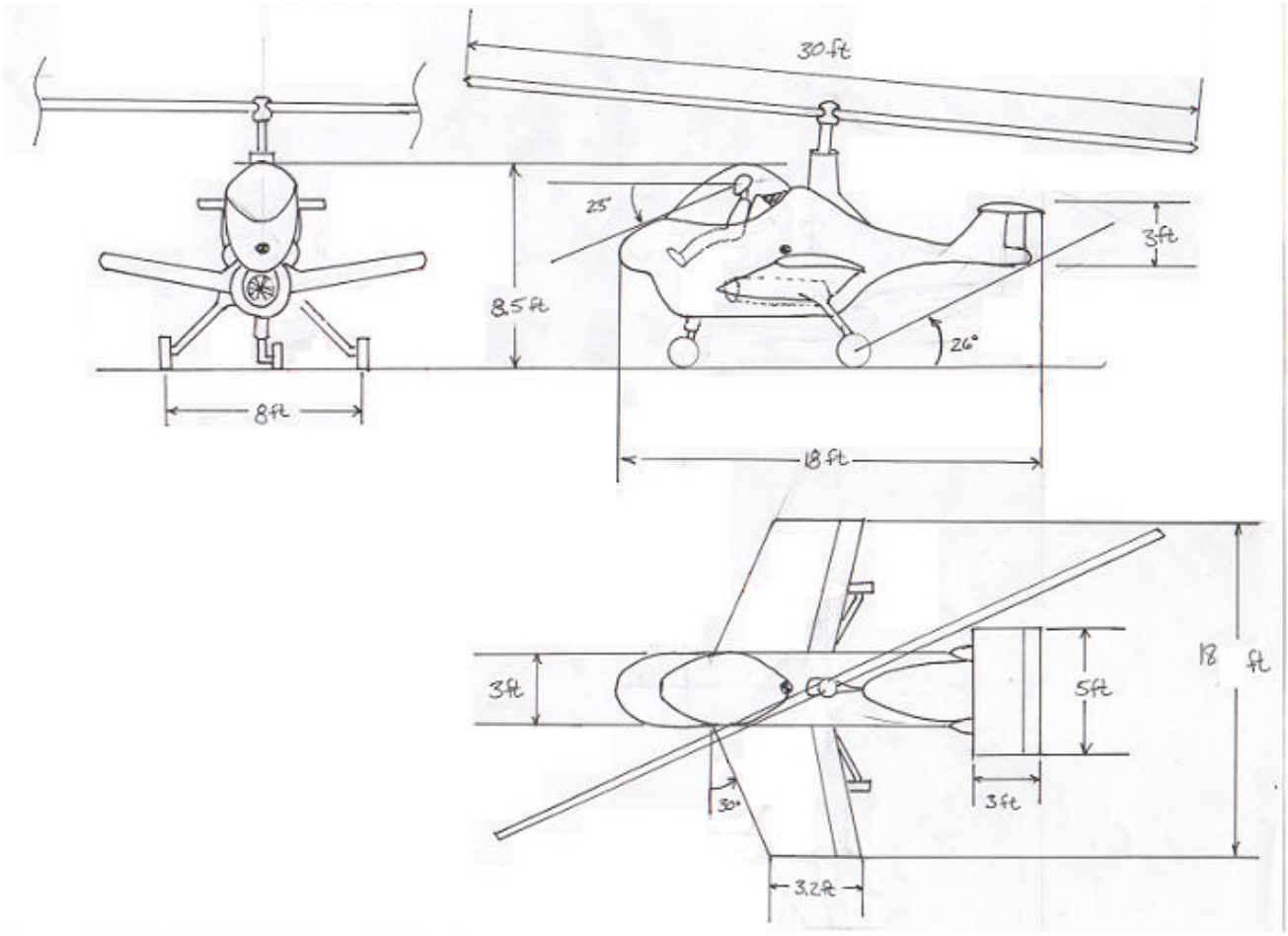

Figure L-9: Sketch of Initial Jet-driven Gyroplane

In a cooperative effort with NASA, called the General Aviation Propulsion (GAP) program, Williams International has developed the FJX-2, a turbofan engine that is much smaller in size than any existing comparator jet engine. This engine weighs only about 445 N (100 lb), yet is rated at 3110 N (700 lb) thrust. The FJX-2 is also expected to perform with efficiency comparable to most piston engines used in aircraft applications.[14] These qualities made the FJX-2 an obvious choice for this gyroplane. Its low weight, low cost, and high thrust-to-weight ratio would help to accelerate the aircraft on the ground enough to allow the extremely short takeoff criteria to be met. Compressed air or exhaust from the engine could be used in various ways to pre-spin the rotor as well, shortening the takeoff distance even more.

Figure L-10 shows the initial concept of the aircraft. It consists of an unpowered, 30 ft diameter rotor, small wings, a large horizontal tail for maximum longitudinal control at slow speeds, lightweight construction, and propulsion provided by the FJX-2. Lateral control is provided by full semi-span flaperons, which can also be used to provide enhanced lift on takeoff. The engine exhaust can be channeled into a duct that spins a turbine. Through a shaft and gearing mechanism, the exhaust could be used to pre-spin the rotor blades. Once the desired rate of rotation is reached, the thrust could be directed back in the horizontal direction, moving the aircraft forward while the blades remain spinning inertially. As the aircraft moves down the

runway, the wings begin to add to the lift already created by the rotors due to its "jumpstart," and the aircraft will be able to take off in a relatively short distance.

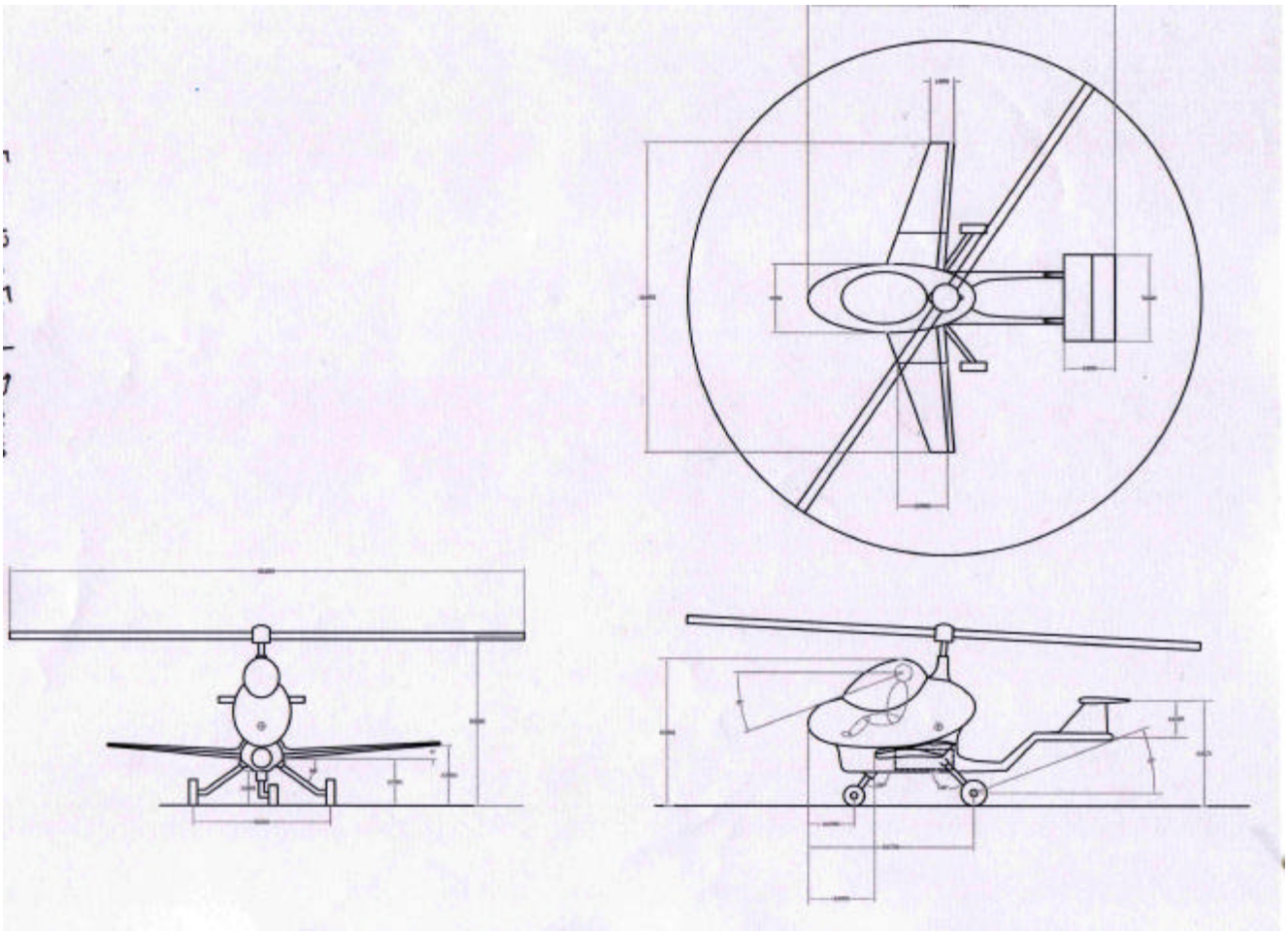

Figure L-10: Sketch of Revised Jet-Driven Gyroplane

After some reevaluation, minor changes were made while the main concept remained the same. The most recent version of the concept is shown in Figure L-9. The rotor remained a diameter of 9.1 m (30 ft), based on several existing gyro designs, including the RAF 2000.[26] However, the method of pre-rotation was changed. The gearing system discussed above would add unnecessary weight, complexity, and cost to the design. It was decided to channel the exhaust gases in a similar manner as discussed above, but instead of using a mechanical device, the exhaust could be ducted down the rotor blades and out through a nozzle at each tip. This would provide a coupled force to start the blades spinning. The idea of tip driven rotor blades was very popular in the early days of helicopter and gyro flight.[27] The problem with using jet engine exhaust is that it poses both a plumbing and a heat transfer nightmare. Therefore it was decided to use an air motor that would use compressed air from the engine's compressor stage. This same method is used with the same engine in the jet-powered concept of the Carter Copter.[1] The blades would remain flat during pre-rotation, and would be "popped" into the proper pitch through a control in the cockpit at a proper time during the takeoff run. Once the blades were pre-rotated to about 300 RPM, the air motor would be cut off and the propulsion

resources directed solely to horizontal acceleration. The blades would remain spinning inertially, possibly with help from weighted tips. Since the time to accelerate should be relatively short due to the light weight of the aircraft, not much loss is expected from the rotor slowing down.

The wing's aspect ratio was increased by making it slightly longer and thinner in an attempt to reduce drag. Full semi-span flaperons were kept, along with the boom-style tail and large vertical and horizontal tail surfaces. The horizontal tail was positioned towards the vertical center of the aircraft to avoid interference from the engine exhaust as well as from the rotor. This causes the tail scrape angle to be larger than the angle of attack that would cause both rotor and wing stall. However, it was assumed that with the wing/rotor combination, exaggerated takeoff rotation would not be needed and this would be included in piloting documentation.

Other features of the design include a bubble canopy for maximum pilot visibility, and a wide wheel base along with considerable dihedral for lateral stability on both the ground and in the air, respectively. Fuel is to be stored partially in the wings and partially in the fuselage. For portability, break points are to be located outboard of the wing fuel tanks at which the wings could be either folded or removed.

The weight of this aircraft was estimated using different methods as shown in Appendix A. The takeoff weight is estimated to be 3780 N (850 lbs) which includes 703 N (158 lbs) of fuel weight. The total takeoff distance was calculated to be about 28 m (92 ft).

L-2.2 Loughborough University's Original Concepts

Loughborough University's team split into 5 groups, each looking at different approaches to solving the problem. Through methods of selection explained later, the choices were narrowed to three concepts for the purpose of further development.

L-2.2.1 Gyroplane

The gyrocopter concept shown in Figure L-11 is a simple piston-powered gyroplane design. Short takeoff is accomplished by means of pre-spinning the main rotor through the use of a simple clutch and drive mechanism from the engine. To optimize cruise performance, the design incorporates a wing on the fuselage that unloads the main rotor at higher flight speeds. Short landing is easily accomplished by this design by means of autorotation of the main rotor, which provides a controllable, near vertical descent. Weight is kept to a minimum through the use of composite material structures in the fuselage.

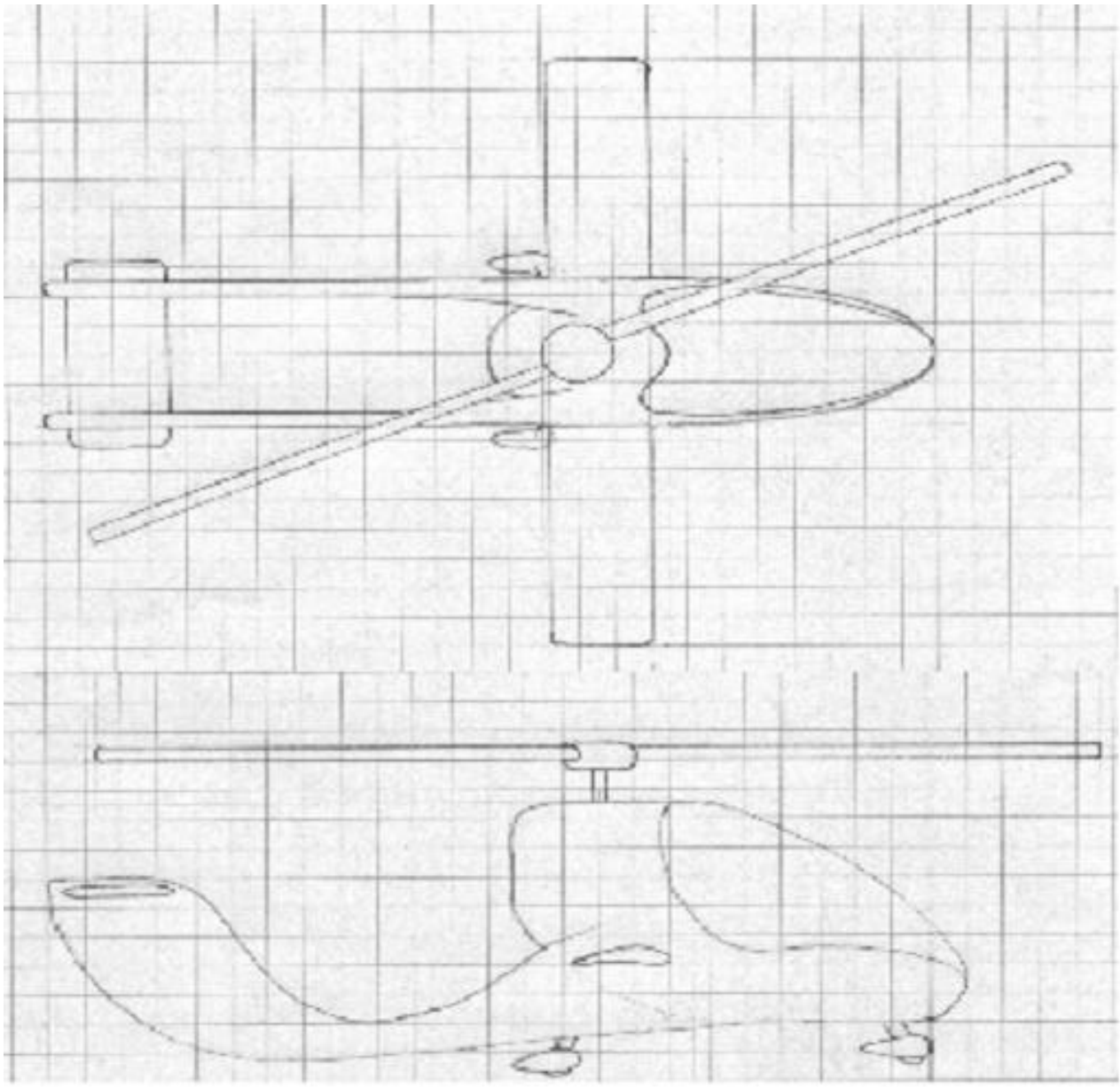

Figure L-11: Sketch of Loughborough's Gyroplane Concept

L-2.2.2 Coaxial Helicopter

Figure L-12 shows a coaxial helicopter concept. The main unique feature of this design is the counter-rotating rotors which alleviates the need for a long tail boom and torque-countering tail rotor. This lightweight helicopter design is small and compact with a specified gross weight of 1962 N (441 lbs) with an overall height of 2.6 m (8.5 ft) and length of 4.4 m (14.4 ft). The two main rotors are both 4 m (13.1 ft) in diameter and power is supplied to them by a specified 60 hp engine through a transmission system. Cruise speed is estimated at slightly over 36 m/s (70 knots), with fuel capacity being 343 N (77 lbs). This design can easily attain the short takeoff and landing requirements through the vertical ascent and descent capability

associated with helicopters. However, the cruise speed would need to be optimized for this particular design to meet requirements.

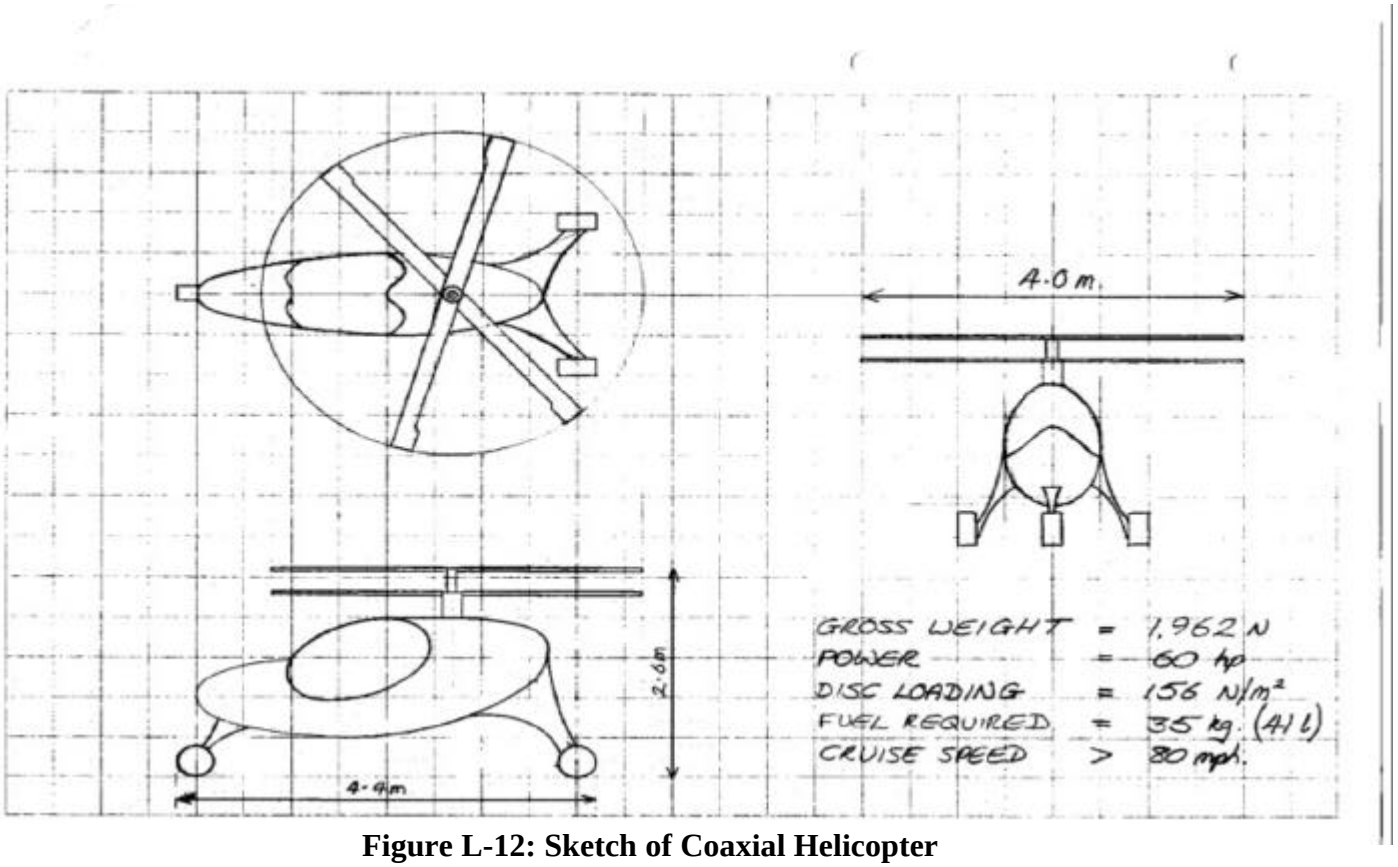

Figure L-12: Sketch of Coaxial Helicopter

L-2.2.3 Joined Wing Concept

A joined wing with twin tilting ducted fans is shown in Figure L-13. This design utilizes a single turboshaft engine housed in the fuselage to drive twin-tilting ducted propellers on the sides of the fuselage. Through the use of composite materials, the empty weight of this design is estimated at 4002 N (900 lbs), with an estimated maximum takeoff weight of 6161 N (1385 lbs). The use of the joined wing brings the overall wingspan to 4 m (13.1 ft), with a total wing area of 7 m^2 (75.3 ft^2) and an effective aspect ratio of 9.2. At 6 m (19.7 ft) in length and 1.8 m (5.9 ft) in height, the fuselage is compact in comparison with many conventional aircraft. This design is currently designed to take off and land vertically by tilting the ducted propellers to meet the short takeoff and landing requirement. With a 336kW (450 horsepower) turboshaft engine specified, cruise speed is estimated at over 103 m/s (200 knots), giving a range of 815 km (440 nautical miles) and an endurance of 2 hours.

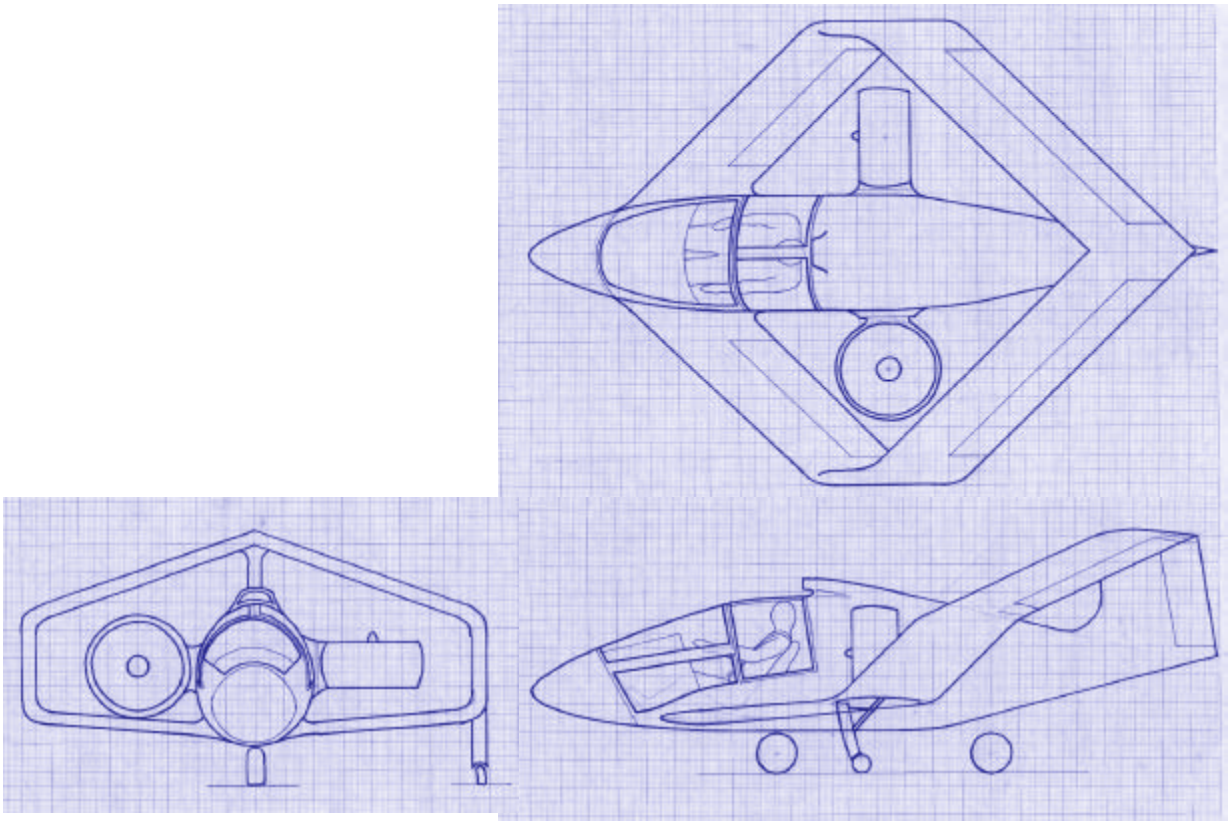

Figure L-13: Sketch of Joined-Wing Concept

L-2.2.4 Jet-bike Concept

A jet-bike concept was also considered. Some key points of this design include vectored or vertical takeoff and landing, relatively high cruise speeds, long endurance of over two hours, and easy transportation. The engine inlet could be as small as 0.6m while still producing large amounts of thrust at lower Mach numbers. These low speeds would be useful for the short takeoff and landing requirements. The high bypass ratio would also decrease the amount of fuel used in cruise. The empty mass of the aircraft is only 65kg which shows how easily it could be transported. Various vertical takeoff and landing aircrafts were researched, and it was found that only a small wing area was needed for vectored or vertical takeoff.

L-2.2.5 Ultralight Concept

Advantages of ultralights include the comfort of a conventional design, low cost, low weight, relatively low power requirement, and good range. There would be a tradeoff between cruise speed and takeoff distance. Also, it was decided that the goals described at the beginning of this report would not allow an aircraft to be included in the ultralight category and this concept would not be pursued any farther.

L-3 SELECTION PROCESS

As with any group design project, it is inevitable that people are going to have different ideas as far as how things should be done. It is also usually true that some ideas are going to be better than others. These facts alone express the need for some sort of process to choose the best course of action for a given situation. The fact that engineering tends to involve tradeoffs can make this process fairly complicated. One design may have some good aspects and some bad aspects, while another may be mediocre across the board. To decide on a concept, methods of comparative analysis were explored to reduce the diverse ideas of 24 people to a single group concept.

The general procedure for selecting a final design concept was fairly simple. The Virginia Tech and Loughborough teams would each develop three concepts. When the Virginia Tech students traveled to Loughborough, the teams would meet to discuss the six concepts. The goal of the one-week visit was to narrow the six down to one. Although there would be room for change, the design chosen would initially be the single concept to be pursued.

The Virginia Tech half of the team began by splitting up into three sub-groups. Each group consisted of three Aerospace Engineers and one Industrial/Systems Engineer. Each of the aerospace engineers was to come up with a concept to meet the design criteria. With the help of the rest of the group, each concept would be developed over the next several weeks. This involved calculations to determine values for weight, takeoff distance, range, and endurance among other parameters.

Before going to Loughborough in November, each subgroup had to narrow its three designs down to one. Although each sub-group decided upon its own selection method, all three were quite similar. Broad rating categories such as performance and ease of operation were defined and given a weighting value. The weighting was included as a measure of a given category's importance relative to other categories. Specific criteria for evaluation were then defined within each category. Each design was then rated according to these specific criteria, either on a "goodness/badness" scale or as a rank relative to the group's other designs. The end result was a single concept for each group. The pusher prop, jet STOL airplane, and jet powered gyroplane were the three designs to survive the evaluation. Once this stage of selection was complete, the three sub-group selection methods were consolidated into a single form shown in Figure L-14. This form was brought to Loughborough along with the three concepts as representative of the Virginia Tech team's selection process.

Category	Category Weight	Criteria	Rank		
			Concept 1	Concept 2	Concept 3
Performance	10	Takeoff Dist.			
		Stall speed			
		Range			
		Endurance			
		Rate of Climb			
		Angle of Climb			
		Takeoff Weight			
		Fuel Weight			
		L/D max			
		AVG			
Cost	8	Cost of Engine			
		Wing-folding			
		Control surfaces			
		AVG			
Ease of Operation	8	Ease of Entry			
		Ease of Flying			
		Ease of Transport			
		AVG			
Serviceability	5	Control System			
		Engine			
		AVG			
Durability	7	Drive System			
		Landing Gear			
		Life of Engine			
		AVG			
Safety	9	Rear engine			
		Side visibility			
		Fuel location			
		Ease of exit			
		Glide			
		AVG			
Misc.	7	Environmental			
		Comfort			
		Payload			
		Aesthetics			
		AVG			
		TOTAL SCORE			

Sum of averages multiplied by appropriate category weight

Figure L-14: Selection Chart

The Loughborough team had its own process for selecting its three concepts. They began by researching methods that could be used to meet the design problem requirements. Five categories of feasible methods were then pursued, including vectored thrust, tilt thrust, gyroplanes, ultra/micro-lights, and helicopters. A sub-group researched each method and then developed a concept according to that method. This differed from the Virginia Tech selection process in that each group was basically assigned a concept to explore, making sure everything was tried. The Virginia Tech method did not necessarily guarantee variety. The group could have ended up bringing three gyroplane designs to England if the selection process deemed them better than other options. Once the Loughborough students had 5 concepts, they were rated in similar fashion to the method employed by the Virginia Tech students. Categories were defined and split into more specific criteria on which to rate each design. Each category was given a

weight, and each of the five designs was rated from 1-10. The top three scores were chosen to go into the pool of six that would be evaluated during the Virginia Tech team's visit.

Once both teams were in Loughborough, they had the task of choosing a single concept that would be concentrated on, at least initially. Before designs could be evaluated, information needed to be exchanged. Both the Virginia Tech and Loughborough teams gave presentations on the three designs they had brought to the table.

With the entire team knowledgeable of all six designs, a common evaluation system needed to be agreed upon. It was decided as a group that elements from both teams' previous systems should be used. The group decided upon the following nine broad categories: performance, weight, cost, safety, durability, ease of operation, serviceability, manufacturability, and miscellaneous. The now combined team of Virginia Tech and Loughborough students split up into groups to determine what sub-categories were important and the weighting factor with which they should be modified. One group would evaluate each of the other groups' sub-category selection and add or delete whatever they felt necessary. In this fashion, a single team selection method was agreed upon.

The consolidated selection method consisted of broad categories broken into more specific criteria to rate each design. Each main category and sub-category was given a weighting factor. The design being rated would be given a score from 1 – 5 in each sub-category. This score was then multiplied by the respective sub-category weighting factors and summed up to obtain the category score. This category score was then divided by the sum of the sub-category weightings and multiplied by the main category weighting to give the final moderated category score. Scores were to be obtained for each category and summed to determine the final score for the design. The highest score would be the chosen design. An example is shown in Figure L-15.

Category	Criteria	Weight	jet conv	
Performance	Takeoff Dist	5	3	15
27	Stall Speed	3	3	9
5	Range	4	3	12
	Cruise Speed (maxR)	4	2	8
	Rate of Climb	3	4	12
	Endurance	3	5	15
	Landing Dist	5	2	10
				81
				15

Figure L-15: Example Ratings of V-tail Jet

The team, which was still split up into category groups, now had the task of rating each of the six designs for the group's assigned category/sub-categories. This proved to be a difficult task, as there were six designs to be rated in nine categories each. After several minutes of chaos, time constraints led to the decision that before the ratings were applied, the field should be narrowed further. This was done by way of a secret ballot vote. The top three designs would move on to be rated while the remaining three would be dropped from consideration. The vote narrowed the six concepts down to the jet STOL (Figure L-8), the pusher prop (Figure L-7), and the joined wing designs (Figure L-13).

These three designs were then rated in the category groups as discussed above. After calculations had been made, there was an astonishing result. The evaluation gave an exact numeric tie between the pusher prop and joined wing designs. At this point the jet STOL design

was dropped and an attempt was made to analyze the scoring differences between the two tied designs. Margin of victory and importance of category were discussed for each category score between the two designs. This resulted in more unorganized discussion, circular arguments, and comparing of apples and oranges. The team agreed that a show of hands vote would make as much sense as anything at this point. The joined wing design won the vote 21 – 3, and would be the concept for future focus (Figure L-16).

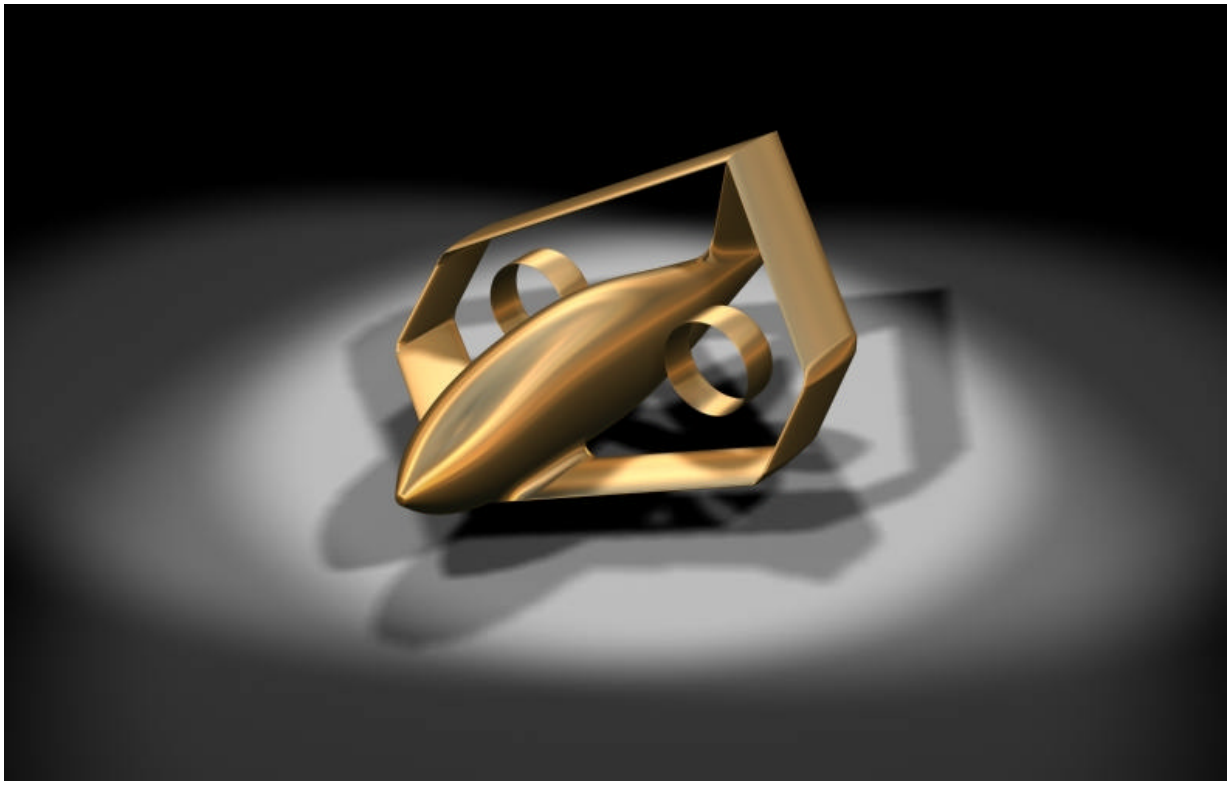

Figure L-16: Design Concept Chosen for Further Development

REFERENCES

1. CarterCopters, LLC., www.cartercopters.com, December 2001.

2. Groen Brothers Aviation, Inc., www.groenbros.com, December 2001.

3. Moller International, www.moller.com/skycar, December 2001.

4. RosAreoSystems, http://rosaerosystems.pbo.ru/english/products/kre4et, December 2001.

5. VSTOL Aircraft Corp., www.vstolaircraft.com, December 2001.

6. Pro Sport Aviation, www.sportlite103.com/freebird, December 2001.

7. "The Flying Flea Archive USA", www.valkyrie.net/~flyingflea/gallery/html, December 2001.

8. STOL CH 701 website: http://www.aircraft-kit.com, December 2001.

9. Avid Aircraft Information Sheet, Avid Aircraft, www.avidaircraft.com, December 2001.

10. Cessna Aircraft Company, "1985 Cessna 152 Information Manual." 1985.

11. Brandt, S., Stiles, R., Bertin, J., and Whitford, R., *Introduction to Aeronautics: A Design Perspective.* AIAA, Reston, VA, 1997.

12. http://www.planopower.com/honda/hondagx610.html, December 2001.

13. "Get In-Line with Moravia, Inc." Moravia, Inc., www.moraviation.com/lom.html, December 2001.

14. "Williams International Product Information," Williams International, http://www.williams-int.com/product/fjx.htm, December 2001.

15. Raymer, Daniel P., *Aircraft Design: A Conceptual Approach*. AIAA. Washington D.C., 1989.

16. Marchman, James F. III, *Introductory Aircraft Performance*, Virginia Tech University Printing, 1996.

17. "The Popular Rotorcraft Association", Popular Rotorcraft Association, Mentone, IN, www.pra.org, December 2001.

18. Roskam, J., *Airplane Design Part II: Preliminary Configuration Design and*

Integration of the Propulsion System, DARCorporation, Lawrence, Kansas, 1997.

19. Thurston, D., *Design for Safety*, McGraw-Hill, New York, 1980.

20. "Textron Lycoming Online", Textron Lycoming, www.lycoming.textron.com, December 2001.

21. Roskam, J., *Airplane Design Part III: Layout Design of Cockpit, Fuselage, Wing, and Empennage: Cutaways and Inboard Profiles*, DARCorporation, Lawrence, Kansas,1989.

22. Donald, D., *The Encyclopedia of Civil Aircraft*, Thunder Bay Press, San Diego, California, 1999.

23. "Eclipse Aviation | EJ22 Engine," Ellipse Aviation, http://www.eclipseaviation.com/500jet/ej22engine.html, December 2001.

24. Jenkinson, Lloyd, "Excerpts from a Forthcoming Book on Aircraft Design," 2001.

25. Davis, Brad, "Gyro Comparisons," *Rotorcraft*, Volume 37, Number 1, Feb-Mar 1999.

26. Rotary Air Force, Inc., *RAF 2000*, www.raf2000.com, December 2001.

27. Lambermont, Paul, *Helicopters and Autogyros of the World*. Cassell and Co., London, 1970.

28. Gessow, Alfred. *Aerodynamics of the Helicopter*, Frederick Ungar Publishing Co., New York, 1967.